Regulation of the Intrahepatic $CD8^+$ T Lymphocyte

Joseph Samuel Dolina
Bordentown, New Jersey

Bachelor of Science, Biology; Bachelor of Science, Chemistry
The College of New Jersey, 2006
Master of Science, Biomedical Sciences
University of Medicine and Dentistry of New Jersey, 2007

A Dissertation presented to the Graduate Faculty
of the University of Virginia in Candidacy for the Degree of
Doctor of Philosophy

Department of Microbiology, Immunology, and Cancer Biology

University of Virginia
August, 2013

For my parents, Joseph Sr. and Katherine,

whose love and support made this work possible.

Modest,
organized
friend,
underground
worker,
let me give you
the wing of my song,
the thrust
of the air,
the soaring
of my ode:
it is born
of your invisible machinery,
it flies
from your tireless
confined mill,
delicate
powerful
entrail,
ever alive and dark.
While
the heart resounds
and attracts
the music of the mandolin,
there, inside,
you filter
and apportion,
you separate
and divide,
you multiply
and lubricate,
you raise
and gather
the threads and the grams
of life, the final
distillate,
the intimate essences.
Submerged
viscus,
measurer
of the blood,
you live
full of hands
and full of eyes,
measuring and transferring
in your hidden
alchemical
chamber.

Yellow
is the matrix
of your red hydraulic flow,
diver
of the most perilous
depths of man,
there forever hidden,
everlasting
in the factory,
noiseless.
And every feeling
or impulse
grew in your machinery,
received some drop
of your tireless
elaboration,
to love you added
fire or melancholy,
let one tiny cell
be in error
or one fiber be worn
in your labor
and the pilot flies into the
wrong sky,
the tenor collapses in a
wheeze,
the astronomer loses a
planet.
Up above, how
the bewitching eyes of the
rose
and the lips
of the matinal carnation
sparkle!
How the maiden
in the river laughs!
And down below,
the filter and the balance,
the delicate chemistry
of the liver,
the storehouse
of the subtle changes:
no one
sees or celebrates it,
but, when it ages
or its mortar wastes away,
the eyes of the rose are
gone,

the teeth of the carnation
wilted
and the maiden silent in
the river.
Austere portion
or the whole
of myself,
grandfather
of the heart,
generator
of energy:
I sing to you
and I fear you
as though you were judge
meter,
implacable indicator,
and if I can not
surrender myself in
shackles to austerity,
if the surfeit of
delicacies,
or the hereditary wine of
my country
dared
to disturb my health
or the equilibrium of my
poetry,
from you,
dark monarch,
giver of syrups and of
poisons,
regulator of salts,
from you I hope for justice:
I love life: Do not betray
me! Work on!
Do not arrest my song.

—Pablo Neruda
'Ode to the Liver'

Translation by
Oriana Josseau Kalant[1]

Regulation of the Intrahepatic $CD8^+$ T Lymphocyte

Abstract

The liver is a tolerogenic environment exploited by persistent infections such as hepatitis B (HBV) and C (HCV) viruses. Using murine models of intravenous (IV) adenovirus and mouse cytomegalovirus (MCMV) infections, I establish that antiviral $CD8^+$ T cells primed directly in the liver acquire a dysfunctional phenotype characterized by a decreased ability to produce pro-inflammatory cytokines and cytolytically kill target cells. During the onset of intrahepatic viral infection, $CD8^+$ T cell infiltration/expansion are accompanied by the upregulation of three core immunoregulatory pathways: IL-10, PD-1/PD-L1, and Tim-3. To examine the role of hepatic myeloid PD-L1 expression during the early phase of viral infection, I administered PD-L1 siRNA encapsulated in lipidoid nanoparticles (LNP) in mice. My studies indicate that Kupffer cells (KC) preferentially engulfed PD-L1 LNP within a short period of time and silenced *Pdl1* during adenovirus and MCMV infections leading to enhanced natural killer (NK) and $CD8^+$ T cell intrahepatic accumulation, effector function, $CD8^+$ T cell-mediated viral clearance, and memory. Without application of PD-L1 LNP, if the dysfunctional liver-primed $CD8^+$ T cells were allowed to expand in the natural setting, these cells also acquired a late phase T regulatory (T_{reg}) cell function on the *in vitro* and *in vivo* priming of naïve $CD8^+$ OT-I T cells. Liver-primed $CD8^+$ T cell (herein renamed $CD8^+$ T_{reg} cells) regulatory activity was independent of PD-1/PD-L1 interaction, IL-10 production, and expression of the canonical Tim-3 ligand, Gal-9. I discovered that $CD8^+$ T_{reg} cell surface Tim-3 controls the expansion of antiviral $CD8^+$ T_{eff} cells by binding to a novel ligand, HMGB-1. HMGB-1, originally identified as a DNA binding protein, may therefore act as a potent cytokine controlling the outcome of acute and chronic viral infections in the liver. Although PD-L1 did not appear to directly play a functional role in $CD8^+$ T_{reg} cell suppression at the late

phase antiviral immune response, PD-1/PD-L1 signaling from KCs during the early phase promoted the development of $CD8^+$ T_{reg} cells. Overall, KC specific PD-1/PD-L1 negative signaling was central in diminishing the early antiviral immune response, whereas Tim-3 limited late phase $CD8^+$ T cell antiviral immunity in the liver. The presence of IL-10-producing, $PD\text{-}1^+PD\text{-}L1^+Tim\text{-}3^+CD8^+$ T cells in the livers of chronic HCV patients raises the possibility that liver-primed $CD8^+$ T cells could play a pivotal role in dampening hepatic T cell responses in the local tissue microenvironment.

Author's Note

The crescendo of past knowledge and human inspiration to explore nature has allowed science to burgeon, improving the quality of life for mankind over the years. Specifically, the scientific method's first use in fighting disease occurred when physicians washed their hands before attending a woman in childbirth and discovered reduced incidences of puerperal fever. Later work conducted by Louis Pasteur led to the first link between microorganisms and disease. As genetics flourished, insights into disease pathology and immunity emerged. At the dawn of a new millennium, immunological research faces new problems as novel pathogens surface, antibiotic resistance rises, and bioterrorism haunts the future. Well-known diseases still remain uncured. Immunological findings are proving to be exceedingly vital, as they provide for effective applications in clinical use.

My interest in pursuing immunological research begins with an undergraduate course entitled "Molecular Immunology and Human Disease." Taught by Dr. Amanda Norvell at The College of New Jersey, this class grasped my mind because I realized that the immune system and diseases are like two armies fighting on a battlefield. Immunology also fascinated me because it is a major hub where different technical skills and biological fields merge. Dr. Norvell's enthusiasm for science as she taught me the basics of the cellular and molecular concepts underlying immunity forced me to realize that I could use science to control the outcome of diseases.

I eventually decided to conduct graduate school level research at the University of Medicine and Dentistry of New Jersey. To further explore the intimate relationship between structure, function, and disease I pursued research under the auspices of Drs.

Nancy Connell and Patricia Fitzgerald-Bocarsly. In Dr. Connell's laboratory I assisted in the development of an early detection system in the event of a bioterrorist attack by infecting human peripheral blood cells and cell lines with BSL-3 select agents and performing microarrays for biomarker and signaling pathway identification. I eventually moved to Dr. Fitzgerald-Bocarsly's laboratory to gain experience with techniques central to immunological research. Here I learned the fundamentals of flow cytometry, ELISA, and fluorescence microscopy in studies investigating CD62L regulation in plasmacytoid dendritic cells by the matrix metalloprotease ADAM17 and IFN-α after herpes simplex virus infection. Overall, these experiences were invaluable and gave me the basic mind and skill set to pursue a career in basic immunology research. I also recognized that I needed to further my education and obtain a doctorate of philosophy degree so I could lead projects and combine my creative nature with a love for science.

My journey consequently progressed to the University of Virginia, founded by Thomas Jefferson and nestled in the foothills of the Blue Ridge Mountains in the picturesque town of Charlottesville. The research community at UVA inspired me because of its values for diligent work and excellence in learning. As I was taking graduate school classes there were many laboratories that peaked my interests, but the laboratory of Dr. Young S. Hahn seized my attention. Dr. Hahn's laboratory studies immune tolerance within the liver, with one side devoted to *in vitro* human hepatitis C virus (HCV) models and the other side employing *in vivo* murine models. The liver itself is a histologically beautiful organ as I remembered from the undergraduate course "Electron Microscopy" taught by Dr. Donald Lovett at The College of New Jersey. Here I learned the microstructural and ultrastructural details of the liver, and the images I captured myself are included in the introduction of this thesis. Further, immunity in the liver is extremely

different compared to any other organ because the hepatic microenvironment is tolerogenic. Tolerance allows diseases such as HCV to persist. Therefore, I set my goals at understanding how existing tolerogenic mechanisms work and to identify new cellular networks the liver employs to dampen immune responses.

I have had the privilege to lead two projects at the University of Virginia. In the first study, Dr. Hahn and I formed a collaboration with Drs. Antonin de Fougerolles, Tatiana Novobrantseva, and Anna Borodovsky of Alnylam Pharmaceuticals in Cambridge Massachusetts where we tested PD-L1 siRNA nanotechnology as a new immunotherapeutic strategy in bypassing the PD-1/PD-L1 immunoregulatory pathway. Working with Dr. Novobrantseva was a pleasure; she not only taught me drug testing protocols and guided the siRNA project, but also offered me excellent career advice and business connections when I visited Boston at a scientific conference. My second research project was discovered based on previous investigations conducted in Dr. Hahn's laboratory characterizing the dysfunction of antigen-specific $CD8^+$ T cells primed in the liver after viral infection. I sat home one night and came to Dr. Hahn's office with an idea: mix exhausted antiviral $CD8^+$ T cells with functionally competent T cells with the hypothesis that these liver-primed T cells had suppressive properties. The liver-primed $CD8^+$ T cells intriguingly did regulate responder T cell proliferation, and it took three years of research to uncover the mechanism of action. During this process of troubleshooting, Dr. Hahn instilled in me the value of patience. During most of my education and previous research I was used to success. However, experiments fail for one reason or another 9 out of 10 times; patience and contemplation of the experimental results are necessary to perfect a technique or further the mechanistic story.

The Hahn laboratory is also a sister laboratory to that of Dr. Thomas Braciale, with whom joint lab meetings and collaborations are a standard. Further, Dr. Braciale challenged me to think more critically with every idea, experiment, and meeting I presented to him. Matthew Hufford, Taeg Kim, and Jie Sun of the Braciale laboratory also assisted in experimental design. Both Drs. Hahn and Braciale were also helpful in meticulously editing my manuscripts for publication, and for that I thank them.

Microscopy and flow cytometry are crucial techniques in immunological research. I would like to thank Sun-Sang Sung for spending the time teaching me proper tissue fixation, immunohistochemistry, and confocal microscopy techniques. Core personnel of the Advanced Microscopy Facility, including Jan Redick and Stacey Guillot, trained and assisted me with imaging on multiple microscopes. Joanne Lannigan and Michael Solga of the University of Virginia Flow Cytometry Core Facility were vital for outlining and performing FACS-sorting and Amnis Imagestream^X experiments.

Outside of the laboratory I would like to thank numerous friends including but not limited to: Hilda Enriquez, Emily Fox, Amelia Hufford, Matthew Hufford, April Inyard, Brandon Kenwood, Isaac Nardi, Virginia Nguyen, Valerie Siclari, and Evan Taddeo. Whenever I was stressed about experiments, Isaac would say ‘let’s mostly plan a SCUBA diving/surfing trip’ to refresh. Virginia would probably just call me a ‘n00b.’ Hilda and April always opened up their homes for visits to New York City and Washington D.C, respectively. I would also like to thank the two most important people in my life, my mother and father, for whom this work is dedicated to. They were always there for me, provided and continue to provide excellent advice for my career and relationships with

people, and offered every kind of emotional and financial support a son could want. And for their unwavering devotion for my continued success, I love them.

On a recent visit back to The College of New Jersey to celebrate my sister, Leslie Dolina, graduating from nursing school, I reunited with Dr. Norvell, and she invited me to present my thesis work as part of her immunology class in the form of a visiting seminar speaker this upcoming fall. Hopefully as I look in the eyes of her undergraduate immunology students I can instill in them some of the scientific vigor ingrained in myself over the past years of my education. Research has taught me many valuable lessons and made it clear that my true passion in the sciences is investigating the immune system in response to disease. If the diseased state is understood at the structural and functional level, perhaps cures can be elucidated, to which I will dedicate the rest of my life.

Table of Contents

List of Figures and Tables

List of Abbreviations

7-AAD	7-actinomycin D	BMDC	bone marrow-derived dendritic cell
α	anti		
αR	α-rosette of glycogen	BrdU	5'-bromodeoxyuridine
βGal	β-galactosidase	BS	basal surface
βME	β-mercaptoethanol	C57BL/6	C57 black 6 (mouse)
ΔC_T	comparative threshold cycle	CAR	Coxsackie and adenovirus receptor
Ab	antibody		
Ad	adenovirus	C LN	celiac lymph node
Ad-LacZ	adenovirus-β-galactosidase	CD	cluster of differentiation
Ad-Ova	adenovirus-ovalbumin	cDNA	complementary DNA
AF	Alexa Fluor	Ce	centriole
ALT	alanine aminotransferase	CFSE	carboxyfluorescein succinimidyl ester
ANOVA	analysis of variance		
AP-1	activator protein 1	Cl-13	Clone-13
APC^1	allophycocyanin	Clod	clodronate
APC^2	antigen presenting cell	Co	collagen
Arm	Armstrong	Cr	crista
AS	apical surface	CTL	cytotoxic T lymphocyte
B	bile ductule	CTLA-4	cytotoxic T lymphocyte antigen 4
Bat3	HLA-B-associated transcript 3		
		Ctrl	control
BC	bile canaliculus	CV	central vein
Bcl	B cell lymphoma	Cy	cyanine

D	day
DAMP	danger associated molecular pattern
DAPI	4',6-diamidino-2 phenylindole
DC	dendritic cell
DMEM	Dulbecco's Modified Eagle medium
DNA	deoxyribonucleic acid
DT	diphtheria toxin
DTR	diphtheria toxin receptor
dTdT	deoxythymidine
eF	eBioscience fluorochrome
eGFP	enhanced green fluorescence protein
EI	endocytotic invagination
ELISA	enzyme-linked immunosorbent assay
En	endothelial cell
EtOH	ethanol
Eu	euchromatin
F	fenestra
FACS	fluorescence-activated cell sorting
Fas	apoptosis stimulating fragment
FasL	apoptosis stimulating fragment ligand
Fc	fragment crystallizable
FITC	fluorescein isothiocyanate
FMO	fluorescence minus one
FoxP3	forkhead box P3
FSC	forward scatter
G	Golgi apparatus
Gal-9	galectin-9
GC	Glisson’s capsule
GITR	glucocorticoid-induced TNFR family related
GM-CSF	granulocyte macrophage colony-stimulating factor
GrB	granzyme B
H	hepatocyte
H & E	hematoxylin and eosin
HA	hepatic artery
HBV	hepatitis B virus
Hc	heterochromatin
HCC	hepatocellular carcinoma
HCV	hepatitis C virus

HEPES	4-(2-hydroxyethyl)-1 piperazineethanesulfonic acid
HIV	human immunodeficiency virus
HL	hepatic lobule
HMGB-1	high-mobility group box 1
HPRT	hypoxanthine phosphoribosyltransferase
HRP	horseradish peroxidase
HSPG	heparin sulfate proteoglycan
HSV	herpes simplex virus
HV	hepatic vein
IFN	interferon
IgG	immunoglobulin G
Ig LN	inguinal lymph node
IL	interleukin
IMDM	Iscove's Modified Dulbecco's medium
IP	intraperitoneal
ITIM	immunoreceptor tyrosine-based inhibitory motif
iT_{reg}	inducible T regulatory
ITSM	immunoreceptor tyrosine-based switch motif
IU	infectious units
IV	intravenous
JAK	Janus kinase
JR	junctional region
KC	Kupffer cell
L	lipid droplet
Lag-3	lymphocyte activation gene 3
Lck	lymphocyte-specific protein tyrosine kinase
LCMV	lymphocytic choriomeningitis virus
Li	lipocyte
LNP	lipidoid nanoparticle
LPS	lipopolysaccharide
LS	lateral surface
LV	lymphatic vessel
LSEC	liver sinusoidal endothelial cell
LSM	laser scanning microscope
Luc	luciferase
Ly	lymphocyte antigen

M	mitochondrion	pAb	polyclonal antibody
Mø	macrophage	PALT	portal tract-associated lymphoid tissue
mAb	monoclonal antibody		
MC	mesothelial cell	PAMP	pathogen associated molecular pattern
MCMV	mouse cytomegalovirus		
MCMV-Ova	MCMV-ovalbumin	panCK	pancytokeratin
MFI	mean fluorescence intensity	PBMC	peripheral blood mononuclear cell
MG	matrix granule		
MHC	major histocompatibility complex	PBS	phosphate buffered saline
		PCR	polymerase chain reaction
mRNA	messenger RNA	PD-1	programmed death 1
Mv	microvillus	PD-L1	programmed death ligand 1
N	nucleus	PD-L2	programmed death ligand 2
NF-κB	nuclear factor kappa-light-chain-enhancer of activated B cells	PE	phycoerythrin
		PEG-DMG	monomethoxy (polyethyleneglycol)-1,2-dimyristoylglycerol
NFAT	nuclear factor of activated T cells		
		PEI	polyethylenimine
NK	natural killer	PerCP	peridinin chlorophyll-A protein
NKT	natural killer T		
NP	nuclear pore	PKB	protein kinase B
Nu	nucleolus	PKR	protein kinase R
OCT	optimal cutting temperature	PLP	periodate-lysine-paraformaldehyde
Ova	ovalbumin		

PMA	phorbol 12-myristate 13-acetate	SDS	sodium dodecyl sulfate
PRR	pattern recognition receptor	SER	smooth endoplasmic reticulum
Ps	pseudopod	SG	secretory granule
PT	portal triad	SH	Src homology
PV	portal vein	SHP	small heterodimer partner
r	recombinant	siRNA	short interfering RNA
R	receptor	SL	secondary lysosome
RACE	rapid amplification of cDNA ends	SOCS	suppressor of cytokine signaling
RAGE	receptor for advanced glycation end products	Src	sarcoma (tyrosine kinase)
		SSC	side scatter
RBC	red blood cell	STAT	signal transducer and activator of transcription
RER	rough endoplasmic reticulum		
		TCR	T cell receptor
Ret	reticulocyte	T_{eff}	T effector
RNA	ribonucleic acid	TEM	transmission electron microscope
RNAi	RNA interference		
RPMI 1640	Roswell Park Memorial Institute 1640 medium	Tet	tetramer
		TGF	transforming growth factor
rRNA	ribosomal RNA	T_{fh}	T follicular helper
S	sinusoid	T_h1	T helper type 1
SC	subcutaneous	T_h2	T helper type 2
SD	space of Disse	T_h3	T helper type 3

Thy1	thymocyte differentiation antigen 1	T_r1	T regulatory type 1
		T_{reg}	T regulatory
Tim-3	T cell immunoglobulin and mucin 3	TV	transendothelial vesicle
		TYK	tyrosine kinase
TJ	tight junction	Vert-X	IL-10 transcriptional reporter (mouse)
TLR	toll-like receptor		
TNF	tumor necrosis factor	VLDL	very low-density lipoprotein

CHAPTER 1

Liver Architecture

Introduction to the Liver as an Organ

The liver is embryologically derived from the digestive tract, and the connection with the small intestine is maintained in adult mammals through the bile duct[2]. Functionally, it is a large mass of glandular tissue having both an exocrine function (secretion of bile) and endocrine function (synthesis of a variety of substances that are eventually released into the bloodstream). In order for the liver to properly perform these two critical tasks, the organ is strategically located. A steady supply of venous blood from the intestinal tract via the portal vein and arterial blood from the hepatic artery is provided. As the liver rests between the intestinal tract and bulk circulation, it receives most of the nutrients absorbed from the gut via the portal vein. Nutrients are taken up by hepatocytes, metabolized, and returned to the blood for storage or the use of other tissues in the body[3]. Further, the liver is known to synthesize lipids, many different kinds of proteins, and urea. Products that are released back into the bloodstream exit the liver through the hepatic vein, which eventually connects to the inferior vena cava of the heart[2].

Hepatic Parenchymal Cellular Organization

Derived from epithelial cells, hepatocytes (H) are arranged in a series of plates between portal triads (PT) and central veins (CV) in a hepatic lobule (HL). Each row of hepatocytes is usually one cell thick, separated by collinear sinusoids (S). Sinusoids form a network of low-resistance blood vessels perfusing the hepatocytes. A

configuration such as this maximizes the exchange of metabolites and other substances between hepatocytes and blood plasma over a large surface area (**Fig. 1.1**)[4].

Hepatocytes are cuboidal and defined by three distinct surfaces. The basal surface (BS) forms the boundary of the hepatocyte that faces sinusoids and the perisinusoidal space of Disse. The lateral surface (LS) delineates the margin of the hepatocyte that forms junctional contacts with other hepatocytes. Lastly, the apical surface (AS) lines a small lumen known as the bile canaliculus, which exists between adjacent hepatocytes (**Fig. 1.2**)[5]. The lateral surface of hepatocytes keeps the plates of hepatocytes intact as this cell surface contains many intercellular junctional complexes tethering hepatocytes. It is known that gap junctions are present along the lateral surface[5]. The junctions along the lateral surface of hepatocytes are not identified here with absolute certainty, but it is likely that this surface serves to attach and to provide communication between neighboring hepatocytes.

Hepatic Nuclei

More than half of hepatocytes contain twice or more (polyploid) the normal content of chromatin and are often binucleate. The nuclei (N) of hepatocytes are typically large compared to other non-parenchymal cells and contain numerous nucleoli (Nu) amongst scattered clusters of chromatin (**Fig. 1.3**). The large number of nucleoli suggests there is an abundance of rRNA production and ribosomal assembly. As the liver synthesizes huge amounts of protein including albumin, prothrombin, and fibrinogen and transports these proteins to the blood plasma, many ribosomes and DNA templates are needed[4].

Hepatic Cell Cytoplasm

Hepatocyte cell cytoplasm has granular appearance due to the abundance of mitochondria (M) (**Fig. 1.2**). Mitochondria are composed of two membranes (inner and outer membranes) where the inner membrane forms folds called cristae (Cr). Matrix granules (MG) also exist inside the mitochondria (**Fig. 1.4**). In order to support such a huge protein synthetic output, energy is needed. Therefore, the cytoplasm of hepatocytes contains a sizeable quantity of mitochondria.

Small particles of medium density are also seen residing in the free cytoplasm of hepatocytes, which are glycogen particles existing as α-rosettes (αR). The α-rosettes of glycogen are closely associated with both the rough and smooth endoplasmic reticula (RER and SER, respectively) (**Fig. 1.4** and **Fig. 1.5**). Carbohydrates are stored in α-rosettes, and hepatocytes are responsible for regulating blood sugar levels. Therefore, this specific configuration within the cytoplasm is important for the export of glucose to the blood stream. As glycogen is broken down into glucose-6-phosphate, this product is converted to glucose within the lumen of the endoplasmic reticulum[6].

Numerous lipid droplets (L) are dispersed in hepatocyte cytoplasm. These droplets lack a lipid bilayer but are rather surrounded by a thin monolayer of phospholipids. Other forms of lipid storage are present as very low-density lipoprotein (VLDL) particles. Contrasting lipid droplets, VLDL particles contain lipids compacted together with protein. Many VLDL particles are observed as membrane-enclosed vesicles often near the periphery of hepatocytes (**Fig. 1.5**). Nevertheless, there is an extensive trend for the storage of lipids in hepatocyte cytoplasm because the liver is responsible for regulating lipid levels in circulation. These lipids are converted to lipoprotein particles and coated

with cholesterols, phospholipids, and proteins in the rough and smooth endoplasmic reticula, eventually forming exocytotic vesicles poised for transport into the blood[3,7].

Hepatic Membrane Systems

Hepatocytes contain a large amount of endoplasmic reticulum. Both rough and smooth varieties are present. The smooth endoplasmic reticulum is randomly dispersed throughout the cytoplasm (**Fig. 1.3** and **Fig. 1.5**). Active protein synthesis in hepatocytes is also supported by the presence of extensive rough endoplasmic reticulum. The rough endoplasmic reticulum is concentrated in areas that are rich in mitochondria (**Fig. 1.2**). In addition, the rough endoplasmic reticulum enfolds the mitochondria exclusively in hepatocytes thereby forming close associations (**Fig. 1.4**)[8]. This association may be important in the synthesis of smooth endoplasmic reticulum and cytochromes. For example, the enzyme Δ-aminolevulinic acid is made in the rough endoplasmic reticulum and transported to the mitochondria. This results in the production of heme inside mitochondria. Heme is transported back to the rough endoplasmic reticulum for the production of microsomal heme protein P450[8]. A close association between the mitochondria and rough endoplasmic reticulum is necessary to maintain this biochemical cycle.

Hepatic Vasculature

The liver is composed of lobes (whose number varies among species), and the functional subunit of the liver is conceptually known as the hepatic lobule. Lobules are arranged in a honeycomb configuration throughout the liver's microstructure (**Fig. 1.1**). Blood enters the hexagonally-shaped lobule at the corners through portal triads (**Fig. 1.6**) and percolates between plates of hepatocytes in sinusoids draining inward towards

a central vein (**Fig. 1.7**). Centrals veins converge into the larger hepatic vein (HV) (**Fig. 1.8**), where the blood exits the liver[4]. Central veins are histologically distinguishable from hepatic veins by their luminal continuation with sinusoids and lack of a squamous endothelial layer. Portal triads are groupings of three main structures: the portal vein (PV), hepatic artery (HA), and bile ductule (B). Lymphatic vessels (LV) are often associated with portal triads as well and guide lymph to the celiac lymph node embedded in the pancreas in mice. The hepatic acinus is a grape-like structure intermediate between lobes and lobules but is difficult to identify via microscopy. Based on the distance lobules lie within hepatic acini (divided in zones 1, 2, and 3) from the main portal tract, they receive qualitatively distinct blood supplies. Zone 1 lies closest to the tract receiving the most oxygenated blood[9].

Two cell types line sinusoids: squamous endothelial cells (En; also known as liver sinusoidal endothelial cells, LSEC) and Kupffer cells (KC). The endothelial lining separates two spaces, the lumen of the sinusoid and the perisinusoidal space of Disse (SD). The space of Disse marks the area between the basal layer of hepatocytes and the endothelial lining. Between endothelial cells, large transcellular gaps called fenestrae (F) are present making the lumen of the sinusoid continuous with the space of Disse (**Fig. 1.9**). The fenestrae in the endothelial lining of *Mus musculus* lack a diaphragm that is present in other species of mammals[4].

Squamous endothelial cells are identified by the presence of many transendothelial (or transplasmalemmal) vesicles (TV) inside an electron-lucent cytoplasm and a relatively small nucleus. The transendothelial vesicles form associations with both the adluminal and abluminal surfaces of the endothelial lining[3]. Further, endothelial cells are

connected together via tight junctions (TJ). Transendothelial vesicles and fenestrae allow for the transport of substances into the perisinusoidal space of Disse across the squamous endothelial lining (**Fig. 1.10** and **Fig. 1.11**)[4].

The perisinusoidal space of Disse is defined as being the area between the basal surface of hepatocytes and the abluminal surface of the endothelial lining. Many parenchymal cell microvilli (Mv) are seen projecting into this region. The microvilli form either a single shaft or branch. The basal surface of hepatocytes also has many endocytotic invaginations (EI) (**Fig. 1.11**). Microvilli serve two main functions: movement of blood plasma in the perisinusoidal space of Disse and increasing the surface area of hepatocytes in this region[2]. This may improve the capability of hepatocytes to transfer matter across this surface. Transport of materials into the parenchymal cells may occur by simple diffusion, protein carriers, channel proteins, and endocytotic vesicle formation. Therefore, these structural elements surrounding the periphery of sinusoids maximize the transport of substances between blood plasma and hepatocytes while allowing erythrocytes and other blood cells to remain sequestered in bulk circulation. Despite physical separation, hepatic microvilli are able to project through fenestrae into the sinusoidal lumen allowing for direct cell-cell contact between hepatocytes and various leukocytes, such as T lymphocytes[10]. Endothelial cells and Kupffer cells are considered major antigen presenting cells in the liver, but hepatocytes may also prime immune responses directly within the liver microenvironment.

Biliary System

Harmful substances are also received and degraded by the liver. Toxic substances are degraded or detoxified by oxidation, hydroxylation, or conjugation. The end products are

eventually expelled into the bile. The bile is a composite material that is excreted into duodenum of the intestinal tract. Bile also manages the emulsification of fats into smaller lipid droplets in the intestinal tract. Therefore, bile is multifaceted and serves digestion and the removal of toxic substances from the body[3].

Bile canaliculi (BC) are small grooves centrally located between adjacent hepatocytes. Numerous microvilli originate from the apical surface of neighboring hepatocytes and protrude into each bile canaliculus facilitating the movement of bile (**Fig. 1.2** and **Fig. 1.5**). This biliary space is separated from other intercellular spaces via flanking tight junctions (TJ). Tight junctions near the bile canaliculi prevent the escape of their contents into the adjacent intercellular space[3]. Other types of junctions between hepatocytes are observed proximal to bile canaliculi along the lateral surfaces (**Fig. 1.5**). Bile canaliculi form a tree-like structure and drain into collecting ducts called the canals of Hering, which further converge into bile ductules. Bile ducts are easily distinguished from other vessels in the liver as they are lined with columnar or cuboidal epithelium (**Fig. 1.6**).

Hepatic Connective Tissue

The liver is encapsulated by a layer of collagenous tissue called Glisson's capsule (GC), surrounded by peritoneal mesothelial cells (MC) (**Fig. 1.12**). The majority of the connective tissue in the liver exists as collagen (Co) within the portal triads (**Fig. 1.13**), but a very fine network of reticulin fibers supports the hepatocytes and liver sinusoidal endothelial cells. In addition, the reticulin network is continuous with collagen found in portal triads and Glisson's capsule[9]. Reticulin stains are often used to diagnose

hepatocyte destruction and regrowth as each hepatocyte is separately surrounded by a cage-like meshwork of reticulin[11].

Kupffer Cells

Kupffer cells are distinguished histologically by the presence of numerous cellular processes. These cells inhabit the lumens of sinusoids, space of Disse, or can form the luminal boundary (**Fig. 1.9**). Kupffer cells are often observed harboring different forms and stages of ingested material derived from cellular debris, viral particles, clot complexes, damaged erythrocytes, immune complexes, and bacteria. Pseudopods (Ps) that project outward from Kupffer cells form junctional regions (JR) with the endothelial lining of the sinusoid and hepatocytes. Kupffer cell cytoplasm contains a large amount of rough endoplasmic reticulum, mitochondria, secondary lysosomes (SL), and secretory granules (SG). Their nuclei are larger than that of endothelial cells and have copious amounts of peripheral heterochromatin (Hc) (**Fig. 1.10**).

Lipocytes

Lipocytes (Li; also known as fat-storing cells, cells of Ito, or stellate cells) reside within the perisinusoidal space of Disse and are much smaller than hepatocytes. Their defining characteristic is an abundance of lipid droplets containing vitamin A. Although hepatocytes store lipid as well, the lipid droplet content of lipocytes constitutes the majority of their cytoplasm. Lipocytes also contain a dilated rough endoplasmic reticulum, numerous Golgi (G), and vesicular bodies (**Fig. 1.14**). The dilated rough endoplasmic reticulum that is observed in this cell type directly correlates with protein production. Concordantly, it is known that this cell type secretes a large amount of extracellular matrices during the development of hepatic cirrhosis and fibrosis. Lipocytes

are also stem cells localized in the liver that give rise to myofibroblastic cells. Bundles of collagenous fibrils may sometimes be observed within the space of Disse serving to maintain overall integrity of liver tissue[2].

Figure 1.1

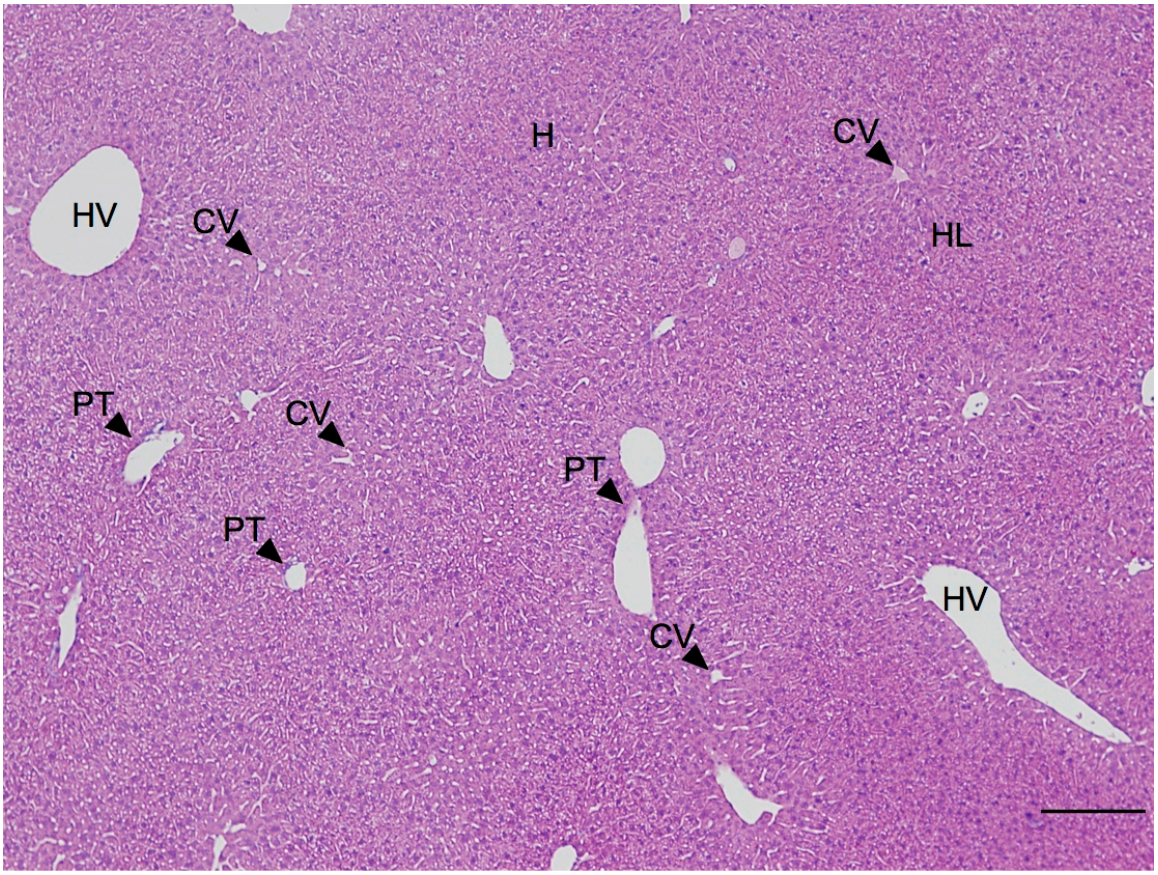

Figure 1.1 Organization of the major liver microstructures is depicted. Hepatocytes (H) are arranged in a series of plates situated between two regions: portal triads (PT) and central veins (CV). Hepatic veins (HV) are also indicated. The functional subunit of the liver is the hexagonal shaped hepatic lobule (HL) through which blood flows to a common central vein. Each lobule is associated with only one central vein. Scale bar, 200 μm.

Figure 1.2

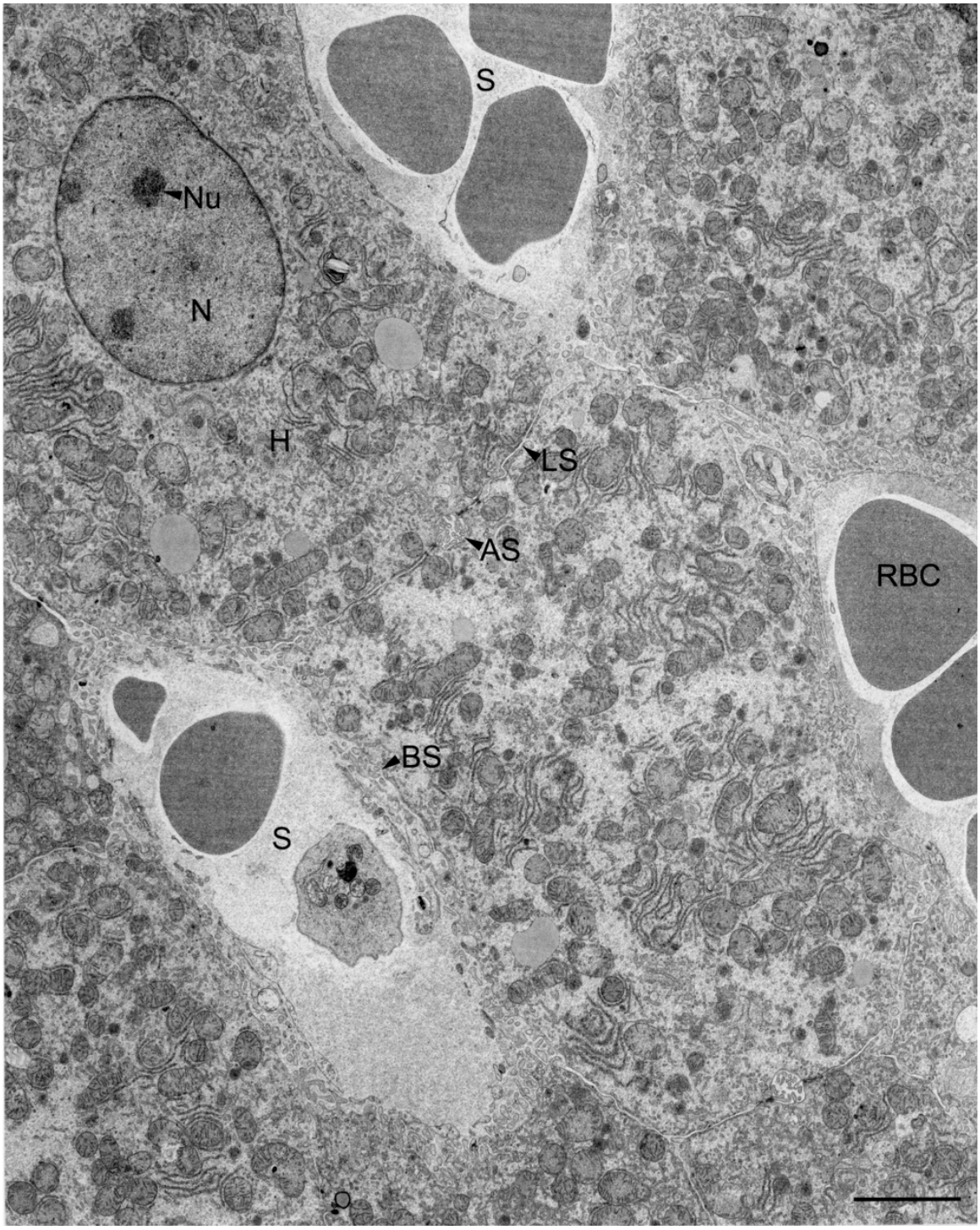

Figure 1.2 Liver parenchymal cells are arranged in a series of plates. Hepatocytes (H) situated between collinear sinusoids (S) containing red blood cells (RBC). The schematic section of a cuboidal hepatocyte illustrates three types of surfaces: basal surfaces (BS) face sinusoids, lateral surfaces (LS) form connections between hepatocytes, and apical surfaces (AS) line a small lumen between neighboring liver cells. Scale bar, 3 μm.

Figure 1.3

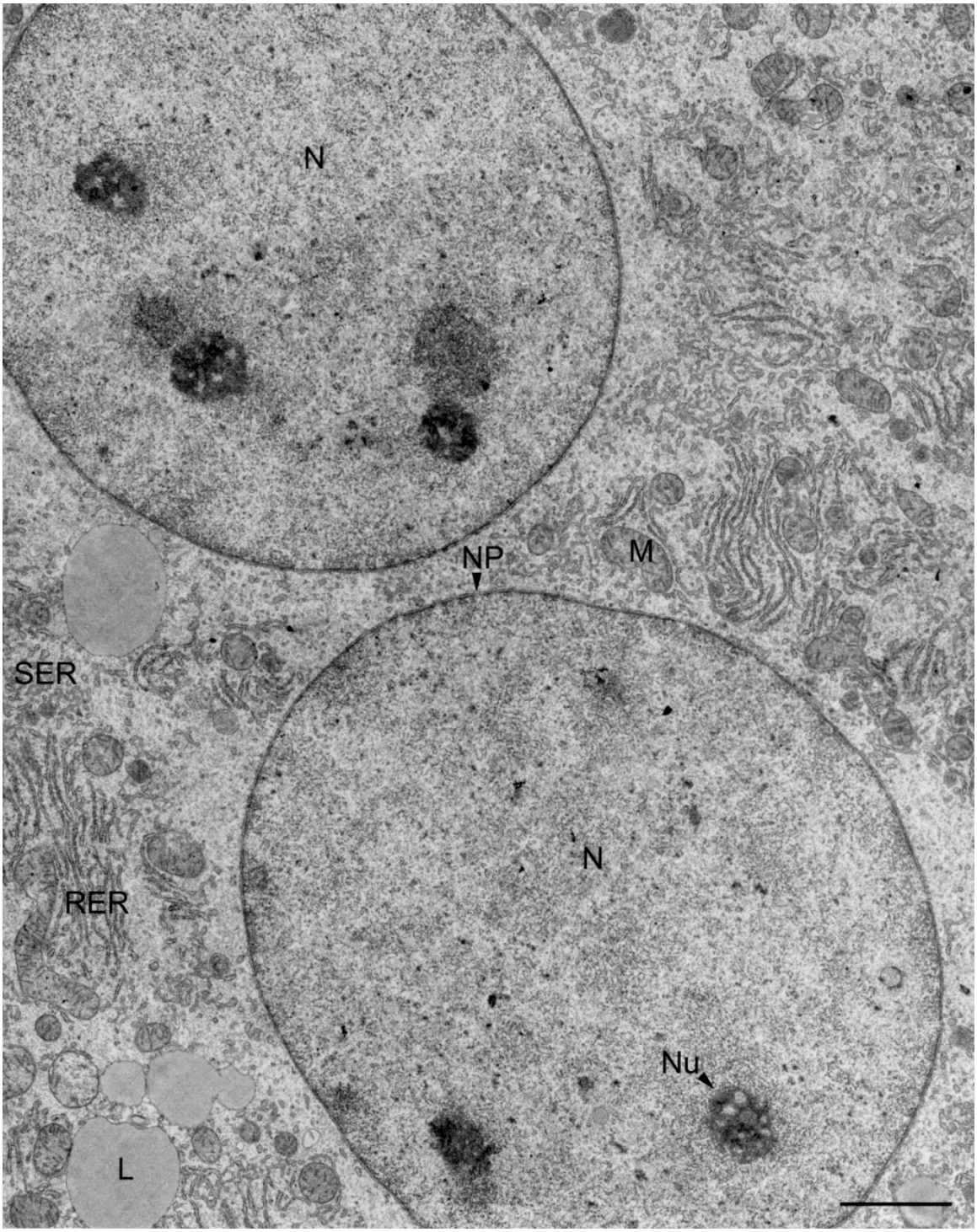

Figure 1.3 Hepatocytes are commonly binucleate. The nuclei (N) are approximately the same size and contain many nucleoli (Nu). Small pores called nuclear pores (NP) exist along the surface of each nucleus. The cytoplasm of a typical hepatocyte contains an abundance of lipid droplets (L), rough endoplasmic reticulum (RER), smooth endoplasmic reticulum (SER), and mitochondria (M). Scale bar, 2 μm.

Figure 1.4

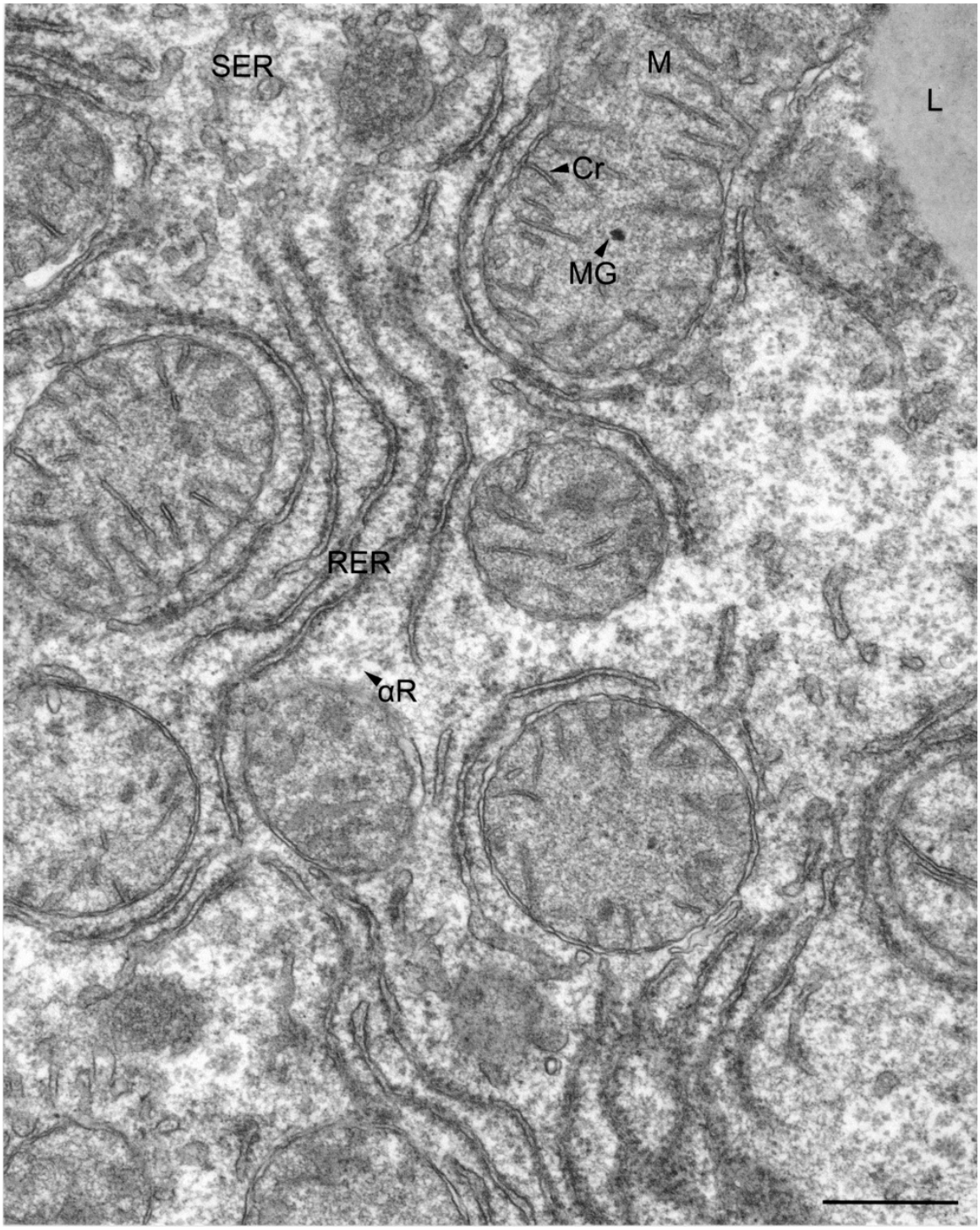

Figure 1.4 The cytoplasm of hepatocytes contains areas plentiful in mitochondria and rough endoplasmic reticulum. Close association between the mitochondria (M) and the rough endoplasmic reticulum (RER) in representative hepatocyte cytoplasm is shown. Cristae (Cr) and matrix granules (MG) typify the mitochondria. Smooth endoplasmic reticulum (SER), lipid droplets (L), and α-rosettes of glycogen (αR) are also included within hepatocyte cytoplasm. Scale bar, 0.5 μm.

Figure 1.5

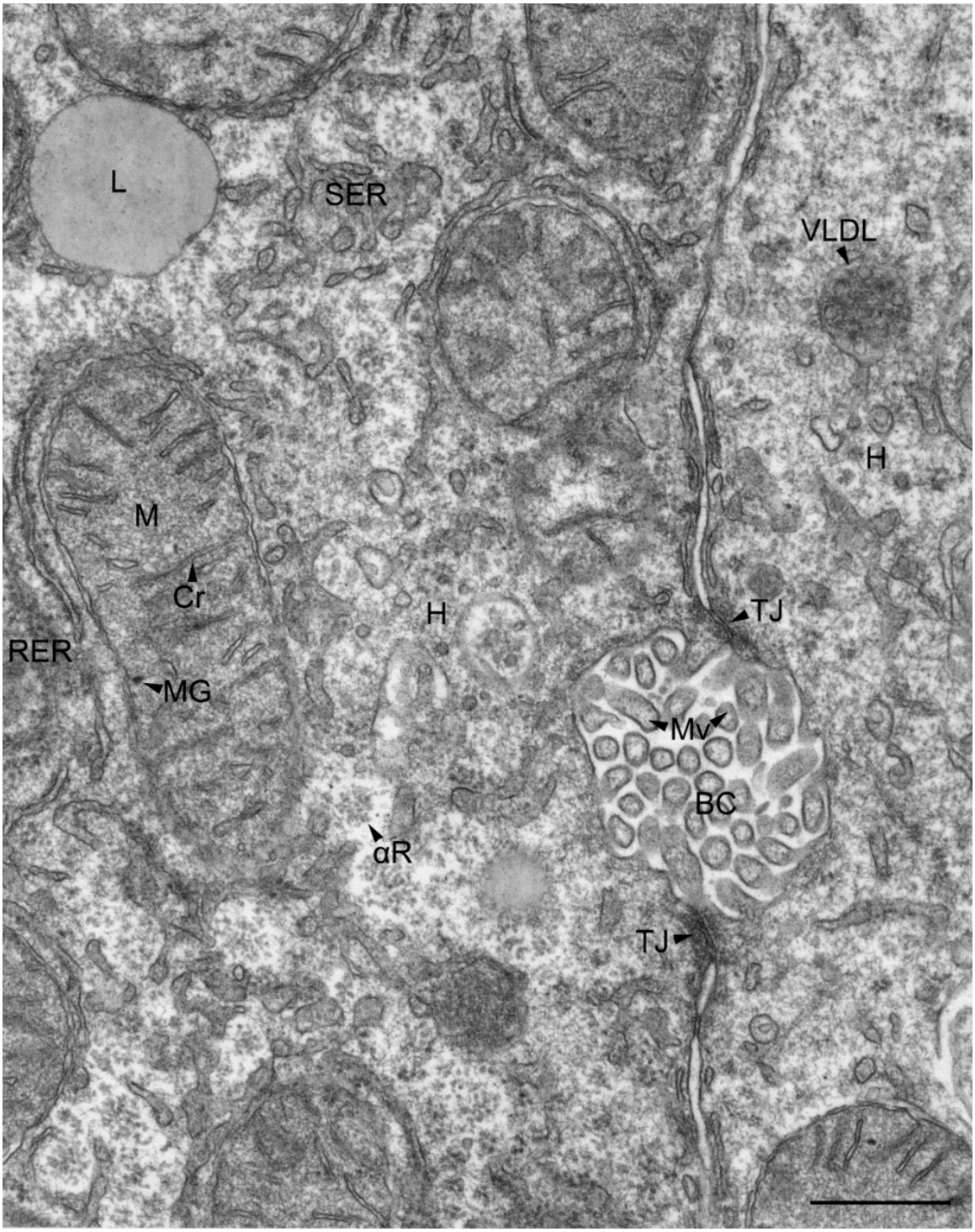

Figure 1.5 Apical and lateral surfaces of the hepatocyte are characterized by junctional complexes and the bile canaliculus. The bile canaliculus (BC) is positioned between adjacent hepatocytes (H). Bile canaliculi contain several microvilli (Mv) originating from parenchymal cells and are sealed by tight junctions (TJ). Rough endoplasmic reticulum (RER), smooth endoplasmic reticulum (SER), lipid droplets (L), α-rosettes of glycogen (αR), vesicles containing very low-density lipoproteins (VLDL), and mitochondria (M) are present in the nearby cytoplasm of typical hepatocytes. Mitochondria are characterized by inner membrane folds known as cristae (Cr) and matrix granules (MG). Scale bar, 0.5 μm.

Figure 1.6

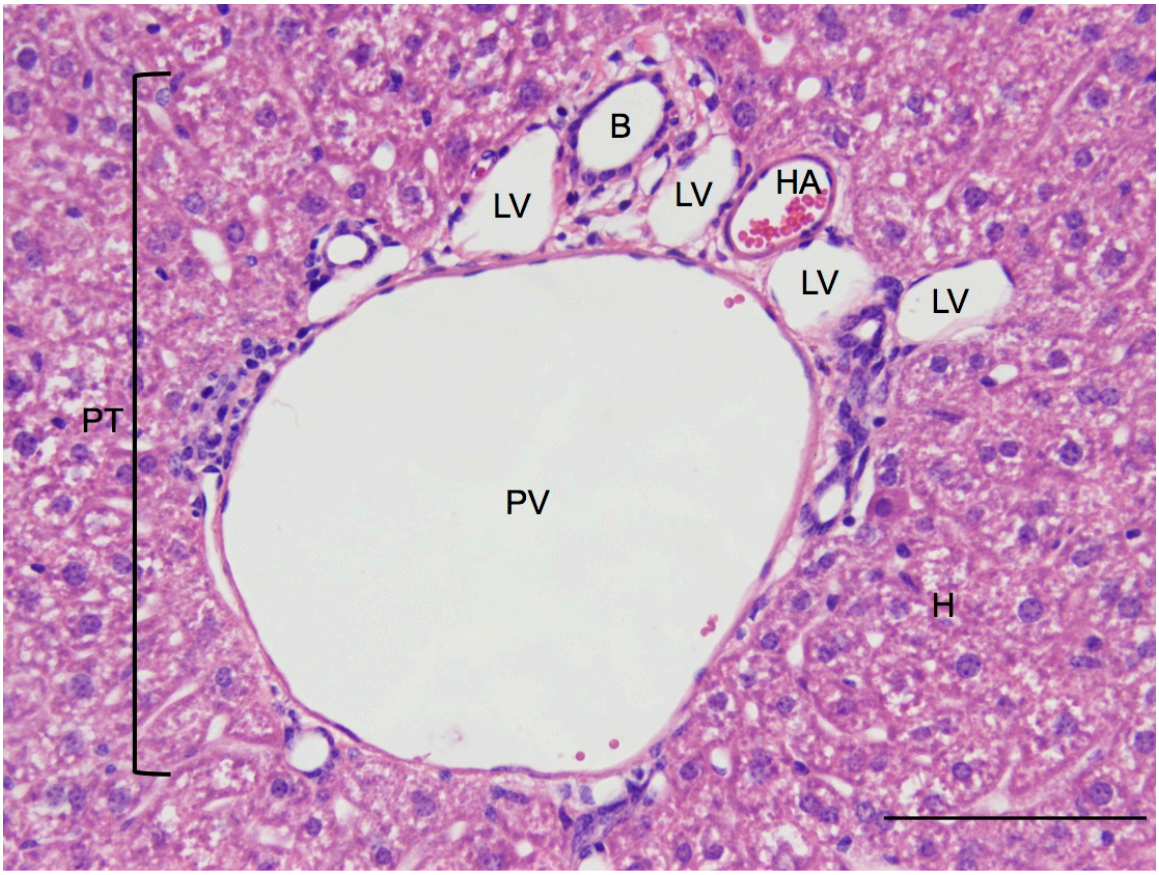

Figure 1.6 Portal triads lie at the corners of hepatic lobules. Hepatocytes (H) surround the portal triad (PT). The portal triad is composed of three structures: the portal vein (PV), hepatic artery (HA), and bile ductules (B). Lymphatic vessels (LV) are often associated with the portal triad. Scale bar, 100 μm.

Figure 1.7

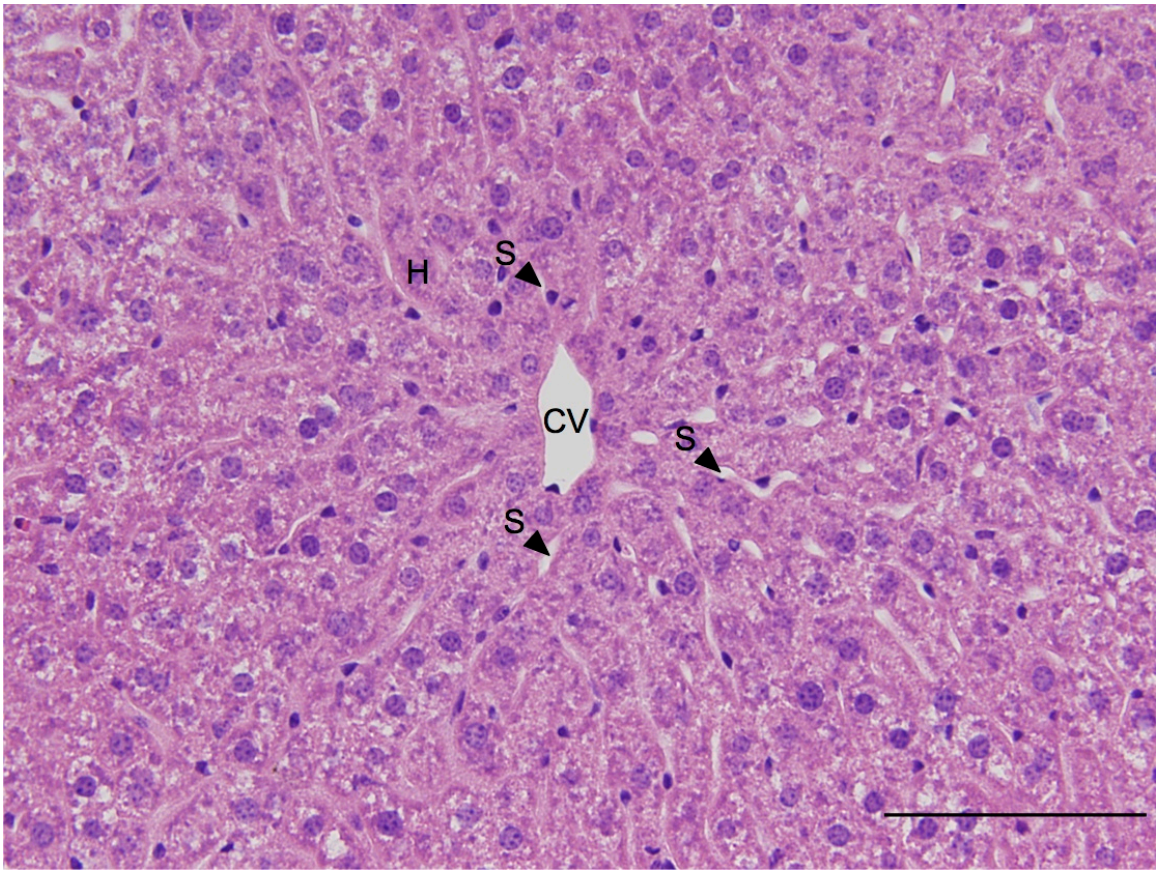

Figure 1.7 Central veins are located at the center of a hepatic lobule. A central vein (CV) is shown draining surrounding sinusoids (S). Hepatocytes (H) exist as one cell thick plates between neighboring sinusoids. Scale bar, 100 μm.

Figure 1.8

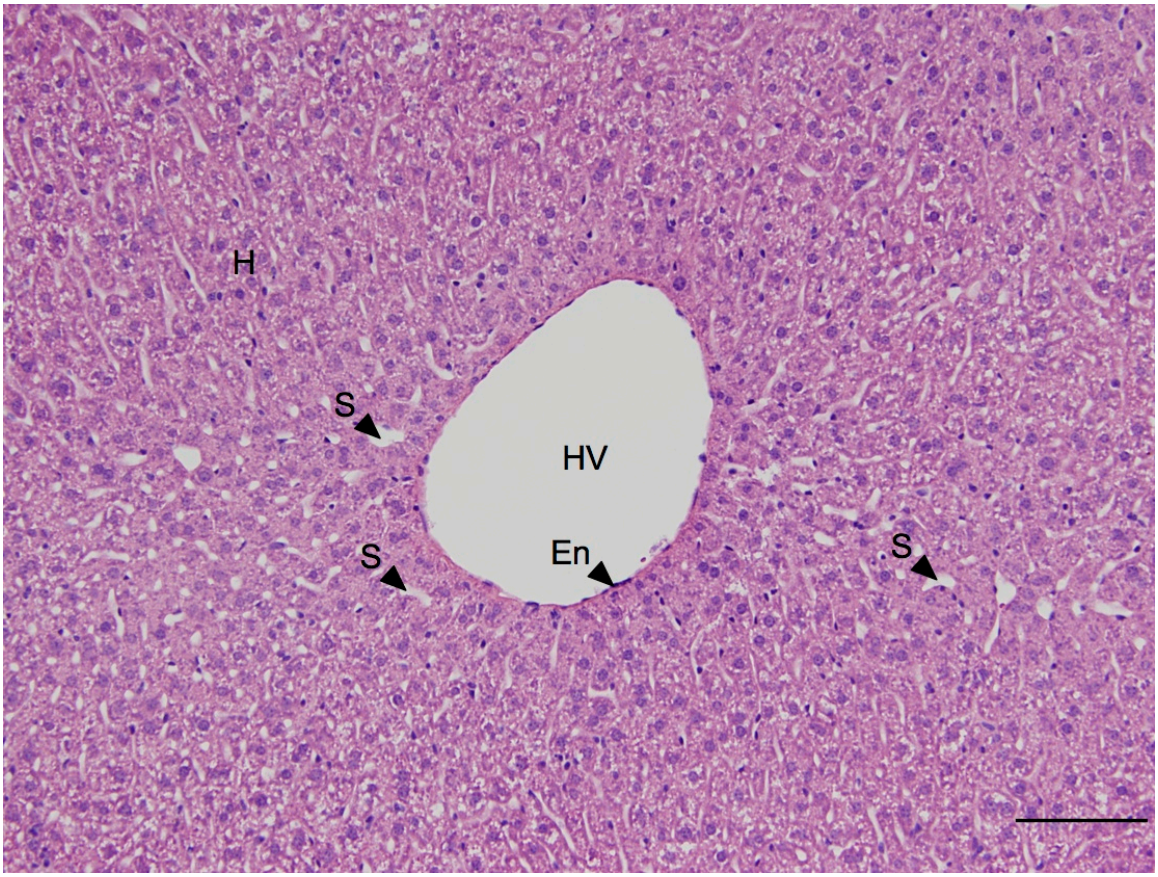

Figure 1.8 Hepatic veins drain central veins. The lumens of hepatic veins (HV) are enclosed by an endothelial (En) lining, which along with their larger size differentiates them from central veins. Hepatocytes (H) and sinusoids (S) are depicted surrounding the hepatic vein, but no direct drainage exists between sinusoids and hepatic veins. Scale bar, 100 μm.

Figure 1.9

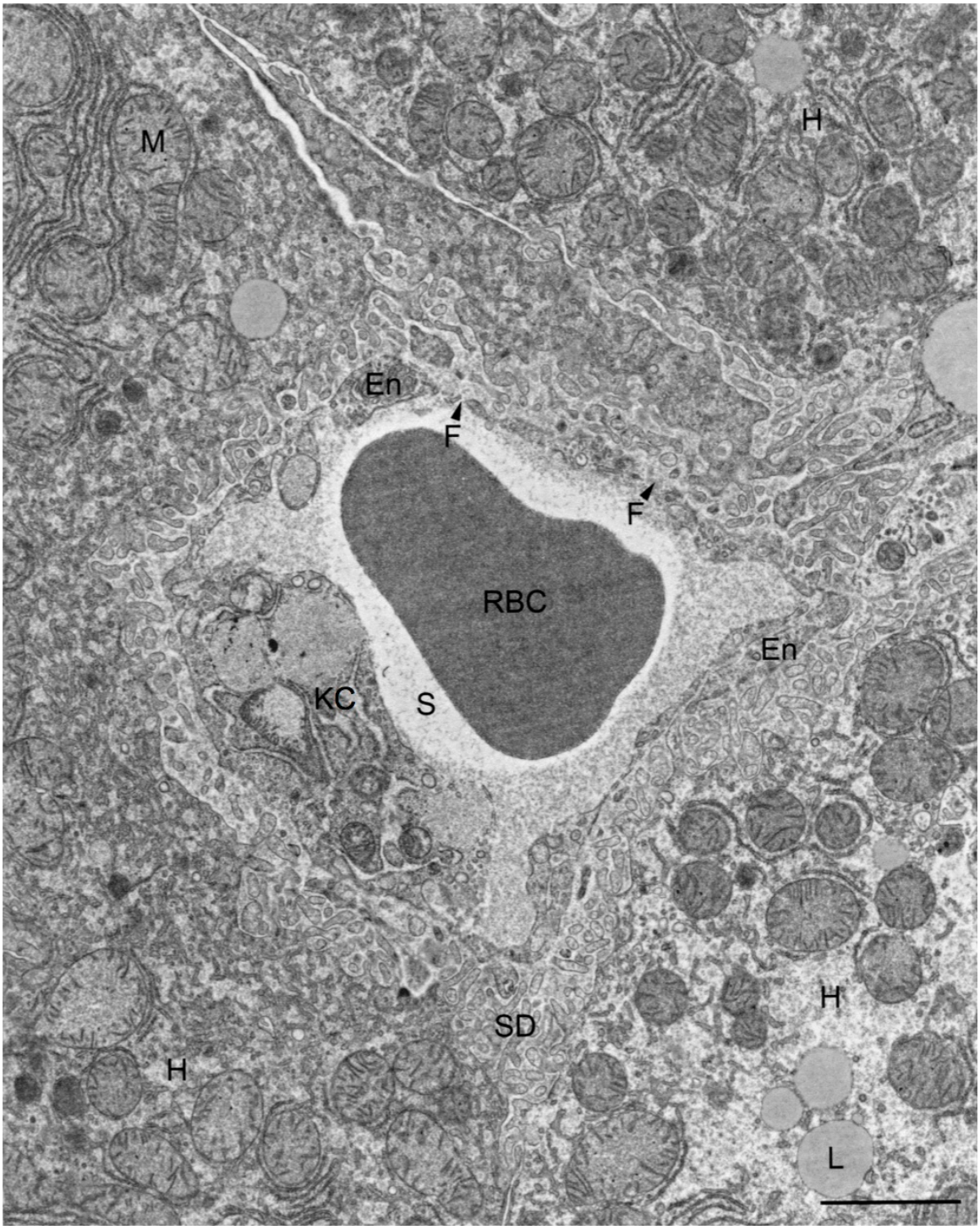

Figure 1.9 Sinusoids form a network of low-resistance blood vessels. A cross section of a hepatic sinusoid (S) containing a red blood cell (RBC) is represented. Sinusoids are surrounded by hepatocytes (H) possessing a large quantity of mitochondria (M) and lipid droplets (L). The lumen of the hepatic sinusoid is lined by a layer of squamous endothelial cells (En). The area between the endothelial cells and hepatocytes is defined as the perisinusoidal space of Disse (SD). The endothelial layer contains fenestrae (F) making the lumen of the sinusoid continuous with the space of Disse. Sinusoids also frequently possess Kupffer cells (KC). Scale bar, 2 μm.

Figure 1.10

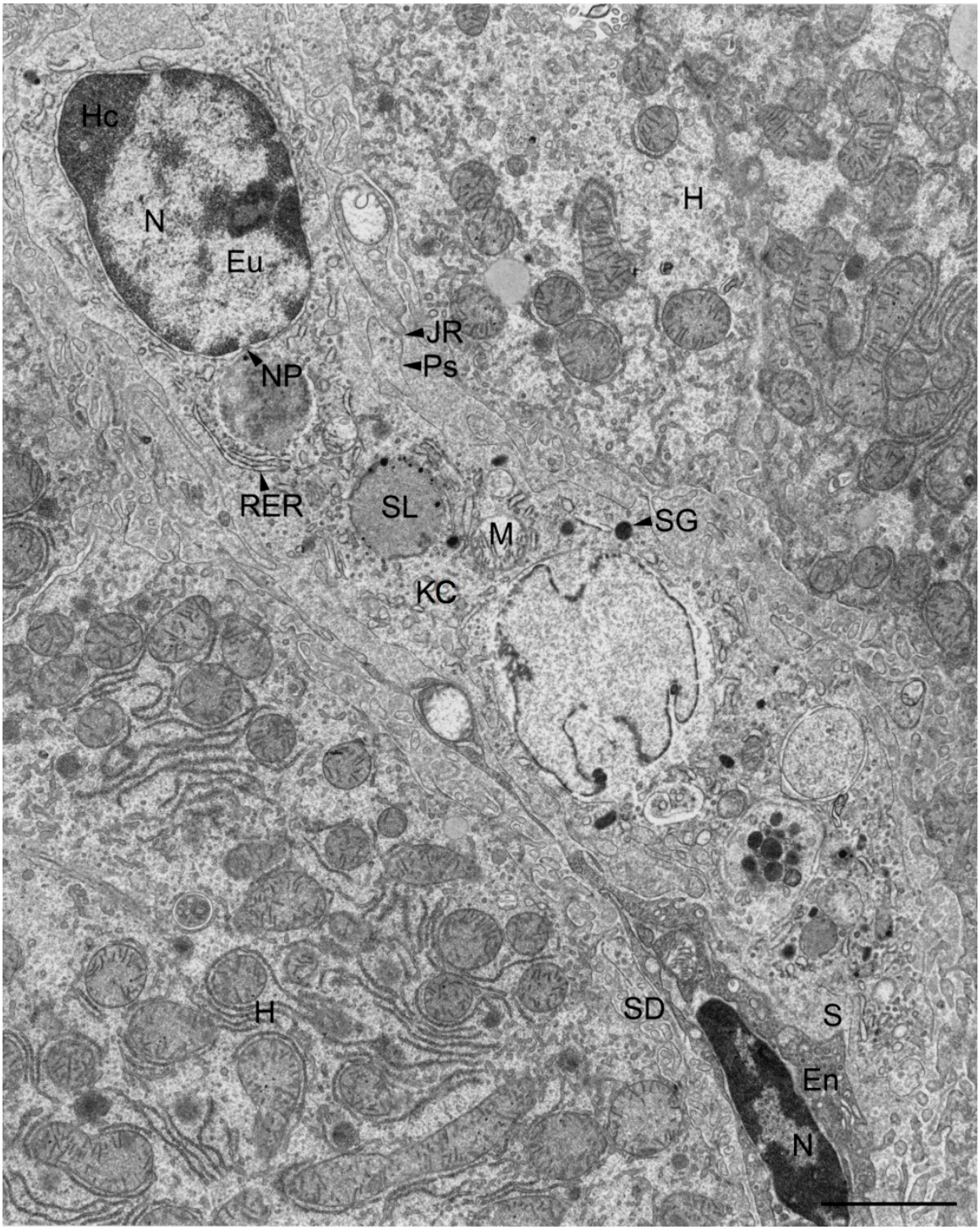

Figure 1.10 Kupffer cells are histologically defined by the presence of pseudopods and internalized cellular debris. A sinusoidal lumen (S) containing a Kupffer cell (KC) surrounded by an endothelial layer (En), perisinusoidal space of Disse (SD), and two hepatocytes (H) is depicted. Phagocytic Kupffer cells are characterized by a nucleus (N) containing many nuclear pores (NP), peripheral heterochromatin (Hc), and central euchromatin (Eu). The nuclei of endothelial cells are typically smaller compared to that of Kupffer cells. Other features common to Kupffer cells include the following: an abundance of secondary lysosomes (SL), mitochondria (M), secretory granules (SG), and extensive rough endoplasmic reticulum (RER). Kupffer cells also form pseudopods (Ps) that sometimes develop junctional regions (JR) with the endothelial layer. Scale bar, 2 μm.

Figure 1.11

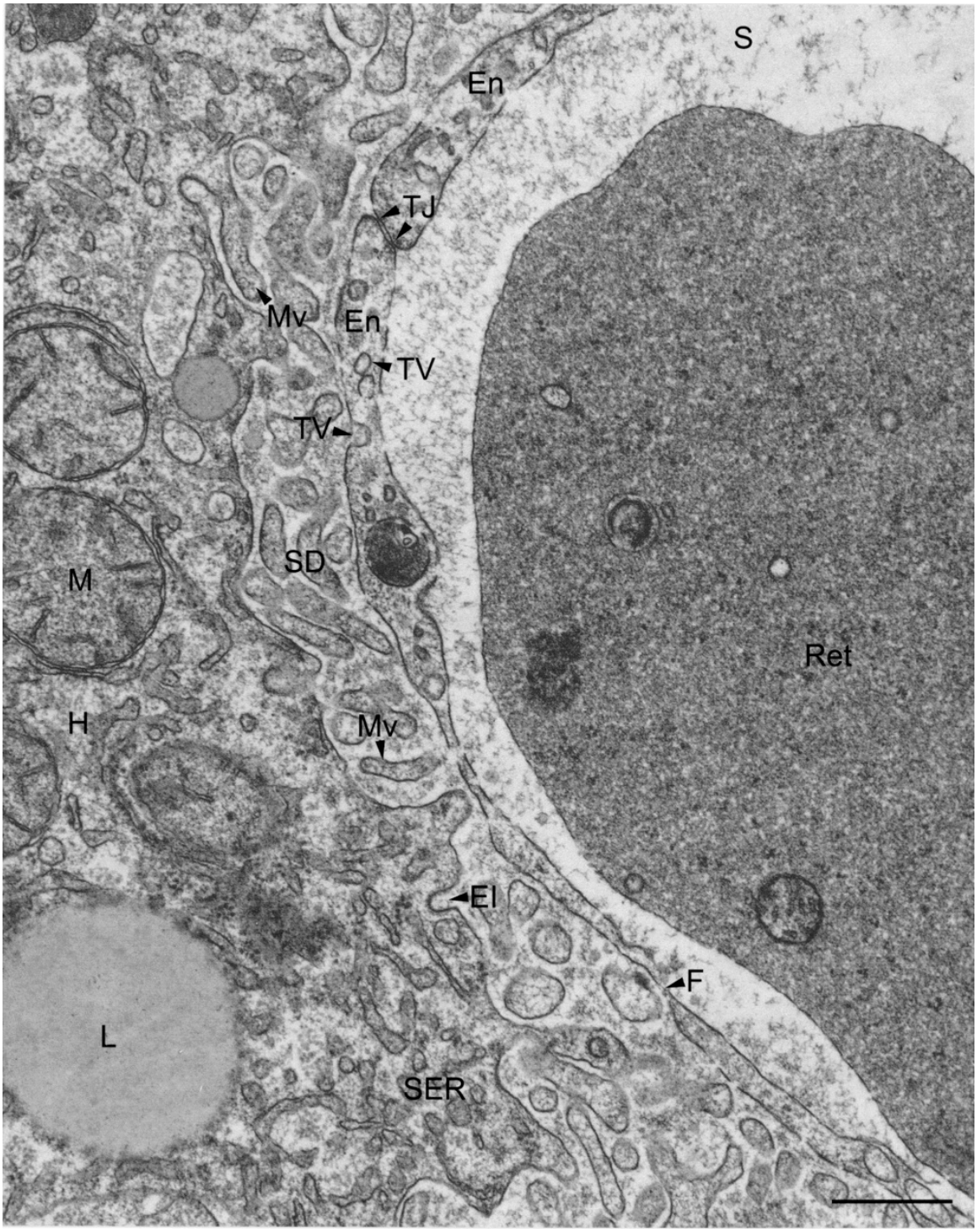

Figure 1.11 The space of Disse is the region existing between liver sinusoidal endothelial cells and hepatocytes. The perisinusoidal region is portrayed demonstrating the ultrastructural elements between hepatocytes (H) and the lumen of sinusoids (S). The presence of mitochondria (M), lipid droplets (L), and smooth endoplasmic reticulum (SER) characterize the periphery of hepatocytes facing sinusoids. Reticulocytes (Ret) are sometimes present inside sinusoids. The endothelial layer (En) separates the perisinusoidal space of Disse (SD) from the lumen of sinusoids. Endothelial cells are tethered by tight junctions (TJ). In addition, endothelial cells contain fenestrae (F) and transendothelial vesicles (TV) inside a relatively electron-lucent cytoplasm. The basal surface of the hepatocyte has many endocytotic invaginations (EI) and microvilli (Mv) that project into the space of Disse. Scale bar, 0.5 μm.

Figure 1.12

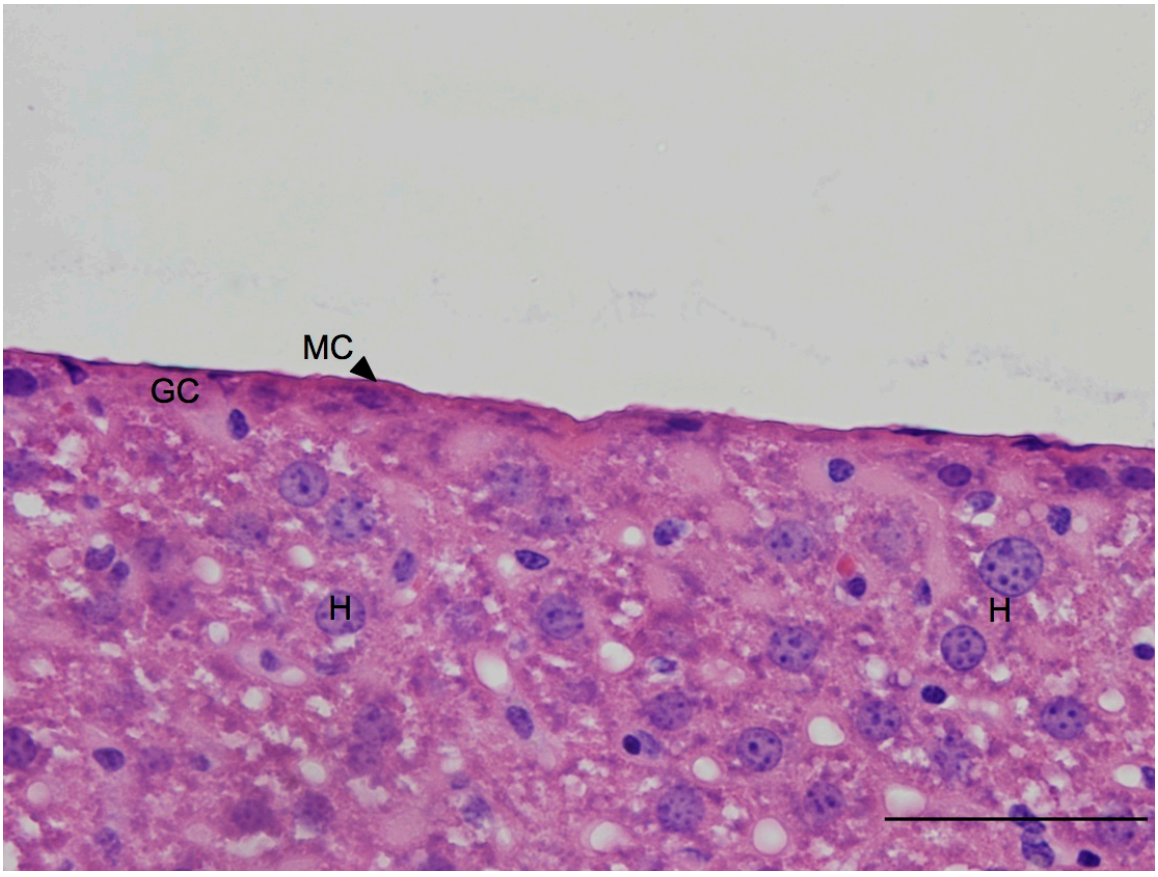

Figure 1.12 A layer of collagenous tissue encapsulates the liver. Glisson's capsule (GC) is a layer of connective tissue surrounding entire lobes of liver lying directly over hepatocytes (H). This structure is further surrounded by a layer of peritoneal mesothelial cells (MC). Scale bar, 50 μm.

Figure 1.13

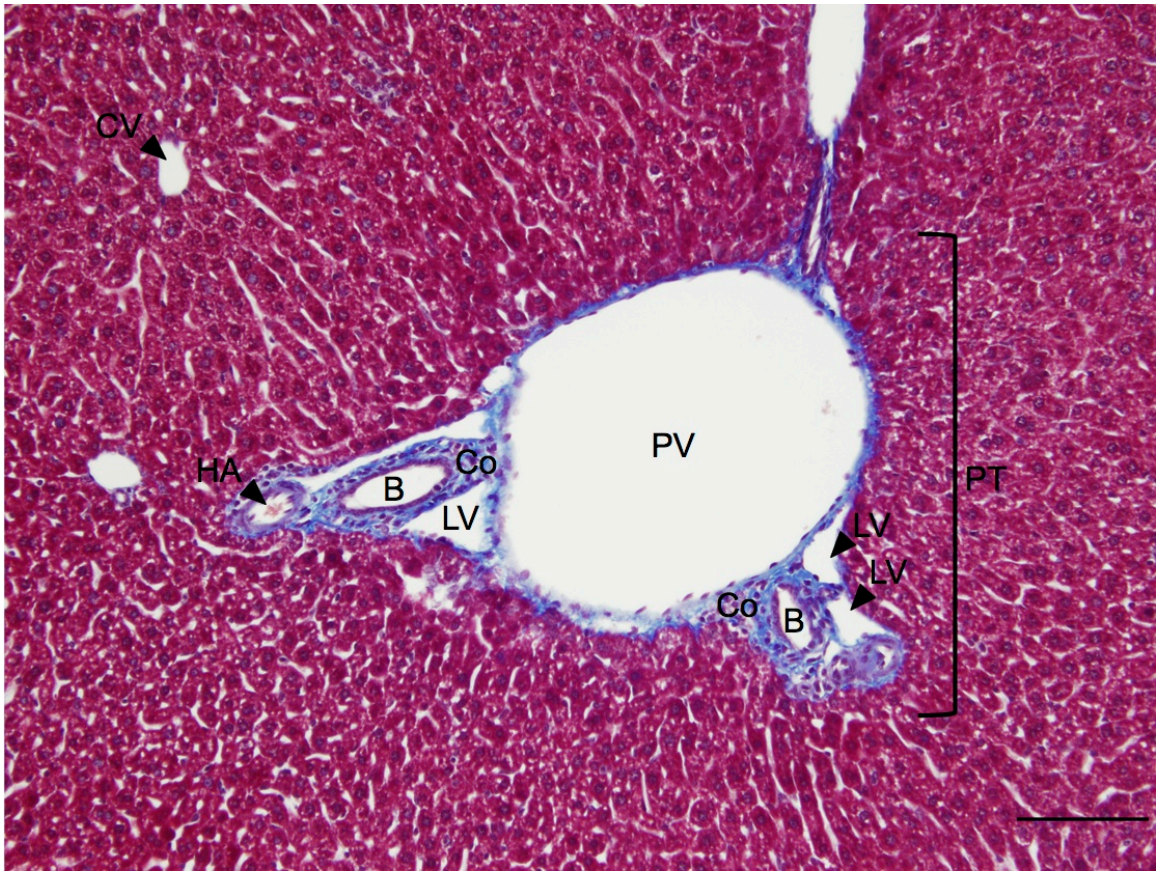

Figure 1.13 The majority of connective tissue is associated with portal triads. A portal triad (PT) comprised of a portal vein (PV), hepatic arteries (HA), bile ductules (B), and associated lymphatic vessels (LV) is depicted. The vast majority of collagen (Co; blue) exists in areas surrounding portal triads and is absent in hepatic lobules and their associated central veins (CV). Scale bar, 100 μm.

Figure 1.14

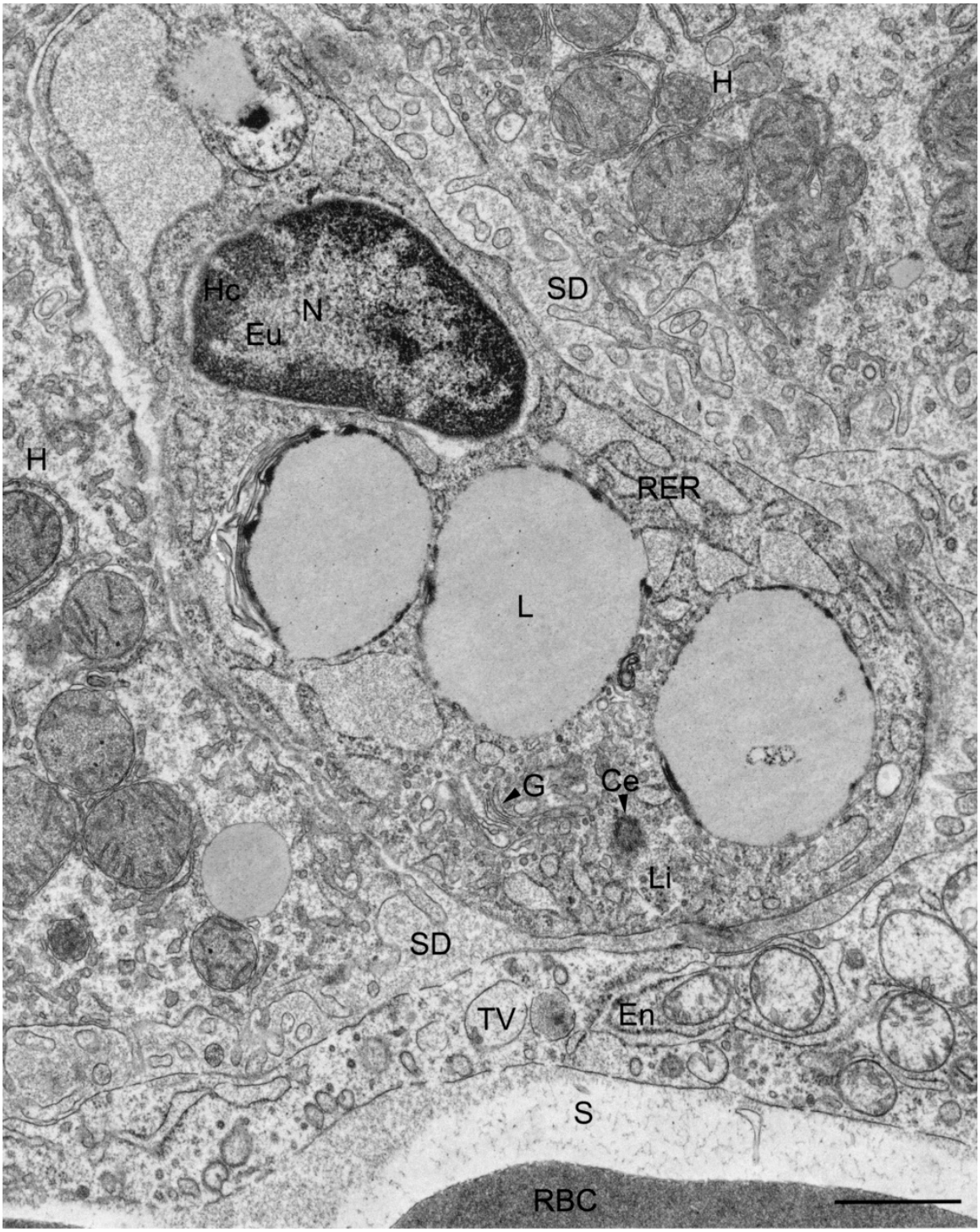

Figure 1.14 Lipocytes form close associations with hepatocytes. A lipocyte (Li) resides within the space of Disse (SD) between hepatocytes (H). A sinusoid (S) containing a red blood cell (RBC) is rendered here. Endothelial cells (En) containing many transendothelial vesicles (TV) retain lipocytes inside the space of Disse and separate from the sinusoidal lumen. Lipocytes are characterized by a large lipid droplet (L) content. Other organelles found within lipocytes include the following: a nucleus (N) containing peripheral heterochromatin (Hc) and central euchromatin (Eu), dilated rough endoplasmic reticulum (RER), Golgi (G), and centrioles (Ce). Scale bar, 1 μm.

Acknowledgments

Electron microscopy and relevant tissue preparation were performed at The College of New Jersey under the supervision and training of Donald Lovett. The University of Virginia Research Histology Core Facility and the University of Virginia Advanced Microscopy Facility kindly assisted in tissue preparation and brightfield imaging, respectively.

Methods

Animals

C57BL/6 mice were used in these experiments (Taconic Farms, Hudson, NY). Animals used were 6 to 10 weeks of age and housed in a pathogen-free facility under protocols approved by the Institutional Animal Care and Use Committees at The College of New Jersey (Ewing, NJ) and the University of Virginia (Charlottesville, VA).

Brightfield Microscopy

For H & E and Gomori's Trichrome staining, excised samples from *Mus musculus* were incubated overnight in 10% buffered formalin acetate (Fisher Scientific, Pittsburgh, PA) at room temperature, washed with 1×PBS, and stored in 70% EtOH prior to paraffin embedding and sectioning. Brightfield microscopy was conducted on an Olympus BX51 microscope (Olympus America Inc., Center Valley, PA).

Transmission Electron Microscopy

Liver tissue collected from *Mus musculus* was sectioned into pieces 1.0 mm thick in chilled 1×PBS containing 1.0 mM $CaCl_2$ and 0.1 M sucrose (pH 7.65). The tissue was then fixed with 4% glutaraldehyde in the same buffer for 3 hrs at room temperature. After rinsing in pure buffer, the tissue was post-fixed in 1% osmium tetroxide for 2 hrs in the same buffer at room temperature, rinsed with glass distilled water, and dehydrated through a graded acetone series. Infiltration with Spurr's resin (10.0 g ERL, 6.8 g DER, 26.0 g NSA, and 0.4 g DMAE) was performed using the Millonig centrifugation protocol (Polysciences Inc., Warrington, PA). Individual hepatic tissue portions were embedded in Spurr's resin for approximately 15 hrs at 70°C.

Monitor sections (0.25-1.5 μm) were prepared, mounted on chrome alum-gelatin subbed glass slides, stained with methylene blue borax, and observed using a light microscope[12]. Thin sections (50-65 nm) of selected blocks were then prepared and mounted on 300 mesh copper grids. All sectioning was performed using a Reichert-Jung Ultracut-E ultramicrotome (Leica, Wetzlar, Germany) equipped with a glass knife.

Thin sections of liver tissue were individually stained with uranyl acetate for 5 min and rinsed in a graded methanol series. The sections were then stained with lead citrate for 2 min and rinsed with boiled glass distilled water. The stained sections of hepatic tissue were observed and characterized using a Hitachi H-7000 transmission electron microscope (Hitachi High Technologies America Inc., Dallas, TX).

CHAPTER 2

Immunology of the Liver: Tolerance

Mononuclear Cell Populations Found in the Liver

The organization of the liver at the microstructural and ultrastructural levels is important for a clear understanding of parenchymal cell interactions with mononuclear cells of the immune system and how antigen is presented in the liver in the context of viral infection. Although many cells possess a single nucleus, mononuclear cells are white blood cells, agranulocytes that can be separated from other parenchymal cells and granulocytes by gradient centrifugation of a solid organ or the peripheral blood. Histodenz and Ficoll gradients are used for separation in the liver and spleen/blood, respectively. Isolating mononuclear cells allows for their subsequent analysis during an immune response.

Mononuclear cells within the liver are defined by cell markers using flow cytometry. Cells are first incubated with a live/dead stain to eliminate dead cells. Forward scatter (area and width) and side scatter (area) gates are next employed to exclude small cell debris and cellular doublets from analysis. CD45 distinguishes hematopoietic cells ($CD45^+$) from non-hematopoietic cells ($CD45^-$). Even though liver sinusoidal endothelial cells (LSEC) are not mononuclear cells, a portion of this cell population is liberated during gradient centrifugation and is defined as $CD105^+CD146^+$. Hepatocytes are completely separated from mononuclear cells due to their large mass, and these cells are not found in the $CD45^-$ fraction.

A NK1.1 versus CD3ε scheme is used to distinguish natural killer (NK) and natural killer T (NKT) cells. NK cells are $NK1.1^+CD3\varepsilon^-$ and NKT cells are $NK1.1^+CD3\varepsilon^+$, where NKT

cells can also be confirmed by their ability to bind CD1d tetramers. Some researchers use NKp46 as a marker defining NK and NKT cells, but it's expression varies and is pliable after viral infection on both cell populations. A portion of NK cells also uniquely express the activation marker Thy1.2 on the C57BL/6 background.

From the NK1.1^{-} gate, a MHC II (I-A/I-E) versus Thy1.2 scatter plot is employed where MHC II$^{lo/hi}$Thy1.2^{-} cells are mostly antigen presenting cells (APC), and the MHC II$^{-/lo}$Thy1.2^{+} gate contains CD4^{+} T cells (Thy1.2^{+}CD4^{+}) and CD8^{+} T cells (Thy1.2^{+}CD8^{+}). Multiple cell populations are found within the MHC II$^{lo/hi}$Thy1.2^{-} gate and are separated based on F4/80 and CD11b staining. Some neutrophils (despite having granulocytic properties) are obtained via gradient centrifugation of liver tissue expressing high levels of CD11b and Ly6G. Other major cell populations found include Kupffer cells (KC), infiltrating monocytes, macrophages (Mø), dendritic cells (DC), and B cells. KCs are CD11b^{lo}F4/80^{hi}, and within the CD11b^{hi}F4/80^{lo} gate reside infiltrating monocytes/Møs (MHC II^{lo}CD11b^{hi}CD11c^{lo}) and conventional DCs (MHC II^{hi}CD11b^{hi}CD11c^{hi}). Since F4/80 staining is exclusively high on KCs, these cells can also be identified via immunofluorescence microscopy. Although not included in this research, the CD11b^{lo}F4/80^{lo} gate likely includes CD103^{+}CD8^{+} DCs, and the CD11b^{-}F4/80^{-} gate contains mostly plasmacytoid DCs (pDC) (B220^{+}CD19^{-}) and a small B cell population (B220^{+}CD19^{+}). This gating scheme is used to identify the immune cells discussed here and analyzed during the course of later experiments (**Fig. 2.1**).

Physiology of the Liver Microenvironment and Tolerance

One theory of how pathogens generally subvert the immune response in the liver is by taking advantage of what is known as 'liver tolerance.' Tolerance in immune responses

to virus is in part due to the environment in which the viral infection occurs. Early transplant studies revealed that the liver is a tolerogenic organ, where increased success rates of transplantation across MHC barriers were achieved without rejection and without the continued need for immunosuppressive drugs compared to other solid organs[13-15]. Further, liver transplant recipients have been shown to be tolerized to receive transplants of other organs in subsequent surgeries[16]. The liver is supplied with 30% of the cardiac yield, and the entire blood volume cycles approximately 360 times per day through the liver in humans[17]. The liver is unique due to its hypoxic blood supply. As previously mentioned, blood is delivered to the liver as a mixture between oxygen rich blood of the hepatic artery and deoxygenated portal blood. Portal vein blood flow constantly exposes the liver to food-derived antigens, environmental toxins, and bacterial products including endotoxin (lipopolysaccharide, LPS)[14,18]. Apart from being metabolized by hepatocytes, the toll-like receptors (TLR) on KCs and LSECs constantly engage these antigens and pathogen associated molecular patterns (PAMP) in the absence of inflammation. This leads to a chronic low level stimulation of NF-κB and high levels of immunosuppressive cytokines such as IL-10 and TGF-β in the liver (endotoxin tolerance theory)[19,20]. The mechanisms contributing to liver tolerance are not well understood, but there is evidence for T cell apoptosis, immune deviation, and active suppression[15].

After viral infection of the liver, CD8$^+$ T cells are primed *in situ* or within the liver draining celiac lymph node (C LN). It has been shown that CD8$^+$ T cells primed in the liver are tolerized to antigen and compete with fully functional CD8$^+$ T cells primed in the C LN. The balance between these two cell populations often determines the outcome of immunity in the liver[21]. Due to the slow blood flow within the liver parenchyma and

unique architecture of the hepatic lobule as discussed previously, immune cells are poised to interact with KCs, LSECs, DCs, and the underlying hepatocytes through fenestrations in the endothelial lining of sinusoids[10,19]. When the liver is depleted of APCs, $CD8^+$ T cell responses can still be primed indicating that the liver itself can act as a secondary lymphoid organ[22]. KCs and LSECs are both able to cross-present antigen and express MHC I/II, CD40, CD80, and CD86, but these cells resemble immature DCs characterized by a poor ability to prime T cell responses. IL-10 production and PD-L1 surface expression have been shown to play key roles within KCs and LSECs in initiating tolerance[20]. During the course of intrahepatic viral infection, the generation of antiviral $CD8^+$ T cells is suboptimal in part due to this defective antigen presentation within the infected liver and a skewed $CD4^+$ T_h1/T_h2 cell balance resulting in their inability to proliferate robustly, to produce critical pro-inflammatory cytokines, and to generate cytolytic effector molecules[14,23].

In the context of hepatitis C virus (HCV) infection, tolerance seems to work to dampen cellular immunity by altering $CD4^+$ and $CD8^+$ T cell responses in chimpanzees and humans. $CD8^+$ T cells lose effector activity during chronic infection of the liver with HCV, and this exhaustion correlates with viral persistence. A mouse model for chronic infection utilizes lymphocytic choriomeningitis virus (LCMV). Throughout chronic LCMV infection, $CD8^+$ T cell exhaustion seems to occur in a hierarchical manner where IL-2/TNF-α production is first lost followed by a loss of IFN-γ production. Once IFN-γ is missing, the $CD8^+$ T cells seem to become completely anergic and succumb to death by apoptosis[24,25].

The liver inhibits CD8$^+$ T cell effector function through a variety of mechanisms, thereby dampening antigen-specific immune responses to viruses. Three key inhibitory pathways that have gained major attention in the last 15 years include the IL-10, PD-1/PD-L1, and Tim-3 immunoregulatory pathways. Acute and chronic viral infections likely exploit these inhibitory pathways in order to actively suppress the host's natural immune response.

Adenovirus and Mouse Cytomegalovirus Infection

The *Adenovirus* (Ad) family contains viruses with linear DNA 35 kb in length enclosed in non-enveloped icosahedral capsids. Recombinant genes (such as *Ova* and *Lacz*) are usually inserted in adenoviruses generated from human serotypes 2 and 5 in order to study antigen-specific immune responses. The icosahedral capsid consists of 240 hexons and 12 pentons made from capsomers. A trimeric glycoprotein fiber topped with a bulbous knob is present on each penton. The knob portion of the glycoprotein primarily binds host cell Coxsackie and adenovirus receptor (CAR), which is highly expressed on hepatocytes. The glycoprotein knob is also known to bind circulating proteins, Factor IX/X and complement C4 binding protein, which form 'molecular bridges' for hepatocyte uptake via heparin sulfate proteoglycan (HSPG) or low-density lipoprotein receptor-related protein. The penton base also binds αV integrin, assisting in viral entry[26]. KCs utilize scavenger, complement, and immunoglobulin Fc-receptors for uptake, and LSECs are known to engulf virus particles, but transgene expression is only achieved in hepatocytes where productive viral infection occurs[27]. Insertion of the transgene is typically accompanied by deletion of the *E1* and *E3* genes rendering the adenovirus a replication-deficient vector[26].

During intravenous (IV) adenovirus delivery, greater than 90% of the virus enters hepatocytes and KCs resulting in a robust NK cell response and a later $CD8^+$ T cell response peaking at day 7 (D7) post-infection. Prior research has demonstrated that IV adenovirus infection results in the expansion of $CD8^+$ T cells with an exhausted phenotype compared to IV infection with replication-competent mouse cytomegalovirus (MCMV)[28]. Furthermore, subcutaneous (SC) adenovirus infection of the left flank leads to the development of functionally competent $CD8^+$ T cells where antigen-specific $CD8^+$ T cells primed directly in the liver are dysfunctional producing significantly less TNF-α, IL-2, IFN-γ (**Fig. 2.2a**), and granzyme B (data not shown). Despite $CD8^+$ T cell differentiation and expansion is highly dependent on IL-2 in most circumstances[29,30], $CD8^+$ T cells do not up-regulate CD25 within the liver 24-48 hours following adenovirus IV infection (**Fig. 2.2b**). The liver-primed $CD8^+$ T cells are also less capable of cytolytically killing target cells *in vivo* (**Fig. 2.3**). Therefore, liver-primed $CD8^+$ T cells responding to acute adenovirus infection resemble the exhausted phenotypes observed after chronic LCMV infections in mice and HCV infection in humans.

Hepatitis C Virus Infection

Upwards of 200 million people are infected with the HCV worldwide, including approximately 4 million cases in the United States. Therefore, control and eradication of this infectious agent represents a major healthcare challenge[31]. Further, 80% of these individuals develop chronic hepatitis characterized by liver fibrosis, cirrhosis, and ultimately hepatocellular carcinoma (HCC)[32]. The only treatment regimen available is IFN-α and ribavirin combination therapy. This treatment has harmful side effects, and its efficacy decreases with certain HCV genotypes and African American decent[33]. HCV

employs strategies to undermine the host immune response, but little is known about how immune deregulation in the liver contributes to persistent viremia.

HCV is an enveloped, positive strand RNA virus within the *Flaviviridae* family. Its genome is approximately 9.5 kb in length, which is translated into a large polyprotein precursor upon endocytosis and release of virus particles into the host cell's cytoplasm. Cleavage by cellular proteases yields structural proteins (core, E1, and E2) located at the N-terminus and C-terminal nonstructural proteins (NS2, NS3, NS4A, NS4B, NS5A, and NS5B) involved in RNA replication[34].

Soon after HCV transmission there is a rapid doubling of the virus, and the first viral protein produced is the N-terminal HCV core precursor protein. The HCV core precursor protein is first localized to the endoplasmic reticulum (ER) via a hydrophobic C-terminal H1 motif, which is later cleaved off, yielding a functional 21 kDa HCV core protein. The mature HCV core protein forms the viral capsid, but it can be found in the nucleus, ER surface, cytoplasm, and in a secreted soluble form[35]. Within infected cells, the core protein has the ability to bind the 60S ribosome, RNA, and tumor necrosis factor receptor (TNFR) family members including the lymphotoxin-β receptor[36,37], TNFR1[38], and Fas[39]. Interaction with these receptors interferes with Fas- and TNF-mediated apoptosis. A decrease in apoptosis of virally infected hepatocytes may contribute to viral persistence. HCV infection also leads to the inhibition of the type I IFN response. IFN-α/β signaling is critical for activating antiviral responses in infected cells, and it also leads to the production of MIP1α, which helps recruit NK cells to the site of infection. NS3-NS4A has been shown to block type I IFN, and specific sequences in E2 and NS5A can decoy and dimerize with protein kinase R (PKR) *in vitro*, respectively. PKR is

responsible for binding dsRNA, and upon binding it phosphorylates the ribosomal subunit, EIF2α, to inhibit protein translation effectively making virally infected cells inert[31]. HCV core protein has been shown to interfere with IFN-α signaling by activating suppressor of cytokine signaling 3 (SOCS3) and inhibiting the nuclear localization of IFN-α activated signal transducers and activators of transcription (STAT)[40,41]. Secreted HCV core can also be found in the serum of infected patients in a prolonged 2-3 month serological window phase following infection before anti-core antibodies are generated[42]. Extracellular core is known to bind the complement receptor, gC1qR, on the surface of T cells and APCs. This ligation not only interferes with complement cascades, but also dampens $CD8^+$ T cell proliferation and IFN-γ production[43-45].

When a HCV *core* transgene is expressed in hepatocytes downstream from the *albumin* promoter in mice that are subsequently infected with adenovirus, viral clearance is delayed and viral-specific $CD8^+$ T cells produce less IFN-γ and TNF-α, whereas the inhibitory PD-1 pathway is enhanced[46]. These results are consistent with previous reports showing HCV core protein is sufficient to dampen $CD8^+$ T cell responses[34,47].

IL-10

First described as a product of T_h2 cells with the ability to inhibit T_h1 cell cytokine synthesis, semi-mature DCs[48], B cells, Møs, and various subsets of $CD4^+$ and $CD8^+$ T cells are now known to produce IL-10. IL-10 is an anti-inflammatory cytokine, and it has been shown to limit $CD8^+$ T cell and T_h1 cell responses, rendering it as a critical pathway in the context of viral infections[49].

IL-10 binds IL-10R, a dimer composed of α and β chains. IL-10Rα is associated with JAK1, and IL-10Rβ is coupled with TYK2. JAK1 and TYK2 are both kinases, but JAK1

primarily phosphorylates the two tyrosine residues on IL-10Rα. STAT3 docks to these tyrosine resides via SH2 domains. STAT3 phosphorylation then results in the formation of STAT homo- and heterodimers, which appear to be critical for most if not all the effects IL-10. STAT3 is typically known for its ability to globally suppress the production of pro-inflammatory cytokines, but downstream STAT3 signaling can also induce other genes such as SOCS3 (involved in inhibiting IL-6 signaling and IFN-γ production) and Bcl-3 (linked to controlling TNF-α induction by binding the p50 subunit of NF-κB)[50,51].

In HCV patients, higher viral titers correlate directly with IL-10, and fibrosis correlates indirectly with exogenous IL-10 therapy. Several studies link certain *Il10* promoter polymorphisms with different clinical outcomes. Furthermore, there appears to be the induction of numerous IL-10-producing, $CD4^+CD25^-FoxP3^-$ and $CD8^+$ T cells within peripheral blood samples and liver biopsies in HCV patients[52-54]. Prior research has shown that within the liver parenchyma most of the HCV-specific $CD8^+$ T cells localize to regions of weak fibrosis and low apoptosis. The HCV-specific $CD8^+$ T cells are able to make IL-10 but unable to produce IFN-γ[53]. These intrahepatic IL-10-producing $CD8^+$ T cells have been identified by another group that additionally shows when these liver infiltrating lymphocytes are stimulated with HCV-peptide they suppress the proliferation of autologous peripheral blood mononuclear cells (PBMC) in co-culture experiments. This is reversible upon anti-IL-10 antibody treatment, indicating some type of equilibrium may exist between cytotoxic T lymphocytes (CTL) and IL-10-producing $CD8^+$ T cells in the liver compartment[54]. One can also speculate from these series of experiments that the intrahepatic $CD8^+$ T cell possesses T regulatory (T_{reg}) cell properties and uses IL-10 and other anti-inflammatory pathways to suppress T cell responses in the context of HCV or other viral infections.

As accumulating evidence suggests that IL-10 signaling is linked to the formation of a chronic infection in HCV patients, a popular mouse model used in the study of the IL-10 pathway is a comparison of acute and chronic LCMV strains, Armstrong (Arm) and Clone-13 (Cl-13), respectively. In the spleens and livers of Cl-13 infected mice, $CD8^+$ T cells are all exhausted in terms of ability to clear virus and produce less TNF-α, IL-2, and IFN-γ when compared to an Arm infection. IL-10 is indeed present in serum of Cl-13 infected mice, and IL-10R expression is equally raised after Arm and Cl-13 inoculations[55]. $CD11c^+$ DCs are capable of producing early IL-10, and this IL-10 seems to drive the development of IL-10-producing $CD4^+$ T cells[56,57]. In IL-$10^{-/-}$ mice, $CD4^+$ T cell IL-2 production is enhanced, and there is greater $CD8^+$ T cell TNF-α production. IFN-γ production and proliferation by $CD4^+$ and $CD8^+$ T cells as well as CTL activity are improved in both IL-$10^{-/-}$ mice and wild-type mice treated with anti-IL-10 antibody[58]. However, if anti-IL-10 antibody is given during the persistent stage of infection, no improvement in T cell responses is observed, suggesting IL-10 shapes the immune response in the acute phase prior to progression to chronicity. In the LCMV model, it is thought that IL-10 acts to skew early IL-2 production leading to an anergic $CD8^+$ T cell[55]. After Cl-13 infection, PD-1 inhibitory receptor expression also appears to be raised on the $CD8^+$ T cell population, discussed below. Anti-IL-10 antibody therapy reduces PD-1 expression in both early and memory responses, suggesting the two inhibitory pathways support each other by unknown molecular mechanisms[59].

PD-1 and PD-L1/2

Signaling through programmed death 1 (PD-1), a member of the CD28 family, inhibits the immune response. Activated T cells, B cells, and myeloid cells induce PD-1

upregulation on their cell surface via NFATc1 binding to the *Pd1* promoter. Currently, it is unclear whether NFATc1 interacts with AP-1 or NF-κB in the 5' regulatory region of *Pd1*[60]. The cytoplasmic tail of PD-1 contains an immunoreceptor tyrosine-based inhibitory motif (ITIM) and an immunoreceptor tyrosine-based switch motif (ITSM). *In vitro* experiments revealed that the tyrosine residue in the ITSM is the most critical in transmitting a PD-1 inhibitory signal. Phosphorylation of ITSM recruits SHP-2, which dephosphorylates molecules such as ZAP70 and CD3ζ in T cells. Upon ligation to either PD-1 ligand 1 (PD-L1) or PD-1 ligand 2 (PD-L2), PD-1 effectively inhibits downstream T cell receptor (TCR) signaling[61]. PD-1 has also been shown to block activation of PKB, phosphotidylinositol-3-OH kinase, and expression of the survival factor, Bcl-x_L[62].

Basal expression of PD-L1 is readily found on T cells, B cells, Møs, and DCs. PD-L1 is further upregulated on T cells and monocytes/Møs following anti-CD3ε antibody and IFN-γ/LPS treatment, respectively[63,64]. PD-L1 is also constitutively expressed on the endothelial linings of non-lymphoid organs including the liver, heart, lung, kidney, salivary gland, and eye. Specifically, LSECs and KCs are known to express PD-L1[65]. Although the functions of PD-L1 and PD-L2 seem to overlap one another, PD-L2 expression is limited to inflammatory Møs and DCs[66]. As PD-L1 expression is regulated by TLR ligation and T_h1 cytokines, PD-L2 expression seems to be increased after IL-4 stimulation (alternative activation by T_h2 cytokines)[67].

Some reports demonstrate that PD-L1 and PD-L2 ligation to PD-1 can also lead to co-stimulation of naïve T cells. For example, when PD-L1 immunoglobulin complex is immobilized on a flask containing T cells stimulated with anti-CD3ε antibody, their proliferation, IL-10, and transient IL-2 production are all enhanced[63]. In a similar

experimental design, other researchers have shown that PD-L2 co-stimulates naïve T cells treated with anti-CD3ε antibody causing them to produce IFN-γ and proliferate to a greater extent[68]. At this point it remains unclear as to how PD-1, a receptor with cytoplasmic ITIM and ITSM domains can actually co-stimulate a cell. Previous work revealed that there might be a separate co-stimulatory receptor that binds PD-L1 and PD-L2 independent of PD-1[69].

Despite controversy, PD-1 seems to play an inhibitory role during acute and chronic viral infections. Antibody blocking of PD-1 *in vitro* reverts the exhausted phenotype of human immunodeficiency virus (HIV)-specific $CD4^+$ and $CD8^+$ T cells to that of a full effector[62]. In patients infected with hepatitis B virus (HBV), PD-L1 is upregulated on myeloid DCs leading to poor activation of T cells in co-culture. If PD-L1 is antibody blocked *in vitro*, the T cells regain function[70]. In acute HCV patients, PD-1 is upregulated on $CD8^+$ T cells, but it is downregulated upon memory formation concurrent with a regain of T cell effector function. If the HCV virus persists leading to a chronic infection, PD-1 levels remain high and the HCV-specific $CD8^+$ T cells remain dysfunctional. *In vitro* blockade of the PD-1/PD-L1 interaction results in enhanced proliferation of the HCV-specific $CD8^+$ T cells[71].

In various studies of chronic viral infections making use of PD-$L1^{-/-}$ mice and blocking antibodies, it is clear that blockade of the PD-1 pathway results in improved $CD8^+$ T cell effector function including an increase in proliferation, cytotoxicity, IFN-γ, and IL-2 production[72,73]. One study in HBV patients showed PD-L1 antibody blockade led to a decrease in IL-10 production, again indicating the pathways may support each other[70]. Additionally, PD-1 decreases anti-CD3ε/CD28 antibody-mediated IL-2 induction in T cell

cultures, but this is reversible upon exogenous application of IL-2. Further, $CD8^+$ T cells seem to be more sensitive to the inhibitory effects of PD-1 possibly owing to their inability to produce copious amounts of IL-2 compared to $CD4^+$ T cells[74]. $CD8^+$ T cells isolated from PD-$1^{-/-}$ mice also lacking $CD4^+$ T cells have an enhanced ability to produce IL-2 and have elevated CD25 (IL-2Rα) expression[75]. Therefore, PD-1 seems to enhance IL-10 signaling but prevents early IL-2 signaling in various immunological model systems.

Tim-3 and Gal-9

The T cell immunoglobulin and mucin (Tim) family is part of the immunoglobulin superfamily and consists of 8 members (Tim-1-8) in the mouse on chromosome 11 and 3 members in humans on chromosome 5. Tim-1, 3, and 4 in the mouse are orthologs of human Tim-1, 3, and 4[76]. Tim-1 was the first member identified as the hepatitis A virus receptor in monkeys (*Havcr1*). Tim-1 contains 60 glycosylation sites, whereas Tim-3 (*Havcr2*) contains 3 in its mucin domain; structural similarity between the two proteins suggest they arose from gene duplication of an ancestral gene[77]. The canonical ligands for Tim-3 include galectin-9 (Gal-9) and phosphatidylserine. Gal-9 recognizes mucin region N- and O-linked glycosylation sites, and phosphatidylserine binds via the FG cleft (featuring phenylalanine-glycine repeats) in the immunoglobulin variable region[76]. The FG cleft is formed by 4 non-canonical cysteines found in all the Tims, but not in other immunoglobulin superfamily members[78]. *E. coli*-derived recombinant Tim-3 tetramers, inherently lacking oligosaccharides, are capable of binding B cells, T cells, DCs, and Møs, suggesting other non-Gal-9 ligands exist[79].

Tim-3 has been mostly studied on T cells but expression is also observed on NK cells, DCs, and monocytes[77]. Several lines of evidence suggest Tim-3 causes decreases in pro-inflammatory cytokine production and apoptosis induction in T cells after engagement with Gal-9 through ill-defined signaling events[76]. A negative signaling role for Tim-3/Gal-9 engagement is highlighted when antibody blockade exacerbates experimental autoimmune encephalomyelitis and type I diabetes in mice[78,80]. Tim-1-3 contain tyrosine phosphorylation motifs, but only one research group has recently uncovered their role and how Tim-3 signaling integrates into the TCR cascade. This occurs through a three-way interaction between Tim-3, the Src-family kinase Lck, and HLA-B-associated transcript 3 (Bat3). In this study, Rangachari *et al.* establish Gal-9 binding to Tim-3 prevents Bat-3 linkage to active Lck, thus modulating downstream TCR signaling[81].

Gal-9 is an S-type lectin. Even though Gal-9 contains two distinct carbohydrate recognition domains joined by a flexible linker, its only known receptor is Tim-3[76]. Gal-9 is particularly abundant in the liver, can be induced in viral infection by IFN-γ within T cells among other cell types, and upon engagement of Tim-3, directly contributes to the exhausted $CD8^+$ T cell phenotype[77,82]. Gal-9 also was shown to promote T_{reg} cell differentiation over T effector (T_{eff}) cell proliferation during viral infection in an ocular herpes simplex virus (HSV) model, chronic HCV infection, and experimental autoimmune arthritis. Therefore, Tim-3 signaling may negatively affect the quality of the T cell response by increasing the T_{reg}:T_{eff} cell ratio[83-85]. Tumor cells are also established to locally produce Gal-1, 3, and 9 contributing to exhaustion[86]. A dampened $CD8^+$ T cell response and poorer prognosis to Epstein-Barr virus associated nasopharyngeal

carcinoma is linked with the release of Gal-9$^+$ exosomes from tumor cells into circulation[87].

Exhaustion within CD8$^+$ T cells during cancer anti-tumor responses, acute viral infection, and chronic viral infections positively correlates with Tim-3 expression. During HIV, HBV, and HCV infections, PD-1 is identified as the primary inhibitory pathway mediating exhaustion; however, its blockade does not fully revert the dysfunctional CD8$^+$ T cell to that of a fully competent effector cell. PD-1$^+$Tim-3$^+$CD8$^+$ T cells indeed exist in a deeper level of exhaustion after LCMV infection with a poorer ability to produce prototypical pro-inflammatory cytokines and a greater propensity to secrete IL-10[88]. During chronic HCV infection, PD-1$^+$Tim-3$^+$CD8$^+$ T cells have defects in proliferation and are the least functional with reduced ability to produce TNF-α, IFN-γ, and CD107a[82,89]. A similar population of exhausted CD8$^+$ T cells expressing PD-1 and Tim-3 was found within tumors in a murine colon cancer model system and within the NY-ESO-1-specific pool of cells recognizing melanoma antigen in humans. Dual anti-PD-L1/Tim-3 antibody blockade restricted tumor growth and improved CD8$^+$ T cell proliferation and TNF-α, IL-2, and IFN-γ production[90,91].

Signal integration between the IL-10, PD-1/PD-L1, and Tim-3 inhibitory pathways in promoting exhaustion is apparent as co-blockade experiments support a role for synergy. How Tim-3 integrates into the anti-inflammatory scheme probably depends on the context of the immune response and microenvironment since Gal-9 and phosphatidylserine can both simultaneously recognize Tim-3. Gal-9$^+$ exosomes can directly bind Tim-3, apoptotic debris together with soluble Gal-9 can crosslink Tim-3, and T cells may intrinsically crosslink Tim-3 on their surface via Gal-9 theoretically creating

three different signaling scenarios[76]. More recently, Tim-3 has also been shown to integrate in the HMGB-1 cascade as HMGB-1 has been shown to bind the same FG site as phosphatidylserine yielding different conformational changes and internal signals, discussed below[92].

RAGE and HMGB-1

High-mobility group box 1 (HMGB-1) was initially described as a non-histone associated, DNA binding protein responsible for DNA organization and transcription[93]. In sterile immunity lacking a pathogen (*e.g.* trauma), necrotic cells release danger signals (alarmins) including HMGB-1, heat shock proteins, S100 proteins, and hyaluronin that can bind pattern recognition receptors (PRR) similar to PAMPs. Matzinger *et al.* proposed this form of immunity is dependent on danger (*i.e.* damage) associated molecular patterns (DAMP) passively released from dying cells[94,95]. HMGB-1 was later found to be actively secreted by monocytes, Møs, DCs, and NK cells through a leaderless mechanism (not secreted through the Golgi apparatus) similar to IL-1 secretion. Rather, hyperacetylation of HMGB-1 and association with secretory lysosomes characterizes its active secretion. Oxidative stress, LPS, polyI:C, IL-1, TNF-α, and IFN-γ stimulate the release of HMGB-1 from Møs and DCs[95].

The major receptor for HMGB-1 is the receptor for advanced glycation end products (RAGE), a member of the immunoglobulin superfamily, but HMGB-1 can also associate with TLR2, TLR4, and TLR9[94]. RAGE is also known to bind other S100 protein family members (S100B, S100P, S100A4, S100A6, S100A8/9, S100A11-13) and prions. Engagement of RAGE leads to a positive signal within the cell dictated by activation of NF-κB. Most key immune cell types (including DCs, NK cells, and T cells) and

endothelial cells express RAGE. Endothelial cell RAGE can associate with Mac-1 to assist in neutrophil adhesion and migration into inflamed tissue[96]. DC engagement of HMGB-1 via RAGE and TLR2, TLR4, and TLR9 has been demonstrated to induce CD80, CD83, and CD86 expression and IL-12 production rendering these cells more potent APCs having an indirect positive effect for T cell priming[97]. HMGB-1 may also increase NK cell IL-2, IFN-γ, and IL-12 production, which in turn may enhance DC/NK cell cross-talk[98]. T cells express RAGE on their surface and within endocytic vesicles, and direct engagement of HMGB-1 boosts a T_h1 cytokine profile in $CD4^+$ T cells and proliferation in both $CD4^+$ and $CD8^+$ T cells[98-102].

Although not traditionally included in the discussion of inhibitory receptor signaling, HMGB-1 was recently discovered to bind Tim-3 within DCs via the Tim-3 FG cleft preventing tumor-derived RNA/DNA activation[103]. Tumor cell derived HMGB-1 has also been shown to decrease anti-tumor immunity in a breast cancer model by enhancing T_{reg} cell production of IL-10[104]. HMGB-1 signaling may therefore have the potential to integrate in the aforementioned immunoregulatory pathways. Depending on the cell type expressing Tim-3 (DC, T_{eff} cell, or T_{reg} cell) and concentration of certain ligands (phosphatidylserine, Gal-9, or HMGB-1) in different immune situations and microenvironments, vastly different outcomes in the NK and T cell responses may occur. Given passive release of HMGB-1 from virally lysed, cytolytically killed, hypoxic, and oxidatively stressed hepatocytes occurs[95] and elevated serum HMGB-1 present during HCV infection directly correlates with liver disease progression[94], HMGB-1 can act as a potent cytokine on immune cells within the liver.

$CD8^+$ T Cell Requirement for $CD4^+$ T Cell Help and IL-2

Recalling that lack of IL-2 production by $CD4^+$ and $CD8^+$ T cells is at least partially controlled by IL-10, PD-1, and Tim-3 signaling events, many researchers believe that deficiency in $CD4^+$ T cell help may be central in initiating $CD8^+$ T cell exhaustion. It is well known that the liver has a lower $CD4^+$:$CD8^+$ T cell ratio compared to most other organs, which may be a reason for the formation of a tolerogenic environment[105]. Other groups have shown that $CD8^+$ T cells can be directly primed by DCs without $CD4^+$ T cell help[106], but functional $CD4^+$ T cells or at least IL-2 are needed to optimize $CD8^+$ T cell effector function[30,107,108]. Treatment of virally anergized $CD8^+$ T cells with exogenous IL-2 also leads to an increase in CD25 expression, and it has been shown that IL-10 treatments can decrease CD25 expression possibly contributing to T cell anergy[109,110]. In the LCMV mouse model, chronic infection of $CD4^{-/-}$ mice (and anti-CD4 antibody depleted mice) with Cl-13 increases viral titers and leaves LCMV-specific $CD8^+$ T cell effectors unable to lyse target cells and produce IFN-γ[111].

Recombinant HCV (rHCV) core protein has also been shown to decrease $CD8^+$ T cell IFN-γ and IL-2 production. This is reversible with exogenous IL-2 treatment. IL-2 seems to be necessary to push a 'semi-effector' CTL to complete its differentiation programming. Addition of rHCV core protein seems to only take effect when added during antigen stimulation in *in vitro* systems lending evidence for the lack of early IL-2 contributing to anergy[112].

More recently, *in vivo* studies of $CD8^+$ T cell dependence on IL-2 has been conducted using IL-2/anti-IL-2 antibody complex. In this technique, IL-2 is mixed with anti-IL-2 antibody (clone S4B6), and then the complex is injected into mice. This complex is able

to bind and crosslink the low affinity IL-2R$\beta\gamma$. Even though anergic $CD8^+$ T cells lack IL-2Rα, this complex is able to bypass this constraint. Injection of the IL-2/anti-IL-2 antibody complex has been shown to increase $CD8^+$ T cell function in different model systems including the chronic LCMV model[113-115].

Figure 2.1

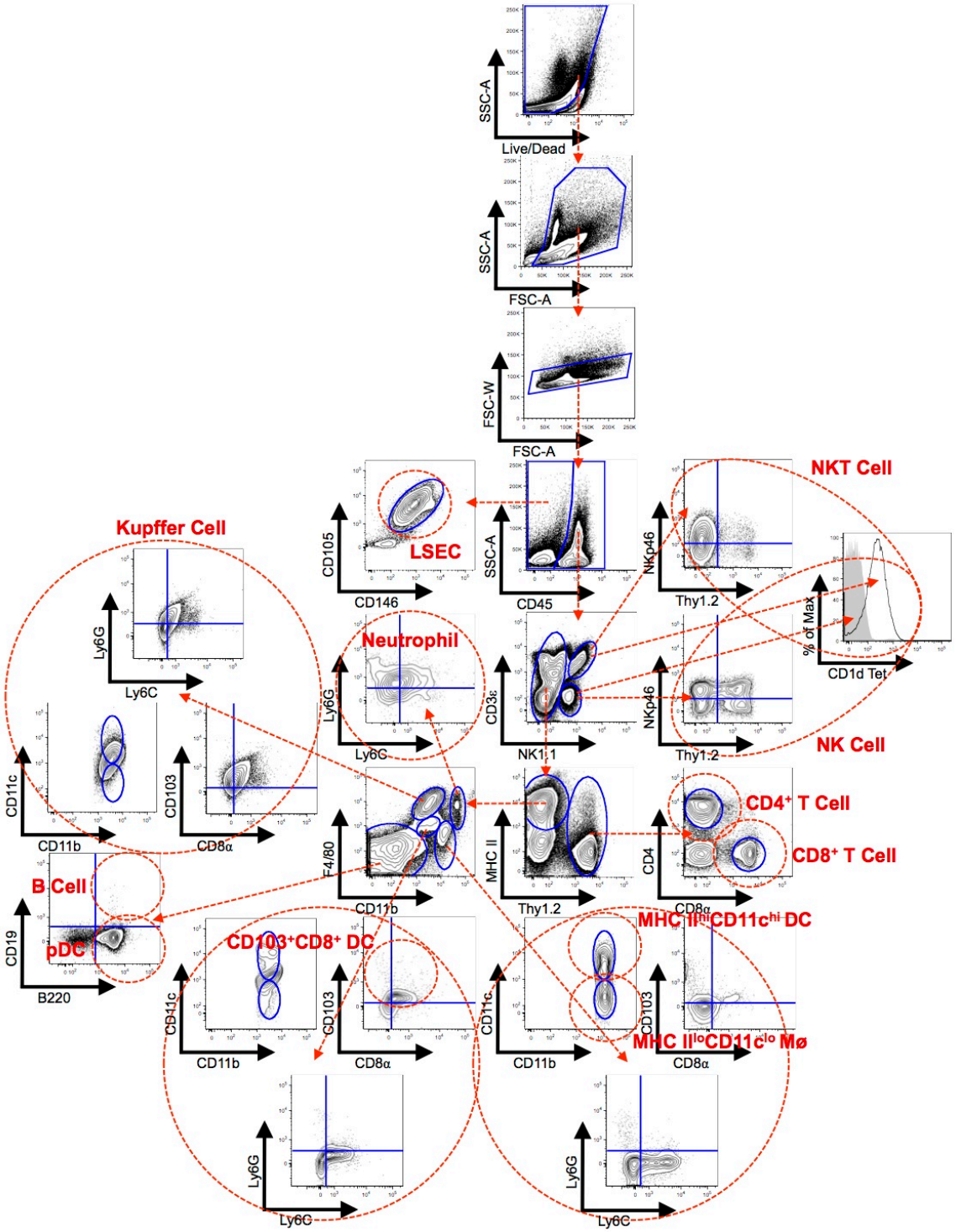
SSC-A
Live/Dead
SSC-A
FSC-A
FSC-W
FSC-A
CD105
LSEC
CD146
SSC-A
CD45
NKp46
Thy1.2
NKT Cell
% of Max
CD1d Tet
Kupffer Cell
Ly6G
Ly6C
Neutrophil
Ly6G
Ly6C
CD3ε
NK1.1
NKp46
Thy1.2
NK Cell
CD11c
CD11b
CD103
CD8α
F4/80
CD11b
MHC II
Thy1.2
CD4
CD8α
CD4+ T Cell
CD8+ T Cell
B Cell
CD19
pDC
B220
CD103+CD8+ DC
CD11c
CD11b
CD103
CD8α
MHC IIhiCD11chi DC
MHC IIloCD11clo Mø
CD11c
CD11b
CD103
CD8α
Ly6G
Ly6C
Ly6G
Ly6C

Figure 2.1 Mononuclear cell populations found in the liver. Mononuclear cells from naïve C57BL/6 mouse livers were harvested and the following cell populations were identified through FACS analysis: LSEC, neutrophil, Kupffer cell, pDC, $CD103^+CD8^+$ DC, MHC $II^{hi}CD11c^{hi}$ DC, MHC $II^{lo}CD11c^{lo}$ monocyte/Mø, NK cell, NKT cell, B cell, $CD4^+$ T cell, and $CD8^+$ T cell. Hepatocytes and stellate cells were not identified via this method.

Figure 2.2

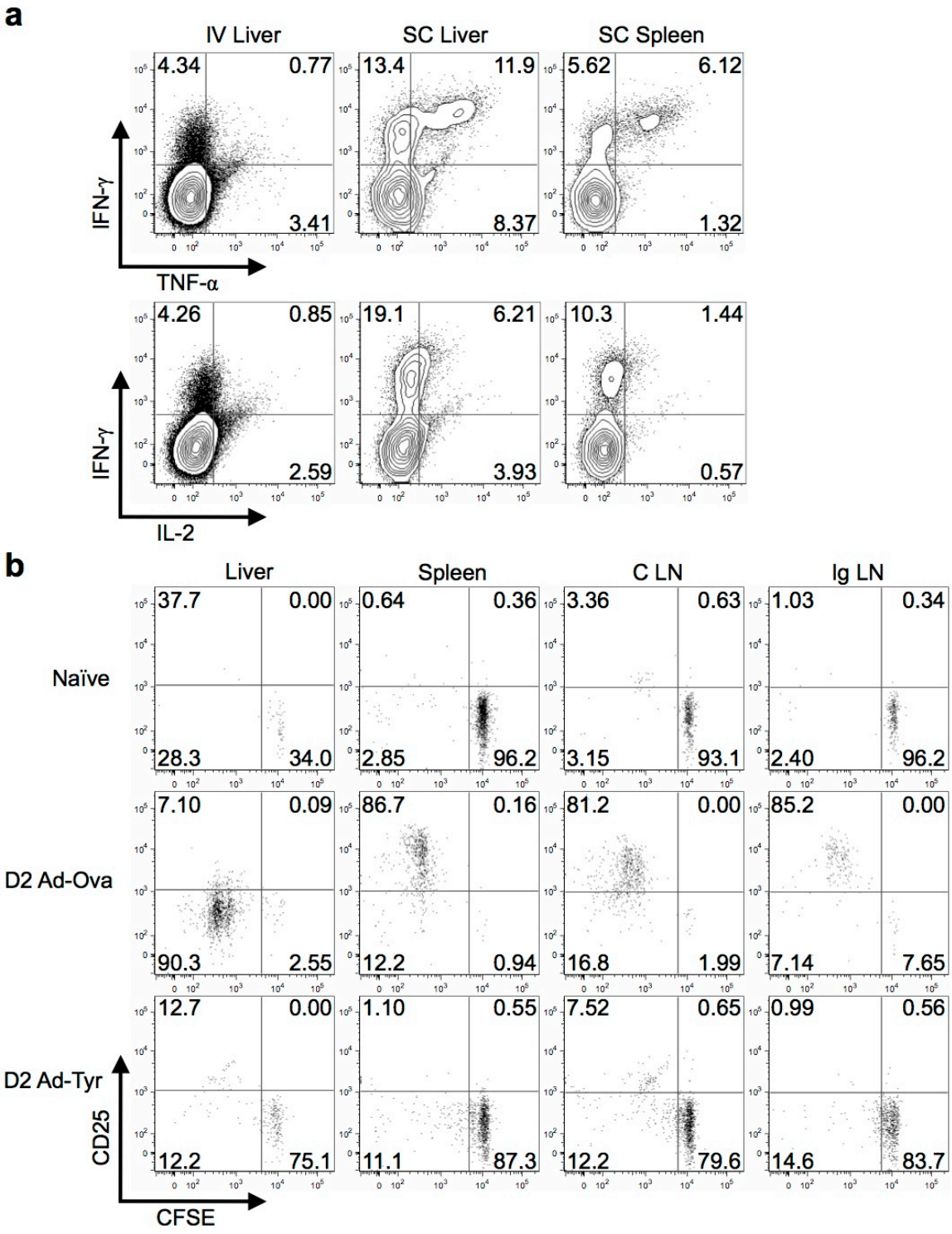
a
IV Liver
SC Liver
SC Spleen
4.34
0.77
3.41
13.4
11.9
8.37
5.62
6.12
1.32
IFN-γ
TNF-α
4.26
0.85
2.59
19.1
6.21
3.93
10.3
1.44
0.57
IFN-γ
IL-2
b
Liver
Spleen
C LN
Ig LN
Naïve
37.7
0.00
28.3
34.0
0.64
0.36
2.85
96.2
3.36
0.63
3.15
93.1
1.03
0.34
2.40
96.2
D2 Ad-Ova
7.10
0.09
90.3
2.55
86.7
0.16
12.2
0.94
81.2
0.00
16.8
1.99
85.2
0.00
7.14
7.65
D2 Ad-Tyr
12.7
0.00
12.2
75.1
1.10
0.55
11.1
87.3
7.52
0.65
12.2
79.6
0.99
0.56
14.6
83.7
CD25
CFSE

Figure 2.2 Liver-primed $CD8^+$ T cells display a dysfunctional antiviral effector cytokine potential. (**a**) C57BL/6 mice were SC or IV infected with 2.5×10^7 IU Ad-Ova, and D7 liver and spleen antigen-specific $CD8^+$ T cell TNF-α, IL-2, and IFN-γ production was assessed after a 5 hr re-stimulation with 2 μg/mL SIINFEKL peptide. (**b**) 2×10^6 CFSE-labeled naïve $Thy1.1^+CD8^+$ OT-I T cells were transferred into C57BL/6 mice one day prior to IV infection with 2.5×10^7 IU Ad-Ova or Ad-Tyr. CFSE dilution of $Thy1.1^+CD8^+$ OT-I T cells was measured in livers, spleens, celiac lymph nodes (C LN), and inguinal lymph nodes (Ig LN) of naïve and infected animals (n = 3 per group). Numbers in the scatter plots represent percentages.

Figure 2.3

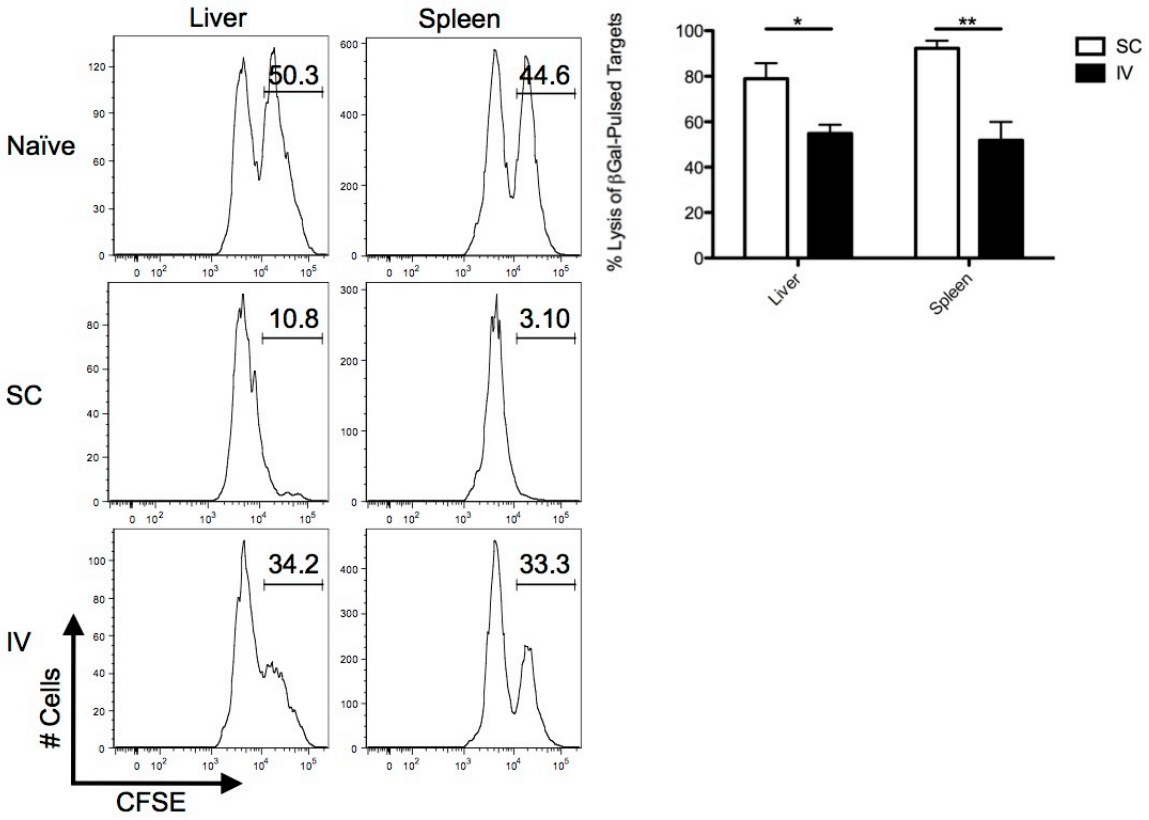
Liver
Spleen
Naïve
SC
IV
50.3
44.6
10.8
3.10
34.2
33.3
Cells
CFSE
% Lysis of βGal-Pulsed Targets
*
**
SC
IV
Liver
Spleen

Figure 2.3 Liver-primed $CD8^+$ T cells are defective in cytolytically killing target cells *in vivo*. (**a,b**) SIINFEKL-pulsed ($CFSE^{lo}$) and ICPMYARV-pulsed ($CFSE^{hi}$) target splenocytes were transferred into naïve, D7 IV Ad-LacZ infected, or D7 SC Ad-LacZ infected mice at a 1:1 ratio. Percent lysis of specific targets was determined in the livers and spleens of recipient mice 18 hrs post-transfer (n = 3 per group). Numbers in the histograms represent percentages. Mean ± s.e.m.; $*P < 0.05$ and $**P < 0.01$.

Acknowledgments

John Lukens of St. Jude Children's Research Hospital was the first to characterize functional differences between $CD8^+$ T cells from SC and IV adenovirus infections. His graduate work at the University of Virginia laid the foundation to subsequent projects described in chapters 4 and 5. NIH Grants DK063222, U19 AI083024, and Immunology Training Fellowship T32 AI07496 supported this work.

Methods

Animals, Infections, and Treatments

C57BL/6 mice were used in these experiments (Taconic Farms, Hudson, NY). *Thy1.1*$^{+/-}$OT-I*(Tcra/Tcrb)*$^{+/-}$ mice were bred from *Thy1.1*$^{+/+}$ and OT-I *(Tcra/Tcrb)*$^{+/+}$*Rag1*^{tm1Mom} mice (Taconic Farms). Animals used were 6 to 10 weeks of age and housed in a pathogen-free facility under protocols approved by the Institutional Animal Care and Use Committee at the University of Virginia (Charlottesville, VA).

Replication-deficient type 5 adenoviruses lacking the *E1* and *E3* genes and expressing the ovalbumin protein (Ad-Ova), β-galactosidase protein (Ad-LacZ), and tyrosinase protein (Ad-Tyr) under the control of the human *Cmv* promoter (Ad-Ova) were provided by Timothy L. Ratliff (Iowa Gene Transfer Vector Core, University of Iowa, Iowa City, IA), Gregory A. Helm (University of Virginia, Charlottesville, VA), and Lisa H. Butterfield (University of Pittsburgh, Pittsburgh, PA), respectively. Mice were infected with 2.5×10^7 infectious units (IU) Ad-Ova via intravenous (IV) injection in the caudal vein or subcutaneous (SC) injection in the left flank.

Liver and Spleen Mononuclear Cell Isolation

Mononuclear cells were isolated from livers and spleens according to previous work[46,116,117]. Briefly, livers were flushed via the portal vein with 0.05% collagenase IV (Sigma-Aldrich, St. Louis, MO) in 1×PBS and washed with Iscove's Modified Dulbecco's Medium (IMDM) containing 10% newborn calf serum. Liver tissue was then homogenized and further digested with 0.05% collagenase IV in 1×PBS. Mononuclear cells were then isolated via Histodenz (Sigma-Aldrich) gradient centrifugation, and the

number of viable cells was determined based on 0.1% Trypan blue (Sigma-Aldrich) exclusion. Whole spleens were harvested, and mononuclear cells were isolated over a Ficoll (Atlanta Biologicals, Lawrenceville, GA) gradient.

In Vivo Cytotoxicity Assay

C57BL/6 splenocytes were pulsed with 2 μg/mL SIINFEKL or ICPMYARV peptide (AnaSpec, Fremont, CA). SIINFEKL-pulsed cells were labeled with 0.2 μM CFSE ($CFSE^{lo}$) and ICPMYARV-pulsed cells were labeled with 2.0 μM CFSE ($CFSE^{hi}$) (Invitrogen, Carlsbad, CA). 20×10^6 mixed splenocytes were transferred IV into naïve, D7 IV Ad-LacZ infected, or D7 SC Ad-LacZ infected mice at a 1:1 ratio ($CFSE^{lo}$:$CFSE^{hi}$). After 18 hrs, liver and spleen mononuclear cells were harvested and the percent lysis of βGal-pulsed targets was determined according to the following formulas[118]:

$$\text{ratio} = (\%\ CFSE^{lo}/\%\ CFSE^{hi})$$

$$\%\ \text{specific lysis} = [1 - (\text{ratio}^{unprimed}/\text{ratio}^{primed})] \times 100$$

Flow Cytometry

The following mAbs were used for cell surface and intracellular staining: anti-CD11b PE-Cy7 (M1/70), anti-CD19 PE (1D3), anti-CD25 APC (PC61), anti-Ly6C APC-Cy7 (AL-21), anti-Ly6G PE (1A8) (BD Biosciences, Franklin Lakes, NJ), anti-CD105 PE (MJ7/18), anti-CD146 AF488 (ME-9F1) (BioLegend, San Diego, CA), anti-B220 PerCP-Cy5.5 (RA3-6B2), anti-CD3ε PerCP-Cy5.5 (145-2C11), anti-CD4 PE (RM4-5), anti-CD8α APC-eF780 (53-6.7), anti-CD11c PerCP-Cy5.5 (N418), anti-CD45 eF450 (30-F11), anti-CD103 PE (2E7), anti-F4/80 APC (BM8), anti-IFN-γ APC (XMG1.2), anti-IL-2 AF488 (JES6-5H4), anti-MHC II (I-A/I-E) FITC (M5/114.15.2), anti-NK1.1 FITC (PK136), anti-NKp46 eF660 (29A1.4), anti-Thy1.2 eF450 (53-2.1), anti-TNF-α PE (MP6-XT22)

(eBioscience, San Diego, CA). Live cells were identified using the Aqua Live/Dead Fixable Dead Cell Stain Kit (Invitrogen). CD1d tetramer containing α-galactosylceramide was used to identify NKT cells (NIH Tetramer Core Facility, Emory University, Atlanta, GA). Cell surface staining of 1.5×10^6 mononuclear cells was performed by first blocking with anti-CD16/CD32 (2.4G2) (Lymphocyte Culture Center, University of Virginia, Charlottesville, VA) followed by specific antibody labeling for 15 min at 4°C in FACS Buffer (1×PBS containing 2% fetal bovine serum and 0.1% NaN_3). Cells were fixed in BD Cytofix/Cytoperm (BD Biosciences). For intracellular cytokine detection, cells were re-stimulated with 2 μg/mL SIINFEKL peptide (AnaSpec), blocked with 1 μL/mL GolgiPlug and 1 μL/mL GolgiStop, and permeabilized with BD Perm/Wash (BD Biosciences). Data were collected on a BD FACS Canto II (BD Immunocytometry Systems, San Jose, CA) and analyzed using FlowJo 8.8.6 software (Tree Star Inc., Ashland, OR).

Statistical Analysis

Significant differences between experimental groups were calculated using the two-tailed Student's t test. Data analysis was performed using Prism 5.0a software (GraphPad Software Inc., La Jolla, CA). Values of $P < 0.05$ were regarded as being statistically significant and noted as * < 0.05 and ** < 0.01.

CHAPTER 3

Rationale and Research Aims

Aim 1: Describe the Kinetics of IL-10, PD-1/PD-L1, Tim-3/Gal-9 Expression During Intrahepatic Viral Infection

Numerous studies report that the IL-10, PD-1, and Tim-3 inhibitory pathways contribute to $CD8^+$ T cell exhaustion during chronic viral infection. Because higher hepatitis C virus (HCV) titers correlate directly with IL-10, fibrosis correlates indirectly with exogenous IL-10 therapy, and numerous studies link certain IL-10 promoter polymorphisms with different clinical outcomes, the IL-10 pathway is central to understanding liver immunology against acute and persisting viruses[52]. In addition, intrahepatic $CD8^+$ T cells produce IL-10 during HCV infection, which to date has not been assigned a specific immunological function[53,54]. With regards to PD-1 and Tim-3, chronic HCV patients have elevated PD-1 and Tim-3 levels on the surface of dysfunctional $CD8^+$ T cells in liver biopsies and peripheral blood samples. *In vitro* blockade of the PD-1/PD-L1 and/or Tim-3/Gal-9 interaction results in enhanced early IL-2/TNF-α production, later IFN-γ production, and proliferation of the HCV-specific $CD8^+$ T cells[71,75,89]. As the balance between these pathways determines the outcome of immune responses to viruses in the liver, their kinetics were first characterized during murine intrahepatic viral infection. With this detailed kinetic analysis, I was better able to address at what time points in the immune response that these pathways functioned.

Since HCV infection only occurs in humans and chimpanzees, I employed an adenovirus murine model to study the early and late kinetics of an acute infection. Adenovirus

infection is targeted to hepatocytes after intravenous (IV) infection, and the early role of inhibitory signaling likely mirrors HCV infection as evidenced by the presence of dysfunctional antiviral CD8$^+$ T cells responding to both viruses (**Fig. 2.2** and **Fig. 2.3**). I hypothesized that early global IL-10 and PD-1/PD-L1 and later Tim-3 presence would characterize the liver microenvironment. The kinetics emulated each other on distinct cell types (particularly the CD8$^+$ T cell) closely since the pathways likely synergized. Further, I also found there was initial burst of IL-10 production from innate immune cells including antigen presenting cells (APCs) such as dendritic cells (DC) and Kupffer cells (KC). Early expression of PD-L1, but not Tim-3, was found on multiple APC types including hepatocytes and liver sinusoidal endothelial cells (LSEC) during this investigation. These analyses also characterized the existence of IL-10-producing, PD-1/PD-L1$^+$Tim-3$^+$CD8$^+$ T cells arising at day 7 (D7) and evaluated their behavior in the context of viral infection of the liver at later time points. After this information was collected and analyzed, I was better able to manipulate my model system via siRNA and antibody-mediated blockade approaches in an effort to determine the effects IL-10, PD-1, and Tim-3 signaling had during early and late phase kinetics with respect to the effector function of virus-specific CD8$^+$ T cells.

Aim 2: Determine the Role of PD-1/PD-L1 Signaling in Early Immunosuppression of NK and CD8$^+$ T Cell Responses Post-Adenovirus Infection

Baseline expression of PD-L1 is found on liver-resident KCs. After hepatic viral infection, high levels of PD-L1 expression on KCs, LSECs, non-resident macrophages (Mø), DCs, natural killer (NK) cells, T cells, and low levels by hepatocytes are observed[65,67]. Further, PD-1 signaling directly inhibits downstream T cell receptor (TCR)

signaling in T cells[61,119,120] and activation of NK cells[121-124]. IV infection with both replication-deficient adenovirus and replication-sufficient MCMV expressing ovalbumin was the model system used in the study of the intrahepatic antiviral immune response.

Blockade of PD-L1 was achieved by delivering PD-L1 siRNA encapsulated in cationic lipidoid nanoparticles (LNP) *in vivo*. Since hepatocytes, KCs, LSECs, non-resident Møs, and DCs play a role in initiating intrahepatic tolerance through PD-1/PD-L1[65,70,73,125], two different formulations of LNP were used: hepatocyte-targeted and myeloid-targeted. Based on the targeting of each drug, the role PD-L1 played on different cell types and the time during which the inhibitory signal initiates immune dysfunction during early intrahepatic viral infection was delineated.

I hypothesized that *in vivo* PD-L1 siRNA-based therapy targeted to myeloid cells in the liver would enhance $CD8^+$ T cell effector function through downregulation of PD-L1. I also expanded my studies by examining NK cells as PD-1 expression on these cells correlates with human disease in chronic HCV patients[126] and other infectious and cancer models[122,123]. I demonstrated KCs preferentially engulfed PD-L1 LNP, and I am the first to show *Pdl1* silencing in the liver resulted in improved NK and $CD8^+$ T cell responses, viral clearance, and $CD8^+$ T cell memory. These data provide a promising NK and $CD8^+$ T cell nucleic acid therapy applicable to ongoing liver-tropic viral infections and hepatocellular carcinoma, vaccine development, and may also be pertinent to other diseases outside the liver governed by similar pathways and cell types.

Aim 3: Characterize the Contribution of Tim-3 Negative Co-Stimulatory Receptor to Regulation of Hepatic Immunity During the Late Phase of Viral Infection

The role of early IL-10 production from APCs was detected, but not explored during the course of these experiments. In addition, Tim-3 expression was not observed on non-T cells in my model system. However, the $CD8^+$ T cells expressed PD-1/PD-L1, Tim-3, and produced IL-10 by D7 to D11 post-infection with adenovirus. Since intrahepatic $CD8^+$ T cells are predicted to have regulatory properties after HCV infection[53,54], I first demonstrated this phenomenon translated within the population of liver-primed $CD8^+$ T cells after adenovirus infection. Indeed, the adenovirus-specific $CD8^+$ T cells acquired a *bona fide* T regulatory (T_{reg}) cell phenotype. These $CD8^+$ T_{reg} cells suppressed naïve OT-I cell proliferation *in vitro* and *in vivo*.

I originally hypothesized that antiviral intrahepatic $CD8^+$ T cells had self-limiting T_{reg} cell properties dependent on their secretion of IL-10, Gal-9, and/or expression of PD-L1. The PD-1/PD-$L1^+$$Tim\text{-}3^+$$CD8^+$ T cells accordingly did not produce Gal-9; moreover, IL-10, PD-L1, and Gal-9 antibody blockades indicated these pathways were not linked to the suppressor mechanism. Interestingly, suppression was dependent on surface expression of Tim-3. Tim-3 acted intrinsically on the $CD8^+$ T_{reg} cell as determined by anti-Tim-3 antibody pre-coating during experimentation and lack of Tim-3 expression on responder $CD8^+$ OT-I T cells.

Tim-3 was recently discovered to bind a novel moiety, HMGB-1, within DCs via its FG cleft preventing tumor-derived RNA/DNA activation[103]. Thus, I formed an alternative hypothesis predicting $CD8^+$ T_{reg} cell surface Tim-3 acted as a decoy receptor, sequestering HMGB-1. I identified a novel mechanism whereby $CD8^+$ T effector (T_{eff})

cell proliferation was negatively affected by the binding and sequestration of HMGB-1 by Tim-3 displayed on intrahepatic $CD8^+$ T_{reg} cells. Contrasting the PD-1/PD-L1-dependent dysfunction observed during the early phase of the immune response to intrahepatic viral infection, Tim-3 negative signaling proved dominant over IL-10 and PD-1/PD-L1 immunoregulation throughout late phase kinetics. Since my model employed adenovirus and a study of acute viral infection, this mechanism may be instrumental in future studies in understanding how acute infection in the liver facilitates the onset of chronic infection.

CHAPTER 4

Lipidoid Nanoparticles Containing PD-L1 siRNA Delivered *In Vivo* Enter Kupffer Cells and Enhance NK and $CD8^+$ T Cell-Mediated Hepatic Antiviral Immunity

Abstract

Effective clinical application of antiviral immunotherapies necessitates enhancing the functional state of natural killer (NK) and $CD8^+$ T cells. An important mechanism for the establishment of viral persistence in the liver is the activation of the PD-1/PD-L1 inhibitory pathway. To examine the role of hepatic myeloid PD-L1 expression during viral infection, I determined the magnitude and quality of antiviral immune responses by administering PD-L1 siRNA encapsulated in lipidoid nanoparticles (LNP) in mice. My studies indicate that Kupffer cells (KC) preferentially engulfed PD-L1 LNP within a short period of time and silenced *Pdl1* during adenovirus and MCMV infection leading to enhanced NK and $CD8^+$ T cell intrahepatic accumulation, effector function (IFN-γ and granzyme B production), $CD8^+$ T cell-mediated viral clearance, and memory. My results demonstrate that PD-L1 knockdown on KCs is central in determining the outcome of liver viral infections, and they represent a new class of gene therapy.

Introduction

The liver maintains a tolerogenic environment from constant exposure to food-derived antigens and bacterial constituents such as lipopolysaccharide via portal blood. While the generation of immune responses including NK and $CD8^+$ T cells clears virus, persistent viral infections such as those by hepatitis C virus (HCV) often take advantage of hepatic tolerance inducing impaired NK and $CD8^+$ T cell responses through activation of negative immunoregulatory pathways[23]. As chronic liver infections including HCV exploit tolerance and remain a worldwide health problem, investigation of these inhibitory pathways and development of novel therapeutic biotechnologies is warranted[31,32,127].

Programmed death 1 (PD-1), a CD28 family member, plays a critical role in suppressing NK and $CD8^+$ T cell responses[72,74,122,123,128-130]. PD-$1^{-/-}$ mice exhibit hyperactive immune responses and develop lymphoproliferative/autoimmune disorders including lupus-like syndrome, arthritis, dilated cardiomyopathy, gastritis, diabetes, hydronephrosis, and graft-versus-host-like disease[61,74,131,132]. PD-1 signaling directly inhibits downstream T cell receptor (TCR) signaling in T cells[61,119,120] and activation of NK cells[121-124]. Baseline expression of PD-1 ligand (PD-L1) is found on liver-resident KCs. After hepatic viral infection, high levels of PD-L1 expression on KCs, liver sinusoidal endothelial cells (LSEC), non-resident macrophages (Mø), dendritic cells (DC), NK cells, T cells, and low levels by hepatocytes are observed[65,67]. Monoclonal antibodies are typically used to block PD-1/PD-L1 negative signaling, but antibodies that interfere with immune suppression sometimes cause off-target side effects seen in clinical trials where ongoing autoimmune diseases similar to those found in PD-$1^{-/-}$ mice are exacerbated[133,134].

Since the discovery of RNA interference (RNAi) by Fire and Mello in 1998[135], short interfering RNA (siRNA) technology is promising in the clinical setting as specific and potent degradation of mRNA target sequences has been achieved *in vivo*[136-138]. Thus far, *in vitro* electroporation of naked PD-L1 siRNA in DCs has been shown to effectively boost their ability to prime T cell responses in a cancer model[139]. Achieving activity in the *in vivo* setting has proven difficult because the use of siRNA as a drug violates the 'Lipinski rules' due to its large size (over 13 kDa), high electrostatic charge (~40 anionic charges on the phosphodiester backbone), and short half-life due to nucleases[140]. As a result, much effort has not only been dedicated to applying siRNA chemical modifications to prevent immunostimulation and increase stability and specificity but also delivery systems. In this study, I tested a novel strategy for controlling *Pdl1* expression through delivery of PD-L1 siRNA encapsulated in a cationic lipidoid nanoparticle (LNP) as the vehicle targeting myeloid cells[141,142]. Previous work with virally infected PD-1$^{-/-}$ mice showed the global absence of PD-1 signaling is characterized by improved immune responses, proliferation, and antigen clearance[65], but the major cell source of PD-L1 and timing of PD-1 signaling is controversial. In contrast, targeted silencing of *Pdl1* in the major disease-causing cell type reduces off-target effects, and the transient nature of PD-L1 siRNA silencing over the use of PD-1$^{-/-}$ and PD-L1$^{-/-}$ mice eliminates the potential of overlapping hyperactive immune responses.

I hypothesized that *in vivo* PD-L1 siRNA-based therapy targeted to myeloid cells in the liver would improve NK and CD8$^+$ T cell responses to localized viral infections. I demonstrate KCs preferentially engulf PD-L1 LNP and are the first to show *Pdl1* silencing in the liver results in improved NK and CD8$^+$ T cell responses, viral clearance, and CD8$^+$ T cell memory. These data provide a promising NK and CD8$^+$ T cell nucleic

acid therapy applicable to ongoing liver-tropic viral infections and hepatocellular carcinoma, vaccine development, and may also be pertinent to other diseases outside the liver governed by similar pathways and cell types. Further, targeting PD-L1 for transient knockdown directly on the disease-causing cell type may be beneficial over monoclonal antibody usage.

Results

Administration of PD-L1 siRNA LNP Abrogates PD-L1 Expression by Kupffer Cells

The nanoparticles in this study were optimized by *in vitro* selection from hundreds of compounds and formulated using C12-200 lipid (**Fig. 4.1**), disteroylphosphatidyl choline, cholesterol, PEG-DMG, and siRNA at a lipid:siRNA weight ratio of 7:1[141]. Due to the cationic nature of LNPs, I hypothesized that highly phagocytic Møs and DCs are key targets *in vivo*, which is supported by a recent study in uninfected rodents and nonhuman primates[142]. Animals were intravenously (IV) injected with fluorochrome-labeled siRNA LNP at day 5 (D5) post-infection with adenovirus (a time point at which most immune cell types, innate and adaptive, are present), and uptake was determined in LSEC, KC, infiltrating monocyte/Mø, DC, CD4$^+$ T cell, CD8$^+$ T cell, and NK cell populations. KCs proficiently engulfed the siRNA LNP over all other cells types examined (**Fig. 4.2a**). Further, only the KCs had internalized the siRNA LNP in perinuclear vesicles (**Fig. 4.2b**) and had the highest fluorescent internalization score (data not shown).

The specific PD-L1 siRNA was selected from 30 candidate sequences, chemically modified to enhance specificity and potency, and formulated into LNPs (PD-L1 LNP). I delivered 0.5 mg/kg PD-L1 LNP IV every other day starting one day prior to infection as pharmacodynamics indicated that this was an appropriate dose for gene silencing[142]. *Pdl1* knockdown was initially confirmed from D5 to D7 in infected livers using luciferase LNP (Luc LNP) as a control (**Fig. 4.3a**). Western blot analysis of total liver PD-L1 also revealed similar kinetics (**Fig. 4.3b**).

I next sought to determine if *Pdl1* silencing was occurring within KCs via an RNAi mechanism. The designed antisense PD-L1 siRNA strand binds positions 932-950 of exon 7 in *Pdl1* with predicted cleavage occurring between positions 940-941 (**Fig. 4.3c**). A 5'-rapid amplification of cDNA ends (5'-RACE) assay performed on total RNA isolated from FACS-sorted KCs established specific and potent silencing of *Pdl1* was occurring via RNAi through detection of the ~250-bp *Pdl1* cleavage product, confirmed by sequencing (**Fig. 4.3d**). Enumeration of sequences revealed that PD-L1 LNP induced cleavage in 93.3% (14/15) of the clones (**Fig. 4.4**). To determine if direct silencing correlated with PD-L1 protein on the surface of antigen presenting cells (APC), PD-L1 surface expression was analyzed on KC, infiltrating monocyte/Mø, and DC populations. Consistent with siRNA LNP uptake data, the most efficient knockdown was observed in KC populations. Similar to reduced uptake capacity by infiltrating monocytes/Møs and DCs, these cells showed modest or no PD-L1 knockdown. KCs had about a two-fold higher level of surface PD-L1 per cell compared to other monocyte/Mø/DC populations (**Fig. 4.3e,f**).

Imaging studies revealed that hepatocytes did not upregulate PD-L1 to any noticeable level post-infection as observed on $F4/80^+$ (KCs) and $CD105^+$ (LSECs) cells (**Fig. 4.5**). Though some PD-L1 knockdown was seen in LSECs, this appeared to be unrelated to direct *Pdl1* silencing as the detectable biodistribution of siRNA LNP excluded these cell types (**Fig. 4.2**). Perhaps microscopic techniques are not sensitive enough to detect low PD-L1 levels, which were observed directly *ex vivo* on non-KCs in these experiments and hepatocytes by Wahl *et al.*[143] or after culture with IFN-γ[144].

To ensure the LNP itself was not drastically altering the maturation status of KCs, CD40, CD80, and CD86 expression was determined on professional hematopoietic APC populations. CD40 and CD86 remained unaltered by Luc LNP, but CD80 was slightly elevated by the LNP on monocyte/Mø and DC populations (**Fig. 4.6**). Together, these data suggest that KCs primarily engulf PD-L1 LNP during viral infection. Unpackaging of PD-L1 siRNA leads to direct RNAi-mediated silencing of *Pdl1* and downregulation of PD-L1 surface expression.

PD-L1 LNP Treatment Augments NK Cell and Antigen-Specific CD8$^+$ T Cell Accumulation, Effector Function, and Memory

Since KCs play a role in initiating intrahepatic tolerance through PD-1/PD-L1[65,125], I hypothesized that CD8$^+$ T cell effector function would be enhanced through downregulation of PD-L1. I also expanded my studies by examining NK cells as PD-1 expression on these cells correlates with human disease in chronic HCV patients[126] and other infectious and cancer models[122,123]. Employing two different hepatic viruses expressing ovalbumin (adenovirus and MCMV), initial analysis of the liver homogenates revealed a significant increase in the number of mononuclear cells isolated following infection after PD-L1 LNP treatment (**Fig. 4.7**). NK cell absolute numbers peaked at D5 and displayed an enhanced kinetic profile after *Pdl1* silencing with both viruses (**Fig. 4.8a**) and produced more granzyme B (GrB) and PMA/ionomycin-induced IFN-γ (**Fig. 4.8b,c**). Improvements in NK cell function were limited to the Thy1.2$^+$ subset. Gating on the entire NK cell population did not reveal any significant trends in effector function.

Furthermore, Ova-specific CD8$^+$ T cell absolute number peaked at D7 and enhanced accumulation to both infections was observed with PD-L1 LNP treatment (**Fig. 4.9a**).

Bulk $CD8^+$ T cell GrB was statistically improved by D5 and continued into D7 where Ova-specific $CD8^+$ T cell GrB was also elevated. In contrast, there was no drastic increase in SIINFEKL peptide-induced IFN-γ by $CD8^+$ T cells following PD-L1 LNP treatment (**Fig. 4.9b,c**). Despite the incomplete acquirement of effector function, $CD8^+$ T cells accumulated/expanded in the liver within distinct clusters of mononuclear cells. The number of foci was significantly higher after PD-L1 LNP treatment at D7 post-Ad-Ova infection, coinciding with the peak in T cell kinetics (**Fig. 4.10a**). The $CD8^+$ T cells in the clusters were associated with MHC II^+ cells, $CD4^+$ T cells, $B220^+$ B cells, and $NKp46^+$ NK cells (**Fig. 4.10b**). At D7 post-Ad-Ova infection, intrahepatic Ova-specific $CD8^+$ T cells were proliferating greater *in situ* following PD-L1 LNP treatment as indicated by Ki-67 staining (**Fig. 4.10c**). When infection was carried out to D40, more Ova Tet^+CD8^+ T cells accumulated in the liver and draining celiac lymph nodes (C LN) but not the spleens and non-draining inguinal lymph nodes (Ig LN) from PD-L1 LNP-treated animals (**Fig. 4.10d**). The Ova Tet^+CD8^+ T cells in the D40 liver were notably $CCR7^-CD62L^-$ (data not shown) and also underwent slightly more pronounced homeostatic cell division incorporating more BrdU (**Fig. 4.10e**). Collectively, these data demonstrate that PD-L1 LNP treatment prior to and during the course of viral infection leads to a superior NK cell and antigen-specific $CD8^+$ T cell response in the acute phase and greater $CD8^+$ T cell memory at later stages.

$CD8^+$ T Cell-Dependent Hepatic Viral Clearance is Enhanced by PD-L1 Pathway Blockade

To test whether silencing of *Pdl1* led to improved viral clearance, hepatocytes were labeled with anti-pancytokeratin (panCK) and anti-Ova antibodies. Virally infected

hepatocytes (panCK$^+$Ova$^+$) could be detected out to D5 in Luc LNP treatment groups and were undetectable in PD-L1 LNP-treated animals (**Fig. 4.11a**). When enumerating the number of infected hepatocytes per mm^2 liver tissue, this difference was statistically significant (**Fig. 4.11b**). Total RNA was also isolated, and *Ova* transcript in Luc LNP and PD-L1 LNP groups was compared at D5 post-infection confirming microscopy results (**Fig. 4.11c**).

Importantly, hepatocytes showed improved structural integrity in PD-L1 LNP-treated mice. This was observed with changes in intermediate-sized filament organization and overall integrity of the hepatocytes. In both naïve and PD-L1-treated animals, intermediate-sized filaments were radially distributed extending from the nucleus to the plasma membrane, and hepatocytes maintained a cuboidal structure. Microtubules, microfilaments, and intermediate-sized filaments are all known to be either disrupted or reorganized during the course of viral infection. In this viral model, Ad-Ova led to a condensation of intermediate-sized filaments, disrupted plasma membrane integrity, and atrophic appearance of hepatocytes. Further, sinusoidal arrangement was altered by Ad-Ova as noted in the anti-CD105 stain. These structural changes were all reversed by PD-L1 LNP almost to the extent where the infected liver microstructure appeared as seen in a naïve liver (**Fig. 4.11a**).

NK cells and CD8$^+$ T cells are largely responsible for clearing virally infected cells in various situations. As responses from these two populations were clearly enhanced by PD-L1 LNP, I next sought to dissect the role played by each cell type for viral clearance. To determine if CD8$^+$ T cells played a role in viral clearance in the liver, mice were given anti-CD8 antibody intraperitoneally (IP) (**Fig. 4.12**). Anti-CD8 antibody treatment had no

effect on D5 viral clearance in Luc LNP-treated animals, but it significantly increased viral load in the PD-L1 LNP treatment group back to levels comparable to untreated or anti-CD8 antibody/Luc LNP-treated animals (**Fig. 4.11c**). Presumably, any residual viral clearance mediated by NK cells was unrelated to siRNA LNP treatment as all enhanced viral clearance due to silencing PD-L1 could be accounted for by the depletion of $CD8^+$ T cells.

Serum alanine aminotransferase (ALT) was significantly increased in PD-L1 LNP-treated animals by D7 (**Fig. 4.13a**). According to a histological analysis of H & E-stained liver sections between D5 and D7, much of the liver was necrotic at D5 (evidenced by vacant spaces between reticulin networks where hepatocytes reside), and signs of hepatocyte regrowth were apparent in both Luc LNP and PD-L1 LNP treatment groups by D7 (**Fig. 4.13b**). The increased ALT in the PD-L1 LNP treatment group directly correlated with the boosted $CD8^+$ T cell absolute number. Indeed, this rise in ALT is the result of transient liver damage as histological studies indicated liver regrowth, but no mortality of mice was observed associated with hepatic injury up to D40 after treatment.

The immunoregulatory function NK cells have on $CD8^+$ T cell responses has been recently reported[124,145,146]. Based on my finding that both NK cell and $CD8^+$ T cell absolute numbers on D5 after infection were increased following PD-L1 LNP treatment (**Fig. 4.8a** and **Fig. 4.9a**) and had a proximal cellular localization on leukocyte aggregates (**Fig. 4.10b**), I hypothesized that cross-talk between NK and $CD8^+$ T cells was occurring, thereby enabling NK cells to influence the generation of $CD8^+$ T cell responses. To test this possibility, I made use of the NKDTR-EGFP mouse. This strain contains a transgene comprised of the 400-bp human *Nkp46* promoter, human

diphtheria toxin (DT) receptor (DTR), and EGFP[147]. When DT is IP injected into these mice selective ablation of NK cells is achieved in either the Luc LNP- or PD-L1 LNP-treated groups (**Fig. 4.14a**). In mice that had received DT, the CD8$^+$ T cell response was completely absent beginning at D5 in either Luc LNP- or PD-L1 LNP-treated mice when Ova-specific T cells first appeared in the liver (**Fig. 4.15a**). The *Nkp46* construct did appear to be mostly specific towards NK cells, but a very small subset of the CD8$^+$ T cells appeared to express the transgene at a low level (**Fig. 4.14b**). To rule out that DT administration was not simply depleting the T cells, congenically mismatched Thy1.1$^+$CD8$^+$ OT-I T cells were transferred into the NKDTR-EGFP mice 24 hours prior to drug treatment and infection. In this scenario, the CD8$^+$ T cells did not expand efficiently when DT was given (**Fig. 4.15b**). This suggests that the NK cells induced by viral infection have a fundamental role in CD8$^+$ T cell priming, irrespective of PD-1/PD-L1 signaling. This is repeatable with anti-NK1.1 depleting antibody (data not shown) and has been shown in the past to be IFN-γ dependent[148]. The increase in NK cell absolute number and increased effector activity may contribute to the enhancement in Ova Tet$^+$CD8$^+$ T cell numbers after PD-L1 LNP treatment. Nevertheless, these results confirm that PD-L1 LNP, like anti-PD-L1 antibody, is able to hasten viral clearance in a CD8$^+$ T cell-dependent manner.

Pdl1-Silenced KCs Directly Improve CD8$^+$ T Cell Expansion and Effector Function

I next examined whether *Pdl1*-silenced KCs directly affected CD8$^+$ T cell effector function. Treatment with PD-L1 LNP was therefore conducted at D5 post-infection. D5 marks the point when NK cells reach their maximum influx in the liver and begin to decline (**Fig. 4.8a**). As expected, when PD-L1 LNP was administered at D5, Ova

Tet^+CD8^+ T cells increased in number for both infections (**Fig. 4.16a**) and they produced significantly more IFN-γ and GrB (**Fig. 4.16b,c**). Delayed PD-L1 LNP treatment still enhanced viral clearance at D7 (**Fig. 4.17**). Collectively, these data imply enhanced viral clearance due to PD-L1 LNP is $CD8^+$ T cell-mediated.

In order to verify this phenotype was due to the presence of *Pdl1*-silenced KCs, clodronate liposomes were IV injected at D3 in order to specifically deplete this population before siRNA LNP delivery at D5. KCs were successfully depleted at a 55 mg/kg clodronate liposome dosage while other monocyte/Mø/DC populations remained unaffected (**Fig. 4.18**). Control liposomes had no effect on $CD8^+$ T cell infiltrate, as a D5 PD-L1 LNP treatment was able to improve Ova-specific $CD8^+$ T cell absolute number comparable to **Fig. 4.16a**. In contrast, depletion of KCs at D3 post-infection with Ad-Ova, regardless of Luc or PD-L1 LNP treatment, resulted in a slight decrease of the Ova-specific $CD8^+$ T cell percentage and absolute number (**Fig. 4.19a**). Similar results were also observed in mice that received no siRNA LNP at D5 (data not shown), ruling out some unknown chemical reaction was occurring between the lipidoid nanoparticle coating containing the siRNA and liposomal membranes surrounding the clodronate. These data suggest KCs are involved in supporting the expansion of virus-specific $CD8^+$ T cells.

In addition, I examined Ova-specific $CD8^+$ T cell effector function in the liver during viral infection by analyzing the production of IFN-γ and GrB. After control liposome administration, IFN-γ production in the PD-L1 LNP group was significantly elevated compared to the Luc LNP group. Furthermore, depletion of KCs by clodronate treatment significantly improved Ova Tet^+CD8^+ T cell IFN-γ production by percentage regardless of

Luc or PD-L1 LNP treatment. IFN-γ MFI also followed a similar trend (**Fig. 4.19b**). Ova Tet^+CD8^+ T cell GrB was not improved via clodronate-mediated KC depletion (data not shown). These results suggest that KCs are a major contributor to regulating $CD8^+$ T cell effector function, in particular, the production of IFN-γ through PD-1/PD-L1 signaling.

Discussion

In this report, I demonstrate that the *in vivo* delivery of PD-L1 siRNA contained within LNPs resulted in specific and potent RNAi-mediated silencing of *Pdl1* mRNA within KCs. During the course of hepatotropic viral infection, KCs preferentially engulfed PD-L1 siRNA encapsulated in LNPs. PD-L1 siRNA escape from small perinuclear vesicles can occur as the cationic properties of the LNP form electrostatic interactions with the anionic lipids of endosomes disrupting membrane integrity (ion-pairing model) leading to an acidified pH where the osmotic pressure from influxing water causes endosomes to swell and rupture (proton sponge effect)[138,149,150]. Depending on the timing of siRNA LNP administration, either before or after the peak in NK cell accretion, *Pdl1* silencing improved NK cell or virus-specific $CD8^+$ T cell effector function. The optimal priming and expansion of $CD8^+$ T cells required NK cell help, but an enhanced, non-redundant role in viral clearance due to PD-L1 downregulation was highly dependent on $CD8^+$ T cell presence. To my knowledge this is the first successful application of *in vivo* siRNA delivery in modulating the immune response in the liver.

The critical role of the KC PD-L1 in impairing $CD8^+$ T cell responses has been well established during hepatic viral infection[46,65] and hepatocellular carcinoma[125]. Notably, my studies demonstrate that viral infection-induced PD-L1 expression is at the highest level per cell on KCs, but low levels of PD-L1 were detected on the surface of LSECs, Møs, and DCs. The precise role of LSEC PD-L1 in antiviral responses still remains unclear because PD-L1 LNP does not achieve differential KC versus LSEC PD-L1 protein knockdown. A recent report by Mueller *et al.* indicated the contribution of hematopoietic versus non-hematopoietic PD-L1 expression to the generation of T cell

responses against LCMV CL-13 infection. In the lungs and spleens of infected animals, hematopoietic cells from PD-L1$^{-/-}$ mice led to improvements in the magnitude and effector function of T cells, whereas non-hematopoietic cells from PD-L1$^{-/-}$ mice separately improved viral clearance. Interestingly, livers in these animals showed different results such that PD-L1$^{-/-}$ on hematopoietic cells was sufficient to improve both T cell responses and viral clearance. Although PD-L1$^{-/-}$ on non-hematopoietic cells seemed to slightly improve liver viral clearance, viral clearance was not optimal unless a global knockdown of PD-L1 was achieved[151]. When KCs were selectively depleted with clodronate liposomes in these series of experiments, CD8$^+$ T cell expansion was diminished, IFN-γ production was improved in Ova-specific CD8$^+$ T cells responding to infection, and GrB was unaltered. Although I cannot rule out the possibility that other cells including inflammatory monocytes/Møs/DCs play a role in boosting CD8$^+$ T cell responses to viral infection in the liver via the PD-1/PD-L1 signaling pathway, these results suggest that KCs are a major contributor to regulating CD8$^+$ T cell expansion and IFN-γ production. Combined, these findings favor the notion that PD-L1 expressed by KCs is central in regulating NK and T cell responses to viruses in the liver.

Prior research has also demonstrated that hepatocyte PD-L1 can directly dampen effector CD8$^+$ T cell responses *in vitro*[143]. Hepatocyte PD-L1 does not play a drastic role in dampening NK and CD8$^+$ T cell responses to adenovirus and MCMV because I have tested another siRNA nanoparticle formulation whereby the PD-L1 siRNA was targeted for uptake specifically by hepatocytes (data not shown). In this case, the nanoparticles were designed to preferentially bind low density lipoprotein (LDL) in circulation, and through LDL receptor-mediated endocytosis, nanoparticles are internalized by interaction with apolipoprotein B100, a protein largely expressed by hepatocytes[152].

Consistent with a low level or lack of PD-L1 expression by hepatocytes after Ad-Ova infection in mice (**Fig. 4.5**), this hepatocyte-specific targeting system did not result in enhanced absolute number or functional data pertaining to total mononuclear cells, NK cells, or T cells (data not shown). In lieu of research performed by Mueller *et al.*, hepatocyte PD-L1 may dampen viral clearance, but it does not appear critical in preventing the priming or expansion of the immune response.

My studies demonstrate that *Pdl1* silencing in KC populations improves NK cell and $CD8^+$ T cell accumulation and function. Upon *Pdl1* silencing at the early phase of viral infection, NK cell functional improvements were limited to the $Thy1.2^+$ population at D5. Interestingly, the Thy1 surface protein has been recently shown to be a NK cell memory marker where Gillard *et al.* found that $Thy1^+$ NK cells protect mice from secondary vaccinia viral infection, are more functional *in vitro*, and expand better when transferred into congenic animals[153]. Although the function of Thy1 has not been fully elucidated, it is believed to be involved with cell-cell interaction and extracellular matrix binding in T cells providing a TCR-independent activation signal[154].

Potential mechanism(s) for superior NK and $CD8^+$ T cell responses by PD-L1 LNP treatment remains to be elucidated. It is likely that enhanced NK and $CD8^+$ T cell responses occur through their direct interaction with *Pdl1*-silenced KCs. As both NK and $CD8^+$ T cells contain CD3ζ, KC PD-L1 may directly engage PD-1 on the surface of these cells, initiating SHP-2-mediated inhibition of an activating CD3ζ/FcRγ/NKp46 or CD3ζ/TCR signal in NK and T cells, respectively. This can lead to increased contact time with the KC characterized by direct enhancements in NK and T cell functional responses[120].

However, NK cells[148,155] can play a role in shaping CD8$^+$ T cell responses. It is possible that CD8$^+$ T cell responses are enhanced indirectly via KC/NK cell cross-talk. In my studies, I observed that PD-L1 LNP-mediated silencing prior to viral infection failed to elicit CD8$^+$ T cell responses when NK cells were depleted or induced poor CD8$^+$ T cell responses incapable of producing IFN-γ in the presence of NK cells. During the expansion phase of the immune response premature NK cell production of IFN-γ may dampen CD8$^+$ T cell effector cytokine production because IFN-γ negatively feedbacks on itself via SOCS1 and SOCS3 induction[156]. At other tissue sites, hyperresponsive NKp46$^+$ NK cells (producing more IFN-γ and surface CD107a) can directly lead to dampened CD4$^+$ and CD8$^+$ T cell responses to MCMV and *Listeria monocytogenes* infections[124]. Additionally, NK cells residing in the liver are also enriched for an inhibitory NKG2A$^+$Ly49$^-$ surface phenotype and are functionally inferior compared to those residing elsewhere. NKG2A/Qa-1b engagement suppresses IFN-γ and favors IL-10 production[117]. In NKDTR-EGFP mice treated with DT the remaining NK cells resistant to depletion had the NKG2A$^+$Ly49$^-$ phenotype (data not shown); therefore, it is possible expansion of this population is detrimental in supporting a CD8$^+$ T cell response. Other reports propose that activated NK cells can directly lyse CD4$^+$ T cells[146] and CD8$^+$ T cells[157], but my data directly contradict this notion because boosting the NK cell response does not lead to a loss of CD8$^+$ T cell accumulation. I hypothesized that an enhancement in intrahepatic NK cell function prematurely dampened CD8$^+$ T cell IFN-γ production in PD-L1 LNP-treated animals[131]. In order to demonstrate that an aberrant increase in liver NK cell function is detrimental to the full-acquisition of CD8$^+$ T cell effector function, I delayed PD-L1 LNP treatment until D5 post-viral infection after the peak in the NK cell response. Bypassing the wave of intrahepatic NK cells responding

to virus, this regimen led to superior $CD8^+$ T cell polyfunctionality. Future studies are needed to determine if dampening PD-1/PD-L1 signaling in intrahepatic NK cells supports an inhibitory population of NKG2A-bearing NK cells or causes influxing NK cells to become hyperresponsive. These results support that *Pdl1* silencing does not override a fundamental NK cell signal required for $CD8^+$ T cell priming.

$CD4^+$ T cells may also influence $CD8^+$ T cell responses[158]. Regarding the contribution of $CD4^+$ T cell help, the analysis of bulk $CD4^+$ T cells indicates that these cells did not significantly expand after viral infection with Ad-Ova nor displayed PD-L1 LNP-mediated functional improvements including IFN-γ (data not shown). This finding is consistent with a series of experiments performed by Wuensch *et al.* demonstrating that after direct intrahepatic infection with adenovirus, the endogenous $CD8^+$ T cell response was not altered in MHC $II^{-/-}$ mice. Additionally, after adoptive transfer of either $CD8^+$ OT-I T cells or $CD4^+$ OT-II T cells, only $CD8^+$ OT-I T cells were capable of expanding in infected recipient mice[106]. Further experimentation is needed to elucidate the immunostimulatory mechanism connecting *Pdl1*-silenced KCs with NK/$CD8^+$ T cell function or the alteration of $CD4^+$ T cell function. Nevertheless, when designing drug treatment protocols for the blockade of PD-1/PD-L1 signaling, it is favorable to delay PD-L1 LNP to a time point between the peaks in NK and T cell kinetics in order to favor optimal priming and prevent dampening of the polyfunctional $CD8^+$ T cell response.

As $CD8^+$ T cell-dependent viral clearance is observed from D5 to D7, the boosted NK and $CD8^+$ T cell accumulation and function were also accompanied by an increase in serum ALT in infected animals at D7. Considering the balance between increased immunity and immunopathology, this is most likely transient as signs of hepatocyte

regrowth are also apparent at D7 and no mortality was observed associated with hepatic injury up to D40 after treatment. In fact, elevated ALT at D7 is correlative evidence that CD8$^+$ T cells are cytolytically killing infected hepatocytes at the peak in their kinetics.

The potential clinical impact of *in vivo* PD-L1 siRNA delivery is promising. siRNA has advantages over antibody- or small molecule inhibitor-based approaches since siRNA is easy to synthesize and lead identification and optimization to targets is rapid. The main challenge in siRNA drug development is targeting and efficaciously delivering the siRNA to the proper organs and disease-causing cell types. C12-200-based LNP can be used to block diseases mainly initiated by myeloid cells of the spleen, liver, and bone marrow due to its bioavailability after IV administration. This was established with LNP comprised of C12-200 lipid containing CCR2 siRNA[159]. IP delivery of polyethylenimine (PEI)-based nanoparticles, a different cationic moiety, containing PD-L1 siRNA was also demonstrated to elicit antitumor immunity in an ovarian tumor model, but PEI and other vehicles including viral delivery systems are often toxic and can stimulate immune responses themselves[160]. *Pdl1* silencing may also be applied to hepatocellular carcinoma because KC PD-L1 upregulation and CD8$^+$ T cell dysfunction correlate with a worse prognosis in humans[125]. Although siRNA technology is still in its infancy, the clinical potential continues beyond curing viral infection including cancer, heart disease, and diabetes.

These data are novel with clear demonstration that *Pdl1* is effectively silenced in KCs via *in vivo* administration of PD-L1 siRNA. Silencing of *Pdl1* effectively improves the NK cell and CD8$^+$ T cell responses to hepatotropic viral infection. Polyfunctional CD8$^+$ T cell responses that could directly clear virally infected cells were only observed if PD-L1 LNP

was given after the wave of accumulating NK cells. It will be exciting in future studies to learn the extent of application of this novel biotechnology from vaccine development toward resolving chronic liver disease and diseases elsewhere controlled by similar mechanisms.

Figure 4.1

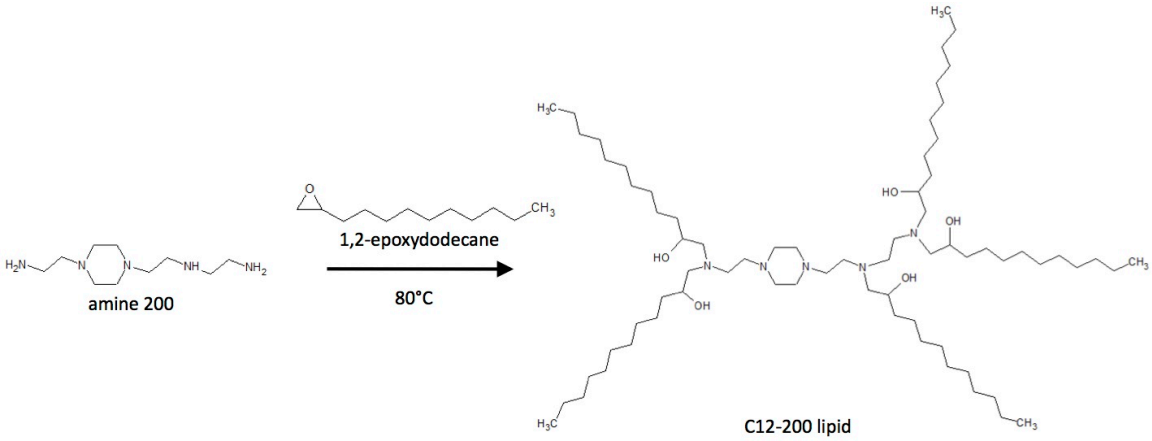

Figure 4.1 Structure of C12-200 lipid. Generation of C12-200 is achieved through Michael addition of amine 200 to 1,2-epoxydodecane for 2 days at 80°C. C12-200 is then mixed with disteroylphosphatidyl choline, cholesterol, PEG-DMG, and siRNA at a final lipid:siRNA weight ratio of 7:1 resulting in lipidoid nanoparticles 70-80 nm in diameter.

Figure 4.2

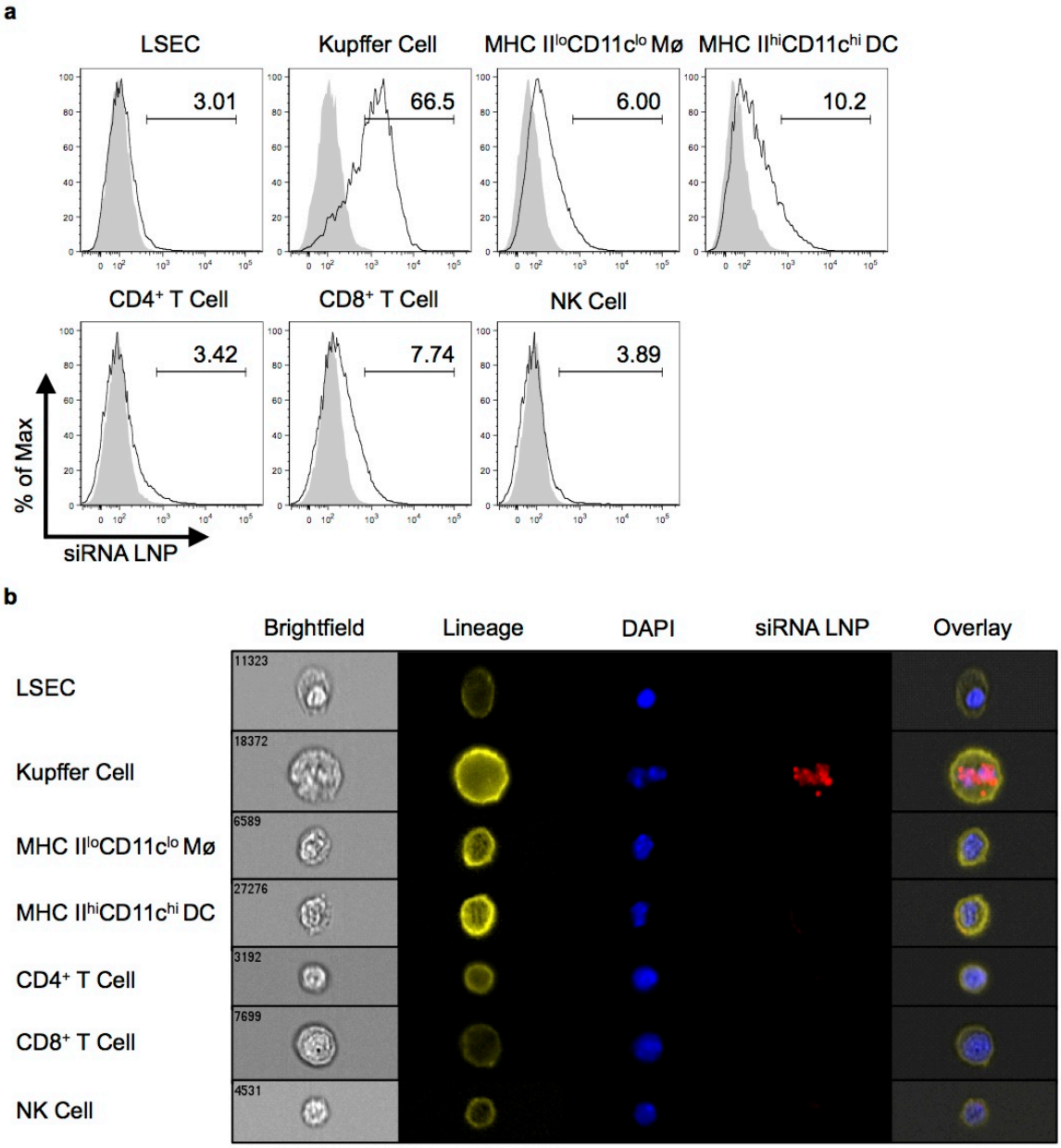
a
LSEC
Kupffer Cell
MHC IIloCD11clo Mø
MHC IIhiCD11chi DC
3.01
66.5
6.00
10.2
CD4+ T Cell
CD8+ T Cell
NK Cell
3.42
7.74
3.89
% of Max
siRNA LNP
b
Brightfield
Lineage
DAPI
siRNA LNP
Overlay
LSEC
Kupffer Cell
MHC IIloCD11clo Mø
MHC IIhiCD11chi DC
CD4+ T Cell
CD8+ T Cell
NK Cell
11323
18372
6589
27276
3192
7699
4531

Figure 4.2 siRNA LNP is primarily engulfed in small vesicles by Kupffer cells within the mononuclear cell pool. At D5 after IV infection with 2.5×10^7 IU Ad-Ova, C57BL/6 mice were IV injected with either Alexa Fluor (AF) 488- or 647-labeled siRNA LNP. (**a**) 1.5 hrs after fluorochrome-labeled siRNA LNP injection, liver mononuclear cells were isolated, and the percentage of nanoparticle uptake was assessed in LSEC ($CD45^-CD105^+CD146^+$), KC ($CD11b^{lo}F4/80^{hi}$), infiltrating monocyte/Mø (MHC $II^{lo}CD11b^{hi}CD11c^{lo}$), DC (MHC $II^{hi}CD11b^{hi}CD11c^{hi}$), $CD4^+$ T cell ($Thy1.2^+CD4^+$), $CD8^+$ T cell ($Thy1.2^+CD8^+$), and NK cell ($NK1.1^+CD3^-$) populations. Filled histograms represent animals that received Luc LNP and numbers indicate percentage. (**b**) Representative images of cells captured by the Amnis Imagestream^X stained with a surface lineage marker (yellow), DAPI (blue), and siRNA LNP (red) are depicted (n = 3 per group).

Figure 4.3

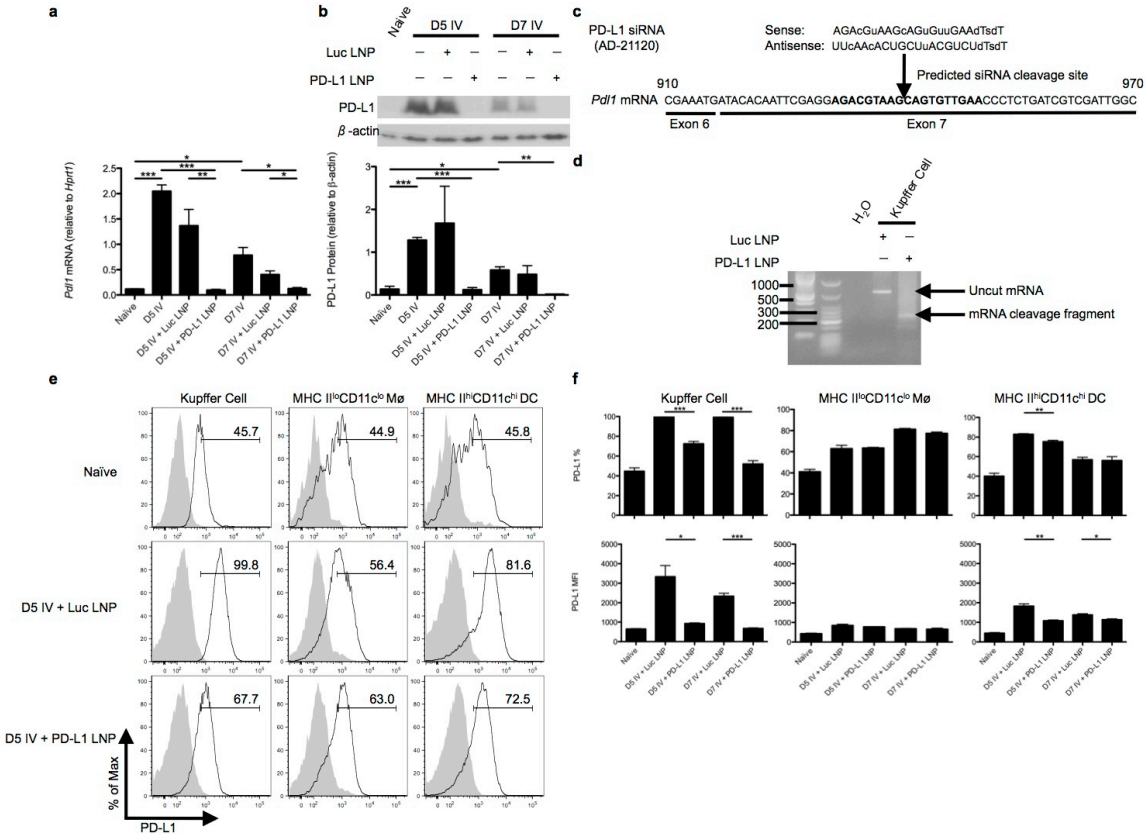
a
b
c
d
e
f
Naïve
D5 IV
D7 IV
Luc LNP
PD-L1 LNP
PD-L1
β -actin
PD-L1 siRNA
(AD-21120)
Sense: AGAcGuAAGcAGuGuuGAAdTsdT
Antisense: UUcAAcACUGCUuACGUCUdTsdT
Predicted siRNA cleavage site
910
970
Pdl1 mRNA CGAAATGATACACAATTCGAGGAGACGTAAGCAGTGTTGAACCCTCTGATCGTCGATTGGC
Exon 6
Exon 7
H2O
Kupffer Cell
1000
500
300
200
Uncut mRNA
mRNA cleavage fragment
Pdl1 mRNA (relative to Hprt1)
PD-L1 Protein (relative to β-actin)
Naïve
D5 IV
D5 IV + Luc LNP
D5 IV + PD-L1 LNP
D7 IV
D7 IV + Luc LNP
D7 IV + PD-L1 LNP
Kupffer Cell
MHC IIloCD11clo Mø
MHC IIhiCD11chi DC
45.7
44.9
45.8
99.8
56.4
81.6
67.7
63.0
72.5
D5 IV + Luc LNP
D5 IV + PD-L1 LNP
% of Max
PD-L1
PD-L1 %
PD-L1 MFI

Figure 4.3 PD-L1 LNP silences *Pdl1* mRNA expression via an RNAi mechanism in Kupffer cells leading to a decrease in PD-L1 protein expression. C57BL/6 mice were IV infected with 2.5×10^7 IU Ad-Ova and received Luc LNP, PD-L1 LNP, or no drug treatment. Whole liver samples were taken at D5 and D7 post-infection. (**a**) *Pdl1* mRNA expression was visualized by Q-PCR (one-way ANOVA/Tukey's post test; n = 3-8 per group), and (**b**) PD-L1 protein expression was assayed by western blotting and densitometry (one-way ANOVA/Tukey's post test; n = 3 per group). (**c**) The PD-L1 siRNA (AD-21120) sequence is depicted. (**d**) At D5 post-infection, C57BL/6 mice were IV injected with either Luc LNP or PD-L1 LNP. 5'-RACE PCR was performed on total RNA isolated from FACS-sorted KCs 4 hrs after LNP injection, and the amplification products from a nested PCR were run on a 1.8% agarose gel. The predicted mRNA cleavage product derived from RNAi-mediated silencing is shown. (**e,f**) PD-L1 expression was assessed by FACS on KCs ($CD11b^{lo}F4/80^{hi}$), infiltrating monocytes/Mø (MHC $II^{lo}CD11b^{hi}CD11c^{lo}$), and DCs (MHC $II^{hi}CD11b^{hi}CD11c^{hi}$) in naïve animals and at D5 to D7 post-infection with PD-L1 LNP or control Luc LNP treatments. Filled histograms represent isotype controls and numbers indicate percentage at D5 post-infection (n = 3 per group). Mean ± s.e.m.; $^*P < 0.05$, $^{**}P < 0.01$, and $^{***}P < 0.001$.

Figure 4.4

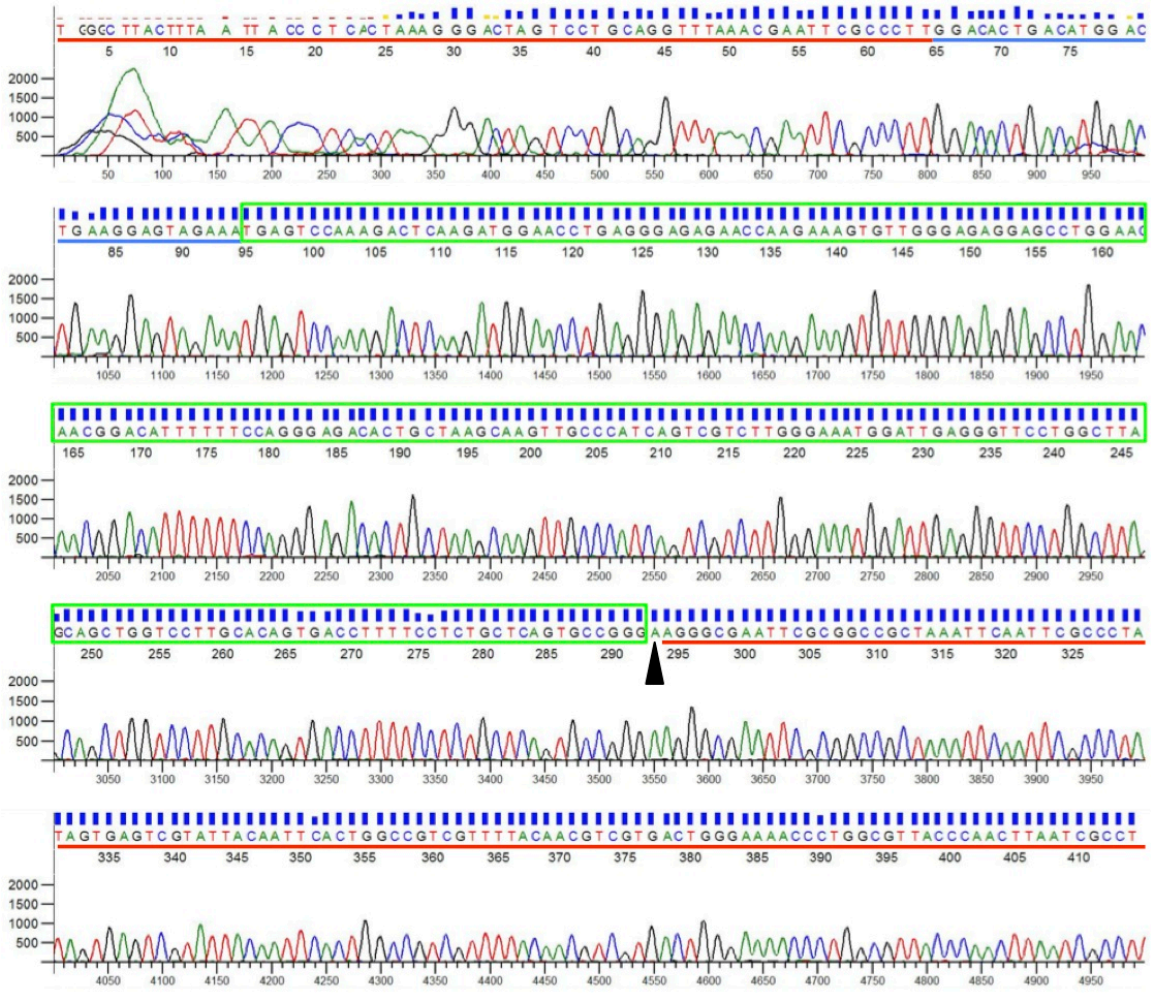
T CGCC TTACTTTA A TT A CC C T CAC T AAA G GG ACTA G T CCT G CAGG T T TAAA C GAA T T C GCCCC T T GG A CAC T G A CA T GG AC
5 10 15 20 25 30 35 40 45 50 55 60 65 70 75
2000
1500
1000
500
50 100 150 200 250 300 350 400 450 500 550 600 650 700 750 800 850 900 950
T G AAGGAGT AGAAA T GAGT CCAAA GACT CAAGA T GGAACCT G AGGGAGAGAACCAAGAAAGT GT T GGGAGAGGAGCCT GGAAC
85 90 95 100 105 110 115 120 125 130 135 140 145 150 155 160
2000
1500
1000
500
1050 1100 1150 1200 1250 1300 1350 1400 1450 1500 1550 1600 1650 1700 1750 1800 1850 1900 1950
AACGGACAT T T T T T CCAGGG AG ACACT G CT AAG CAAGT T GCCCA T CAGT CGT CT T GGGAAAT GGAT T GAGGGT T CCT GGCT T A
165 170 175 180 185 190 195 200 205 210 215 220 225 230 235 240 245
2000
1500
1000
500
2050 2100 2150 2200 2250 2300 2350 2400 2450 2500 2550 2600 2650 2700 2750 2800 2850 2900 2950
GCAGCT GGT CCT T GCACAGT GACCT T T T CCT CT GCT CAGT GCCGGG AAGGGCGAAT T CGCGGCCGCT AAAT T CAAT T CGCCCT A
250 255 260 265 270 275 280 285 290 295 300 305 310 315 320 325
2000
1500
1000
500
3050 3100 3150 3200 3250 3300 3350 3400 3450 3500 3550 3600 3650 3700 3750 3800 3850 3900 3950
TAGT GAGT CGT AT T ACAAT T CACT GGCCGT CGT T T T ACAACGT CGT GACT GGGAAAACCCT GGCGT T ACCCAACT T AAT CGCCT
335 340 345 350 355 360 365 370 375 380 385 390 395 400 405 410
2000
1500
1000
500
4050 4100 4150 4200 4250 4300 4350 4400 4450 4500 4550 4600 4650 4700 4750 4800 4850 4900 4950

Figure 4.4 The predicted cleavage fragment found in Kupffer cells treated with PD-L1 LNP has sequence homology with full length *Pdl1* mRNA. The ~250-bp band found in the lane of PD-L1 LNP-treated KCs was cut and inserted into a pCR4-TOPO vector. *E. coli* were transformed with this construct and select clones were sequenced. Sequence derived from vector (red underscore), 5'-RACE oligonucleotide (blue underscore), 3'-A addition for vector insertion (arrow), and *Pdl1* mRNA cleavage fragment (green box) are depicted. This sequence is representative of five selected clones all having sequence derived from *Pdl1* mRNA.

Figure 4.5

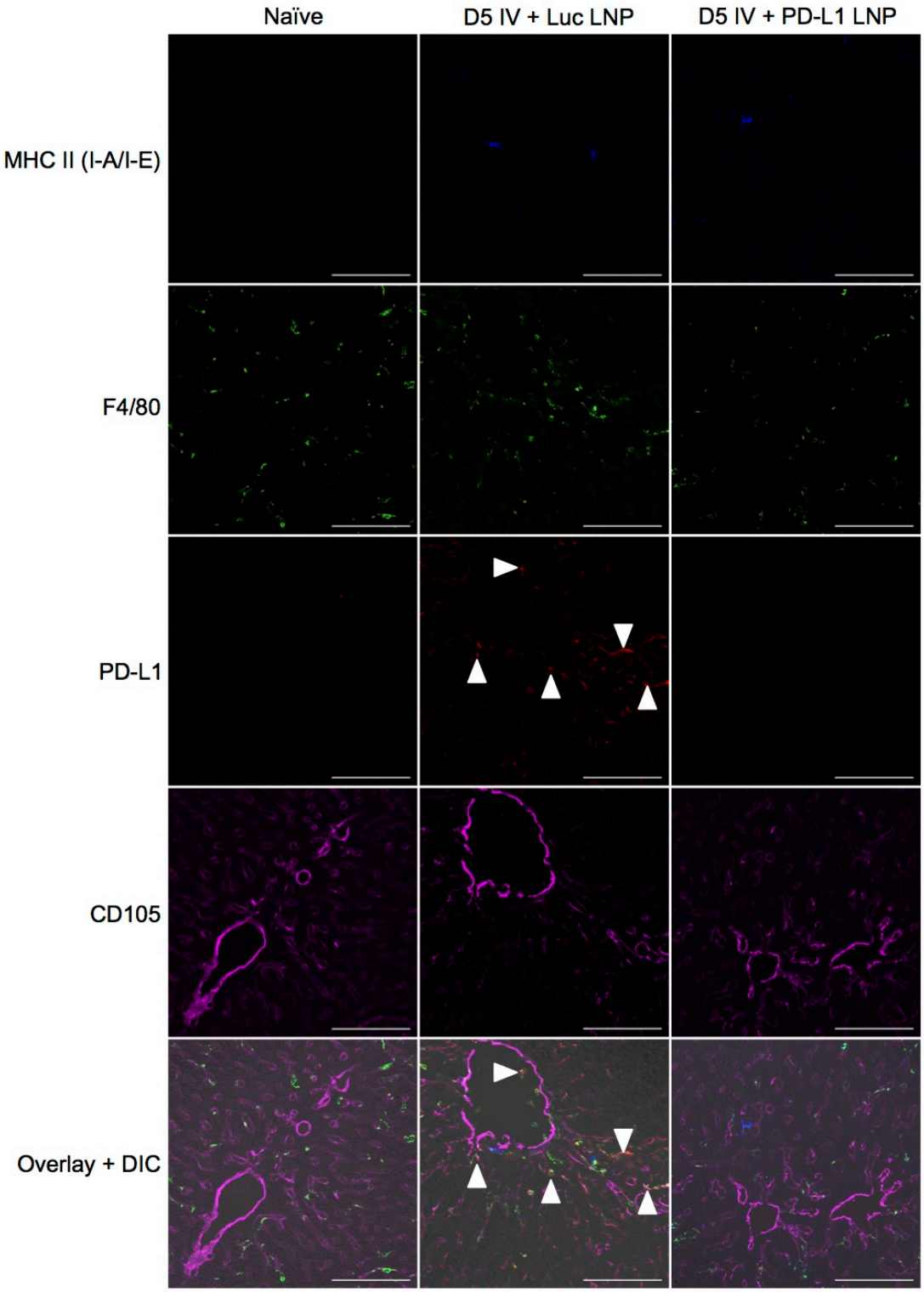
Naïve
D5 IV + Luc LNP
D5 IV + PD-L1 LNP
MHC II (I-A/I-E)
F4/80
PD-L1
CD105
Overlay + DIC

Figure 4.5 PD-L1 is preferentially downregulated on F4/80^{+} cells and CD105^{+} cells, but not hepatocytes, after PD-L1 LNP treatment. PLP-fixed/OCT-frozen liver cross sections were acquired from naïve C57BL/6 mice or mice at D5 after IV infection with 2.5×10^{7} Ad-Ova that had received either full regimen Luc LNP or PD-L1 LNP. Representative microscopy of sections stained with anti-MHC II (I-A/I-E) (blue) denoting DCs, anti-F4/80 (green) marking KCs, anti-PD-L1 (red), and anti-CD105 (magenta) labeling LSECs is shown (n = 3 per group). Scale bar, 100 μm.

Figure 4.6

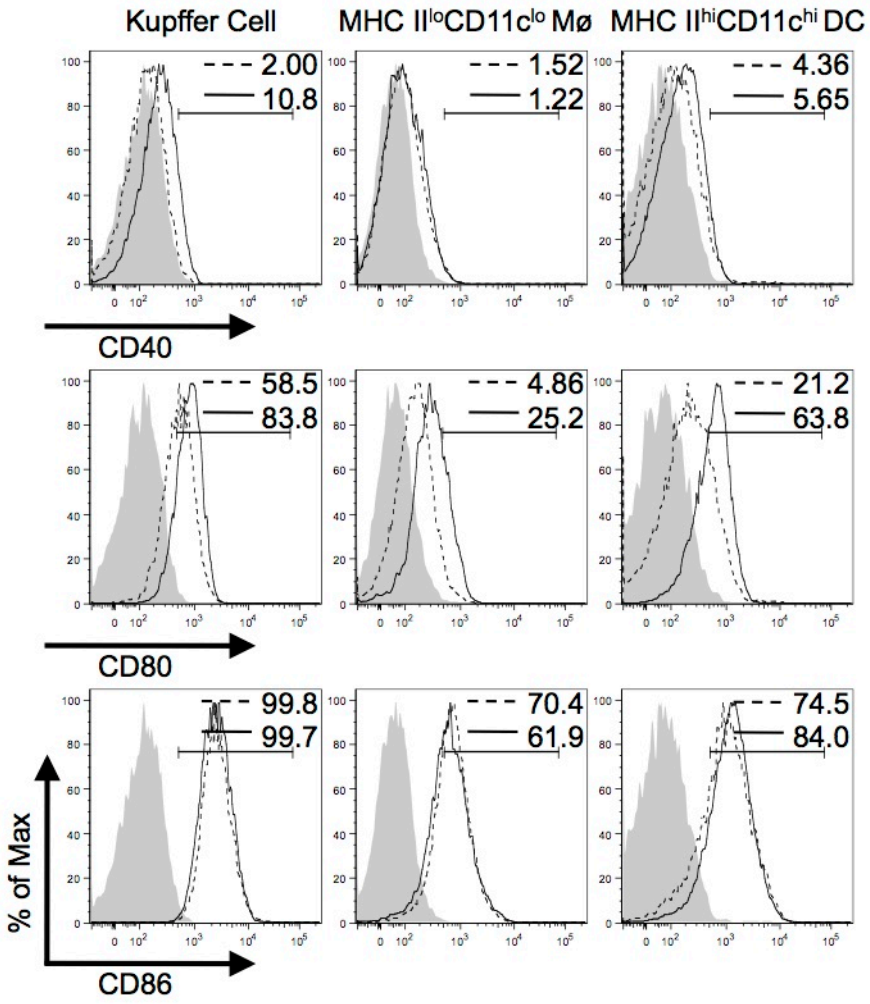
Kupffer Cell
MHC II^{lo}CD11c^{lo} Mø
MHC II^{hi}CD11c^{hi} DC
2.00
10.8
1.52
1.22
4.36
5.65
CD40
58.5
83.8
4.86
25.2
21.2
63.8
CD80
99.8
99.7
70.4
61.9
74.5
84.0
% of Max
CD86

Figure 4.6 LNP enhances APC maturation. C57BL/6 mice were IV infected with 2.5×10^7 IU Ad-Ova and received Luc LNP or no drug treatment. Whole liver samples were taken at D5 post-infection. CD40, CD80, and CD86 expression was assessed by FACS on KCs ($CD11b^{lo}F4/80^{hi}$), infiltrating monocytes/Mø (MHC $II^{lo}CD11b^{hi}CD11c^{lo}$), and DCs (MHC $II^{hi}CD11b^{hi}CD11c^{hi}$) at D5 post-infection with Luc LNP (solid line) or no treatment (dashed line). Filled histograms represent isotype controls and numbers indicate percentage (n = 3 per group).

Figure 4.7

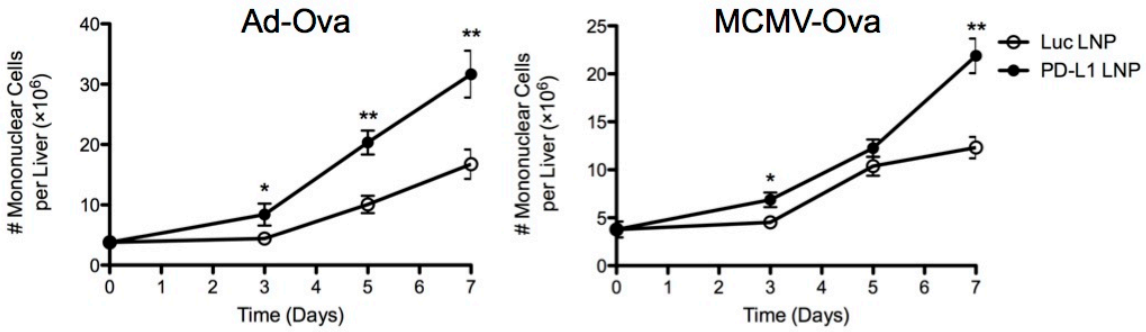
Ad-Ova
MCMV-Ova
Mononuclear Cells per Liver (×10^6)
Time (Days)
Luc LNP
PD-L1 LNP
*
**

Figure 4.7 PD-L1 LNP augments liver mononuclear infiltrate. Live mononuclear cells isolated from the livers of C57BL/6 mice IV infected with 2.5×10^7 IU Ad-Ova or 1×10^4 IU MCMV-Ova were quantified after full regimen Luc or PD-L1 LNP treatment. Trypan blue exclusion was used to assess the number of viable cells (n = 3-7 per group). Mean ± s.e.m.; $^*P < 0.05$ and $^{**}P < 0.01$.

Figure 4.8

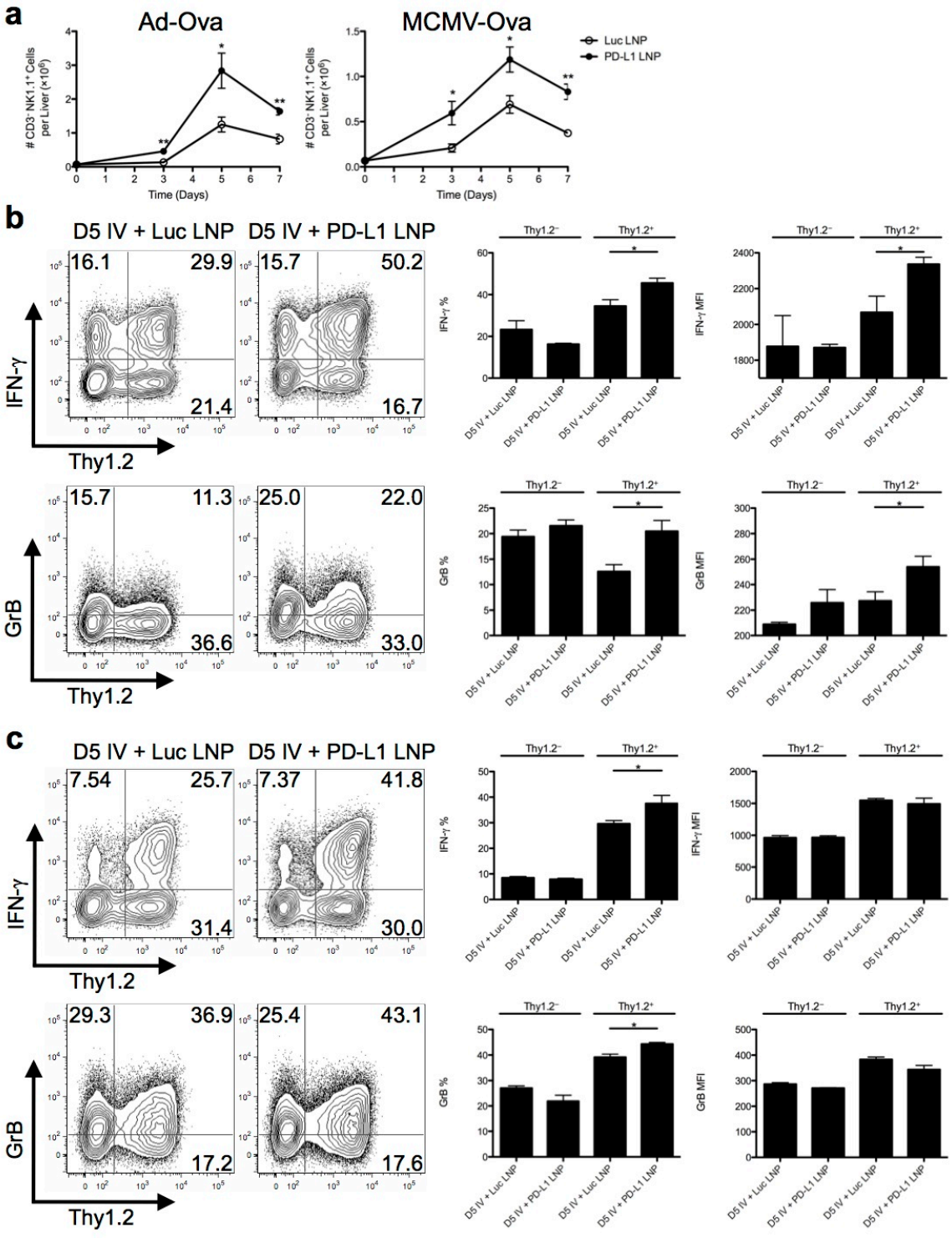
a
Ad-Ova
MCMV-Ova
Luc LNP
PD-L1 LNP
CD3⁻ NK1.1⁺ Cells per Liver (×10⁶)
Time (Days)
b
D5 IV + Luc LNP
D5 IV + PD-L1 LNP
16.1
29.9
21.4
15.7
50.2
16.7
IFN-γ
Thy1.2
15.7
11.3
36.6
25.0
22.0
33.0
GrB
Thy1.2⁻
Thy1.2⁺
IFN-γ %
IFN-γ MFI
GrB %
GrB MFI
c
7.54
25.7
31.4
7.37
41.8
30.0
29.3
36.9
17.2
25.4
43.1
17.6

Figure 4.8 NK cell function and accumulation are enhanced by full regimen PD-L1 LNP therapy in response to Ad-Ova and MCMV-Ova infection. C57BL/6 mice were IV infected with 2.5×10^7 IU Ad-Ova or 1×10^4 IU MCMV-Ova and either received Luc LNP or PD-L1 LNP at days -1, 1, and 3. (**a**) Liver mononuclear cells were collected, and NK cells ($CD3^-NK1.1^+$) were enumerated at days 0, 3, 5, and 7 (n = 3-5 per group). NK cell IFN-γ was assessed after a 5 hr re-stimulation with 5 ng/mL PMA and 500 ng/mL ionomycin, and GrB was determined directly *ex vivo* for both (**b**) Ad-Ova (n = 3-7 per group) and (**c**) MCMV-Ova (n = 3-4 per group) at D5 post-infection. Numbers in the scatter plots represent percentages. Mean ± s.e.m.; $*P < 0.05$ and $**P < 0.01$.

Figure 4.9

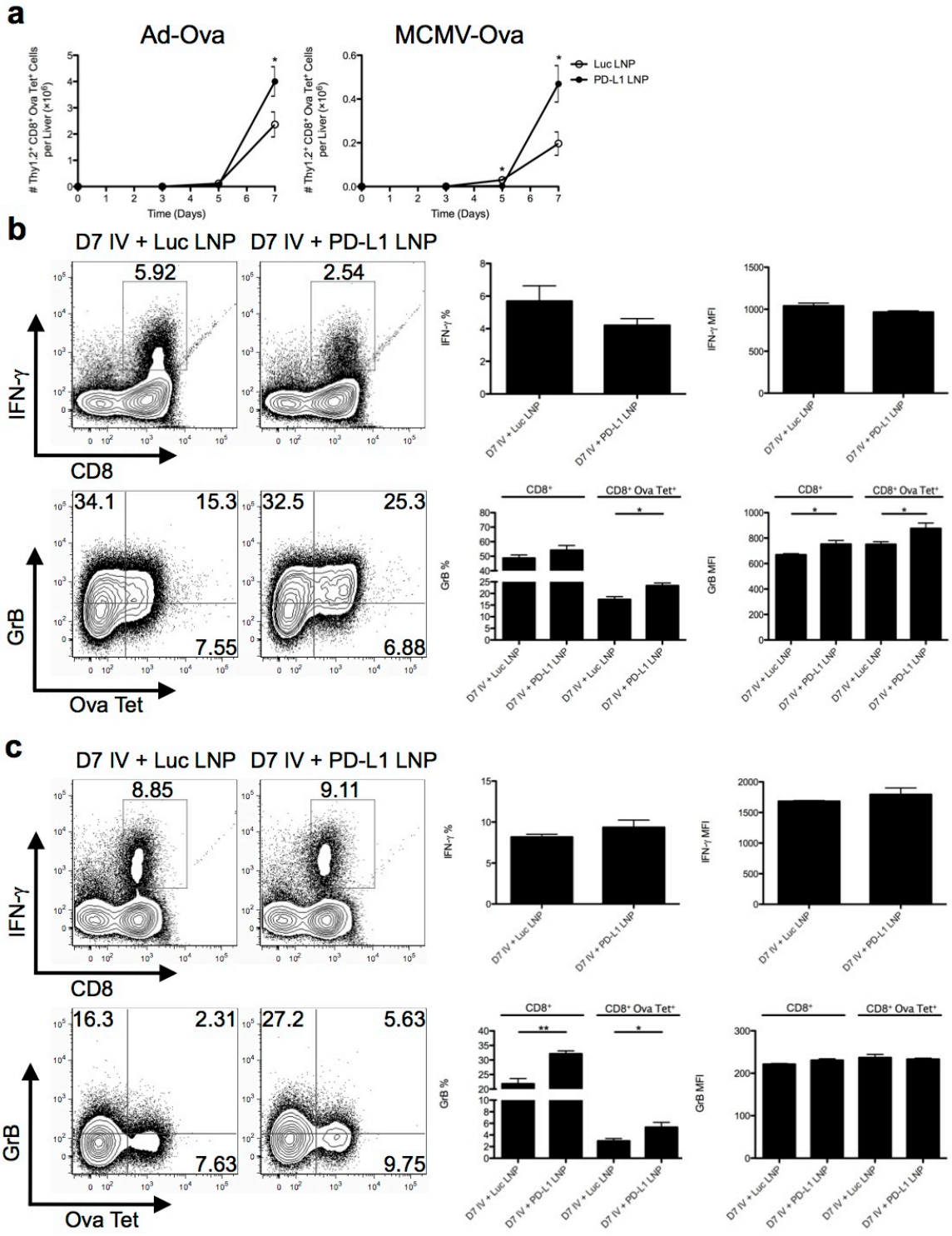
a
Ad-Ova
MCMV-Ova
Thy1.2+ CD8+ Ova Tet+ Cells per Liver (×10^6)
Time (Days)
Luc LNP
PD-L1 LNP
b
D7 IV + Luc LNP
D7 IV + PD-L1 LNP
5.92
2.54
IFN-γ
CD8
34.1
15.3
7.55
32.5
25.3
6.88
GrB
Ova Tet
IFN-γ %
IFN-γ MFI
GrB %
GrB MFI
CD8+
CD8+ Ova Tet+
c
8.85
9.11
16.3
2.31
7.63
27.2
5.63
9.75

Figure 4.9 Ova-specific $CD8^+$ T cell cytolytic function and accumulation are enhanced by full regimen PD-L1 LNP therapy in response to Ad-Ova and MCMV-Ova infection. C57BL/6 mice were IV infected with 2.5×10^7 IU Ad-Ova or 1×10^4 IU MCMV-Ova and either received Luc LNP or PD-L1 LNP at days -1, 1, 3, and 5. (**a**) Liver mononuclear cells were collected and the number of Ova-specific $CD8^+$ T cells (Ova Tet^+CD8^+) was determined at days 0, 3, 5, and 7 (n = 3-7 per group). Antigen-specific $CD8^+$ T cell IFN-γ was assessed after a 5 hr re-stimulation with 2 μg/mL SIINFEKL peptide, and GrB was determined directly *ex vivo* for both (**b**) Ad-Ova (n = 3-4 per group) and (**c**) MCMV-Ova (n = 3-4 per group) infections. Numbers in the scatter plots represent percentages. Mean ± s.e.m.; $*P < 0.05$ and $**P < 0.01$.

Figure 4.10

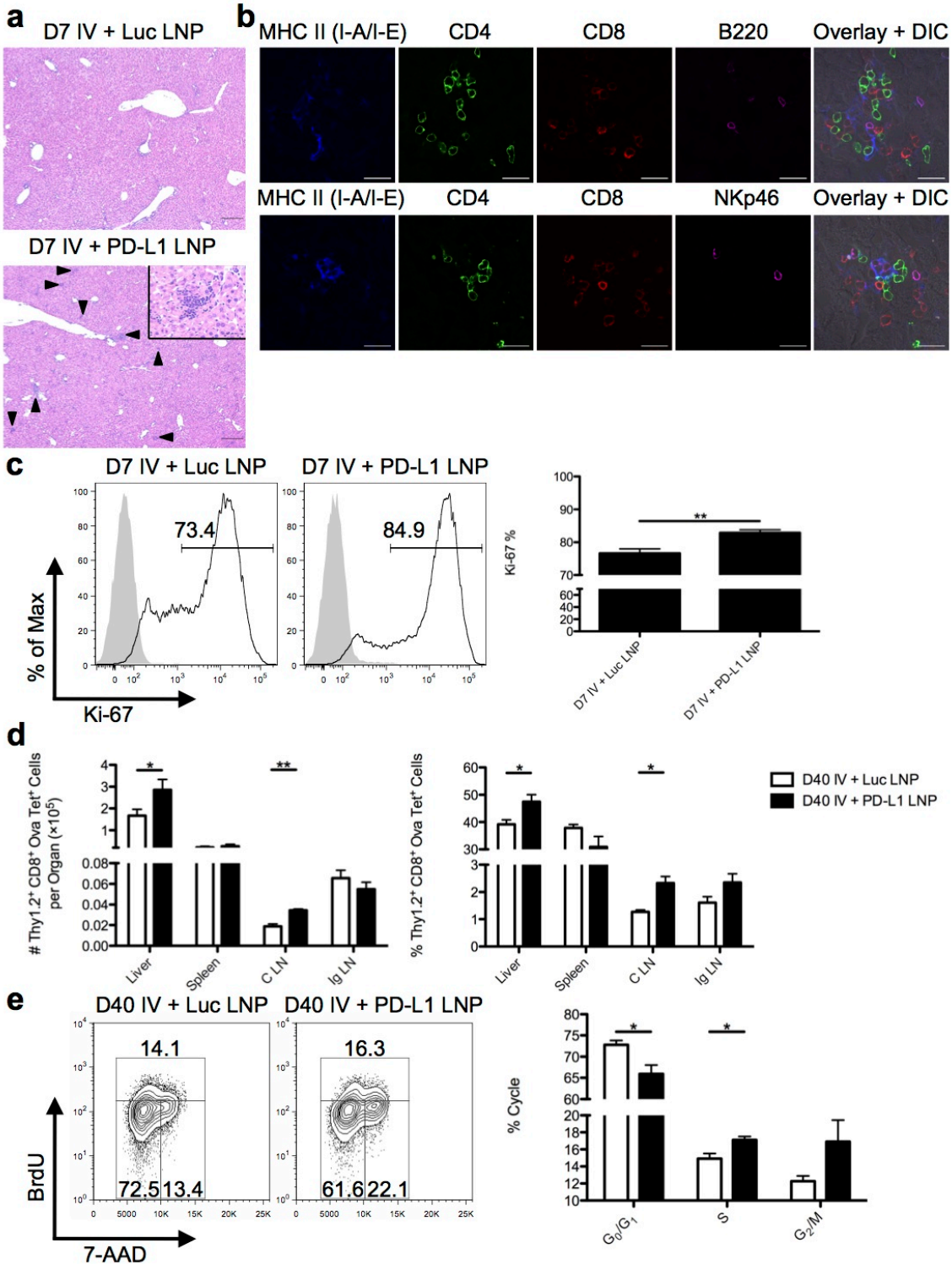
a
D7 IV + Luc LNP
D7 IV + PD-L1 LNP
b
MHC II (I-A/I-E)
CD4
CD8
B220
Overlay + DIC
MHC II (I-A/I-E)
CD4
CD8
NKp46
Overlay + DIC
c
D7 IV + Luc LNP
D7 IV + PD-L1 LNP
73.4
84.9
% of Max
Ki-67
Ki-67 %
D7 IV + Luc LNP
D7 IV + PD-L1 LNP
d
Thy1.2+ CD8+ Ova Tet+ Cells per Organ (×10^5)
% Thy1.2+ CD8+ Ova Tet+ Cells
Liver
Spleen
C LN
Ig LN
D40 IV + Luc LNP
D40 IV + PD-L1 LNP
e
D40 IV + Luc LNP
D40 IV + PD-L1 LNP
14.1
16.3
72.5
13.4
61.6
22.1
BrdU
7-AAD
% Cycle
G0/G1
S
G2/M

Figure 4.10 Full PD-L1 LNP treatment regimen boosts $CD8^+$ T cell accumulation in clusters, acute proliferation, memory, and long-term homeostatic proliferation. C57BL/6 mice were IV infected with 2.5×10^7 IU Ad-Ova and either received Luc LNP or PD-L1 LNP at days -1, 1, 3, and 5. (**a**) D7 liver sections from Ad-Ova-infected C57BL/6 mice were collected and stained with H & E. Arrows indicate discrete clusters. Scale bar, 200 μm. Inlay depicts lobular clusters in the D7 PD-L1 LNP-treated mice contained cells of mononuclear origin (n = 6 per group). Scale bar, 50 μm. (**b**) PLP-fixed/OCT-frozen liver cross sections from D7 livers were stained with anti-MHC II (I-A/I-E) (blue), anti-CD4 (green), anti-CD8 (red), anti-B220 (magenta-upper panel), anti-NKp46 (magenta-lower panel) (n = 3 per group). Scale bar, 20 μm. (**c**) Ki-67 presence was determined through FACS analysis of Ova Tet^+CD8^+ T cells at D7 post-infection (n = 3 per group). (**d**) At D40 post-infection, the number and percentage of Ova Tet^+CD8^+ T cells was determined in the liver, spleen, C LN, and Ig LN (n = 3-7 per group). (**e**) 7 days prior to a D40 harvest, 0.5 mg BrdU was administered IP daily to mice. The number Ova Tet^+CD8^+ T cells in G_0/G_1, S, and G_2/M cell cycles was determined based on anti-BrdU/7-AAD staining (n = 3-4 per group). Numbers in the histograms and scatter plots represent percentages. Mean ± s.e.m.; $^*P < 0.05$ and $^{**}P < 0.01$.

Figure 4.11

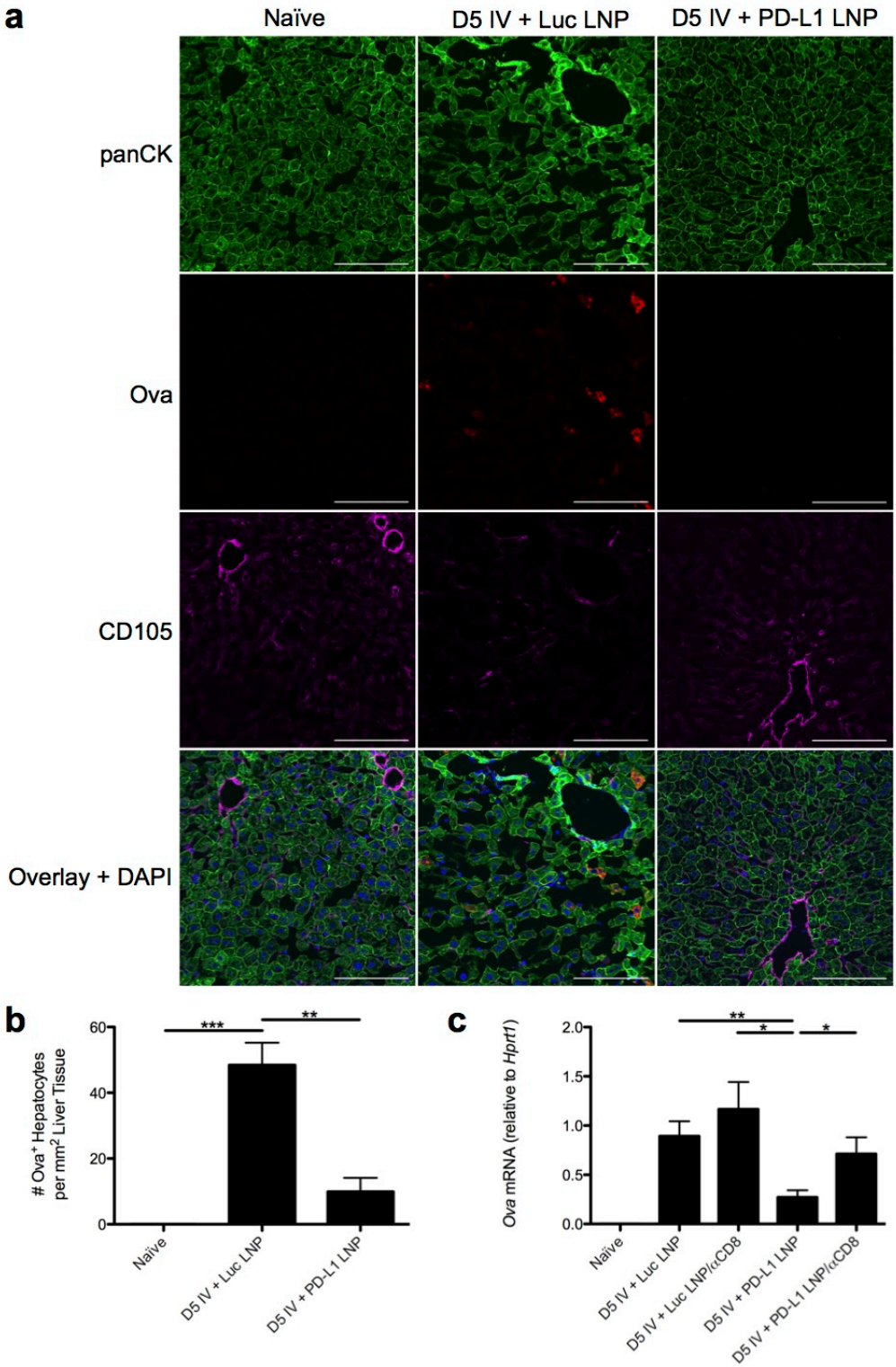
a
Naïve
D5 IV + Luc LNP
D5 IV + PD-L1 LNP
panCK
Ova
CD105
Overlay + DAPI
b
Ova+ Hepatocytes per mm2 Liver Tissue
60
40
20
0
***
**
Naïve
D5 IV + Luc LNP
D5 IV + PD-L1 LNP
c
Ova mRNA (relative to Hprt1)
2.0
1.5
1.0
0.5
0.0
**
*
*
Naïve
D5 IV + Luc LNP
D5 IV + Luc LNP/αCD8
D5 IV + PD-L1 LNP
D5 IV + PD-L1 LNP/αCD8

Figure 4.11 PD-L1 LNP enhances $CD8^+$ T cell-mediated viral clearance. PLP-fixed/OCT-frozen liver cross sections were obtained from naïve C57BL/6 mice or mice at D5 after IV infection with 2.5×10^7 Ad-Ova that had received either full regimen Luc LNP or PD-L1 LNP. (**a**) Sections were stained with anti-panCK (green) signifying hepatocytes, anti-Ova (red) marking virally infected cells, anti-CD105 (magenta) for LSECs, and DAPI (blue) with a representative collection of images shown. Scale bar, 100 μm. (**b**) Hepatocytes that were virally infected ($panCK^+Ova^+$ cells) were enumerated per field of view D5 post-infection (one-way ANOVA/Tukey's post test; n = 3 per group). (**c**) Total RNA from D5 whole liver samples was collected and *Ova* mRNA was measured by Q-PCR. To deplete $CD8^+$ T cells, 300 μg anti-CD8 Ab was administered IP to C57BL/6 mice 1 day prior to infection along with full regimen Luc or PD-L1 LNP (one-way ANOVA/Tukey's post test; n = 4-9 per group). Mean ± s.e.m.; $^*P < 0.05$, $^{**}P < 0.01$, and $^{***}P < 0.001$.

Figure 4.12

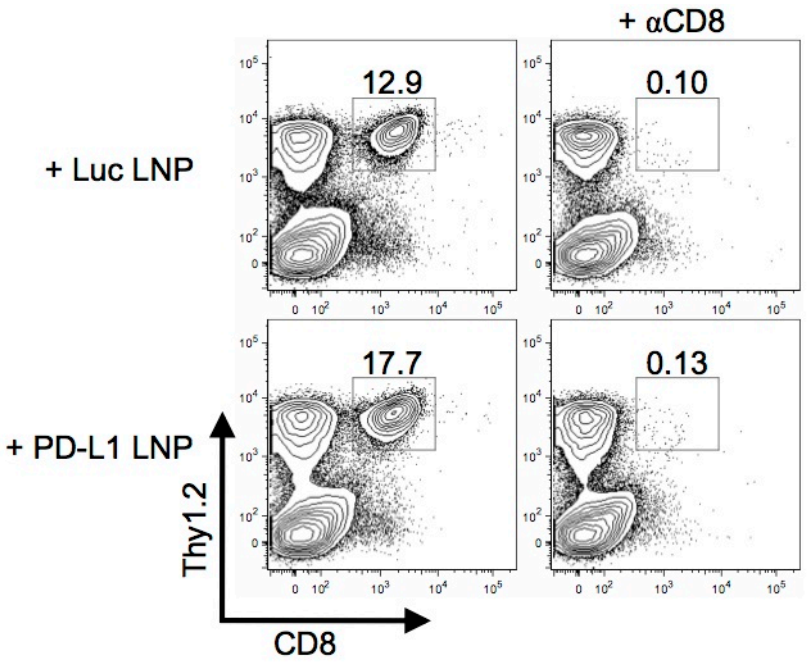

Figure 4.12 Anti-CD8 antibody effectively depletes $CD8^+$ T cells. C57BL/6 mice received 300 μg anti-CD8 Ab IP 1 day prior to infection along with full regimen Luc or PD-L1 LNP. The mice were IV infected with 2.5×10^7 Ad-Ova. The depletion of $CD8^+$ T cells ($Thy1.2^+CD8^+$) was confirmed by FACS analysis at D5 post-infection (n = 4-5 per group). Numbers in the scatter plots represent percentages.

Figure 4.13

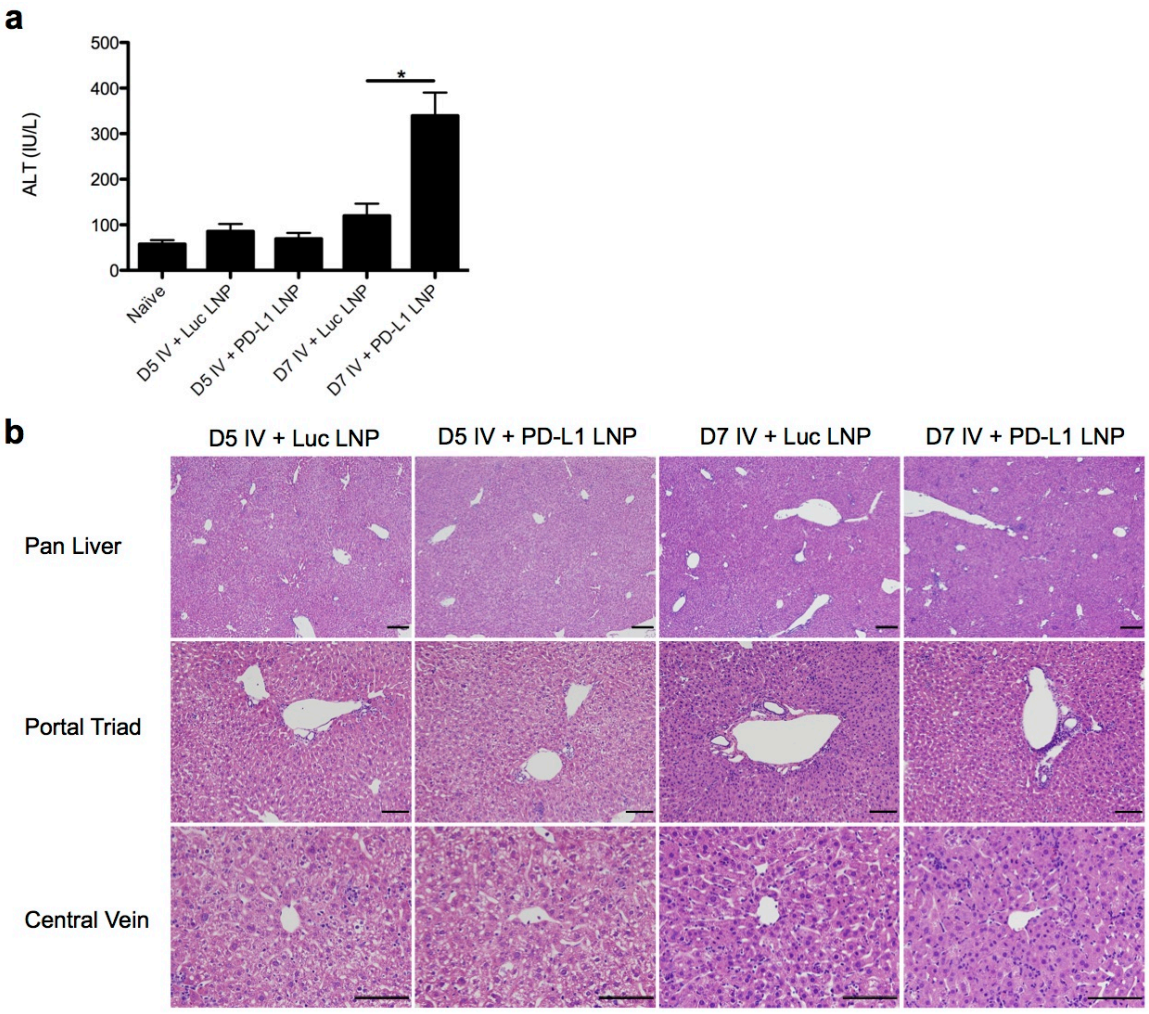
a
ALT (IU/L)
500
400
300
200
100
0
*
Naïve
D5 IV + Luc LNP
D5 IV + PD-L1 LNP
D7 IV + Luc LNP
D7 IV + PD-L1 LNP
b
D5 IV + Luc LNP
D5 IV + PD-L1 LNP
D7 IV + Luc LNP
D7 IV + PD-L1 LNP
Pan Liver
Portal Triad
Central Vein

Figure 4.13 Hepatocyte lysis peaks at D7 post-infection. C57BL/6 mice were IV infected with 2.5×10^7 IU Ad-Ova and either received Luc LNP or PD-L1 LNP at days -1, 1, 3, and 5. (**a**) Serum ALT was assessed in naïve, D5, and D7 Ad-Ova-infected animals (one-way ANOVA/Tukey's post test; n = 3 per group). (**b**) D5 and D7 liver sections from Ad-Ova-infected mice were collected and stained with H & E (n = 6 per group). Pan liver scale bar, 200 μm; portal triad scale bar, 100 μm; central vein scale bar, 100 μm. Mean ± s.e.m.; $*P < 0.05$.

Figure 4.14

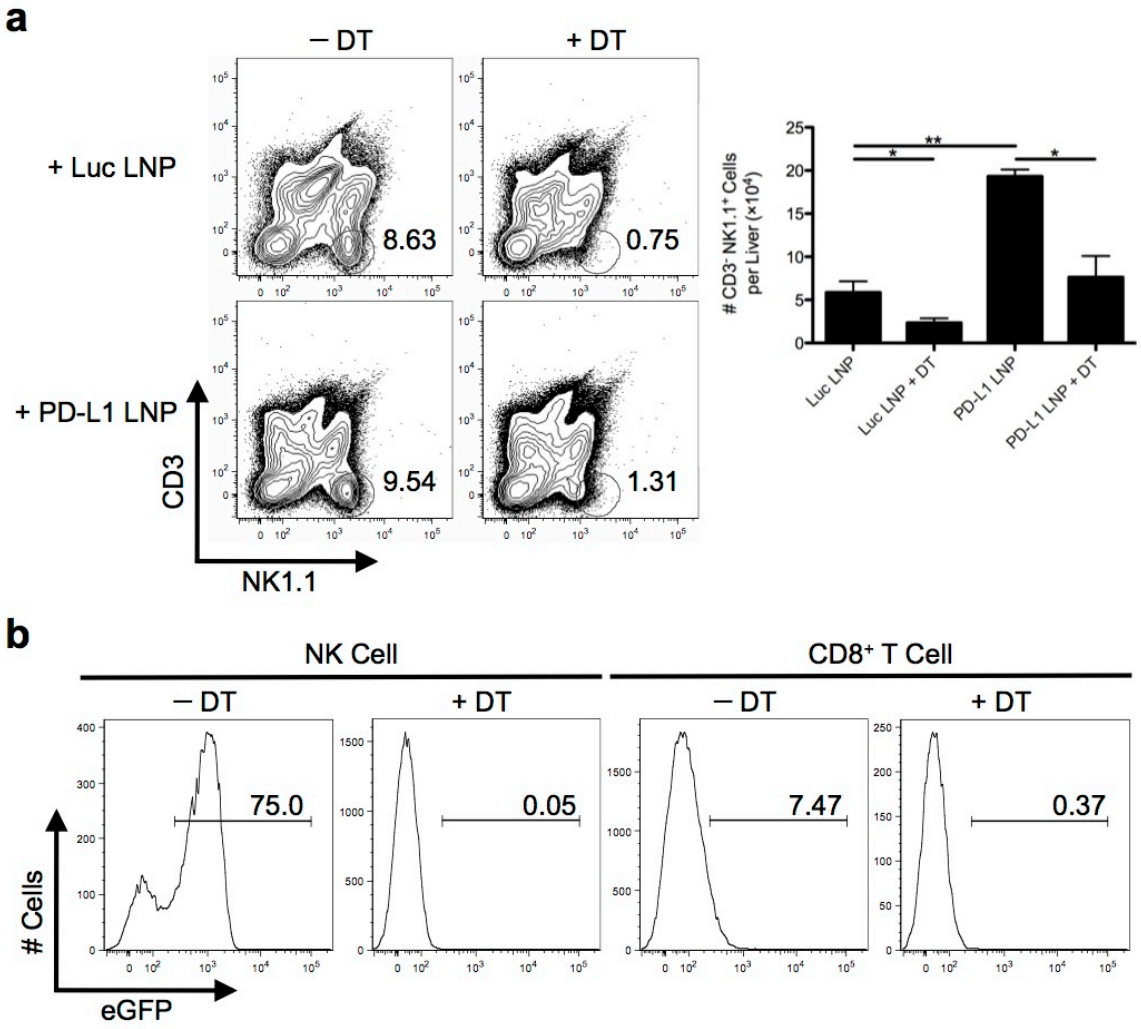
a
− DT
+ DT
+ Luc LNP
+ PD-L1 LNP
8.63
0.75
9.54
1.31
CD3
NK1.1
CD3- NK1.1+ Cells per Liver (×10⁴)
Luc LNP
Luc LNP + DT
PD-L1 LNP
PD-L1 LNP + DT
b
NK Cell
CD8+ T Cell
− DT
+ DT
75.0
0.05
7.47
0.37
Cells
eGFP

Figure 4.14 Diphtheria toxin effectively depletes NK cells in NKDTR-EGFP mice. NKDTR-EGFP mice were IV infected with 2.5×10^7 IU Ad-Ova, and either received full regimen Luc LNP or PD-L1 LNP. (**a**) DT-treated and control livers were collected, and the number of NK cells in the mononuclear pool was determined (one-way ANOVA/Tukey's post test; n = 3-5 per group). (**b**) eGFP expression was characterized in NK cells ($CD3^-NK1.1^+$) and $CD8^+$ T cells ($Thy1.2^+CD8^+$) with and without DT administration (n = 3-5 per group). Numbers in the scatter plots and histograms represent percentages. Mean ± s.e.m.; $^*P < 0.05$ and $^{**}P < 0.01$.

Figure 4.15

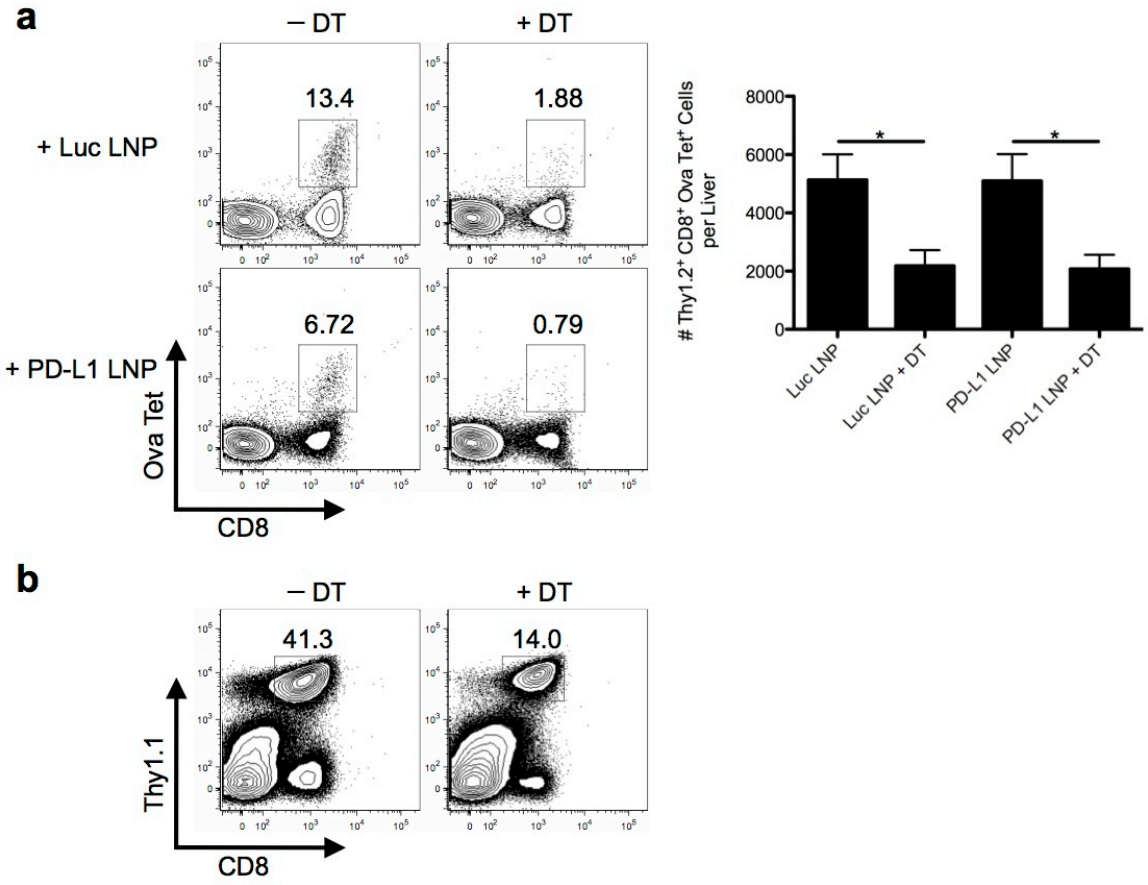
a
– DT
+ DT
+ Luc LNP
13.4
1.88
+ PD-L1 LNP
6.72
0.79
Ova Tet
CD8
Thy1.2+ CD8+ Ova Tet+ Cells per Liver
8000
6000
4000
2000
0
*
*
Luc LNP
Luc LNP + DT
PD-L1 LNP
PD-L1 LNP + DT
b
– DT
+ DT
41.3
14.0
Thy1.1
CD8

Figure 4.15 $CD8^+$ T cell priming is dependent on NK cell presence irrespective of *Pdl1* silencing. (**a**) NKDTR-EGFP mice were IV infected with 2.5×10^7 IU Ad-Ova, and either received full regimen Luc LNP or PD-L1 LNP. In addition, experimental groups were divided into mice that received DT or did not. Liver mononuclear cells were collected at D5 and the number of Ova Tet^+CD8^+ T cells was determined by flow cytometry (n = 3-4 per group). (**b**) 1×10^5 $CD8^+$ splenocytes from a $Thy1.1^+$ OT-I mouse were transferred into NKDTR-EGFP mice 2 days prior to infection. LNP treatment commenced 1 day prior to infection, and the number of $Thy1.1^+CD8^+$ T cells in the liver was established at D5 post-infection (n = 3 per group). Numbers in the scatter plots represent percentages. Mean ± s.e.m.; $*P < 0.05$ and $**P < 0.01$.

Figure 4.16

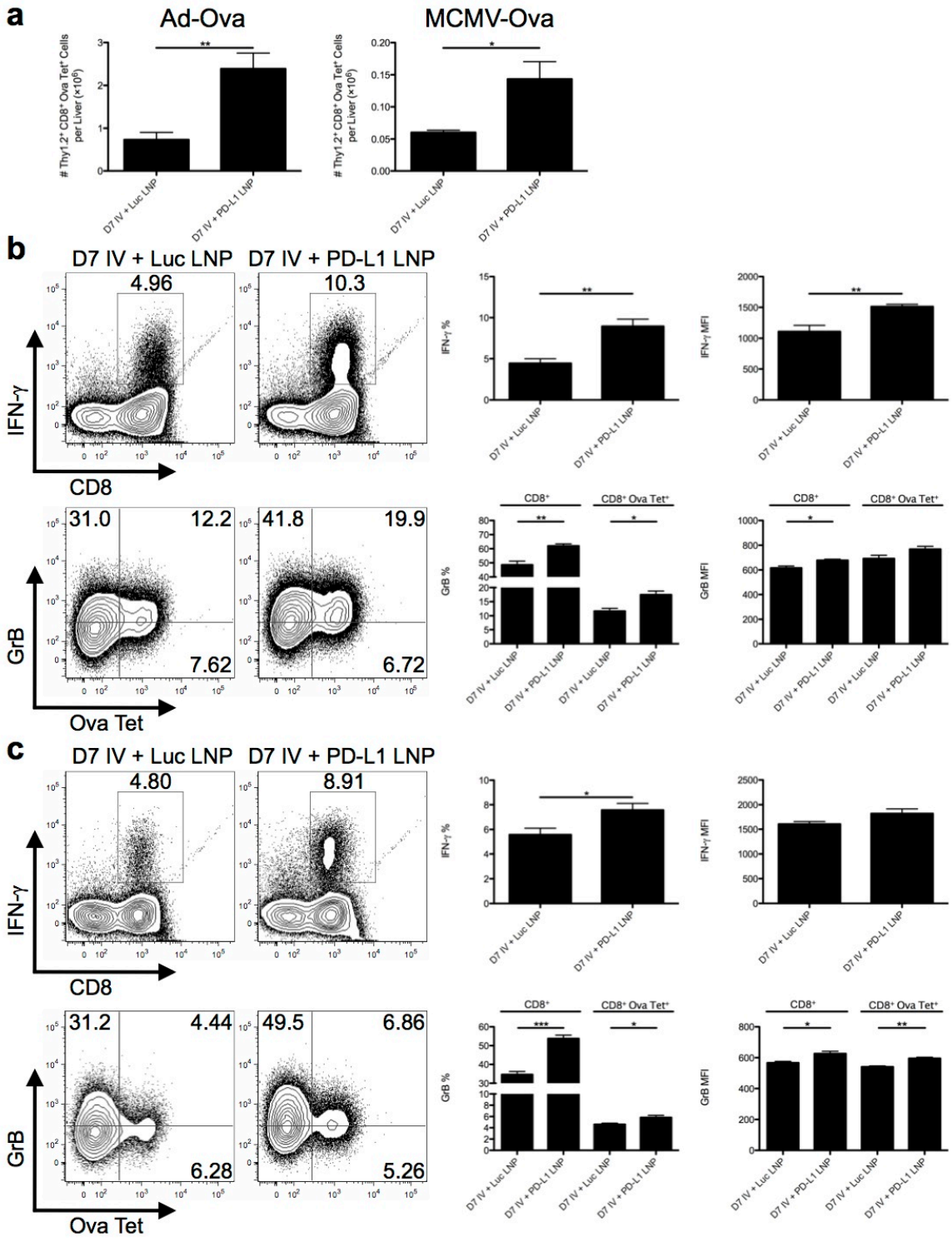
a
Ad-Ova
MCMV-Ova
Thy1.2+ CD8+ Ova Tet+ Cells per Liver (×10^6)
D7 IV + Luc LNP
D7 IV + PD-L1 LNP
b
D7 IV + Luc LNP
D7 IV + PD-L1 LNP
4.96
10.3
IFN-γ
CD8
IFN-γ %
IFN-γ MFI
31.0
12.2
7.62
41.8
19.9
6.72
GrB
Ova Tet
CD8+
CD8+ Ova Tet+
GrB %
GrB MFI
c
4.80
8.91
31.2
4.44
6.28
49.5
6.86
5.26

Figure 4.16 D5 PD-L1 LNP treatment enhances $CD8^+$ T cell accumulation and full effector function. C57BL/6 mice were IV infected with either 2.5×10^7 IU Ad-Ova or 1×10^4 IU MCMV-Ova, (**a**) and the number of Ova Tet^+CD8^+ T cells was determined at D7 post-infection (n = 4 per group). In all experimental groups, Luc LNP or PD-L1 LNP was injected at only D5, after the peak in NK cell presence. Antigen-specific $CD8^+$ T cell IFN-γ was assessed after a 5 hr re-stimulation with 2 μg/mL SIINFEKL peptide, and GrB was determined directly *ex vivo* for both (**b**) Ad-Ova (n = 4 per group) and (**c**) MCMV-Ova (n = 4 per group) infections. Numbers in the scatter plots represent percentages. Mean ± s.e.m.; **P* < 0.05, ***P* < 0.01, and ****P* < 0.001.

Figure 4.17

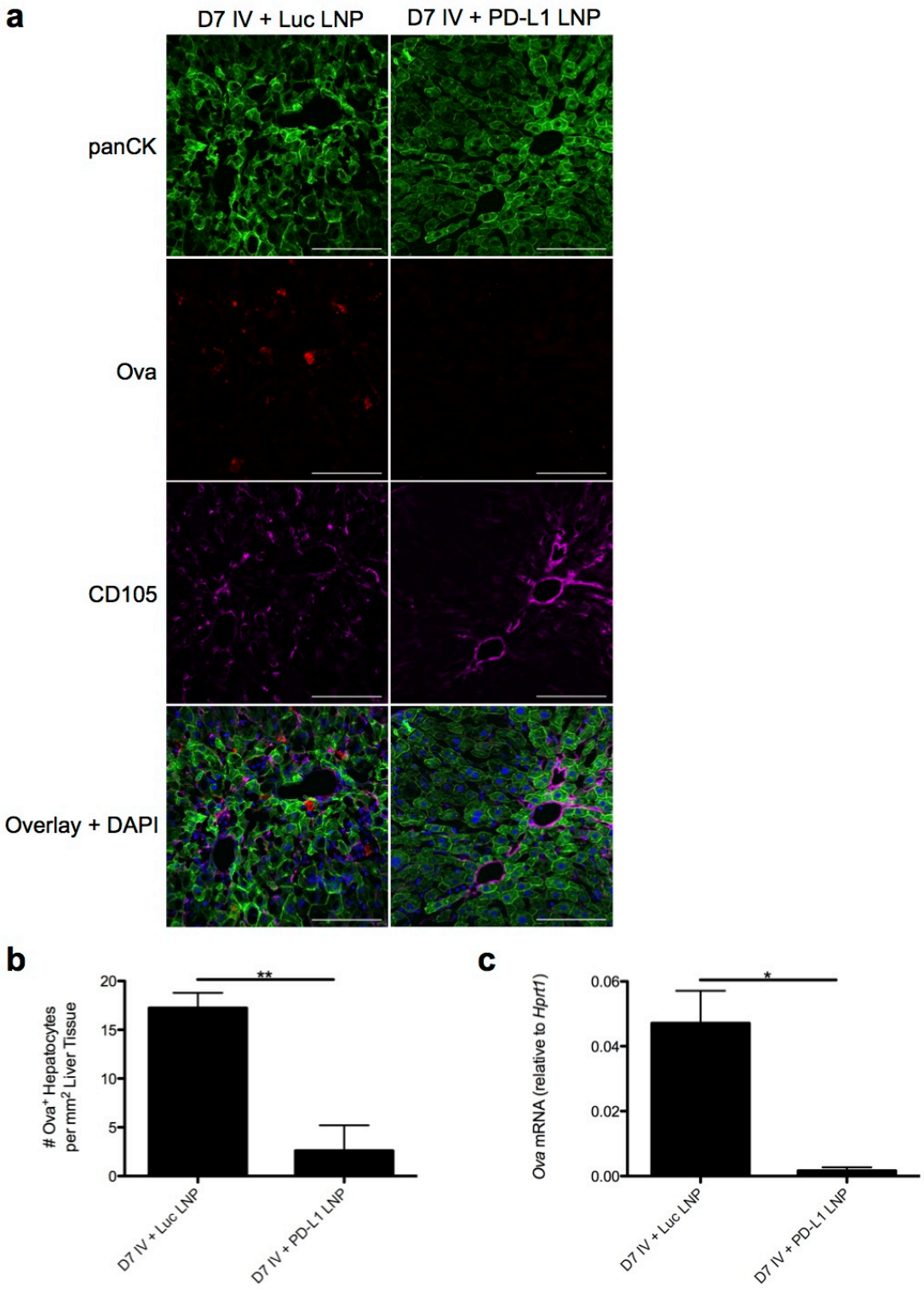
a
D7 IV + Luc LNP
D7 IV + PD-L1 LNP
panCK
Ova
CD105
Overlay + DAPI
b
Ova+ Hepatocytes per mm2 Liver Tissue
20
15
10
5
0
**
D7 IV + Luc LNP
D7 IV + PD-L1 LNP
c
Ova mRNA (relative to Hprt1)
0.06
0.04
0.02
0.00
*
D7 IV + Luc LNP
D7 IV + PD-L1 LNP

Figure 4.17 Enhanced viral clearance is observed during the D5 delay of PD-L1 LNP treatment. PLP-fixed/OCT-frozen liver cross sections were collected from naïve C57BL/6 mice or mice at D7 after IV infection with 2.5×10^7 Ad-Ova that had received Luc LNP or PD-L1 LNP administered at D5. (**a**) Sections were stained with anti-panCK (green), anti-Ova (red), anti-CD105 (magenta), and DAPI (blue). A representative collection of images is shown (n = 3 per group). Scale bar, 100 μm. (**b**) Hepatocytes that were virally infected ($panCK^+Ova^+$ cells) were enumerated per field of view D7 post-infection (n = 3 per group). (**c**) From the same animals used for microscopy, total RNA from a whole liver sample was taken prior to fixative application and *Ova* mRNA was measured by real-time PCR (n = 3 per group). Mean ± s.e.m.; $*P < 0.05$ and $**P < 0.01$.

Figure 4.18

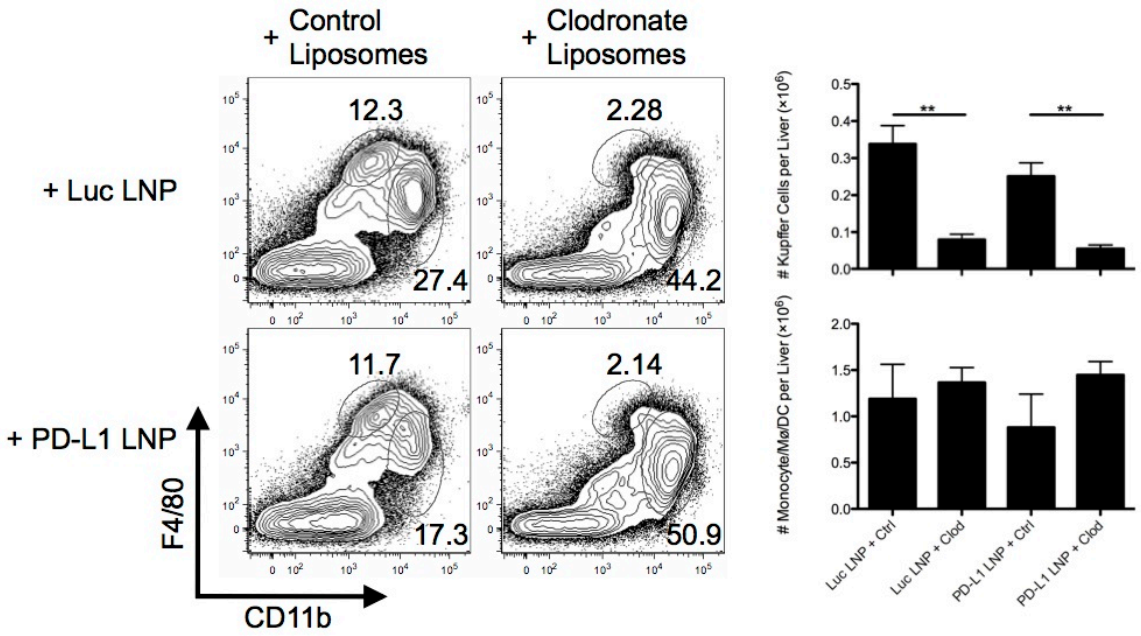
+ Control Liposomes
+ Clodronate Liposomes
+ Luc LNP
+ PD-L1 LNP
12.3
27.4
2.28
44.2
11.7
17.3
2.14
50.9
F4/80
CD11b
Kupffer Cells per Liver (×10⁶)
Monocyte/Mø/DC per Liver (×10⁶)
**
**
Luc LNP + Ctrl
Luc LNP + Clod
PD-L1 LNP + Ctrl
PD-L1 LNP + Clod

Figure 4.18 Clodronate liposomes effectively deplete Kupffer cells. C57BL/6 mice were IV infected with 2.5×10^7 Ad-Ova, IV injected with control or 55 mg/kg clodronate liposomes at D3 post-infection, and IV injected with 0.5 mg/kg Luc or PD-L1 LNP at D5 post infection. In a MHC $II^+Thy1.2^-$ gate, the specific depletion of KCs ($F4/80^+CD11b^{lo}$) compared to monocyte/Mø/DC populations ($CD11b^{hi}$) was confirmed by FACS analysis at D7 post-infection (n = 3 per group). Numbers in the scatter plots represent percentages. Mean ± s.e.m.; $^{**}P < 0.01$.

Figure 4.19

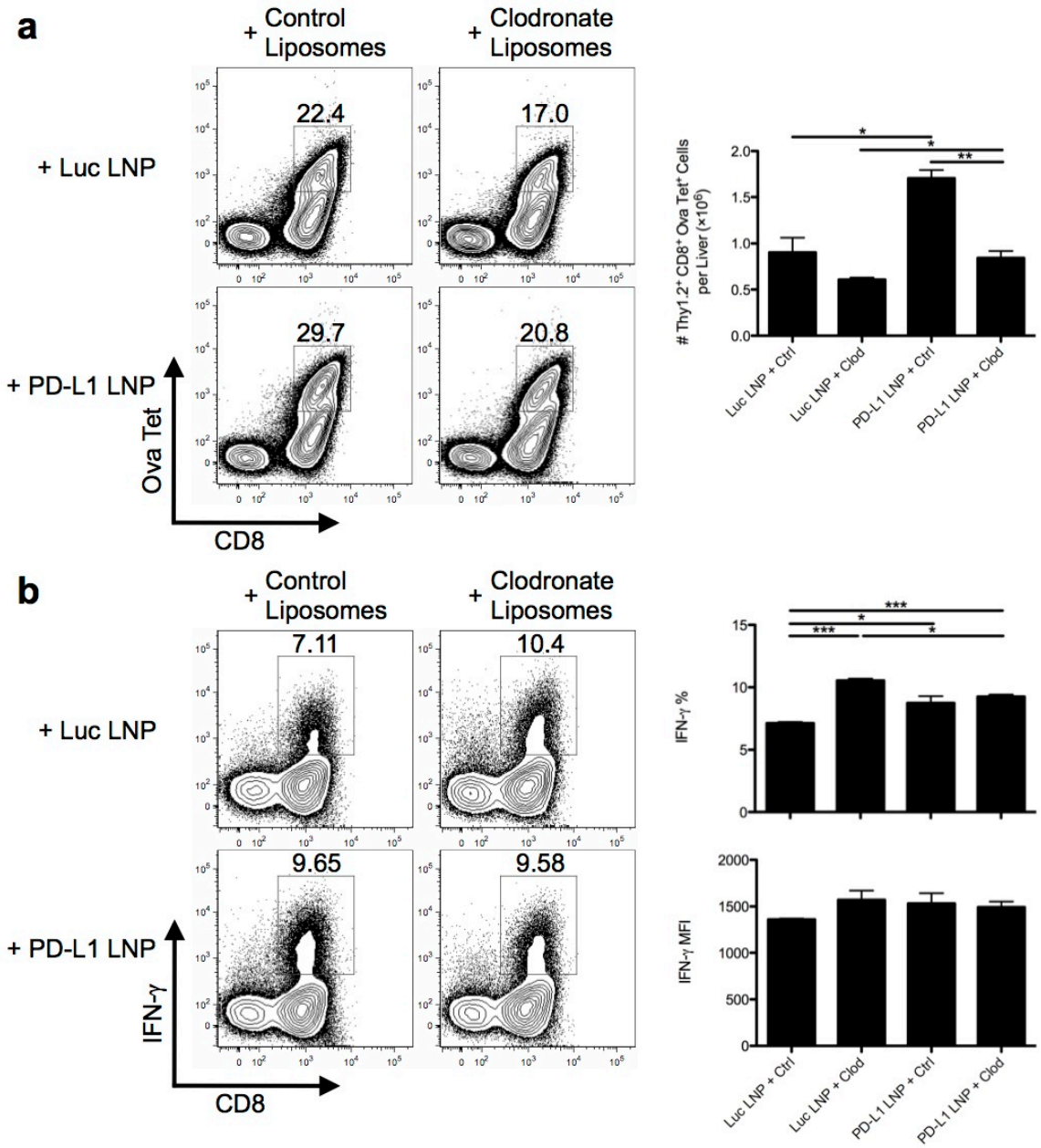
a
+ Control Liposomes
+ Clodronate Liposomes
+ Luc LNP
+ PD-L1 LNP
22.4
17.0
29.7
20.8
Ova Tet
CD8
Thy1.2+ CD8+ Ova Tet+ Cells per Liver (×10^6)
Luc LNP + Ctrl
Luc LNP + Clod
PD-L1 LNP + Ctrl
PD-L1 LNP + Clod
b
7.11
10.4
9.65
9.58
IFN-γ
IFN-γ %
IFN-γ MFI

Figure 4.19 Kupffer cells are necessary for optimal expansion of $CD8^+$ T cells and mediate their IFN-γ production. C57BL/6 mice were IV infected with 2.5×10^7 IU Ad-Ova, IV injected with control or 55 mg/kg clodronate liposomes at D3 post-infection, and IV injected with Luc or PD-L1 LNP at D5 post-infection. (**a**) The number of Ova Tet^+CD8^+ T cells was calculated at D7 post-infection in each experimental group (one-way ANOVA/Tukey's post test; n = 3 per group). (**b**) IFN-γ was assessed after a 5 hr re-stimulation with 2 μg/mL SIINFEKL peptide (one-way ANOVA/Tukey's post test; n = 3 per group). Numbers in the scatter plots represent percentages. Mean ± s.e.m.; $*P < 0.05$, $**P < 0.01$, and $***P < 0.001$.

Acknowledgments

I thank Alnylam Pharmaceuticals siRNA synthesis and formulation groups for providing PD-L1 siRNA and LNP nanoparticles. This project was in part formed through a collaboration initiated by Antonin de Fougerolles, and I am grateful for a pilot grant on behalf of Alnylam Pharmaceuticals. I also give gratitude to Tatiana Novobrantseva and Anna Borodovsky of Alnylam Pharmaceuticals for contributions to editing and experimental design. The University of Virginia Research Histology Core Facility and the University of Virginia Advanced Microscopy Facility kindly assisted in tissue preparation and confocal/brightfield imaging. Michael Solga and the University of Virginia Flow Cytometry Core Facility contributed to performing and outlining FACS-sorting and Amnis Imagestream^X experiments. NIH Grants DK063222, U19 AI083024, and Immunology Training Fellowship T32 AI07496 supported this work.

Methods

PD-L1 siRNA Selection and LNP Preparation

A total of 30 siRNAs with 100% homology with *Mus musculus Pdl1* (sequence NM_021893.2) were selected using proprietary algorithms. Single-strand RNAs were produced, annealed into duplexes[161], and transfected into BNL and NMuLi liver epithelial cell lines using Lipofectamine RNAiMAX transfection reagent (Invitrogen, Carlsbad, CA) at 0.1 nM and 10 nM. mRNA levels were quantified 24 hrs after transfection by Q-PCR and normalized to *Mus musculus Gapdh* (Applied Biosystems, Foster City, CA). siRNA showing best knockdown were selected for 12 point dose-response ranging from 10 nM to 0.01 pM to determine the IC_{50} values. The most potent duplex with the sequence

Sense: AGAcGuAAGcAGuGuuGAAdTsdT

Antisense: UUcAAcACUGCUuACGUCUdTsdT

was selected for scale up and LNP formulation. As a negative control a siRNA duplex for luciferase was used, with the sequence

Sense: cuuAcGcuGAGuAcuucGAdTsdT

Antisense: UCGAAGuACUcAGCGuAAGdTsdT

Small case letters represent residues with 2'-OMe modifications. Deoxythymidine (dTdT) was added to 3'-ends to protect from exonuclease degradation. PD-L1 specific and control siRNAs were formulated into 70-80 nm LNPs with C12-200 as the primary cationic lipid as described[141].

Animals, Infections, and Treatments

C57BL/6 mice were used in these experiments (Taconic Farms, Hudson, NY). NKDTR-EGFP mice were kindly provided by Eric Vivier (Centre d'Immunologie de Marseille-

Luminy, Université de la Méditerranée, Marseille, France)[147]. *Thy1.1*$^{+/-}$OT-I*(Tcra/Tcrb)*$^{+/-}$ mice were bred from *Thy1.1*$^{+/+}$ and OT-I *(Tcra/Tcrb)*$^{+/+}$*Rag1*^{tm1Mom} mice (Taconic Farms). Animals used were 6 to 10 weeks of age and housed in a pathogen-free facility under protocols approved by the Institutional Animal Care and Use Committee at the University of Virginia (Charlottesville, VA).

Replication-deficient type 5 adenovirus lacking the *E1* and *E3* genes and expressing the ovalbumin protein (Ad-Ova) under the control of the human *Cmv* promoter was provided by Timothy L. Ratliff (Iowa Gene Transfer Vector Core, University of Iowa, Iowa City, IA). Mouse cytomegalovirus expressing the ovalbumin protein fused to the transferrin receptor (MCMV-Ova) under the control of the HCMV *Ie1* promoter (*Miep*) was provided by Ann B. Hill (Oregon Health and Science University, Portland, Oregon). Mice were infected with 2.5×10^7 infectious units (IU) Ad-Ova or 1×10^4 IU MCMV-Ova via intravenous (IV) injection in the caudal vein.

Mice were IV injected with 0.5 mg/kg LNP containing luciferase siRNA (Luc LNP) or PD-L1 siRNA (PD-L1 LNP) at days -1, 1, 3, and 5 or only day 5 relative to day 0 infection. For siRNA LNP uptake experiments, mice were IV injected with 0.5 mg/kg AF488- or AF647-labeled siRNA LNP at day 5 post-infection, and liver mononuclear cells were harvested 1.5 hrs later (Alnylam Pharmaceuticals, Cambridge, MA). For CD8$^+$ T cell depletion, mice were intraperitoneally (IP) injected with 300 μg anti-CD8 (2.43) (BioXCell, West Lebanon, NH) 1 day prior to infection. For NK cell depletion, mice were given 250 ng diphtheria toxin (DT) from *Corynebacterium diphtheriae* (Sigma-Aldrich, St. Louis, MO) IP at days -1, 1, and 3 relative to day 0 infection. For Kupffer cell depletion, mice were IV injected with control or clodronate liposomes (Encapsula NanoSciences,

Nashville, TN) at day 3 post-infection. Clodronate liposomes were titrated prior to prevent an off-target effect, and a low concentration (55 mg/kg) achieved differential tissue Kupffer cell and tissue/blood-borne/bone marrow monocyte/Mø/DC depletion.

Quantitative Reverse-Transcription PCR

Total RNA was isolated using the Trizol method (Invitrogen) and reverse-transcribed using High Capacity RNA-to-cDNA Master Mix (Applied Biosystems). Q-PCR was performed using Fast SYBR Green Master Mix (Applied Biosystems) on an AB StepOne Plus Real-Time PCR System. QuantiTect primers for *Gallus gallus Ova*, *Mus musculus Pdl1* (Qiagen, Valencia, CA), and self-designed primers for *Mus musculus* hypoxanthine phosphoribosyltransferase (*Hprt1*)

Forward: 5'-CTCCGCCGGCTTCCTCCTCA-3'

Reverse: 5'-ACCTGGTTCATCATCGCTAATC-3'

were used for detection. Data were generated by the comparative threshold cycle (ΔC_T) method by normalizing to *Hprt1*.

5'-RACE PCR

C57BL/6 mice were given 0.5 mg/kg Luc LNP or PD-L1 LNP IV, and KCs were isolated by FACS-sorting 4 hrs later. Approximately 50 ng of RNA isolated from sorted cells using the GenElute Mammalian Total RNA Miniprep Kit (Sigma-Aldrich) was used for 5'-RACE PCR using the GeneRacer Kit (Invitrogen). Briefly, RNA was dephosphorylated for 1 hr at 50°C with calf intestinal alkaline phosphatase (CIAP), decapped for 1 hr at 37°C with tobacco acid pyrophosphatase (TAP), and ligated to an RNA oligonucleotide for 1 hr at 37°C with T4 RNA ligase. RNA was reverse-transcribed using a *Pdl1* gene-specific primer

Reverse: 5'-GACCTCTGTGTTCCCTGCTTG-3'

with SuperScript III RT (Invitrogen). Nested PCR was performed using Platinum *Taq* DNA Polymerase High Fidelity (Invitrogen) on a BioRad C1000^{TM} Thermal Cycler (BioRad, Hercules, CA). First round *Pdl1* PCR primers

Forward: 5'-CGACTGGAGCACGAGGACACTGA-3'

Reverse: 5'-ACGGAGGATGCTAAGCAGCAGTTG-3'

and nested *Pdl1* PCR primers

Forward: 5'-GGACACTGACATGGACTGAAGGAGTA-3'

Reverse: 5'-CCCGGCACTGAGCAGAGGAAAAG-3'

were used for detection. PCR products were separated by electrophoresis on a 1.8% agarose gel. cDNA bands were excised, purified on S.N.A.P. columns, and incubated for 4 hrs at 16°C with pCR4-TOPO vector. TOP10 *Escherichia coli* chemically competent cells were transformed and plated overnight at 37°C (Invitrogen). Ampicillin-resistant clones were expanded; plasmids were isolated using a QIAprep Spin Miniprep Kit (Qiagen) and sequenced on an AB 3730 DNA Analyzer using M13 reverse primers (Invitrogen).

Western Blot

Whole liver sections were homogenized, protein concentration was determined using the Pierce BCA Protein Assay Kit (Thermo Scientific, Rochester, NY), and proteins were resolved by electrophoresis on 10% SDS-polyacrylamide gels and transferred to nitrocellulose membranes. Membranes were then incubated with biotinylated anti-PD-L1 (pAb), biotinylated anti-β-actin (AC-15), and streptavidin-HRP (R&D Systems, Minneapolis, MN) followed by visualization with SuperSignal West Pico

Chemiluminescent Substrate (Thermo Scientific). Optical densitometry was performed using ImageJ 1.38x software (NIH, USA).

ALT Assay

Mice were sacrificed by lethal injection of sodium pentobarbital (Nembutal; Abbott Laboratories, Chicago, IL) and bled via the retro-orbital venous plexus. The concentration of alanine aminotransferase (ALT) was determined by mixing 20 μL serum with 200 μL liquid ALT working buffer (Pointe Scientific, Canton, MI). The reaction was incubated for 180 s at 37°C. Absorbance was read at 0, 60, 120, and 180 s time points at 340 nm using a PowerWave XS Microplate Spectrophotometer (BioTek, Winooski, VT).

Liver Mononuclear Cell Isolation

Mononuclear cells were isolated from livers according to previous work[46,116,117]. Briefly, livers were flushed via the portal vein with 0.05% collagenase IV (Sigma-Aldrich) in 1×PBS and washed with Iscove's Modified Dulbecco's Medium (IMDM) containing 10% newborn calf serum. Liver tissue was then homogenized and further digested with 0.05% collagenase IV in 1×PBS. Mononuclear cells were then isolated via Histodenz (Sigma-Aldrich) gradient centrifugation, and the number of viable cells was determined based on 0.1% Trypan blue (Sigma-Aldrich) exclusion.

Flow Cytometry

The following mAbs were used for cell surface and intracellular staining: anti-CD4 PerCP-Cy5.5 (RM4-5), anti-CD11b PE-Cy7 (M1/70), anti-CD40 PE (3/23), anti-Ki-67 PE (B56) (BD Biosciences, Franklin Lakes, NJ), anti-CD105 AF647 (MJ7/18), anti-CD105

PE (MJ7/18), anti-CD146 AF488 (ME-9F1), anti-MHC II (I-A/I-E) AF680 (M5/114.15.2), anti-Thy1.2 AF594 (53-2.1) (BioLegend, San Diego, CA), anti-CD3ε PerCP-Cy5.5 (145-2C11), anti-CD8α APC-eF780 (53-6.7), anti-CD11c PerCP-Cy5.5 (N418), anti-CD45 eF450 (30-F11), anti-CD80 PE (16-10A1), anti-CD86 PE (GL1), anti-F4/80 APC (BM8), anti-F4/80 PE (BM8), anti-IFN-γ APC (XMG1.2), anti-MHC II (I-A/I-E) FITC (M5/114.15.2), anti-NK1.1 APC (PK136), anti-NK1.1 FITC (PK136), anti-PD-L1 PE (M1H5), anti-Thy1.2 eF450 (53-2.1) (eBioscience, San Diego, CA), and anti-granzyme B PE (GB12) (Invitrogen). H2-K^b Ova-tetramer (SIINFEKL) APC (MHC Tetramer Core Laboratory, Baylor College of Medicine, Houston, TX) was used to identify Ova-specific $CD8^+$ T cells. Cell surface staining of 1.5×10^6 mononuclear cells was performed by first blocking with anti-CD16/CD32 (2.4G2) (Lymphocyte Culture Center, University of Virginia, Charlottesville, VA) followed by specific antibody labeling for 15 min at 4°C in FACS Buffer (1×PBS containing 2% fetal bovine serum and 0.1% NaN_3). Cells were fixed in BD Cytofix/Cytoperm (BD Biosciences). For intracellular cytokine detection, cells were re-stimulated with 5 ng/mL PMA and 500 ng/mL ionomycin (Sigma-Aldrich) or 2 μg/mL SIINFEKL peptide (AnaSpec, Fremont, CA), blocked with 1 μL/mL GolgiPlug and 1 μL/mL GolgiStop, and permeabilized with BD Perm/Wash (BD Biosciences). For BrdU cell proliferation assays, 0.5 mg BrdU was administered IP daily to mice, and cells were stained with anti-BrdU FITC and 7-AAD using the BrdU Flow Kit (BD Biosciences). Data were collected on a BD FACS Canto II (BD Immunocytometry Systems, San Jose, CA) and analyzed using FlowJo 8.8.6 software (Tree Star Inc., Ashland, OR). For analysis of PCR products, cells were sorted on an iCyt Reflection Cell Sorter (iCyt Mission Technology, Champaign, IL). For visualization of cells, images were captured on an Amnis Imagestream^X. Internalization scores were calculated using IDEAS 4.0

software (Amnis Corporation, Seattle, WA) by creating a cytoplasmic mask eroded 5 pixels in from the cell membrane defined by the brightfield image. The fraction of fluorescent pixels in the fluorochrome-labeled siRNA LNP channel was calculated as a ratio of pixels inside versus outside the mask[162].

Microscopic Studies

Livers were flushed with 1×PBS and periodate-lysine-paraformaldehyde fixative (PLP), excised, and then incubated in PLP for 3 hrs at 4°C according to previous work[163]. After passage over a sucrose gradient, livers were frozen in OCT, sectioned at 5 μm thickness, blocked with 2.4G2 solution (2.4G2 media containing anti-CD16/32, 30% chicken/donkey/horse serum, and 0.1% NaN_3), and stained with anti-Ova AF647 (pAb) (Antibodies-Online), anti-CD4 AF488 (RM4-5), anti-CD8α AF555 (53-6.7), anti-CD105 AF555 (MJ7/18), anti-CD105 AF647 (MJ7/18), anti-F4/80 AF488 (CI:A3-1), anti-MHC II (I-A/I-E) Pacific Blue (M5/114.15.2), anti-NKp46 AF647 (pAb) (BioLegend), anti-B220 APC (RA3-6B2) (eBioscience), anti-PD-L1 AF555 (pAb) (R&D Systems), DAPI (Roche, Indianapolis, IN), and anti-panCK AF488 (C-11) (Sigma-Aldrich). Confocal microscopy was performed on a Zeiss LSM-700 microscope, and the data were analyzed using Zen 2009 Light Edition software (Carl Zeiss MicroImaging GmbH, Jena, Germany). For H & E staining, excised samples were incubated overnight in 10% buffered formalin acetate (Fisher Scientific, Pittsburgh, PA) at room temperature, washed with 1×PBS, and stored in 70% EtOH prior to paraffin embedding and sectioning. Brightfield microscopy was conducted on an Olympus BX51 microscope (Olympus America Inc., Center Valley, PA).

Statistical Analysis

Significant differences between experimental groups were calculated using the two-tailed Student's t test or one-way ANOVA (with group comparisons ≥ 3). Data analysis was performed using Prism 5.0a software (GraphPad Software Inc., La Jolla, CA). Values of $P < 0.05$ were regarded as being statistically significant and noted as * < 0.05, ** < 0.01, and *** < 0.001.

CHAPTER 5

Liver-Primed $CD8^+$ T Cells Suppress Antiviral Adaptive Immunity Through Gal-9-Independent Tim-3 Engagement of HMGB-1

Abstract

The liver is a tolerogenic environment exploited by persistent infections such as hepatitis B (HBV) and C (HCV) viruses. In a murine model of intravenous (IV) hepatotropic adenovirus infection, liver-primed antiviral $CD8^+$ T cells fail to produce pro-inflammatory cytokines and do not display cytolytic activity characteristic of effector $CD8^+$ T cells generated by infection at an extrahepatic, *i.e.* subcutaneous (SC), site. Importantly, the liver-generated $CD8^+$ T cells also appear to have a T regulatory (T_{reg}) cell function exemplified by their ability to limit proliferation of antigen-specific T effector (T_{eff}) cells *in vitro* and *in vivo* via Tim-3 expressed by the $CD8^+$ T_{reg} cells. Regulatory activity did not require recognition of the canonical Tim-3 ligand Gal-9 but was dependent on $CD8^+$ T_{reg} cell surface Tim-3 binding to the alarmin HMGB-1. Thus, virus-specific $Tim\text{-}3^+CD8^+$ T cells operating through HMGB-1 recognition in the setting of acute and chronic viral infections of the liver may act to dampen hepatic T cell responses in the liver microenvironment and as a consequence limit immune mediated tissue injury or promote the establishment of persistent infections with viruses such as HCV.

Introduction

Immune cells within the normal (non-inflamed) liver are maintained within a state of active tolerance due to continuous exposure to microbe-derived pathogen associated molecular patterns (PAMP), toxins, and food-derived antigens, which stimulate high level production of immunoregulatory molecules (*e.g.* IL-10, TGF-β, and PD-L1)[19,20,23]. Hepatotropic viruses adapted for efficient replication and persistence in the liver have evolved to take advantage of this critical window leading to dysfunctional adaptive immune responses characterizing acute (adenovirus)[28,116,164] and chronic (HBV and HCV)[18,31,127] infections. Cytotoxic $CD8^+$ T cells are the main cell type responsible for clearing virally infected cells in an antigen-specific manner. During the course of intrahepatic viral infection, the generation of antiviral $CD8^+$ T_{eff} cells is suboptimal in part due to defective antigen presentation within the infected liver and a skewed $CD4^+$ T_h1/T_h2 cell balance resulting in their inability to proliferate robustly, to produce critical pro-inflammatory cytokines, and to generate cytolytic effector molecules[14,23]. Understanding the mechanisms that orchestrate the development of this dysfunctional intrahepatic $CD8^+$ T cell response is critical for antiviral immunotherapy target selection and development.

Another factor limiting intrahepatic $CD8^+$ T cell responses to virus infection of the liver is the development of inducible T regulatory (iT_{reg}) cells of the $CD4^+$ (T_h3 and T_r1)[165] and $CD8^+$ lineages[54]. Initial studies identifying T_{reg} cells acting in an antigen-specific manner included an investigation of chronic HCV infection in the livers of a cohort of pregnant women that received HCV contaminated anti-D immunoglobulin[166]. Currently, it is established that foreign antigen, IL-2, IL-10, TGF-β, galectin-9 (Gal-9), and/or PD-1/PD-

L1 signaling can influence the differentiation of iT_{reg} cells[80,83-85,167,168]. Further, suppression of T cell responses is mediated through a variety of antigen-specific cell contact dependent and independent mechanisms including IL-2 sequestration[169], release of anti-inflammatory cytokines (IL-10 and TGF-β)[53,54,165,170-172], chemokine production (CCL4)[173], CTLA-4 co-stimulation[174], Fas/FasL or perforin killing[175-177], granzyme B (GrB) negative feedback loops[178], and negative PD-1/PD-L1 signaling[179-181]. Thus far, distinguishing T_{eff} from T_{reg} cell populations within the infected liver has proven difficult since the expression of cell markers characteristic of T_{reg} cells such as FoxP3, Helios, CTLA-4, GITR, CD25, CD38, CD103, CD127, Lag-3, Ly49 inhibitory receptors, and TNFR is quite variable[165,175,182,183].

Intrahepatic $CD8^+$ T cells responding to acute and chronic HCV viral infections are capable of producing IL-10 and co-express PD-1, PD-L1, and Tim-3. There is compelling evidence suggesting that simultaneous blockade of these corresponding pathways can improve antiviral immunity within the liver[82,88,89,184] as well as immunity to tumors[56,91] prompting the development of novel therapeutics to modulate these regulatory elements. $CD8^+$ T cell derived IL-10 can reduce IL-12R, IL-2, IFN-γ, and Tbet expression in an autocrine loop[49,165,185]. In addition, IL-10 can decrease antigen presenting cell (APC) MHC II and co-stimulatory molecule expression and IL-12 and TNF-α production[50,51,165]. Programmed death 1 (PD-1), a CD28 family member, upon engagement with PD-1 ligand (PD-L1), plays a critical role in suppressing $CD8^+$ T cell responses via direct SHP-2-mediated inhibition of phosphorylation events and Ca^{++} fluxes downstream of the T cell receptor (TCR) signal[61,74,119,120,128-130]. Within the ectodomain of Tim-3, a member of the T cell immunoglobulin and mucin (Tim) family, Gal-9 recognizes mucin region N- and O-linked glycosylation sites, and

phosphatidylserine binds via the FG cleft in the immunoglobulin variable region[76]. Gal-9 is particularly abundant in the liver, can be induced in viral infection by IFN-γ within T cells among other cell types, and upon engagement of Tim-3 dampens CD8$^+$ T cell IL-2, IFN-γ, and proliferation through ill-defined signaling events[76,77,81,82,88,91]. *E. coli*-derived recombinant Tim-3 tetramers, inherently lacking oligosaccharides, are capable of binding B cells, T cells, dendritic cells (DC), and macrophages (Mø), suggesting other non-Gal-9 ligands exist[79].

Tim-3 was recently discovered to bind a novel moiety, high-mobility group box 1 (HMGB-1), within DCs via its FG cleft preventing tumor-derived RNA/DNA activation[103]. HMGB-1 is classified under the alarmins, which conventionally relay danger (*i.e.* damage) associated molecular pattern (DAMP) signals to APCs. HMGB-1 was first identified as a chromatin associated protein stabilizing histone formation and facilitating transcription[95]. Although passively released by necrotic cells, HMGB-1 active secretion from monocytes, Møs, DCs, and NK cells has been observed[93]. Upon binding the receptor for advanced glycation end products (RAGE) expressed by DCs and T cells, HMGB-1 can act as a cytokine directly shaping maturation and proliferation, respectively[96-100,102].

I originally hypothesized that antiviral intrahepatic CD8$^+$ T cells had self-limiting T_{reg} cell properties dependent on their secretion of IL-10, Gal-9, and/or expression of PD-L1. Accordingly, the PD-1/PD-L1$^+$Tim-3$^+$CD8$^+$ T cells did not produce Gal-9; moreover, IL-10, PD-L1, and Gal-9 antibody blockades indicated these pathways were not linked to the suppressor mechanism. Surprisingly, I found that intrahepatic CD8$^+$ T_{reg} cell surface Tim-3 acts as a decoy receptor. *In vitro* co-cultures and *in vivo* models together indicated that CD8$^+$ T_{eff} cell proliferation was negatively affected by the binding and

sequestration of HMGB-1 by Tim-3 displayed on intrahepatic $CD8^+$ T_{reg} cells. The discovery that Tim-3/HMGB-1 interaction occurs on the surface of T_{reg} cells adds to the vast array of mechanisms aforementioned responsible for limiting T_{eff} cell responses. This may explain why initial acute infection in the liver facilitates the onset of chronic infection, where naïve $CD8^+$ T cells are unable to become efficiently activated by viral-derived antigen.

Results

PD-1 and Tim-3 Co-Expression is Enhanced on Antigen-Specific CD8$^+$ T Cells in Response to Hepatic Viral Infection

To examine the potential roles of PD-1/PD-L1 and Tim-3 inhibitory signaling during intrahepatic antiviral immune responses, I first characterized inhibitory receptor expression on CD8$^+$ T cells responding to SC or IV adenovirus administration. SC infection of the left flank leads to a local immune response in the skin where DCs uptake and present antigen as they enter the afferent lymphatic vessels of the inguinal lymph node (Ig LN). Naïve CD8$^+$ T cells primed in the Ig LN eventually re-circulate to distal organs, including the liver and spleen. Conversely, during IV infection, greater than 90% of the adenovirus targets the liver, where mainly hepatocytes are transduced[28]. Ova-specific CD8$^+$ T cells primed directly in the liver by DCs, Kupffer cells, or hepatocytes themselves produce significantly less TNF-α, IL-2, and IFN-γ (**Fig. 2.2a**) and granzyme B (data not shown) compared to CD8$^+$ T cells that have trafficked from the Ig LN in response to adenovirus expressing ovalbumin (Ad-Ova). Further, despite CD8$^+$ T cell differentiation and expansion is highly dependent on IL-2 in most circumstances[29,30], CD8$^+$ T cells do not up-regulate CD25 within the liver 24-48 hrs following Ad-Ova IV infection (**Fig. 2.2b**).

A kinetic analysis of the IV infection reveals that the peak in both bulk and Ova-specific intrahepatic CD8$^+$ T cell absolute number occurs at day 7 (D7) (**Fig. 5.1a**). The peak in PD-1 and Tim-3 expression on bulk CD8$^+$ T cells also occurs at D7, coinciding with maximal release of cytokine (**Fig. 5.2a**). CD8$^+$ T cells uniquely co-express PD-1 and Tim-3 during IV infection of the liver. Further, co-expression of these receptors is

enriched on Ova Tet$^+$CD8$^+$ T cells. Despite much fewer CD8$^+$ T cells infiltrate the livers and spleens of SC infected mice, the frequency of Ova-specific CD8$^+$ T cells is comparable. In addition, IV infection with a different adenoviral vector expressing β-galactosidase (Ad-LacZ) produces similar results analogous to Ad-Ova regarding PD-1 and Tim-3 surface expression (**Fig. 5.1b,c**). PD-L1, the major ligand for PD-1 in this model, followed a bimodal kinetic pattern, with no differences observed between infection groups up to D7 and continued elevation at later time points in the IV infected liver. Gal-9 expression was detected on naïve and SC splenic CD8$^+$ T cells, but was lost or shed on liver-primed CD8$^+$ T cells by D7 (**Fig. 5.2a,b**). In summary, liver-primed CD8$^+$ T cells have pronounced co-expression of PD-1/PD-L1 and Tim-3.

Liver-Primed CD8$^+$ T Cells Exert a T_{reg} Suppressor Function on the Priming of Naïve CD8$^+$ T Cells *In Vitro* via Linked Suppression

Since PD-1 and Tim-3 inhibitory signaling plays a major role in dampening CD8$^+$ T cell immune responses to a variety of cancers and acute/chronic viral infections, I hypothesized that CD8$^+$ T cells primed in the liver were actively contributing to a dysfunctional intrahepatic immune response via mechanisms related to PD-1 and Tim-3 signaling. Parting from the traditional view relating to inward negative signaling from PD-1 and Tim-3 explaining CD8$^+$ T cell dysfunction, I envisioned the intrahepatic CD8$^+$ T cells possessing an outward T_{reg} cell function related to these pathways affecting naïve CD8$^+$ T cell activation and expansion. In order to model this, I first utilized an *in vitro* system employing TCR transgenic OT-I T cells, where Thy1 congenically mismatched CFSE-labeled naïve CD8$^+$ OT-I T cells were placed in culture with equal numbers of CD8$^+$ T cells from the D7 SC spleen or IV liver. Bone marrow-derived dendritic cells

(BMDC) matured for 7 days in rIL-4 and rGM-CSF, pulsed with an ovalbumin derived octapeptide sequence ($Ova_{257-264}$:SIINFEKL) served as the antigenic stimulant. By D2 and D3 of co-culture, the SC $CD8^+$ T cells did not affect OT-I T cell division, whereas the IV $CD8^+$ T cells suppressed OT-I T cell division by three standards: the number of dividing OT-I T cells, division index, and percent suppression (**Fig. 5.3a,b**). This suppressive effect of IV infected liver-derived $CD8^+$ T cells was observed over a range of OT-I:IV $CD8^+$ T ratios (**Fig. 5.3c**). Significantly less IL-2 and IFN-γ could be detected in the supernatants collected from OT-I/IV $CD8^+$ T cell co-cultures (**Fig. 5.3d**) consistent with lowered surface expression of CD25 and intracellular detection of IFN-γ/CD107a within OT-I T cells (**Fig. 5.3e**).

To confirm the IV $CD8^+$ T cells possessed a *bona fide* T_{reg} phenotype and were not simply killing the BMDCs or competing with OT-I T cells for access to antigen, multiple parameters were examined. First, the SC $CD8^+$ T cells which were characterized by a similar Ova Tet^+ frequency (**Fig. 5.1b**) and had more cytolytic potential in killing targets *in vitro* and *in vivo* (**Fig. 2.3**) could not regulate OT-I T cells. Second, T_{regs} are known to be highly sensitive to antioxidants including β-mercaptoethanol (βME)[172], and addition of βME to the co-cultures completely inhibited IV $CD8^+$ T cell suppression (**Fig. 5.4**). Third, competition with OT-I T cell access to peptide/MHC I complex was not observed because pretreatment of the IV $CD8^+$ T cells with Mitomycin C did not reverse suppression (**Fig. 5.5a**). Therefore, these data suggest intrahepatic $CD8^+$ T cells are indeed genuine $CD8^+$ T_{reg} cells.

$CD4^+$ and $CD8^+$ T_{reg} cells mediate suppression through two main paths: linked and bystander suppression. Linked suppression involves antigen recognition of peptides by

T_{reg} and T_{eff} cells on the same APC, and bystander suppression occurs when T_{reg} cells mediate suppression through the secretion of inhibitory cytokines or sequestration of growth factors[167]. To determine if the intrahepatic $CD8^+$ T_{reg} cells were required to recognize the same peptide on the BMDC as the responding $CD8^+$ OT-I T_{eff} cells, I IV infected mice with Ad-LacZ, isolated the intrahepatic $CD8^+$ T_{reg} cells, and discovered that $CD8^+$ T_{reg} cells that could not recognize $Ova_{257-264}$ could not regulate OT-I T cell expansion. However, if BMDCs were pulsed with both $Ova_{257-264}$ and a β-galactosidase derived octapeptide sequence ($\beta Gal_{497-504}$:ICPMYARV) simultaneously, βGal-specific $CD8^+$ T_{reg} cells indeed suppressed OT-I T cell division (**Fig. 5.6a,b**). Therefore, intrahepatic $CD8^+$ T_{reg} cells regulate via linked suppression.

Cellular Markers and Properties Associated with Liver-Primed $CD8^+$ T_{reg} Cells

Hallmarks of $CD4^+$ T_{reg} cells include their lack of IL-2 transcript and production, FoxP3 and CD25 expression, and inability to proliferate[186]. FoxP3, together with Helios, bind the *Il2* promoter, maintaining it in a hypoacetylated state[187]. T_r1 cells are another group of T_{reg} cells known to mediate suppression via secretion of IL-10[165], and IL-10 promoter polymorphisms correlate with worse HCV prognosis and clinical response to IFN-α/ribavirin therapy[57]. Further, peripheral blood and intrahepatic $CD8^+$ T cells isolated from humans bearing HCV are also observed to produce IL-10[53,54]. In my model, I analyzed a panel of markers and found that the intrahepatic Ova Tet^+CD8^+ T_{reg} cells had markedly diminished *Il2* and *Foxp3* mRNA but maintained enhanced levels of *Il10*, *Havcr2*, *Pdc1*, and *Ikzf2* mRNA (**Fig. 5.7a**). Elevated Helios intracellular expression (**Fig. 5.7b**) and IL-10 cytokine production (**Fig. 5.8a,b**) along with a diminished IL-2 axis marked $CD8^+$ T_{reg} cells. The $CD8^+$ T_{reg} cells were $GITR^+$, but CD25, CD103, CD127, and

CTLA-4 surface expression was absent. Kim *et al*. have shown that Qa-1 restriction and the presence of inhibitory Ly49 receptors define a subset of CD8$^+$ T_{reg} cells[175]; I could not detect surface expression of Ly49 receptors, but low levels of NKG2A and Qa-1 expression were apparent (**Fig. 5.7b** and data not shown).

To explore the role of IL-10 in intrahepatic CD8$^+$ T_{reg} cells, I infected IL-10 transcriptional reporter expressing eGFP (Vert-X) mice with Ad-Ova and FACS-sorted eGFP$^+$ and eGFP$^-$CD8$^+$ T_{reg} cells from the liver at D7 post-infection. eGFP$^+$CD8$^+$ T_{reg} cells maintained similar amounts of *Havcr2*, *Pdc1*, and *Ikzf2* mRNA (**Fig. 5.7c**). eGFP positivity correlated with PD-1 and Tim-3 expression, but not with antigen specificity (**Fig. 5.7d**). I also found that eGFP$^+$CD8$^+$ T_{reg} cells were more effective at suppressing OT-I T cell division *in vitro* (**Fig. 5.9a**). However, blockade of IL-10 through the use of anti-IL-10R antibody could not reverse suppression (**Fig. 5.9b**). These data indicate IL-10 phenotypically marks the CD8$^+$ T_{reg} cell, but does not appear to have a central role in suppressor function.

CD8$^+$ T_{reg} Cells Suppress T_{eff} Cells in a Tim-3-Dependent Manner

CD8$^+$ T_{reg} cells were then pre-coated with anti-PD-L1 and anti-Tim-3 antibodies prior to co-culture. Anti-PD-L1 antibody had no effect on improving OT-I T cell division, but anti-Tim-3 antibody partially rescued D3 OT-I T division (**Fig. 5.10a**). Further analysis revealed the number of dividing OT-I T cells, division index, and percent suppression were improved after Tim-3 blockade (**Fig. 5.10b**). A greater concentration of IL-2 and IFN-γ cytokine was present in the supernatants collected from OT-I/IV CD8$^+$ T_{reg} cell co-cultures with anti-Tim-3 antibody pre-coating (**Fig. 5.10c**). As OT-I T cells were proliferating more extensively with anti-Tim-3 antibody treatment, they began to

downregulate CD25 expression (a feature of $CD8^+$ T_{eff} terminal differentiation)[188]. No differences were observed in IFN-γ production or CD107a cycling to the surface per cell (**Fig. 5.10d**). PD-L1/Tim-3 co-blockade did not reveal a synergistic effect as observed by others during intrahepatic viral infection[88,89]. Rather, PD-L1 blockade seemed to have a dominant negative effect on OT-I T cell priming. Importantly, cross-linking Tim-3 on the surface of $CD8^+$ T_{reg} cells did not induce intrinsic cell death or alter absolute numbers in the co-culture (data not shown), improve proliferation after anti-CD3ε and anti-CD28 antibody mediated stimulation (**Fig. 5.5b**), or recover IL-2 and IFN-γ production (**Fig. 5.11**). Nevertheless, Tim-3 blockade appeared to inhibit $CD8^+$ T_{reg} cell ability to suppress $CD8^+$ T_{eff} proliferation.

Nascent $CD8^+$ T Cell Expansion During Liver and Lymph Node Antiviral Immune Responses is Suppressed by Intrahepatic $CD8^+$ T_{reg} Cells *In Vivo*

I next examined whether liver-primed $CD8^+$ T_{reg} cells could regulate the expansion of $CD8^+$ T_{eff} cells *in vivo*. To this end, naïve, Ad-Ova, and Ad-LacZ infected mice were re-infected with mouse cytomegalovirus expressing ovalbumin (MCMV-Ova) at D7 post-adenovirus infection, and the livers were analyzed at D14. D7 marks the peak in $CD8^+$ T cell kinetics within the liver, after which absolute numbers drastically decline (**Fig. 5.1a**). Livers excised from mice immunized with Ad-Ova vector harbored a lower absolute number of viable mononuclear cells per liver, whereas no significant difference was observed with mice that had received Ad-LacZ (**Fig. 5.12a**). Further, endogenous intrahepatic $CD8^+$ T cells isolated from mice that received Ad-Ova produced a reduced amount of TNF-α and IFN-γ compared to mice infected with MCMV-Ova alone or a combination of Ad-LacZ and MCMV-Ova. IL-2 could not be detected after a peptide-

based re-stimulation (**Fig. 5.12b**). These results recapitulate *in vitro* data indicating $CD8^+$ T_{reg} cells act in an antigen-specific manner (**Fig. 5.6**).

By nature of the experimental design, antigen specific responses could not be accurately described *in vivo* due to overlying immune responses generating $CD8^+$ T cells of the same specificity. Therefore, a similar experiment was conducted where mice received naïve $Thy1.1^+CD8^+$ OT-I T cells at D7 prior to MCMV-Ova infection. In this trial, the numbers of $Thy1.1^+CD8^+$ OT-I T cells in the livers of mice pre-infected with Ad-Ova were reduced. Further, intraperitoneal (IP) delivery of anti-Tim-3 antibody at D5 and D6 improved their absolute number (**Fig. 5.12c**). As before, no improvements in TNF-α, IL-2, and IFN-γ were observed per cell (**Fig. 5.12d**). These series of experiments suggest that the liver microenvironment is physically capable of regulating subsequent infections of similar antigen specificities dependent on Tim-3, but the role of the $CD8^+$ T_{reg} cell *in vivo* remained to be elucidated.

To more directly demonstrate the immunoregulatory effect of liver-primed $CD8^+$ T_{reg} cells on antigen-specific $CD8^+$ T_{eff} cell responses *in vivo*, D7 Ad-Ova SC splenic $CD8^+$ T cells and D7 IV liver $CD8^+$ T_{reg} cells were adoptively transferred into naïve C57BL/6 mice along with CFSE-labeled naïve $Thy1.1^+CD8^+$ OT-I T cells. IV $CD8^+$ T_{reg} cells were left alone or pre-coated with anti-PD-L1 or anti-Tim-3 antibodies. The recipient mice were then SC infected with Ad-Ova and analyzed at D3. A notable reduction in the size in the draining Ig LN was observed in mice that had received IV $CD8^+$ T_{reg} cells, and this was annulled with anti-Tim-3 pre-coating (**Fig. 5.13a**). Few OT-I T cells entered non-draining secondary lymphoid organs, the spleen and celiac lymph node (C LN). Within the Ig LN, IV $CD8^+$ T_{reg} cells diminished the number of dividing OT-I T cells, division index, and

elevated percent suppression. In this case, pre-coating IV $CD8^+$ T_{reg} cells with anti-Tim-3 antibody restored OT-I T cell proliferation kinetics *in vivo* beyond that of animals that had received OT-I T cells alone (**Fig. 5.13b,c**). It is entirely possible that the mechanism underlying this phenomenon acted on the cells *ex vivo* prior to transfer or within the blood, but it was confirmed both IV $CD8^+$ T_{reg} cells and OT-I T cells were trafficking to the substance of the paracortical cell mass (T cell zone) most likely via high endothelial venules within the Ig LN by D2 (**Fig. 5.13d**). Anti-Tim-3 antibody induced proliferation also rapidly decreased CD25 expression on the terminally dividing OT-I T cells consistent with observations *in vitro* (data not shown). Collectively, these data imply IV $CD8^+$ T_{reg} cells suppress $CD8^+$ T_{eff} cell proliferation via surface Tim-3 *in vitro* and *in vivo*.

Tim-3/HMGB-1 Binding and Internalization Mediates $CD8^+$ T_{reg} Cell Suppression and Acts Independently of Gal-9

I originally hypothesized that IV $CD8^+$ T_{reg} cells were producing Gal-9, whose binding to Tim-3 on the surface of $CD8^+$ T_{eff} cells was mediating suppression. This seemed unlikely because *Lgals9* mRNA and Gal-9 protein could not be detected within IV $CD8^+$ T_{reg} cells (**Fig. 5.7a** and **Fig. 5.2**, respectively), Tim-3 acted intrinsically on the IV $CD8^+$ T_{reg} cell highlighted by anti-Tim-3 antibody pre-coating, and $CD8^+$ OT-I T cells were devoid of Tim-3 receptor expression (**Fig. 5.14**). Chiba *et al.* recently discovered that Tim-3 can bind HMGB-1 in its FG loop within DC early endosomes[103], and other research groups have identified that HMGB-1 can act as a cytokine boosting DC maturation and IL-12 production along with direct and indirect effects on T cell proliferation[96-100,102]. These data raised the possibility that Tim-3 displayed by liver-primed $CD8^+$ T_{reg} cells may be binding HMGB-1. Since HMGB-1 has been reported to

be a ligand for the activating receptor RAGE displayed on $CD8^+$ T cells, I questioned if the interaction between HMGB-1 and Tim-3 on the surface of $CD8^+$ T_{reg} cells may affect the augmentation of T cell activation associated with RAGE engagement. To explore this possibility, I examined the impact of HMGB-1 blockade on OT-I T cell proliferation in culture with $Ova_{257-264}$ pulsed BMDCs with or without $CD8^+$ T_{reg} cells. Consistent with published results, blockade of HMGB-1 diminished OT-I T cell proliferation in cultures devoid of $CD8^+$ T_{reg} cells. However, when $CD8^+$ T_{reg} cells were included in culture OT-I T cell proliferation decreased as expected, which was unaffected by HMGB-1 blockade (**Fig. 5.15a**). Thus, the $CD8^+$ T_{reg} cells employ suppression independent of HMGB-1, or these cells effectively control the concentration of HMGB-1 through a Tim-3-dependent mechanism.

To examine the contribution of Tim-3 displayed by $CD8^+$ T_{reg} cells on OT-I proliferation, I considered the impact of Tim-3 blockade. As before, Tim-3 blockade partially reversed $CD8^+$ T_{reg} cell mediated suppression. Importantly, simultaneous blockade with anti-HMGB-1 and anti-Tim-3 antibodies in the culture media restored $CD8^+$ T_{reg} cell suppression (**Fig. 5.15a).** Gal-9 did not appear to be involved in this mechanism because rGal-9 could neither impede OT-I T cell division, nor could addition of anti-Gal-9 antibody to the media of OT-I/IV $CD8^+$ T_{reg} cell co-cultures reverse suppression (**Fig. 5.15b**). These results suggest that blockade of HMGB-1 abrogates the enhancement in proliferation after Tim-3 blockade.

Tim-3 was indeed capable of binding HMGB-1, as rTim-3Fc chimeric protein co-immunoprecipitated with HMGB-1 present in the supernatants collected from BMDC and BMDC/OT-I T cell cultures (**Fig. 5.15c**). Both endogenous $CD8^+$ T cells collected from

the D7 IV infected liver and OT-I T cells expanding in culture expressed the archetypical receptor for HMGB-1, RAGE, rendering $CD8^+$ T cells capable of responding to this growth factor in this model (**Fig. 5.15d,e**). I next determined if Tim-3 interaction with HMGB-1 could also explain the phenotypes observed *in vivo*. A histological analysis of D7 Ad-Ova infected livers revealed that the $CD8^+$ T cells were exclusively sequestering HMGB-1 on their surface and cytoplasm (**Fig. 5.15f**). Given that DCs are a potent source of HMGB-1 within the lymph node during T cell activation, $CD8^+$ T_{reg} cells may also have sequestered HMGB-1 once transferred and trafficked to the Ig LN of SC infected mice. IV $CD8^+$ T_{reg} cells were remarkably observed to actively bind and uptake HMGB-1 within intracellular vesicles in the *in vivo* lymph node experimental approach, and HMGB-1 co-localized with $CD8^+$ T_{reg} cell Tim-3. Anti-Tim-3 antibody pre-coated IV $CD8^+$ T_{reg} cells were clearly defective in internalizing HMGB-1 (**Fig. 5.15g,h**). These results describe a novel mechanism in which Tim-3 on the surface of IV $CD8^+$ T_{reg} cells binds HMGB-1, hampering $CD8^+$ T_{eff} cell proliferation between cells of the same specificities.

HMGB-1 in my model system could promote the expansion of T cells directly, or indirectly affect T cell proliferation by binding DC RAGE enhancing the expression of co-stimulatory receptors and secretion of IL-12. A microarray analysis of total RNA isolated from FACS-sorted $Ly6C^+$ Kupffer cells and $CD11b^+$ DCs/Møs at D7 post-Ad-Ova infection revealed that virus induced upregulation of *Hmgb1* within these cells (**Table 5.1**). However, when the *in vitro* suppression assay was repeated with BMDCs matured from *Rage*$^{-/-}$ mice, anti-Tim-3 antibody pre-treatment of the liver-primed $CD8^+$ T_{reg} cells was still able to effectively reverse suppression (**Fig. 5.16**). These results support that the notion that during viral infection, APCs actively secrete HMGB-1, and Tim-3

displayed by $CD8^+$ T_{reg} cells directly affects $CD8^+$ T_{eff} cell proliferation by sequestering HMGB-1.

Discussion

In this report I demonstrate that hepatic viral infection results in the generation and expansion of a novel population of $CD8^+$ T cells with regulatory activity. These $CD8^+$ T_{reg} cells routinely co-expressed PD-1, PD-L1, and Tim-3 and were distinguished by Helios and GITR phenotypic markers. Regulatory activity was independent of PD-L1 expression and IL-10 production by the $CD8^+$ T_{reg} cells but was critically dependent on Tim-3 expression. Furthermore, Tim-3 displayed by $CD8^+$ T_{reg} cells bound HMGB-1 on the surface of the $CD8^+$ T_{reg} cells preventing $CD8^+$ T_{eff} cell expansion in a Gal-9-independent manner. Given secretion of HMGB-1 by activated and mature APCs in response to PAMPs or pro-inflammatory cytokines and the role of HMGB-1 as a critical growth factor for TCR-engaged $CD8^+$ T_{eff} cells, I present a novel model where intrahepatic $CD8^+$ T_{reg} cells limit $CD8^+$ T_{eff} cell expansion via Tim-3-mediated HMGB-1 sequestration (**Fig. 5.17**). These findings are the first report to demonstrate a role for Tim-3 as a major contributor to $CD8^+$ T_{reg} cell regulatory function in the liver during viral infection.

Previous studies have shown that liver infiltrating $CD25^+FoxP3^+CD4^+$ T_{reg} cells dampen immune responses to hepatic viral infection[189]. My data do not argue against the contribution of $CD4^+$ T_{reg} cells on limiting hepatic immune responses. However, $FoxP3^+CD4^+$ T_{reg} cells are found in the naïve liver but do not significantly expand after adenovirus infection (data not shown). This finding is consistent with a series of experiments performed by Wuensch *et al.* demonstrating that after direct intrahepatic infection with adenovirus, the endogenous $CD8^+$ T cell response was not altered in MHC $II^{-/-}$ mice[106]. In the case of chronic HCV infection, Tim-3 is upregulated on $CD4^+$ iT_{reg}

cells[85]. As a result, Tim-3 binding of HMGB-1 could theoretically play a similar role on $CD25^+FoxP3^+CD4^+$ T_{reg} cells. More research is needed to determine if during chronic infection with HCV, $CD4^+$ and $CD8^+$ T_{reg} cells may use Tim-3 to continuously sequester HMGB-1 being released by necrotic hepatocytes and activated APCs. This mechanism may contribute to the transition from acute to chronic infection and/or allow virus to persist during later stages of chronic disease.

Similar to conventional $CD25^+FoxP3^+CD4^+$ T_{reg} cells, Helios might be involved in inhibiting *Il2* transcription in $CD8^+$ T_{reg} cells since $CD8^+$ T_{reg} cells did not express *Il2* mRNA or IL-2 protein but maintained elevated intranuclear/cellular Helios[182]. This lack of IL-2 production by $CD8^+$ T_{reg} cells also explains their failure to proliferate after anti-CD3ε/CD28 antibody re-stimulation or compete with OT-I T cells following co-culture with BMDCs. Intrahepatic $CD8^+$ T_{reg} cells were also unable to proliferate in the presence or absence of Tim-3 blockade, suggesting that $CD8^+$ T_{reg} cell engulfment HMGB-1 is incapable to overcome exhaustion when the *Il2* locus is transcriptionally repressed. These results indicate that Helios may be central in propagating dysfunction within the $CD8^+$ T cell pool by blocking NFAT/AP-1 access to the *Il2* promoter converting them to a regulatory cell type and could be a reliable marker for defining intrahepatic $CD8^+$ T_{reg} cells.

The suppressive function exerted by liver-primed $CD8^+$ T_{reg} cells occurred in an antigen-specific manner, where recognition of peptide/MHC I complex on the APC by both the $CD8^+$ T_{reg} and T_{eff} cell was necessary and sufficient for Tim-3 to control suppression. It was recently shown that the Tim-3 signaling is intracellularly linked to the TCR via the Src-family kinase Lck through annealing to HLA-B-associated transcript 3 (Bat3). In this

study, Rangachari *et al.* establish Gal-9 binding to Tim-3 prevents Bat-3 linkage to active Lck, thus modulating downstream TCR signaling[81]. Although Gal-9 and HMGB-1 recognize different regions of Tim-3, it is appreciated that conformational changes due to Tim-3 binding its ligands is intimately linked to the TCR. My results support the notion that suppression of $CD8^+$ T_{eff} cells is co-dependent on $CD8^+$ T_{reg} cell TCR recognition of antigen and Tim-3 binding HMGB-1.

Although blockade of Tim-3 improved OT-I T cell proliferation in an HMGB-1-dependent manner, an enhancement in IL-2 and IFN-γ production was only detected in the culture supernatant and not on a per cell basis by percent positive cells or mean fluorescence intensity. This indicates that the elevated pro-inflammatory cytokine production was linked with the enhanced proliferation of the responder OT-I T cells. To date, HMGB-1 has been shown to improve proliferation of both $CD4^+$ and $CD8^+$ T cells, but enhanced levels of cytokines have only been associated with supporting a $CD4^+$ T_h1 cell response[98,102]. It is possible that HMGB-1 only affects proliferation within $CD8^+$ T_{eff} cells. Conversely, the TCR is one of the most complex signaling molecules in nature, having ten ITAM motifs, where most receptors utilize two. Guy *et al.* revealed that different multiplicities of ITAM and strength TCR signaling uncouples proliferation and cytokine production. This effect was dependent on TCR affinity for peptide, where superagonists and strong peptides induced proliferation while weak peptides sufficiently led to maximal IL-2 secretion[190]. Ovalbumin was used as the model antigen in these experiments, where the OT-I T cells receive a strong TCR signal. Since strength of signal dictates T cell proliferation or cytokine production, I may have masked a role for Tim-3/HMGB-1 in regulating $CD8^+$ T_{eff} cell cytokine production. In the future, it is worth employing another transgenic system where the responder T cells recognize a weaker peptide/MHC I

complex. Alternatively, BMDCs could be pulsed with mutated ovalbumin derived peptides providing a suboptimal TCR signal.

Gal-9 and HMGB-1 are both present during the course of viral infection of the liver and cancer. I speculate that Tim-3 has different roles on T_{reg} and T_{eff} cells depending on the microenvironment. During antiviral immune responses, including chronic HCV infection, Gal-9 is expressed and released by a wide variety of cells in response to elevated production of IFN-γ[76,77,81,82,88,91]. Apart from activated APCs releasing HMGB-1, it can be passively released by virally lysed, cytolytically killed, hypoxic, and oxidatively stressed hepatocytes[95]. Further, a dampened $CD8^+$ T cell response and poorer prognosis to Epstein-Barr virus associated nasopharyngeal carcinoma is linked with the release of Gal-9^+ exosomes from tumor cells into circulation[87]. HMGB-1 released from tumor cells also has divergent functions, either activating DCs or promoting tumor angiogenesis, growth, invasion, and metastasis[98,104]. Since the binding sites for Gal-9 and HMGB-1 are distally located on Tim-3 mucin and immunoglobulin variable regions, respectively, simultaneous recognition of both ligands is also possible. In this context, the concentrations of Gal-9 and HMGB-1 along with their different avidities for Tim-3 during viral infection and cancer could balance the adaptive immune response in multiple ways. Prior research is limited because the RMT3-23 clone of anti-Tim-3 antibody is effective at blocking both Gal-9 and HMGB-1 affinity for Tim-3[103,191]. Consequently, a fundamental role for HMGB-1 may have been overlooked in different disease models.

IL-10, PD-1/PD-L1, and Tim-3 signaling forms a supportive network for the synergistic expression of the receptors themselves and their ability to inhibit the effector function of antiviral $CD8^+$ T_{eff} cells[55,59,70,88,90,91,192]. Moreover, PD-L1 expression by T_{reg} cells has

been reported to play a role in mediating suppressor function in some laboratories[179-181]. However, both IL-10 and PD-1/PD-L1 engagement were not involved in the suppressive function of $CD8^+$ T_{reg} cells in my studies. Since IL-10 and PD-L1 are dispensable to the function of T_{reg} cells in my model, I do not exclude the possibility that signaling from these inhibitory pathways or their synergy with Tim-3 may also affect the development of $CD8^+$ T_{reg} cells *in situ* thereby altering their balance with $CD8^+$ T_{eff} cells[168].

Approximately 600 million people worldwide are in danger of developing chronic liver disease due to HBV and HCV infections, and only a subset of these patients respond to IFN-α/ribavirin therapy[127]. Simultaneous blockade of the IL-10, PD-1/PD-L1, and Tim-3 inhibitory pathways has potential clinical efficacy. Even though Tim-3-targeted therapies have not yet been tested in humans, the safety of blocking different inhibitory pathways varies. For example, anti-CTLA-4 antibody clinical trials were accompanied with the onset of autoimmunity, whereas anti-PD-L1 antibodies yielded fewer side effects[134]. Additionally, PD-1 can ligate PD-L1 or PD-L2, and PD-L1 can bind CD80 and a putative co-stimulatory receptor[133]. Moreover, elevated serum HMGB-1 during HCV infection directly correlates with liver disease progression[94]. Thus, HMGB-1 sequestration by T_{reg} cell Tim-3 may not be sufficient to suppress T_{eff} cells under conditions of extensive liver injury and HMGB-1 release. One must therefore consider disease progression, signaling pathway integration, and ligand concentration, accessibility, and avidity for receptors in the design of immunotherapeutic strategies.

In summary, these data describe a novel mechanism where Tim-3 binds HMGB-1 on liver-primed $CD8^+$ T_{reg} cells suppressing the proliferation of $CD8^+$ T_{eff} cells during acute adenovirus infection in an antigen-specific manner. This observation may provide a

framework for future studies of Tim-3, where consideration for ligand access of both Gal-9 and HMGB-1 is warranted. Translation to human liver disease is to be expected given that a similar population of IL-10-producing, PD-1/PD-$L1^+$Tim-3^+CD8^+ T cells is present in the liver biopsies of chronic HCV patients. The $CD8^+$ T_{reg} cell population that arises after viral infection of the liver could be indicated by intranuclear/cellular Helios and *Il10* transcript, but more defining markers are needed to separate $CD8^+$ T_{reg} cells from functional and dysfunctional $CD8^+$ T_{eff} cells. Understanding how tolerance spreads in the antiviral intrahepatic $CD8^+$ T cell population is essential in developing immunotherapies in the clinic. The scope of this research extends to numerous human diseases including cancer, autoimmune diseases such as diabetes, alloimmunity, heart disease, and allergy governed by a T_{reg}/T_{eff} cell balance.

Figure 5.1

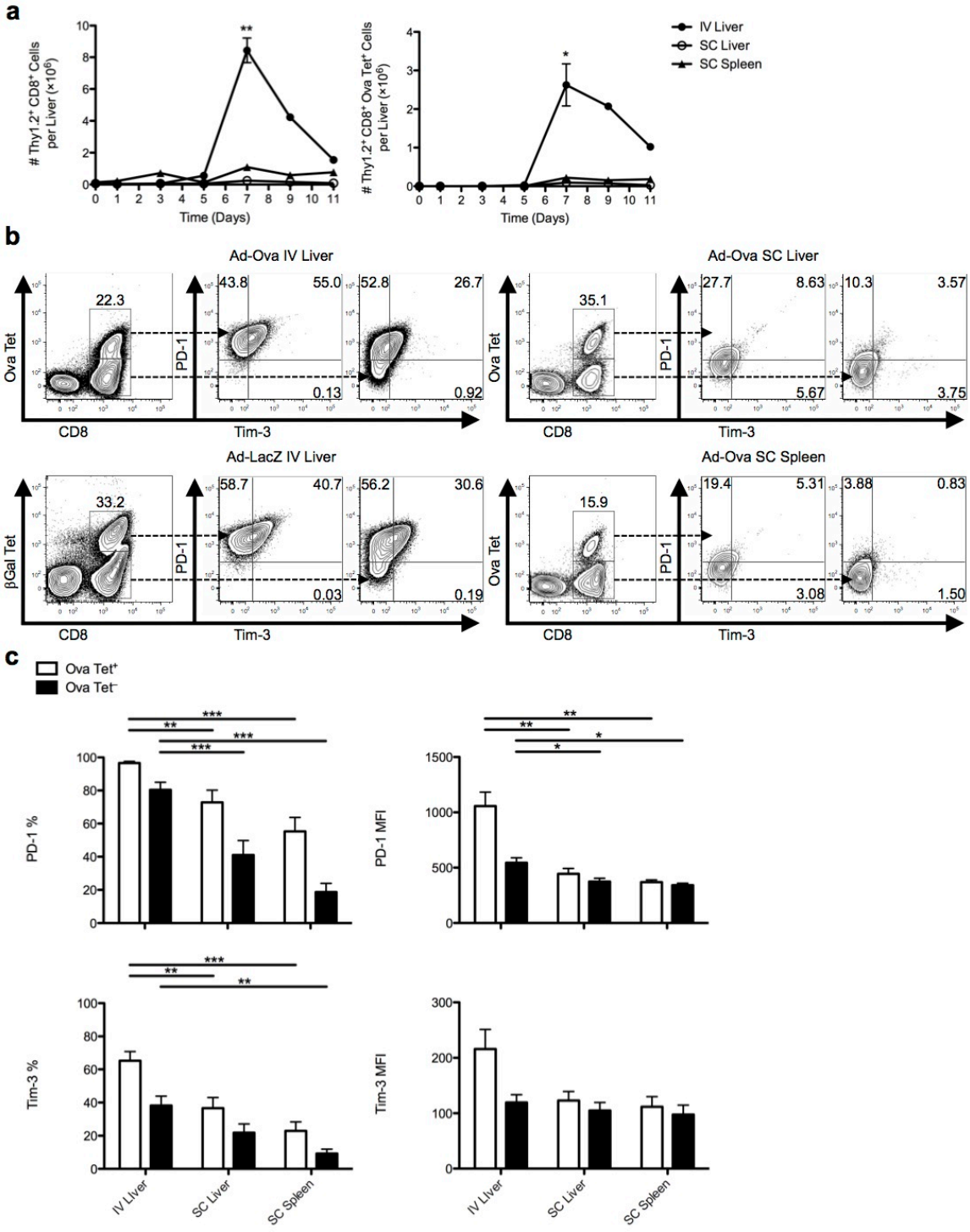
a
Thy1.2+ CD8+ Cells per Liver (×10^6)
Time (Days)
Thy1.2+ CD8+ Ova Tet+ Cells per Liver (×10^6)
Time (Days)
IV Liver
SC Liver
SC Spleen
b
Ad-Ova IV Liver
Ad-Ova SC Liver
Ad-LacZ IV Liver
Ad-Ova SC Spleen
Ova Tet
βGal Tet
PD-1
CD8
Tim-3
22.3
43.8
55.0
52.8
26.7
0.13
0.92
35.1
27.7
8.63
10.3
3.57
5.67
3.75
33.2
58.7
40.7
56.2
30.6
0.03
0.19
15.9
19.4
5.31
3.88
0.83
3.08
1.50
c
Ova Tet+
Ova Tet−
PD-1 %
PD-1 MFI
Tim-3 %
Tim-3 MFI
IV Liver
SC Liver
SC Spleen

Figure 5.1 PD-1 and Tim-3 are co-expressed on liver-primed $CD8^+$ T cells after IV adenovirus infection. C57BL/6 mice were SC or IV infected with 2.5×10^7 IU Ad-Ova. (**a**) Liver and spleen mononuclear cells were collected and the number of bulk and Ova-specific $CD8^+$ T cells (Ova Tet^+CD8^+) were determined at days 0, 1, 3, 5, 7, 9, and 11. (**b,c**) Co-expression of PD-1 and Tim-3 was determined directly *ex vivo* for Ova Tet^+ and Ova Tet^- populations of $CD8^+$ T cells at D7 post-infection. Ad-Ova IV infection in the liver was also compared to D7 livers from Ad-LacZ IV infected C57BL/6 mice (one-way ANOVA/Tukey's post test; n = 4-9 per group). Numbers in the scatter plots represent percentages. Mean ± s.e.m.; $*P < 0.05$, $**P < 0.01$, and $***P < 0.001$.

Figure 5.2

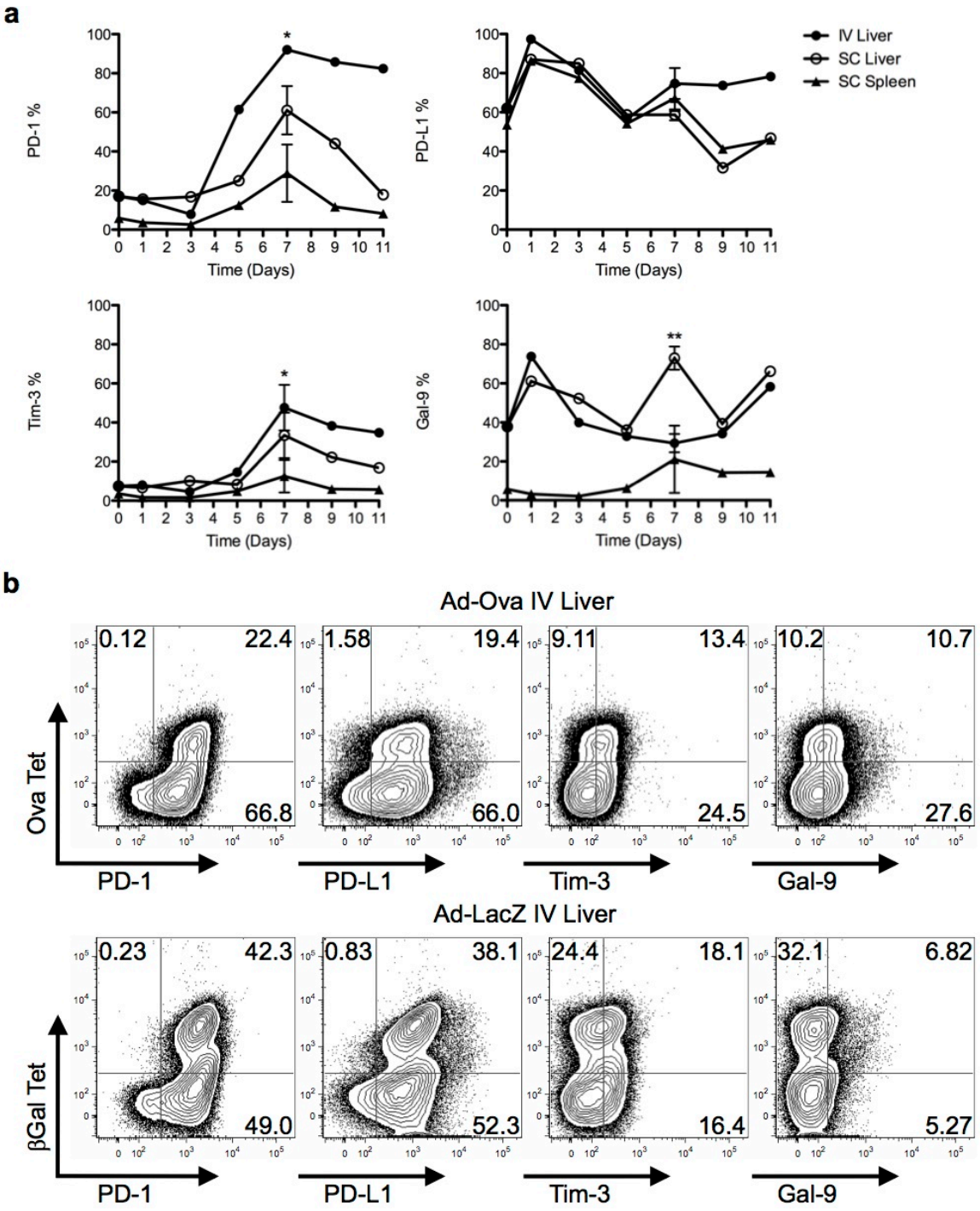
a
PD-1 %
PD-L1 %
Tim-3 %
Gal-9 %
Time (Days)
IV Liver
SC Liver
SC Spleen
b
Ad-Ova IV Liver
Ad-LacZ IV Liver
Ova Tet
βGal Tet
PD-1
PD-L1
Tim-3
Gal-9
0.12
22.4
66.8
1.58
19.4
66.0
9.11
13.4
24.5
10.2
10.7
27.6
0.23
42.3
49.0
0.83
38.1
52.3
24.4
18.1
16.4
32.1
6.82
5.27

Figure 5.2 PD-1 and Tim-3 inhibitory pathways peak at D7 following IV adenovirus administration. C57BL/6 mice were SC or IV infected with 2.5×10^7 IU Ad-Ova, and (**a**) percent surface expression of PD-1, PD-L1, Tim-3, and Gal-9 was determined directly *ex vivo* on bulk liver and spleen $CD8^+$ T cells at days 0, 1, 3, 5, 7, 9, and 11 (one-way ANOVA/Tukey's post test; n = 3 per group). (**b**) D7 antigen-specific expression of PD-1, PD-L1, Tim-3, and Gal-9 on liver $CD8^+$ T cells responding to Ad-Ova and Ad-LacZ IV infection is displayed (n = 3 per group). Numbers in the scatter plots represent percentages. Mean ± s.e.m.; $*P < 0.05$ and $**P < 0.01$.

Figure 5.3

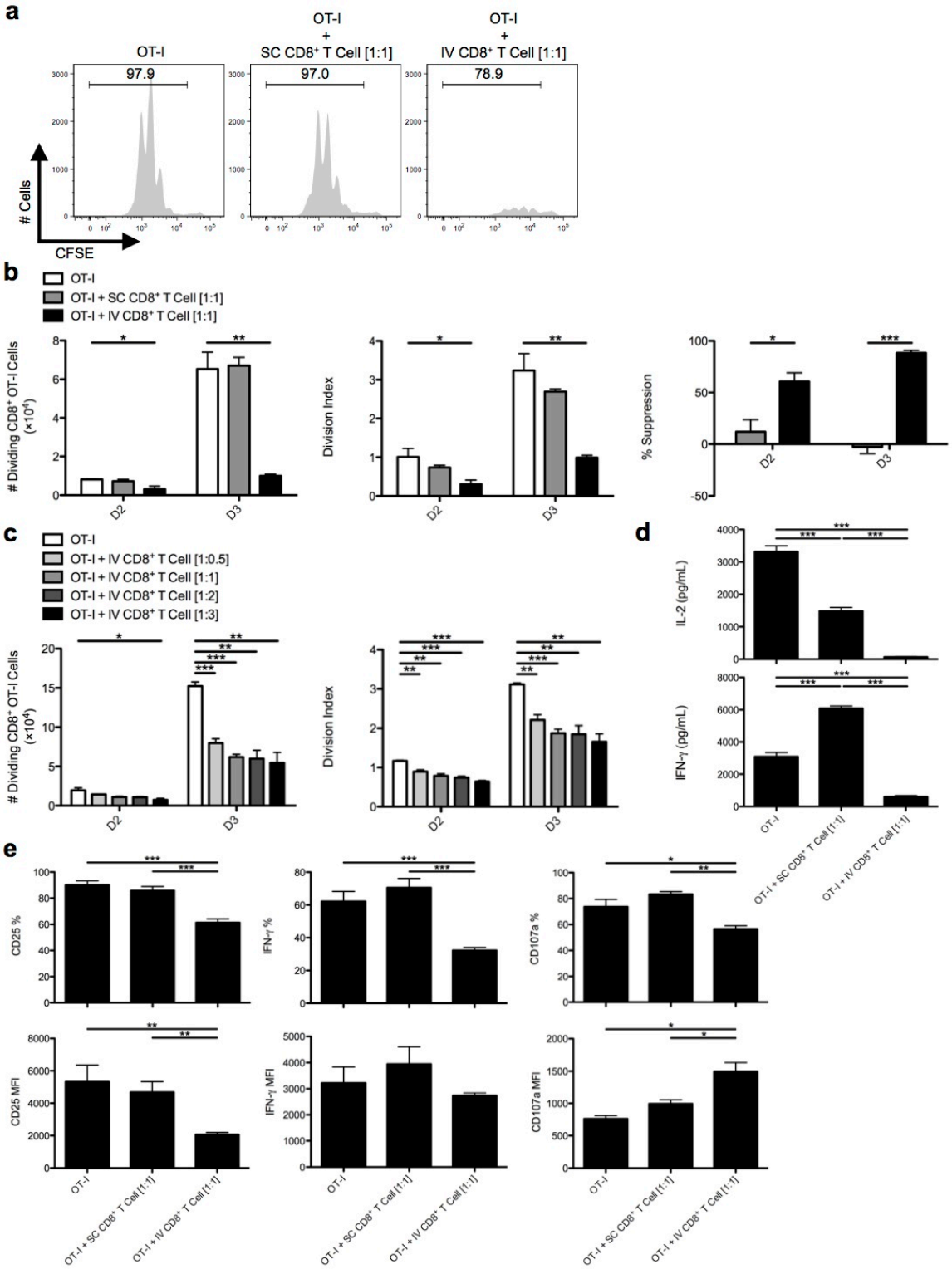
a
OT-I
OT-I + SC CD8+ T Cell [1:1]
OT-I + IV CD8+ T Cell [1:1]
97.9
97.0
78.9
Cells
CFSE
b
OT-I
OT-I + SC CD8+ T Cell [1:1]
OT-I + IV CD8+ T Cell [1:1]
Dividing CD8+ OT-I Cells (×10^4)
Division Index
% Suppression
D2
D3
c
OT-I
OT-I + IV CD8+ T Cell [1:0.5]
OT-I + IV CD8+ T Cell [1:1]
OT-I + IV CD8+ T Cell [1:2]
OT-I + IV CD8+ T Cell [1:3]
Dividing CD8+ OT-I Cells (×10^4)
Division Index
d
IL-2 (pg/mL)
IFN-γ (pg/mL)
OT-I
OT-I + SC CD8+ T Cell [1:1]
OT-I + IV CD8+ T Cell [1:1]
e
CD25 %
IFN-γ %
CD107a %
CD25 MFI
IFN-γ MFI
CD107a MFI

Figure 5.3 $CD8^+$ T cells from the livers of IV infected animals suppress the activation and expansion of naïve $CD8^+$ OT-I T cells *in vitro*. C57BL/6 mice were SC or IV infected with 2.5×10^7 IU Ad-Ova, and (**a**) bulk $CD8^+$ T cells were isolated from D7 SC spleens and IV livers then cultured with CFSE-labeled naïve $Thy1.1^+CD8^+$ OT-I T cells at a 1:1 ratio. SIINFEKL-pulsed BMDCs were used as the source of antigen, and co-cultures were analyzed at D3. (**b**) The number of dividing OT-I T cells, division index, and percent suppression displayed by either SC $CD8^+$ T cells or IV $CD8^+$ T cells were calculated at D2 and D3 of culture. (**c**) Naïve $Thy1.1^+CD8^+$ OT-I T cells were also cultured at various ratios relative to $CD8^+$ T cells collected from the livers of IV infected mice (1:0.5, 1:1, 1:2, and 1:3). (**d**) The concentrations of IL-2 and IFN-γ were measured in the D3 culture supernatants by ELISA. (**e**) CD25 expression was determined directly *ex vivo*, CD107a expression was ascertained after a 5 hr culture with GolgiStop + anti-CD107a Ab cocktail, and IFN-γ was quantified after a 5 hr re-stimulation with 2 μg/mL SIINFEKL peptide on D3 $Thy1.1^+CD8^+$ OT-I T cells (one-way ANOVA/Tukey's post test; n = 5-12 per group). Numbers in the histograms represent percentages. Mean ± s.e.m.; $^*P < 0.05$, $^{**}P < 0.01$, and $^{***}P < 0.001$.

Figure 5.4

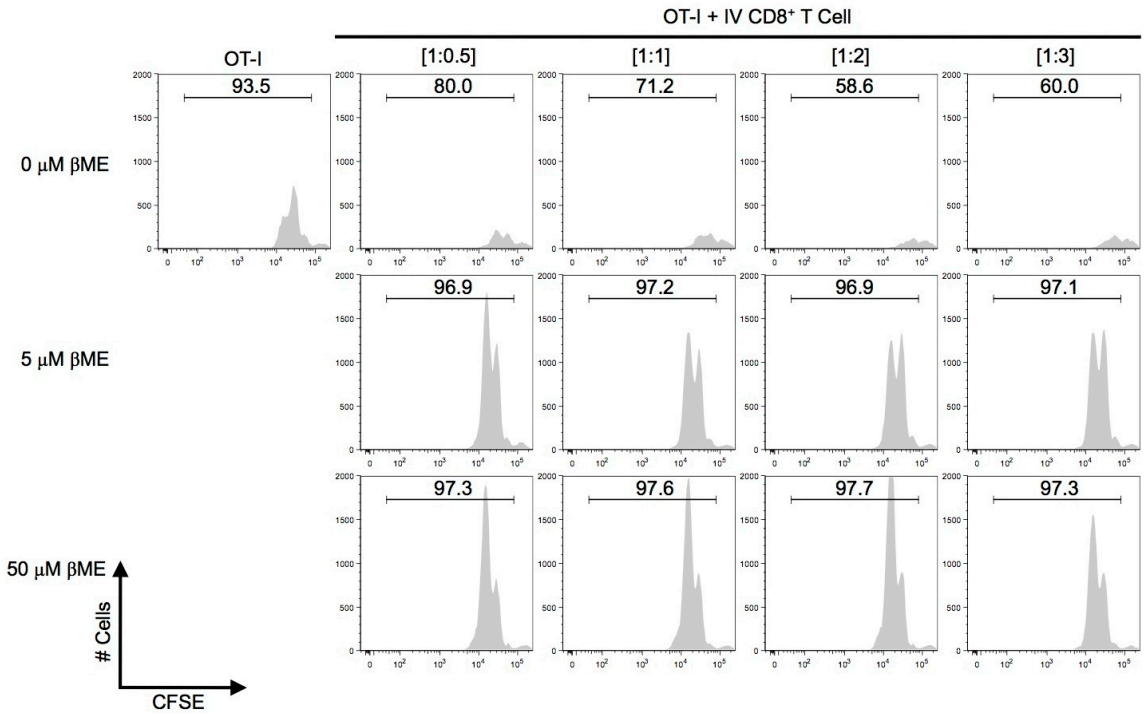
OT-I + IV CD8+ T Cell
OT-I
[1:0.5]
[1:1]
[1:2]
[1:3]
0 μM βME
5 μM βME
50 μM βME
93.5
80.0
71.2
58.6
60.0
96.9
97.2
96.9
97.1
97.3
97.6
97.7
97.3
Cells
CFSE

Figure 5.4 β-mercaptoethanol blocks $CD8^+$ T_{reg} cell suppression of $CD8^+$ OT-I T cells *in vitro*. C57BL/6 mice were IV infected with 2.5×10^7 IU Ad-Ova, and bulk $CD8^+$ T cells were isolated from D7 IV livers then cultured with CFSE-labeled naïve $Thy1.1^+CD8^+$ OT-I T cells at a 1:1 ratio. SIINFEKL-pulsed BMDCs were used as the source of antigen, and co-cultures were analyzed at D2. βME was included in the co-cultures at the indicated concentrations (n = 3 per group). Numbers in the histograms represent percentages.

Figure 5.5

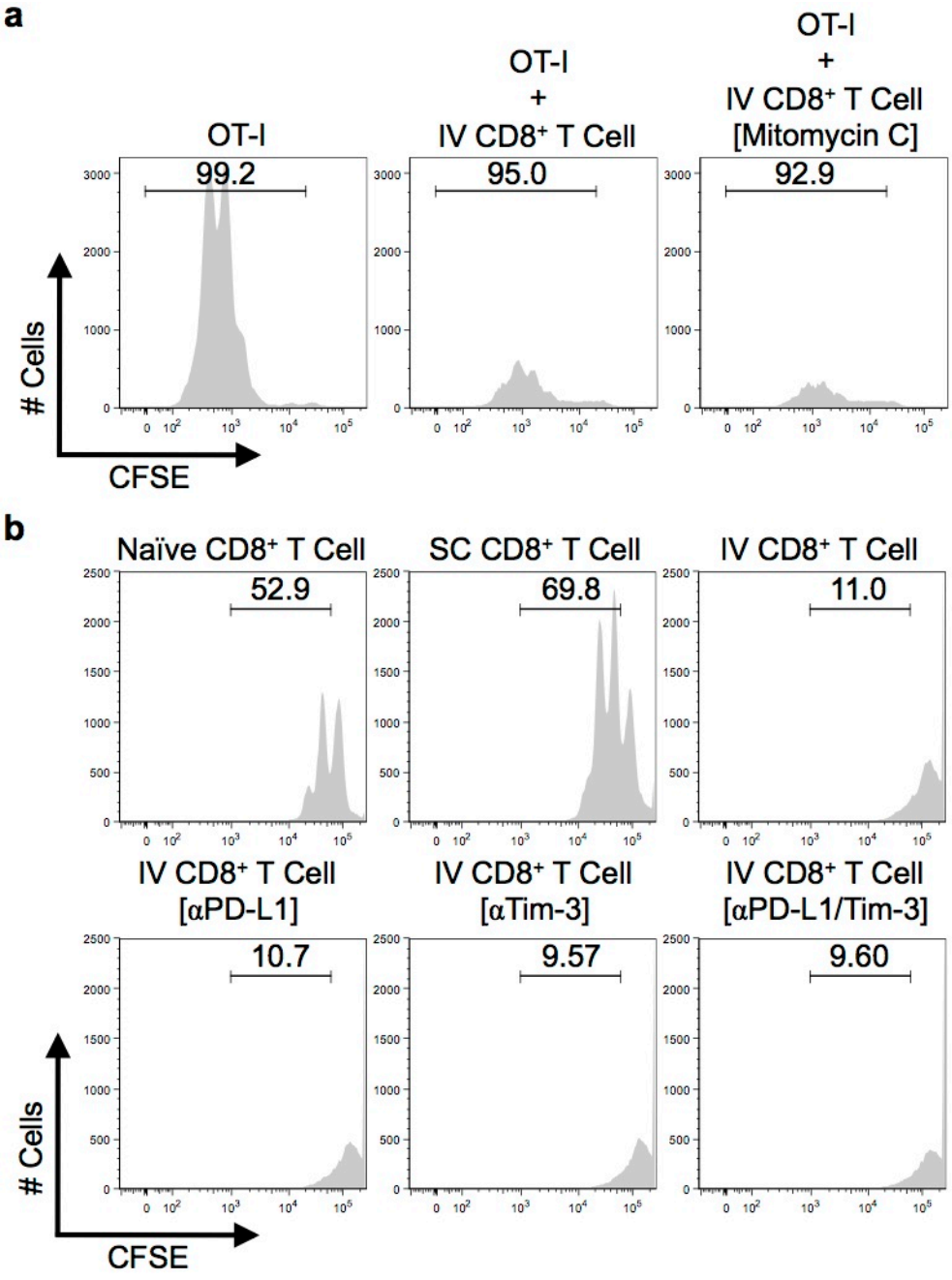
a
OT-I
99.2
OT-I
+
IV CD8+ T Cell
95.0
OT-I
+
IV CD8+ T Cell
[Mitomycin C]
92.9
Cells
CFSE
b
Naïve CD8+ T Cell
52.9
SC CD8+ T Cell
69.8
IV CD8+ T Cell
11.0
IV CD8+ T Cell
[αPD-L1]
10.7
IV CD8+ T Cell
[αTim-3]
9.57
IV CD8+ T Cell
[αPD-L1/Tim-3]
9.60
Cells
CFSE

Figure 5.5 $CD8^+$ T_{reg} cells are defective in proliferation and do not compete with $CD8^+$ OT-I T cells for access to peptide/MHC I complex. C57BL/6 mice were IV infected with 2.5×10^7 IU Ad-Ova, and (**a**) bulk $CD8^+$ T_{reg} cells isolated from D7 IV livers were cultured with CFSE-labeled naïve $Thy1.1^+CD8^+$ OT-I T cells at a 1:1 ratio. SIINFEKL-pulsed BMDCs were used as the source of antigen, and co-cultures were analyzed at D3. Prior to *in vitro* co-culture, $CD8^+$ T_{reg} cells were treated with Mitomycin C to inhibit the potential proliferation from this population of cells. (**b**) $CD8^+$ T cells taken from naïve liver, D7 SC spleen, and D7 IV liver were labeled with CFSE and re-stimulated *in vitro* with plate-bound anti-CD3ε Ab and soluble anti-CD28 Ab. Anti-PD-L1 Ab and/or anti-Tim-3 Ab were included during culture. CFSE dilution was determined at D2 (n = 3 per group). Numbers in the histograms represent percentages.

Figure 5.6

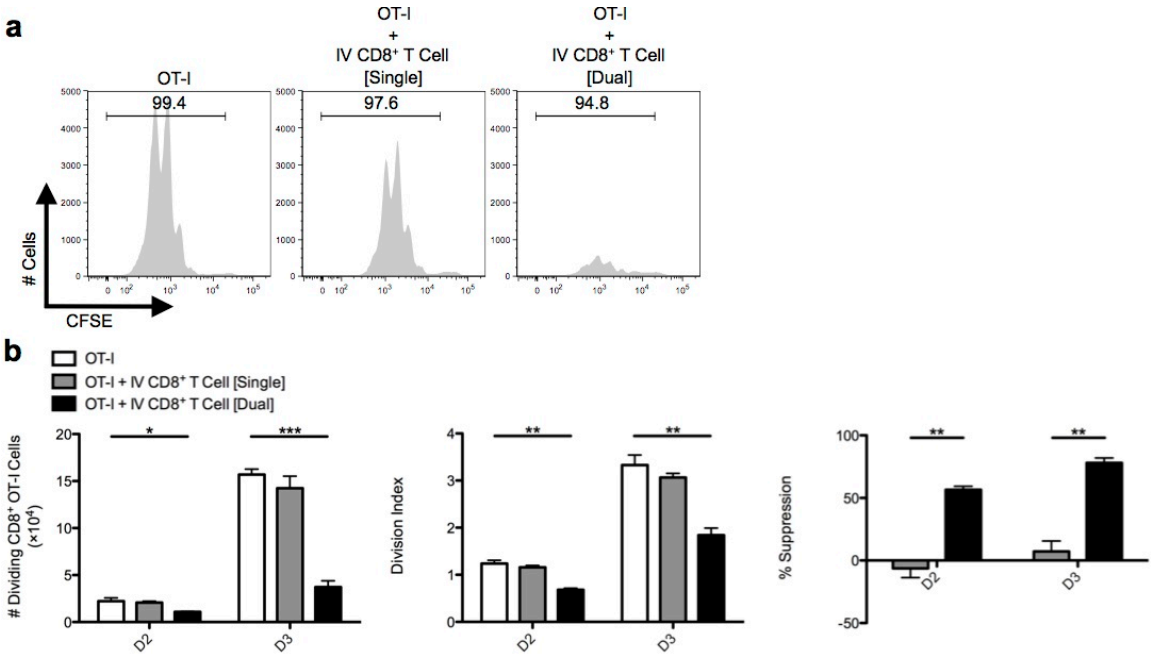
a
OT-I
OT-I + IV CD8+ T Cell [Single]
OT-I + IV CD8+ T Cell [Dual]
99.4
97.6
94.8
Cells
CFSE
b
OT-I
OT-I + IV CD8+ T Cell [Single]
OT-I + IV CD8+ T Cell [Dual]
Dividing CD8+ OT-I Cells (×10⁴)
Division Index
% Suppression
D2
D3

Figure 5.6 Liver-primed $CD8^+$ T_{reg} cells restrain $CD8^+$ OT-I T cell outgrowth in an antigen-specific manner. (**a**) $CD8^+$ T_{reg} cells were isolated from D7 livers of C57BL/6 mice IV infected with 2.5×10^7 IU Ad-LacZ and cultured with CFSE-labeled naïve $Thy1.1^+CD8^+$ OT-I T cells at a 1:1 ratio. SIINFEKL (Single)- or SIINFEKL/ICPMYARV (Dual)-pulsed BMDCs were used as the source of antigen, and CFSE dilution was determined at D3. (**b**) The number of dividing OT-I T cells, division index, and percent suppression by IV $CD8^+$ T_{reg} cells were assessed after D2 and D3 of culture (one-way ANOVA/Tukey's post test; n = 6 per group). Numbers in the histograms represent percentages. Mean ± s.e.m.; $*P < 0.05$, $**P < 0.01$, and $***P < 0.001$.

Figure 5.7

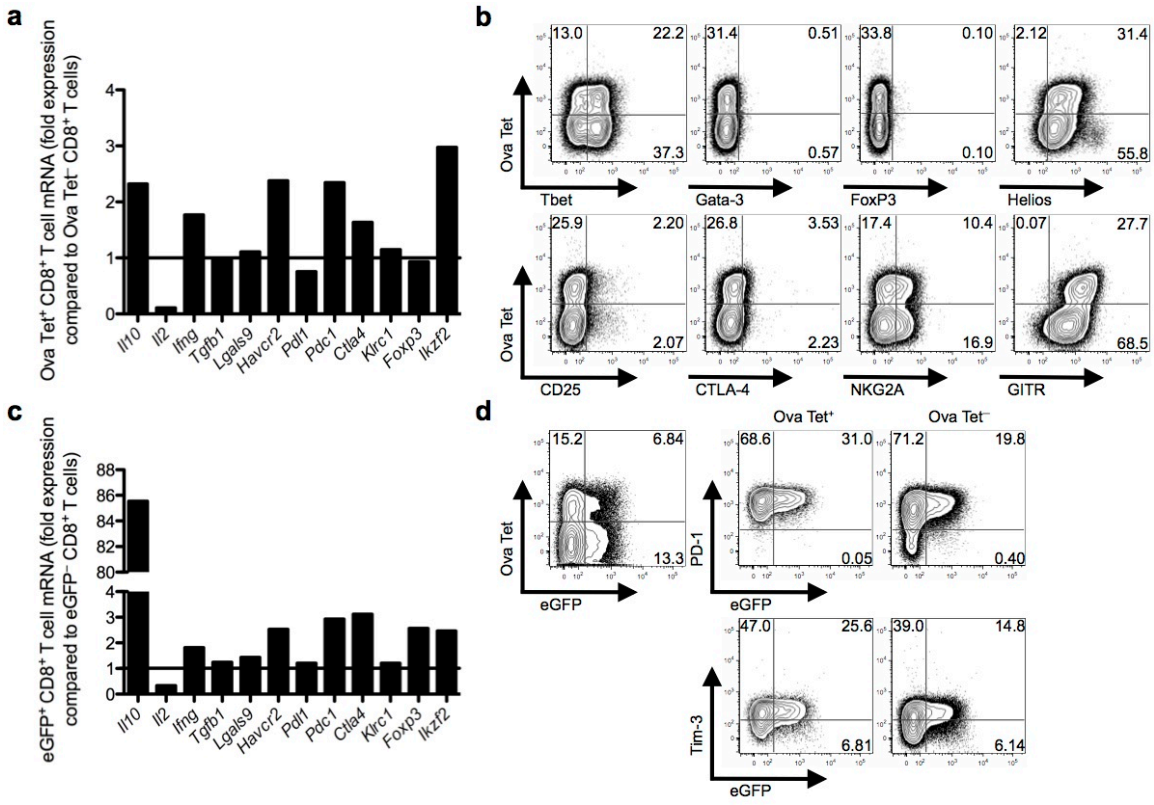
a
Ova Tet+ CD8+ T cell mRNA (fold expression compared to Ova Tet− CD8+ T cells)
Il10
Il2
Ifng
Tgfb1
Lgals9
Havcr2
Pdl1
Pdc1
Ctla4
Klrc1
Foxp3
Ikzf2
b
Ova Tet
Tbet
Gata-3
FoxP3
Helios
CD25
CTLA-4
NKG2A
GITR
c
eGFP+ CD8+ T cell mRNA (fold expression compared to eGFP− CD8+ T cells)
d
Ova Tet+
Ova Tet−
PD-1
Tim-3
eGFP

Figure 5.7 The phenotype of liver $CD8^+$ T_{reg} cells display some canonical T_{reg} markers. C57BL/6 mice were IV infected with 2.5×10^7 IU Ad-Ova, D7 liver mononuclear cells were isolated, and total RNA was collected from FACS-sorted Ova Tet^+ and Ova Tet^-CD8^+ T_{reg} cells. (**a**) *Il10* (IL-10), *Il2* (IL-2), *Ifng* (IFN-γ), *Tgfb* (TGF-β), *Lgals9* (Gal-9), *Havcr2* (Tim-3), *Pdl1* (PD-L1), *Pdc1* (PD-1), *Ctla4* (CTLA-4), *Klrc1* (NKG2A), *Foxp3* (FoxP3), and *Ikzf2* (Helios) mRNA was measured by Q-PCR. (**b**) Expression of intranuclear/cellular Tbet/Gata-3/FoxP3/Helios, and surface CD25/CTLA-4/NKG2A/GITR was determined on $CD8^+$ T_{reg} cells from the livers of IV infected mice. (**c**) Similarly, transcript from FACS-sorted $eGFP^+CD8^+$ T_{reg} cells was compared to that of $eGFP^-CD8^+$ T_{reg} cells from D7 IV infected Vert-X mice. (**d**) PD-1 and Tim-3 surface expression along the eGFP profile was separately assessed on Ova Tet^+ and Ova Tet^-CD8^+ T_{reg} cells (n = 3 per group). Numbers in the scatter plots represent percentages.

Figure 5.8

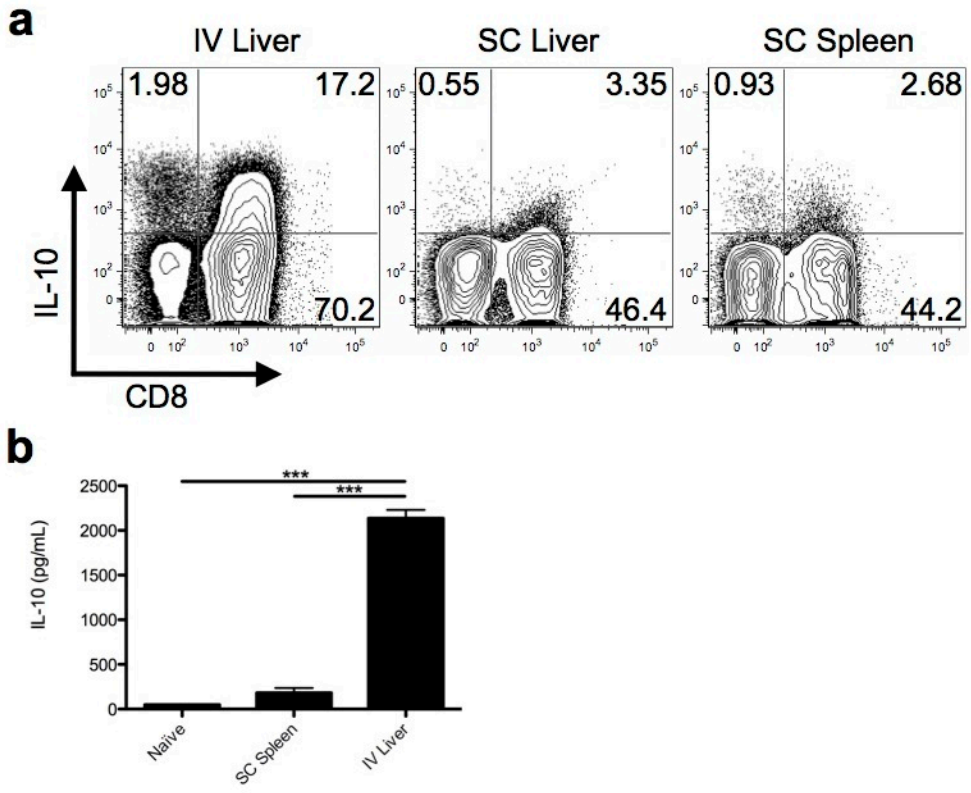
a
IV Liver
SC Liver
SC Spleen
1.98
17.2
70.2
0.55
3.35
46.4
0.93
2.68
44.2
IL-10
CD8
b
IL-10 (pg/mL)
2500
2000
1500
1000
500
0
***
***
Naïve
SC Spleen
IV Liver

Figure 5.8 Intrahepatic $CD8^+$ T cells produce IL-10. (**a**) C57BL/6 mice were SC or IV infected with 2.5×10^7 IU Ad-Ova. Endogenous D7 liver and spleen T cell IL-10 production was assessed after a 5 hr re-stimulation with 5 ng/mL PMA and 500 ng/mL ionomycin. (**b**) $CD8^+$ T cells taken from naïve liver, D7 SC spleen, and D7 IV liver were re-stimulated *in vitro* with plate-bound anti-CD3ε Ab and soluble anti-CD28 Ab. The concentration of IL-10 was measured in the D2 culture supernatant by ELISA (one-way ANOVA/Tukey's post test; n = 3 per group). Numbers in the scatter plots represent percentages. Mean ± s.e.m.; ***$P < 0.001$.

Figure 5.9

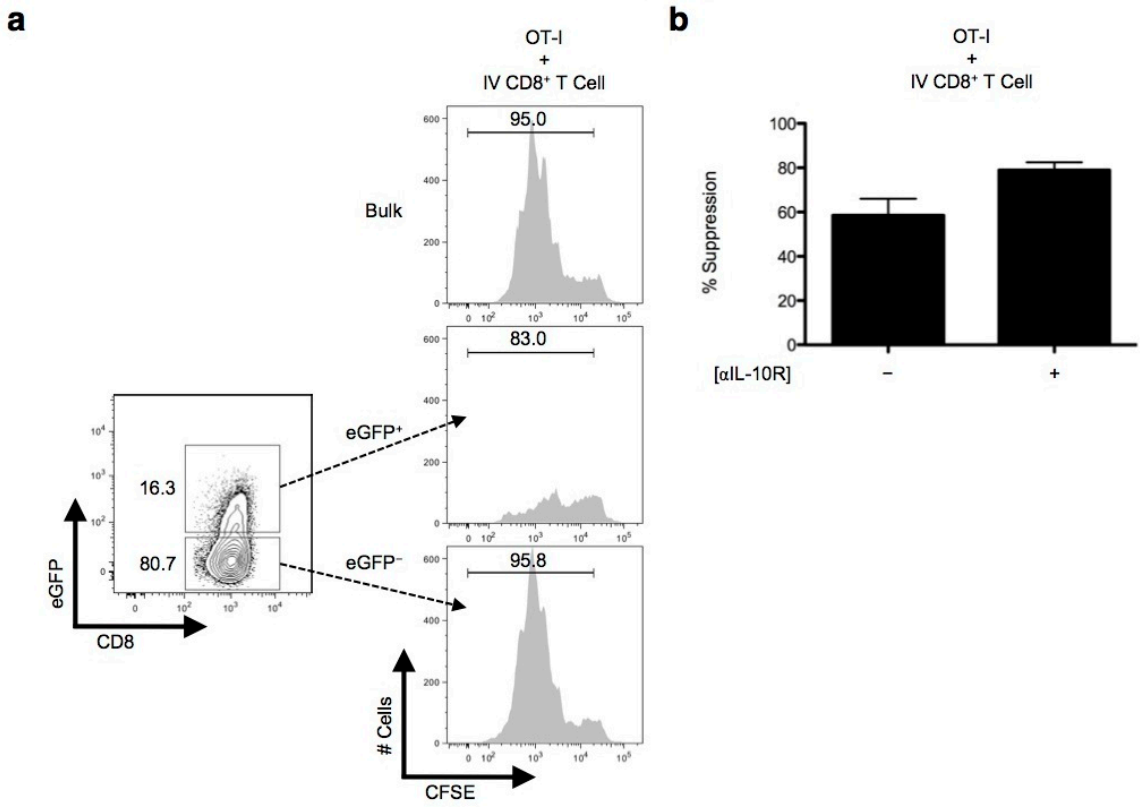
a
OT-I
+
IV CD8⁺ T Cell
Bulk
95.0
83.0
95.8
eGFP⁺
eGFP⁻
16.3
80.7
eGFP
CD8
Cells
CFSE
b
OT-I
+
IV CD8⁺ T Cell
% Suppression
100
80
60
40
20
0
[αIL-10R]
–
+

Figure 5.9 $eGFP^+CD8^+$ T_{reg} cells are more potent suppressors compared to $eGFP^-CD8^+$ T_{reg} cells from IL-10 transcriptional reporter mice. (**a**) Representative *in vitro* suppression assays from bulk $CD8^+$ T_{reg} cells and FACS-sorted $eGFP^+CD8^+$ T_{reg} cells or $eGFP^-CD8^+$ T_{reg} cells from D7 Ad-Ova IV infected C57BL/6 and Vert-X mice, respectively, co-cultured with CFSE-labeled naïve $Thy1.1^+CD8^+$ OT-I T cells at a 1:1 ratio are depicted (n = 3 per group). (**b**) D3 percent suppression by D7 Ad-Ova liver-primed $CD8^+$ T_{reg} cells during co-culture with CFSE-labeled naïve $Thy1.1^+CD8^+$ OT-I T cells at a 1:1 ratio and SIINKFEKL-pulsed BMDCs is displayed. Select wells also contained anti-IL-10R Ab in the media during culture (n = 3 per group). Numbers in the histograms and scatter plots represent percentages. Mean ± s.e.m.

Figure 5.10

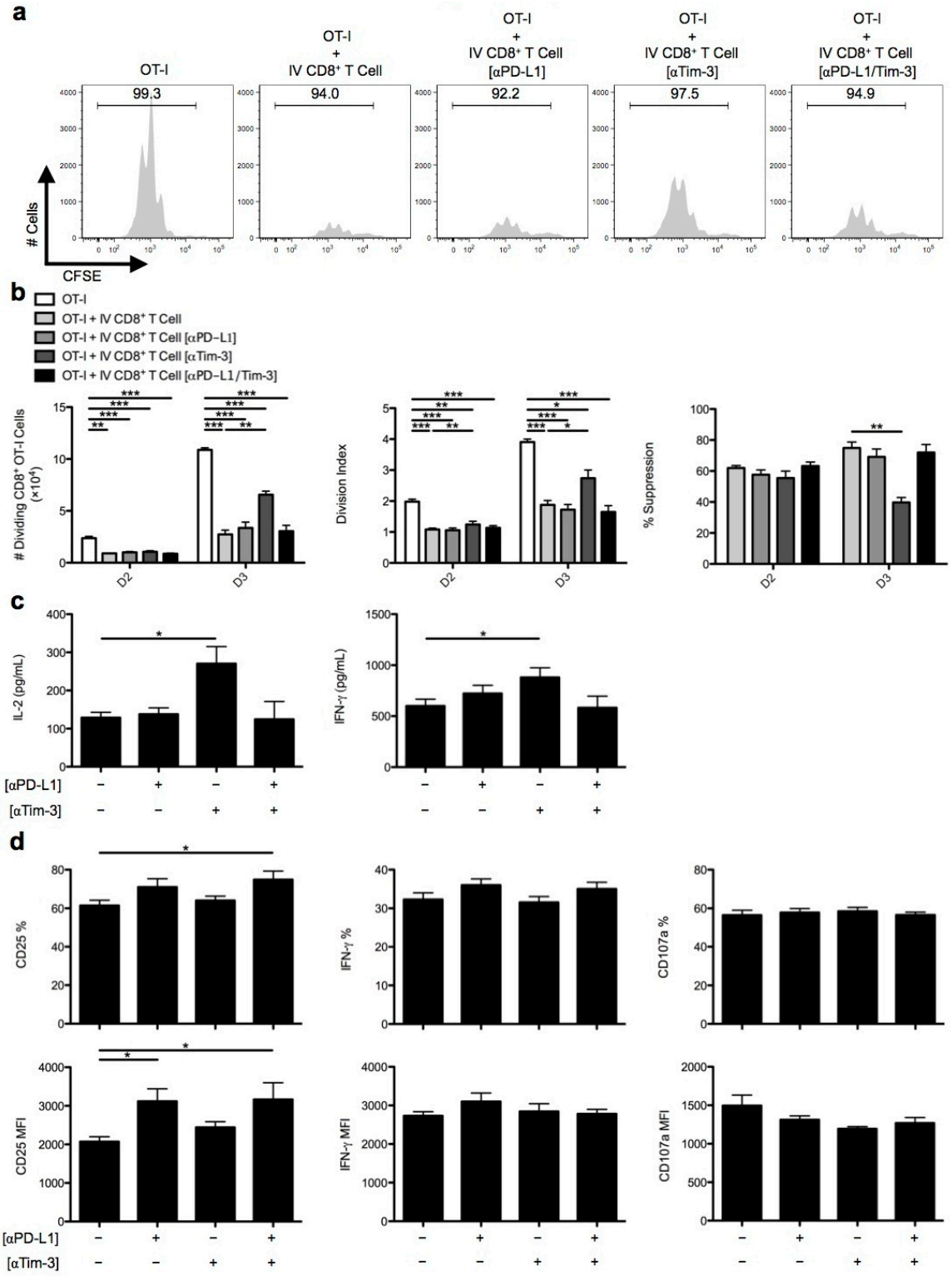
a
OT-I
OT-I + IV CD8⁺ T Cell
OT-I + IV CD8⁺ T Cell [αPD-L1]
OT-I + IV CD8⁺ T Cell [αTim-3]
OT-I + IV CD8⁺ T Cell [αPD-L1/Tim-3]
99.3
94.0
92.2
97.5
94.9
Cells
CFSE
b
OT-I
OT-I + IV CD8⁺ T Cell
OT-I + IV CD8⁺ T Cell [αPD-L1]
OT-I + IV CD8⁺ T Cell [αTim-3]
OT-I + IV CD8⁺ T Cell [αPD-L1/Tim-3]
Dividing CD8⁺ OT-I Cells (×10⁴)
Division Index
% Suppression
D2
D3
c
IL-2 (pg/mL)
IFN-γ (pg/mL)
[αPD-L1]
[αTim-3]
d
CD25 %
IFN-γ %
CD107a %
CD25 MFI
IFN-γ MFI
CD107a MFI
[αPD-L1]
[αTim-3]

Figure 5.10 *In vitro* $CD8^+$ T_{reg} cell suppression is dictated by the Tim-3 inhibitory pathway. C57BL/6 mice were IV infected with 2.5×10^7 IU Ad-Ova, and (**a**) bulk $CD8^+$ T_{reg} cells were isolated from D7 IV livers. Before co-culture with CFSE-labeled naïve $Thy1.1^+CD8^+$ OT-I T cells at a 1:1 ratio and SIINKFEKL-pulsed BMDCs, the $CD8^+$ T_{reg} cells were left alone or pre-coated with anti-PD-L1 Ab, anti-Tim-3 Ab, or both. Cell cultures were analyzed at D3 for CFSE dilution. (**b**) The number of dividing OT-I T cells, division index, and percent suppression displayed by IV $CD8^+$ T_{reg} cells were calculated at D2 and D3 of culture. (**c**) The concentrations of IL-2 and IFN-γ were measured in the D3 culture supernatants by ELISA. (**d**) CD25 expression was determined directly *ex vivo*, CD107a expression was ascertained after a 5 hr culture with GolgiStop + anti-CD107a Ab cocktail, and IFN-γ was quantified after a 5 hr re-stimulation with 2 μg/mL SIINFEKL peptide on D3 $Thy1.1^+CD8^+$ OT-I T cells in wells containing $CD8^+$ T_{reg} cells (one-way ANOVA/Tukey's post test; n = 6-9 per group). Numbers in the histograms represent percentages. Mean ± s.e.m.; $^*P < 0.05$, $^{**}P < 0.01$, and $^{***}P < 0.001$.

Figure 5.11

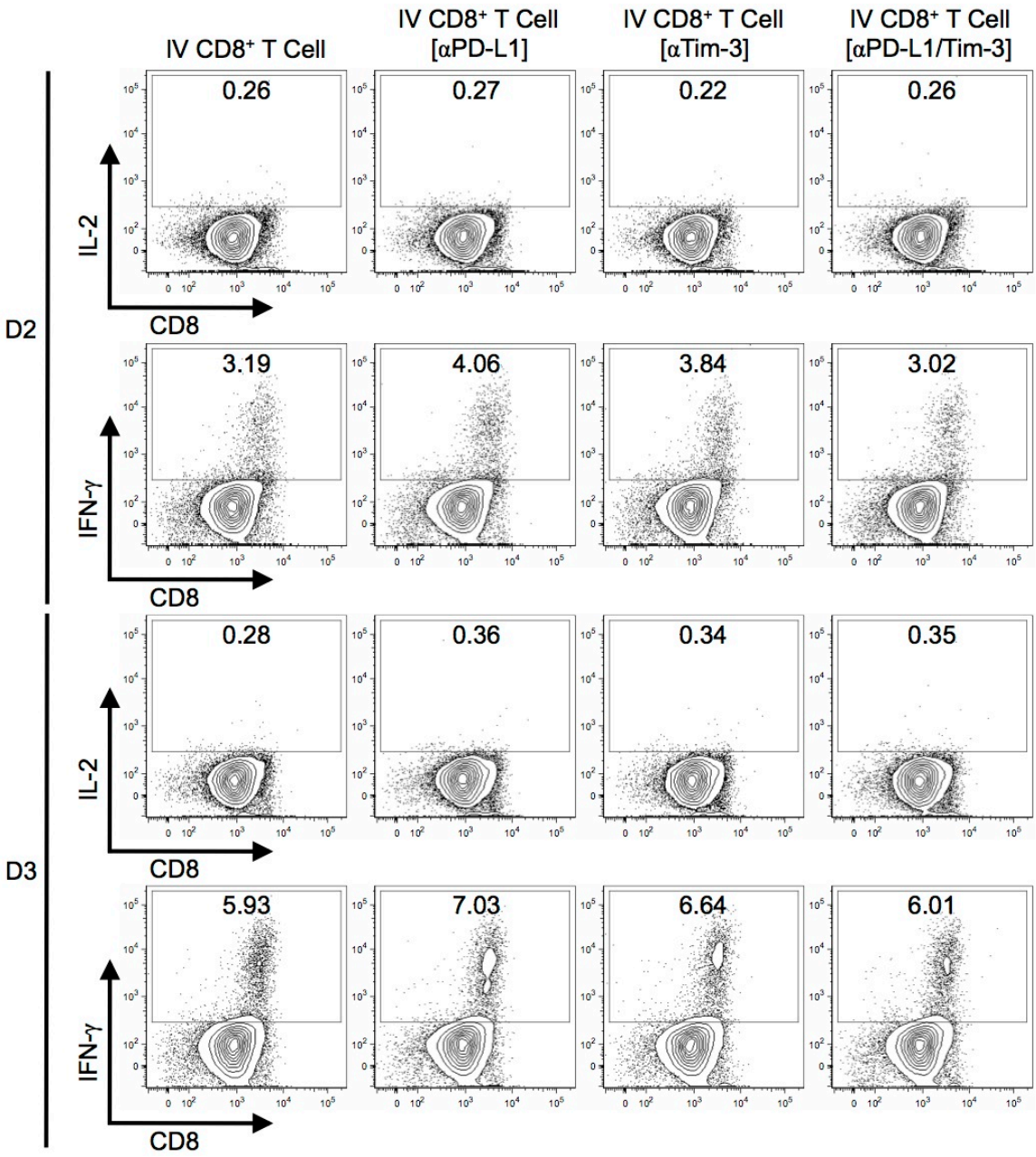
IV CD8+ T Cell
IV CD8+ T Cell [αPD-L1]
IV CD8+ T Cell [αTim-3]
IV CD8+ T Cell [αPD-L1/Tim-3]
D2
D3
IL-2
IFN-γ
CD8
0.26
0.27
0.22
0.26
3.19
4.06
3.84
3.02
0.28
0.36
0.34
0.35
5.93
7.03
6.64
6.01

Figure 5.11 Treatment with anti-PD-L1 antibody or anti-Tim-3 antibody does not improve $CD8^+$ T_{reg} cell cytokine production. C57BL/6 mice were IV infected with 2.5×10^7 IU Ad-Ova, and bulk $CD8^+$ T_{reg} cells were isolated from D7 IV livers. Before co-culture with CFSE-labeled naïve $Thy1.1^+CD8^+$ OT-I T cells at a 1:1 ratio and SIINKFEKL-pulsed BMDCs, the $CD8^+$ T_{reg} cells were left alone or pre-coated with anti-PD-L1 Ab, anti-Tim-3 Ab, or both. Antigen-specific $Thy1.1^-CD8^+$ T_{reg} cell IL-2 and IFN-γ were quantified after a 5 hr re-stimulation with 2 μg/mL SIINFEKL peptide on D2 and D3 after co-culture (n = 3 per group). Numbers in the scatter plots represent percentages.

Figure 5.12

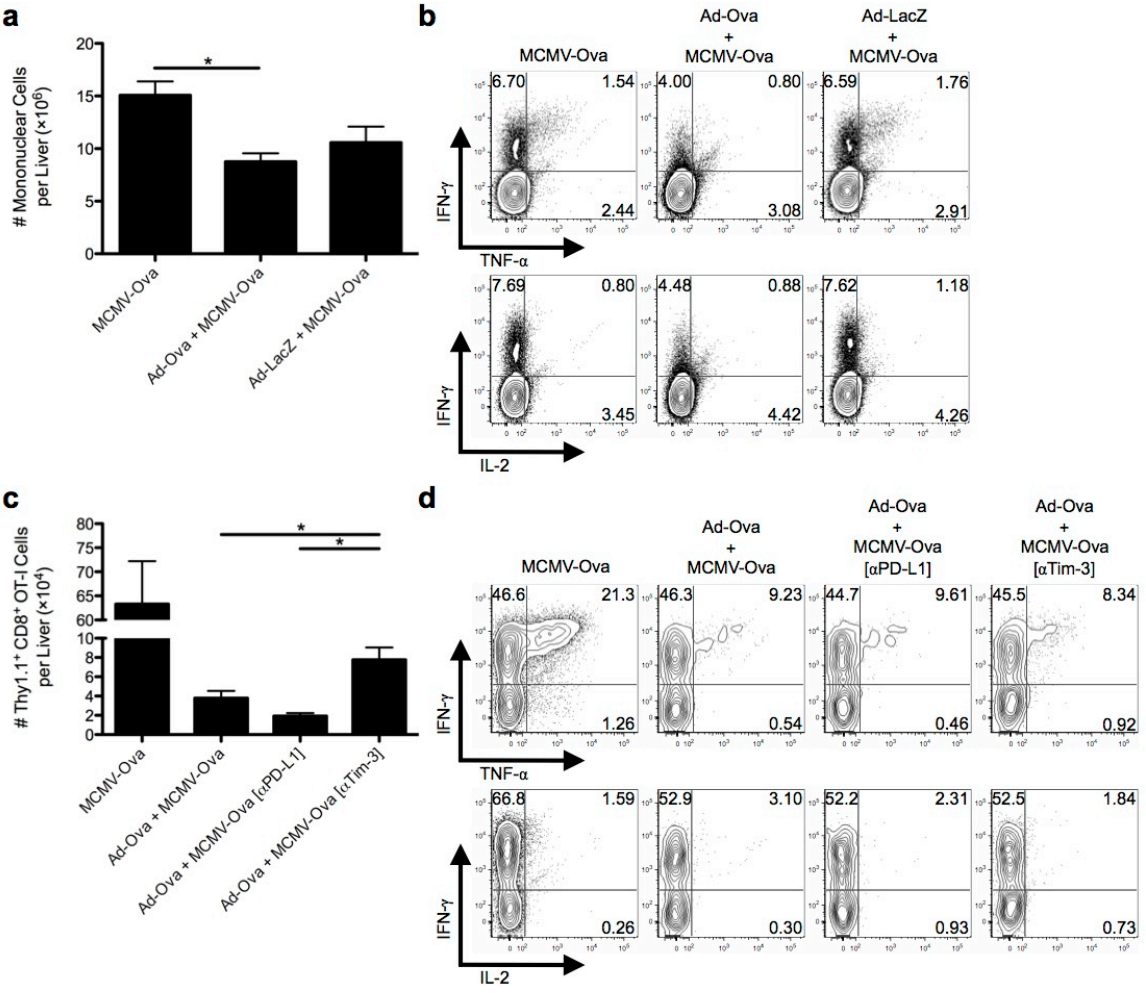
a
Mononuclear Cells per Liver (×10^6)
MCMV-Ova
Ad-Ova + MCMV-Ova
Ad-LacZ + MCMV-Ova
b
MCMV-Ova
Ad-Ova + MCMV-Ova
Ad-LacZ + MCMV-Ova
IFN-γ
TNF-α
IL-2
c
Thy1.1+ CD8+ OT-I Cells per Liver (×10^4)
MCMV-Ova
Ad-Ova + MCMV-Ova
Ad-Ova + MCMV-Ova [αPD-L1]
Ad-Ova + MCMV-Ova [αTim-3]
d
MCMV-Ova
Ad-Ova + MCMV-Ova
Ad-Ova + MCMV-Ova [αPD-L1]
Ad-Ova + MCMV-Ova [αTim-3]
IFN-γ
TNF-α
IL-2

Figure 5.12 Tim-3 blockade improves antigen-specific hepatic secondary immune responses to viral infection. C57BL/6 mice were IV infected with 2.5×10^7 IU Ad-Ova, Ad-LacZ, or left uninfected. At D7, all 3 experimental groups were IV infected with 1×10^4 IU MCMV-Ova. (**a**) The number of live mononuclear cells isolated from the livers of D14 infected animals was enumerated. Trypan blue exclusion was used to assess the number of viable cells. (**b**) Endogenous $CD8^+$ T cell TNF-α, IL-2, and IFN-γ were quantified at D14 after a 5 hr re-stimulation with 2 μg/mL SIINFEKL peptide (one-way ANOVA/Tukey's post test; n = 3 per group). (**c,d**) In a parallel experiment, 5×10^5 naïve $Thy1.1^+CD8^+$ OT-I T cells were transferred at D7. C57BL/6 mice were left untreated or were administered 300 μg anti-PD-L1 Ab or anti-Tim-3 Ab IP at D5 and D6 prior to a D7 MCMV-Ova infection. The number of $Thy1.1^+CD8^+$ OT-I T cells and their TNF-α, IL-2, and IFN-γ production was assessed in the livers of infected animals at D14. Cytokine detection was achieved after a 5 hr re-stimulation with 2 μg/mL SIINFEKL peptide (one-way ANOVA/Tukey's post test; n = 3 per group). Numbers in the scatter plots represent percentages. Mean ± s.e.m.; $^*P < 0.05$.

Figure 5.13

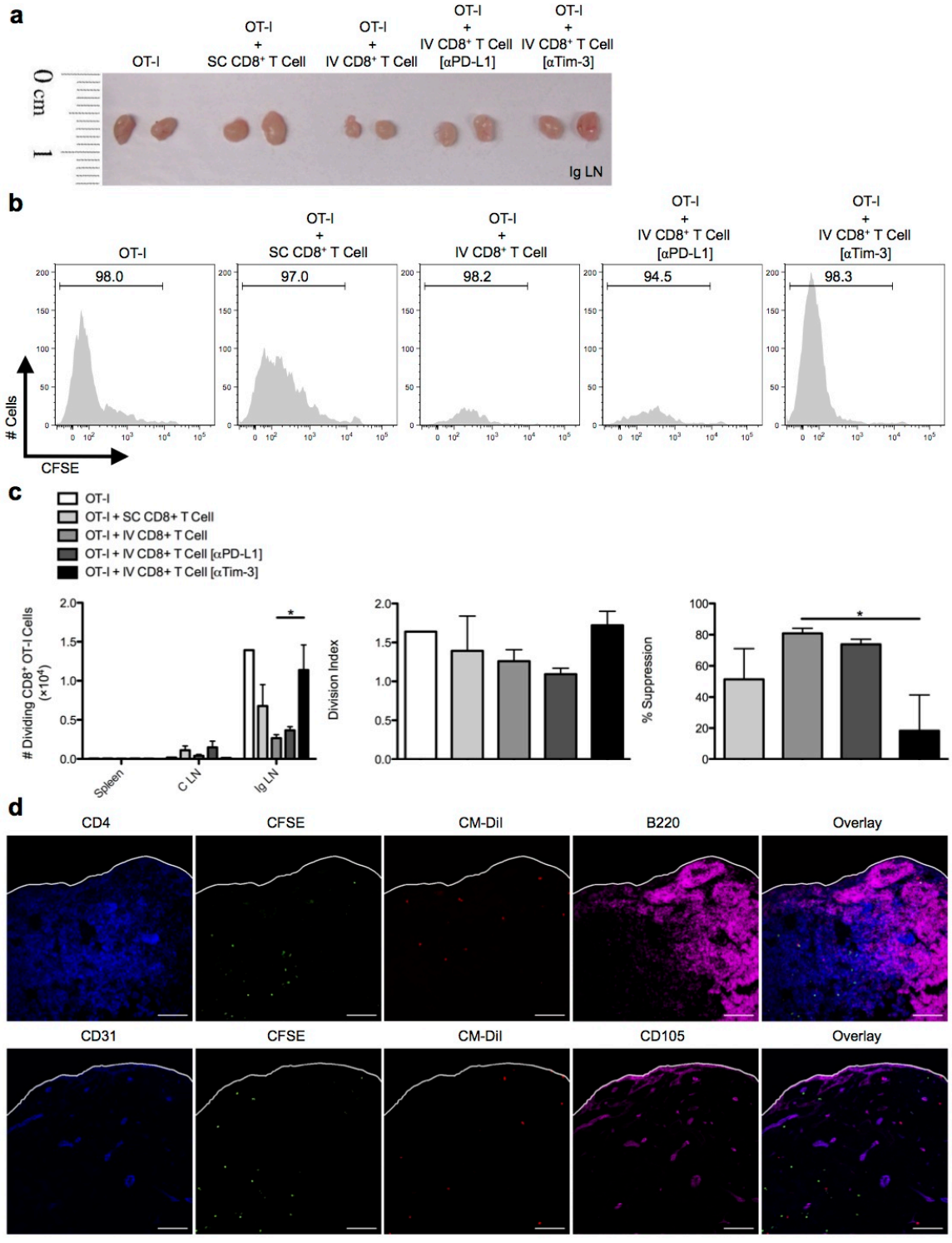
a
OT-I
OT-I + SC CD8⁺ T Cell
OT-I + IV CD8⁺ T Cell
OT-I + IV CD8⁺ T Cell [αPD-L1]
OT-I + IV CD8⁺ T Cell [αTim-3]
0 cm
1
Ig LN
b
OT-I
OT-I + SC CD8⁺ T Cell
OT-I + IV CD8⁺ T Cell
OT-I + IV CD8⁺ T Cell [αPD-L1]
OT-I + IV CD8⁺ T Cell [αTim-3]
98.0
97.0
98.2
94.5
98.3
Cells
CFSE
c
OT-I
OT-I + SC CD8+ T Cell
OT-I + IV CD8+ T Cell
OT-I + IV CD8+ T Cell [αPD-L1]
OT-I + IV CD8+ T Cell [αTim-3]
Dividing CD8⁺ OT-I Cells (×10⁴)
Spleen
C LN
Ig LN
Division Index
% Suppression
d
CD4
CFSE
CM-DiI
B220
Overlay
CD31
CFSE
CM-DiI
CD105
Overlay

Figure 5.13 *In vivo* $CD8^+$ T_{reg} cell suppression of SC primed OT-I T cells entering draining lymph nodes is regulated by Tim-3. C57BL/6 mice were SC or IV infected with 2.5×10^7 IU Ad-Ova, and bulk $CD8^+$ T cells were isolated from D7 SC spleens and IV livers. D7 $CD8^+$ T_{reg} cells from IV infected livers were left alone or pre-coated with anti-PD-L1 Ab or anti-Tim-3 Ab. CFSE-labeled naïve $Thy1.1^+CD8^+$ OT-I T cells alone or in combination with $CD8^+$ T cells from infected spleens and livers at a 1:2 ratio, respectively, were adoptively transferred into naïve C57BL/6 mice. Shortly thereafter, these recipient mice were SC infected. At D3 post-infection, the spleens, C LN, and (**a,b**) Ig LN were harvested, and (**c**) the number of dividing OT-I T cells was determined in each organ. The division index and percent suppression of OT-I T cells in the Ig LN is displayed (one-way ANOVA/Tukey's post test; n = 3-6 per group). (**d**) CM-DiI-labeled $CD8^+$ T_{reg} cells from D7 IV infected liver (red) and CFSE-labeled naïve $Thy1.1^+CD8^+$ OT-I T cells (green) were transferred in a similar experiment and Ig LNs were harvested at D2 SC post-infection. PLP-fixed/OCT-frozen Ig LN cross sections were stained with anti-CD4 (blue-upper panel), anti-CD31 (blue-lower panel), anti-B220 (magenta-upper panel), and CD105 (magenta-lower panel) (n = 3 per group). Scale bar, 100 μm. Numbers in the histograms represent percentages. Mean ± s.e.m.; $*P < 0.05$.

Figure 5.14

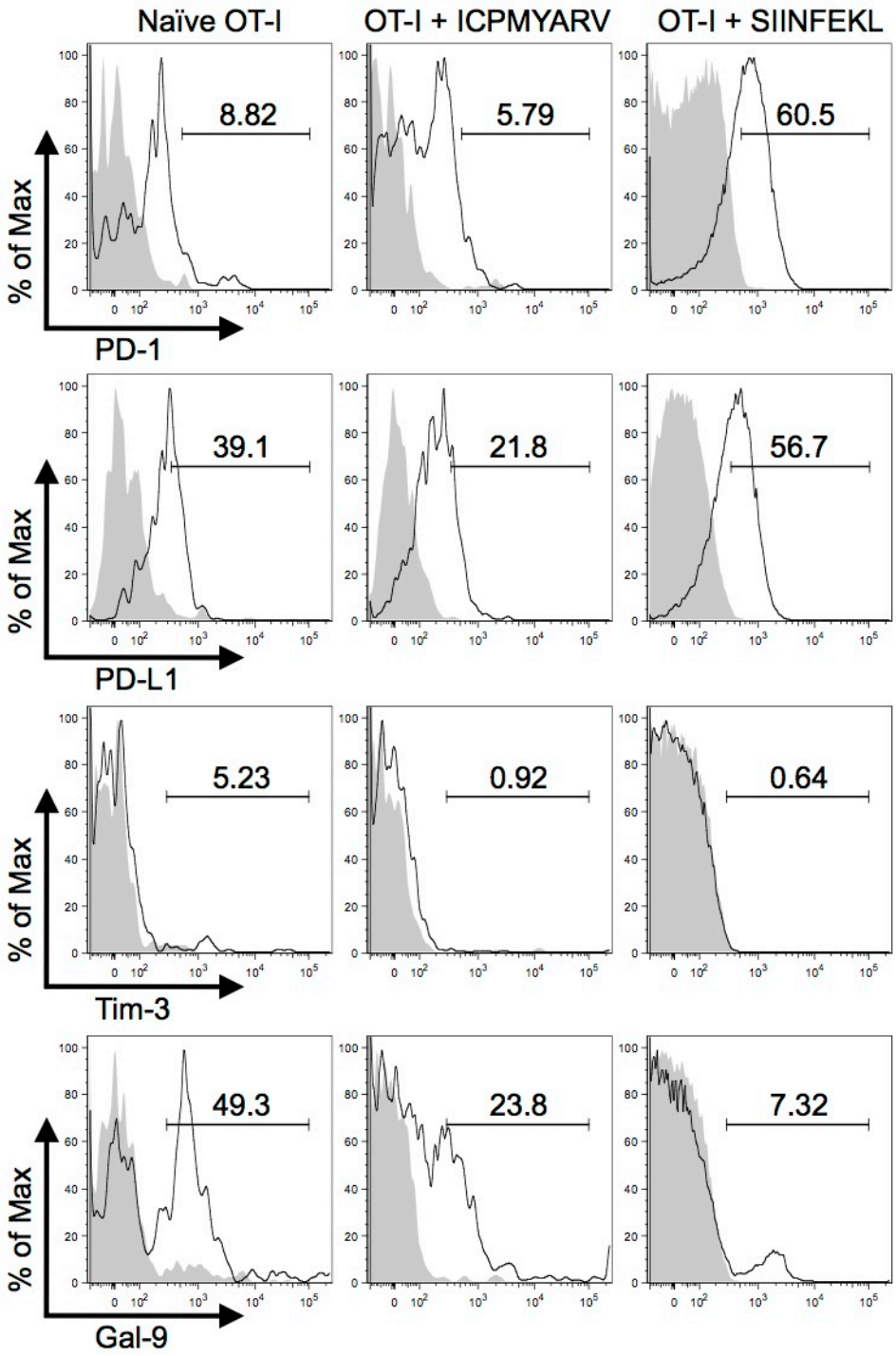
Naïve OT-I
OT-I + ICPMYARV
OT-I + SIINFEKL
% of Max
PD-1
8.82
5.79
60.5
PD-L1
39.1
21.8
56.7
Tim-3
5.23
0.92
0.64
Gal-9
49.3
23.8
7.32

Figure 5.14 Primed $CD8^+$ OT-I T cells differentially up-regulate PD-1/PD-L1 and Tim-3/Gal-9 surface expression. Naïve $Thy1.1^+CD8^+$ OT-I T cells were stimulated *in vitro* with un-pulsed, ICPMYARV-pulsed, or SIINFEKL-pulsed BMDCs and analyzed at D2 for surface expression of PD-1, PD-L1, Tim-3, and Gal-9 (n = 3 per group). Numbers in the histograms represent percentages.

Figure 5.15

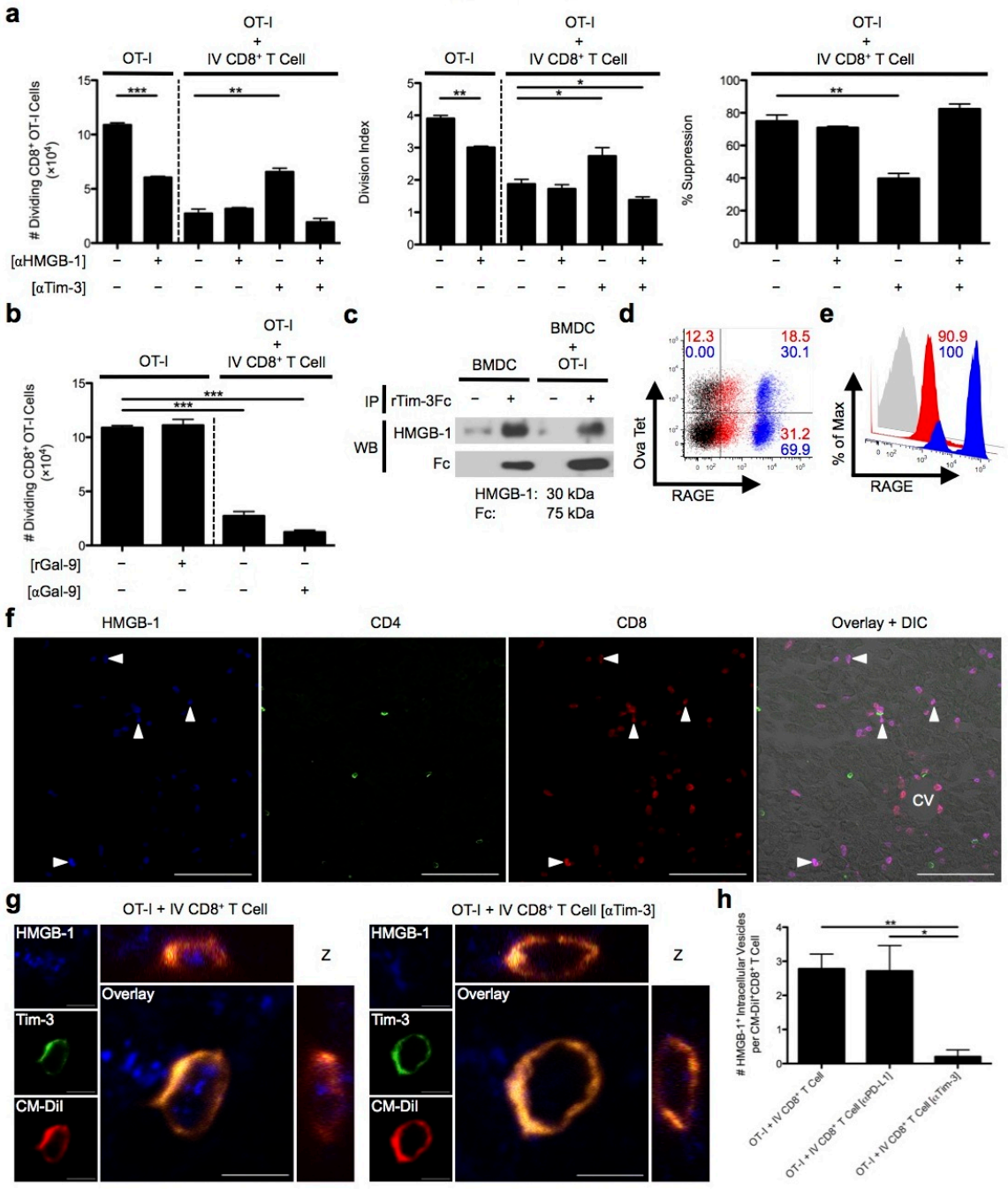
a
OT-I
OT-I + IV CD8⁺ T Cell
Dividing CD8⁺ OT-I Cells (×10⁴)
Division Index
% Suppression
[αHMGB-1]
[αTim-3]
b
[rGal-9]
[αGal-9]
c
BMDC
BMDC + OT-I
IP
rTim-3Fc
WB
HMGB-1
Fc
HMGB-1: 30 kDa
Fc: 75 kDa
d
Ova Tet
RAGE
12.3
0.00
18.5
30.1
31.2
69.9
e
% of Max
90.9
100
f
HMGB-1
CD4
CD8
Overlay + DIC
CV
g
OT-I + IV CD8⁺ T Cell
OT-I + IV CD8⁺ T Cell [αTim-3]
Tim-3
CM-DiI
Overlay
Z
h
HMGB-1⁺ Intracellular Vesicles per CM-DiI⁺CD8⁺ T Cell
OT-I + IV CD8⁺ T Cell
OT-I + IV CD8⁺ T Cell [αPD-L1]
OT-I + IV CD8⁺ T Cell [αTim-3]

Figure 5.15 Tim-3 binding to HMGB-1 controls $CD8^+$ T_{reg} cell suppression independent of Gal-9. (**a**) D7 Ad-Ova primed $CD8^+$ T_{reg} cells were isolated from livers, left alone or pre-coated with anti-Tim-3 Ab, and co-cultured with CFSE-labeled naïve $Thy1.1^+CD8^+$ OT-I T cells at a 1:1 ratio and SIINKFEKL-pulsed BMDCs. Select wells also contained anti-HMGB-1 Ab in the media during culture. D3 CFSE dilution and number of dividing OT-I T cells, division index, and percent suppression by IV $CD8^+$ T_{reg} cells were evaluated (one-way ANOVA/Tukey's post test; n = 6 per group). (**b**) The number of dividing OT-I T cells was also determined when rGal-9 was included in the media with OT-I T cells alone and when anti-Gal-9 Ab was included in the media of OT-I/$CD8^+$ T_{reg} cell co-cultures (n = 3 per group). (**c**) Supernatants from media obtained from BMDCs maturing in the presence of rIL-4 and rGM-CSF and from D1 BMDC co-culture with OT-I T cells were incubated with rTim-3Fc chimeric protein for 1 hr, followed by immunoprecipitation with protein A/G and immunoblot analysis with anti-HMGB-1 Ab or anti-human Fc (n = 3 per group). RAGE surface (red) and intracellular (blue) expression on (**d**) endogenous $CD8^+$ T cells from livers D7 post-infection with Ad-Ova and (**e**) OT-I T cells after D3 culture with SIINFEKL-pulsed BMDCs compared to FMO (black and grey, respectively) is depicted (n = 3 per group). (**f**) PLP-fixed/OCT-frozen liver cross sections from D7 livers were stained with anti-HMGB-1 (blue), anti-CD4 (green), and anti-CD8 (red). Central vein (CV) is indicated (n = 6 per group). Scale bar, 100 μm. (**g**) 3D orthogonal view representative of PLP-fixed/OCT-frozen Ig LN cross sections from C57BL/6 mice that received CM-DiI-labeled $CD8^+$ T_{reg} cells from D7 infected liver (red) and CFSE-labeled naïve $Thy1.1^+CD8^+$ OT-I T cells stained with anti-HMGB-1 (blue) and anti-Tim-3 (green) is shown. Scale bar, 5 μm. (**h**) From the same Ig LN tissue sections, quantification of intracellular HMGB-1^+ perinuclear vesicles within uncoated, anti-PD-L1

Ab pre-coated, and anti-Tim-3 Ab pre-coated $CD8^+$ T_{reg} cells was assessed per cell in images (one-way ANOVA/Tukey's post test; n = 3 per group). Numbers in the histograms and scatter plots represent percentages. Mean ± s.e.m.; *P < 0.05, **P < 0.01, and ***P < 0.001.

Table 5.1

Gene	Protein	Fold Change	Accession #
Hmgb1	HMGB-1	2.466	BF166000
Il18	IL-18	2.422	NM_008360
Ifna5	IFN-α5	2.039	NM_010505
Il12b	IL-12β (p40)	1.494	AF128214
Tnfa	TNF-α	0.616	NM_013693
Il1b	IL-1β	0.438	BC011437
Pdl1	PD-L1	0.363	NF_021893
Il6	IL-6	0.400	NM_031168
Il10	IL-10	0.038	NM_010548
Havcr2	Tim-3	N/A	N/A

Table 5.1 Liver resident macrophage populations upregulate *Hmgb1* in response to adenovirus infection. Total RNA was collected from FACS-sorted Ly6C$^+$ Kupffer cells and CD11b$^+$ DCs/Møs isolated from the liver. Gene expression from a microarray analysis relative to other CD11b$^+$ DC/Mø populations is displayed (n = 3 per group).

Figure 5.16

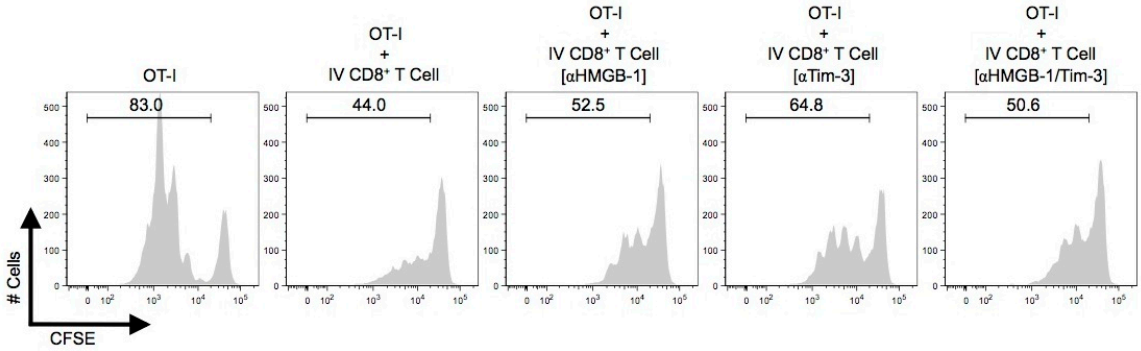
OT-I
OT-I + IV CD8+ T Cell
OT-I + IV CD8+ T Cell [αHMGB-1]
OT-I + IV CD8+ T Cell [αTim-3]
OT-I + IV CD8+ T Cell [αHMGB-1/Tim-3]
83.0
44.0
52.5
64.8
50.6
Cells
CFSE

Figure 5.16 Tim-3-mediated *in vitro* $CD8^+$ T_{reg} cell suppression is unaltered in the presence of *Rage*$^{-/-}$ BMDCs. C57BL/6 mice were IV infected with 2.5×10^7 IU Ad-Ova, and bulk $CD8^+$ T_{reg} cells were isolated from D7 IV livers. Before co-culture with CFSE-labeled naïve $Thy1.1^+CD8^+$ OT-I T cells at a 1:1 ratio and SIINKFEKL-pulsed *Rage*$^{-/-}$ BMDCs, the $CD8^+$ T_{reg} cells were left alone or pre-coated with anti-Tim-3 Ab. Select wells also contained anti-HMGB-1 Ab in the media during culture. Cell cultures were analyzed at D3 for CFSE dilution (n = 3 per group). Numbers in the histograms represent percentages.

Figure 5.17

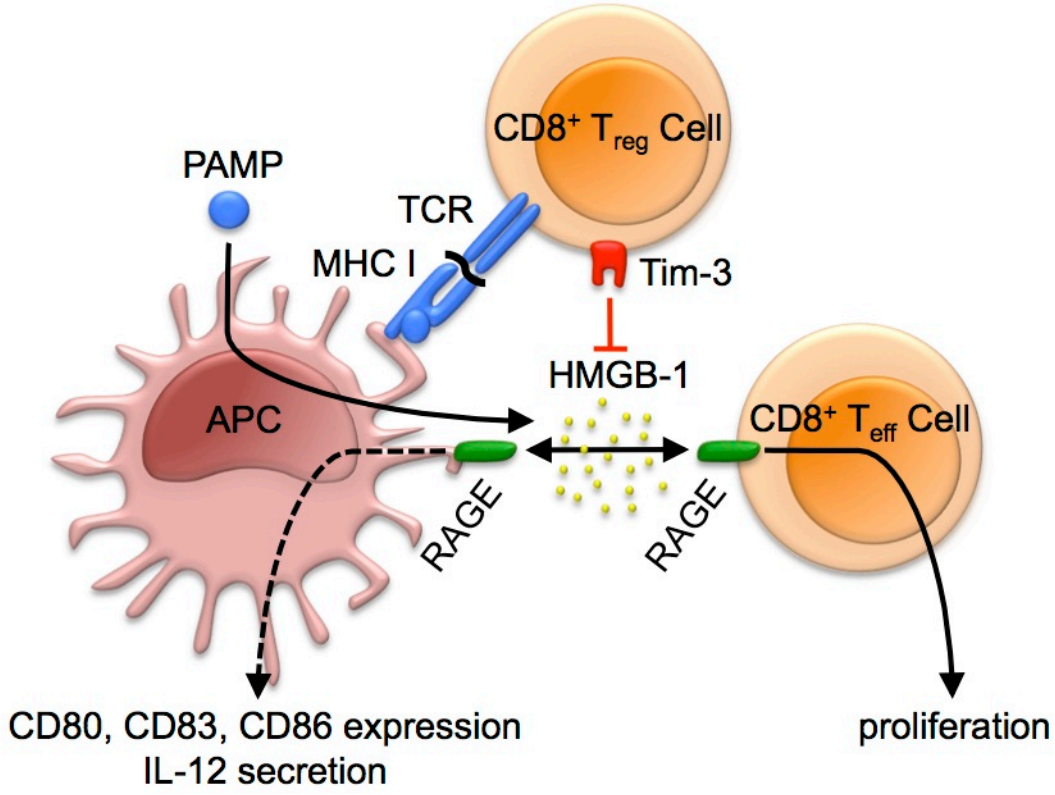
CD8+ Treg Cell
PAMP
TCR
MHC I
Tim-3
HMGB-1
APC
CD8+ Teff Cell
RAGE
RAGE
CD80, CD83, CD86 expression
IL-12 secretion
proliferation

Figure 5.17 Mechanism of liver $CD8^+$ T_{reg} cell suppression. $CD8^+$ T_{reg} cells recognize peptide/MHC I complex on the surface of an APC. This engagement event licenses Tim-3 to sequester HMGB-1, preventing HMGB-1 binding to RAGE in pro-inflammatory microenvironments thus precluding $CD8^+$ T_{eff} cell expansion. Since APCs are known to express RAGE, it is possible that sequestration of HMGB-1 also prevents maturation characterized by CD80, CD83, and CD86 up-regulation and IL-12 production from these cell populations.

Acknowledgments

After pilot experiments established a $CD8^+$ T_{reg} cell phenotype, Jie Sun at Indiana University kindly aided in optimizing $CD8^+$ T cell co-culture experiments. I also thank Taeg Kim and Hai-Chon Lee of the University of Virginia for their contributions in experimental design. Sun-Sang Sung and the University of Virginia Advanced Microscopy Facility assisted in confocal imaging. Michael Solga and the University of Virginia Flow Cytometry Core Facility contributed to performing and outlining FACS-sorting experiments. NIH Grants DK063222, U19 AI083024, and Immunology Training Fellowship T32 AI07496 supported this work.

Methods

Animals and Infections

Thy1.2$^{+/+}$ C57BL/6 mice were used in these experiments (Taconic Farms, Hudson, NY). *Thy1.1*$^{+/-}$ OT-I*(Tcra/Tcrb)*$^{+/-}$ mice were bred from *Thy1.1*$^{+/+}$ and OT-I*(Tcra/Tcrb)*$^{+/+}$*Rag1*^{tm1Mom} mice (Taconic Farms). IL-10 transcriptional reporter (Vert-X) mice provided by Christopher Karp were generated by insertion of a neomycin-IRES-eGFP cassette between the endogenous stop site and polyadenosine site of *Il10*. The neomycin cassette was floxed out using *Zp3-cre* mice (The Jackson Laboratory, Bar Harbor, ME), and heterozygous mice were interbred to generate homozygous mice[193]. *Rage*$^{-/-}$ mice were obtained from the laboratory of Victor E. Laubach (University of Virginia, Charlottesville, VA). Animals used were 6 to 10 weeks of age and housed in a pathogen-free facility under protocols approved by the Institutional Animal Care and Use Committee at the University of Virginia (Charlottesville, VA).

Replication-deficient type 5 adenoviruses lacking the *E1* and *E3* genes and expressing the ovalbumin protein (Ad-Ova) or β-galactosidase protein (Ad-LacZ) under the control of the human *Cmv* promoter were provided by Timothy L. Ratliff (Iowa Gene Transfer Vector Core, University of Iowa, Iowa City, IA) and Gregory A. Helm (University of Virginia, Charlottesville, VA), respectively. Mouse cytomegalovirus expressing the ovalbumin protein fused to the transferrin receptor (MCMV-Ova) under the control of the HCMV *Ie1* promoter (*Miep*) was provided by Ann B. Hill (Oregon Health and Science University, Portland, Oregon). Mice were infected with 2.5×10^7 infectious units (IU) Ad-Ova/LacZ/Tyr or 1×10^4 IU MCMV-Ova via intravenous (IV) injection in the caudal vein or subcutaneous (SC) injection in the left flank.

Quantitative Reverse-Transcription PCR

Total RNA was isolated using the Trizol method (Invitrogen, Carlsbad, CA) and reverse-transcribed using High Capacity RNA-to-cDNA Master Mix (Applied Biosystems, Foster City, CA). Q-PCR was performed using Fast SYBR Green Master Mix (Applied Biosystems) on an AB StepOne Plus Real-Time PCR System. QuantiTect primers for *Mus musculus Il10*, *Il2*, *Ifng*, *Tgfb*, *Lgals9*, *Havcr2*, *Pdl1*, *Pdc1*, *Ctla4*, *Klrc1*, *Foxp3*, *Ikzf2* (Qiagen, Valencia, CA), and self-designed primers for *Mus musculus* hypoxanthine phosphoribosyltransferase (*Hprt1*)

Forward: 5'-CTCCGCCGGCTTCCTCCTCA-3'

Reverse: 5'-ACCTGGTTCATCATCGCTAATC-3'

were used for detection. Data were generated by the comparative threshold cycle (ΔC_T) method by normalizing to *Hprt1*.

Microarray Analysis

Total RNA was isolated using the Trizol method (Invitrogen). Microarray analysis was performed at the Virginia Bioinformatics Institute (Virginia Polytechnic Institute and State University, Blacksburg, VA) using an Agilent 2100 BioAnalyzer (Agilent Technologies, Santa Clara, CA).

ELISA

IL-10 ELISAs were performed on diluted D2 supernatants of magnetically sorted, anti-CD3ε and anti-CD28 antibody re-stimulated $CD8^+$ T cells; IL-2 and IFN-γ ELISAs were performed on diluted D3 supernatants from *in vitro* suppression assays (BD Biosciences, Franklin Lakes, NJ). Each sandwich ELISA was incubated with 1×TMB Substrate

Solution (eBioscience, San Diego, CA), and the reaction was stopped with 1 M H_2SO_4. Absorbance was read at 450 nm using a PowerWave XS Microplate Spectrophotometer (BioTek, Winooski, VT).

Immunoprecipitation and Western Blot

Supernatants were collected from bone marrow dendritic cell (BMDC) cultures or D1 BMDC/OT-I co-cultures. 5 μg of recombinant mouse Tim-3 fused to human IgG_1 chimeric protein (rTim-3Fc) (R&D Systems, Minneapolis, MN) was added to 500 μL supernatant for 1 hr at room temperature. Immunoprecipitation was achieved via addition of Protein A/G PLUS-Agarose (Santa Cruz Biotechnology, Dallas, TX) overnight at 4°C. Proteins were resolved by electrophoresis on 10% SDS-polyacrylamide gels and transferred to nitrocellulose membranes. Membranes were then incubated with rabbit anti-HMG1/2/3 (pAb) (Santa Cruz Biotechnology), biotinylated anti-human IgG (pAb) (SouthernBiotech, Birmingham, AL), HRP-linked anti-rabbit IgG (pAb) (Cell Signaling Technology, Danvers, MA), and streptavidin-HRP (R&D Systems) followed by visualization with SuperSignal West Pico Chemiluminescent Substrate (Thermo Scientific, Rochester, NY).

Liver and Spleen Mononuclear Cell Isolation

Mononuclear cells were isolated from livers and spleens according to previous work[46,116,117]. Briefly, livers were flushed via the portal vein with 0.05% collagenase IV (Sigma-Aldrich, St. Louis, MO) in 1×PBS and washed with Iscove's Modified Dulbecco's Medium (IMDM) containing 10% newborn calf serum. Liver tissue was then homogenized and further digested with 0.05% collagenase IV in 1×PBS. Mononuclear cells were then isolated via Histodenz (Sigma-Aldrich) gradient centrifugation, and the

number of viable cells was determined based on 0.1% Trypan blue (Sigma-Aldrich) exclusion. Whole spleens were harvested, and mononuclear cells were isolated over a Ficoll (Atlanta Biologicals, Lawrenceville, GA) gradient.

In vitro Suppression Assay

BMDCs were matured for one week in Roswell Park Memorial Institute (RPMI) Medium 1640 containing 10% HyClone fetal bovine serum, 15 mM HEPES Buffer, 50 μM βME, 20 ng/mL recombinant mouse IL-4 (rIL-4), and 20 ng/mL recombinant mouse GM-CSF (rGM-CSF) (eBioscience). 5×10^3 BMDCs were placed in each well of a 96-well round bottom plate, pulsed for 5 hrs with 10 ng/mL SIINFEKL or ICPMYARV peptides (AnaSpec, Fremont, CA), then cultured with 5×10^4 CFSE-labeled (Invitrogen) naïve $Thy1.1^+CD8^+$ OT-I T cells per reaction. $CD8^+$ T cells from SC or IV infected C57BL/6 mice were then added at the appropriate ratio. $CD8^+$ T cells were positively sorted using magnetic beads linked to anti-CD8α (Miltenyi Biotec, Auburn, CA) in all relevant experiments. βME was removed after peptide pulsing in a wash before T cell co-culture.

In vivo Suppression Assay

For *in vivo* liver responses, 5×10^5 CFSE-labeled naïve $Thy1.1^+CD8^+$ OT-I T cells were transferred into naïve, D7 Ad-Ova infected, or D7 Ad-LacZ infected C57BL/6 mice prior to IV MCMV-Ova infection. For *in vivo* lymph node responses, 3×10^6 $CD8^+$ T cells from SC or IV infected C57BL/6 mice were co-transferred with 1.5×10^6 CFSE-labeled naïve $Thy1.1^+CD8^+$ OT-I T cells into naïve C57BL/6 mice. Shortly after, these mice were SC infected. At D3 post-infection, the inguinal lymph nodes (Ig LN), celiac lymph nodes (C LN), and spleens were harvested.

In vitro T cell Activation

2×10^5 CFSE-labeled $CD8^+$ T cells were placed in a 96-well flat bottom plate coated with 1 μg/mL anti-CD3ε (145-2C11) (BD Biosciences) in RPMI Medium 1640 containing 10% HyClone fetal bovine serum, 15 mM HEPES Buffer, 50 μM βME, and 2 μg/mL anti-CD28 (37.51) (eBioscience).

Antibody Blockade and Cell Treatments

In vivo whole animal blockade of PD-L1 and Tim-3 at D5 and D6 post-Ad-Ova infection was conducted prior to MCMV-Ova infection at D7 via intraperitoneal (IP) injection of 300 μg anti-PD-L1 (10F.9G2) or anti-Tim-3 (RMT3-23) (BioXCell, West Lebanon, NH). For *in vitro* and *in vivo* lymph node blockade, $CD8^+$ T_{reg} cells were pre-coated with 20 μg/mL anti-PD-L1 and/or anti-Tim-3 for 1 hr at 37°C prior to culture or transfer, respectively. In order to inhibit proliferation of $CD8^+$ T_{reg} cells during *in vitro* co-culture, cells were treated with 50 μg/mL Mitomycin C (Sigma-Aldrich) for 20 min at 37°C, washed, then placed in co-culture with CFSE-labeled naïve $Thy1.1^+CD8^+$ OT-I T cells. 1.0 μg/mL recombinant mouse Gal-9 (rGal-9) (R&D Systems), 20 μg/mL anti-Gal-9 (RG9-1), 20 μg/mL anti-IL-10R (1B1.3A) (BioXCell), and 0.5 μg/mL anti-HMGB-1 (pAb) (eBioscience) were added to culture media in relevant experiments.

Flow Cytometry

The following mAbs were used for cell surface and intracellular staining: anti-CD25 APC (PC61), anti-IL-2 APC (JES6-5H4) (BD Biosciences), anti-Gal-9 AF647 (108A2), anti-Gal-9 PE (108A2), anti-PD-L1 PE-Cy7 (10F.9G2) (BioLegend, San Diego, CA), anti-CD8α APC-eF780 (53-6.7), anti-CD25 PE (PC61), anti-CD107a eF660 (1D4B), anti-

CTLA-4 PE (UC10-4B9), anti-FoxP3 PE (FJK-16s), anti-Gata-3 PE (TWAJ), anti-GITR PE (DTA-1), anti-Helios PE (22F6), anti-IFN-γ APC (XMG1.2), anti-IL-2 AF488 (JES6-5H4), anti-IL-10 APC (JES5-16E3), anti-NKG2A PE (16a11), anti-PD-1 FITC (J43), anti-PD-1 PE (J43), anti-Tbet PE (4B10), anti-Thy1.2 eF450 (53-2.1), anti-Tim-3 PE (RMT3-23), anti-Tim-3 AF647 (RMT3-23), anti-TNF-α PE (MP6-XT22) (eBioscience), and anti-RAGE AF647 (MAB11795) (R&D Systems). H2-K^b Ova-tetramer (SIINFEKL) APC (MHC Tetramer Core Laboratory, Baylor College of Medicine, Houston, TX) and H2-K^b βGal-tetramer (ICPMYARV) PE (MHC Tetramer Core Facility, NIAID, Atlanta, GA) were used to identify Ova-specific and βGal-specific $CD8^+$ T cells, respectively. Cell surface staining of 1.5×10^6 mononuclear cells was performed by first blocking with anti-CD16/CD32 (2.4G2) (Lymphocyte Culture Center, University of Virginia, Charlottesville, VA) followed by specific antibody labeling for 15 min at 4°C in FACS Buffer (1×PBS containing 2% fetal bovine serum and 0.1% NaN_3). Cells were fixed in BD Cytofix/Cytoperm (BD Biosciences). For nuclear transcription factor staining, cells were stained using the FoxP3 Staining Set (eBioscience). CD107a expression was assessed after a 5 hr culture with GolgiStop (BD Biosciences) + anti-CD107a Ab cocktail. For intracellular cytokine detection, cells were re-stimulated with 5 ng/mL PMA and 500 ng/mL ionomycin (Sigma-Aldrich) or 2 μg/mL SIINFEKL peptide (AnaSpec), blocked with 1 μL/mL GolgiPlug and 1 μL/mL GolgiStop, and permeabilized with BD Perm/Wash (BD Biosciences). Data were collected on a BD FACS Canto II (BD Immunocytometry Systems, San Jose, CA) and analyzed using FlowJo 8.8.6 software (Tree Star Inc., Ashland, OR). For analysis of PCR products and sorting of $CD11b^+$ DC/Møs and $Ly6C^+$ Møs, Ova Tet^+ from Ova Tet^-CD8^+ T cells, and $eGFP^+$ from $eGFP^-$ Vert-X $CD8^+$ T cells

prior to culture, cells were sorted on an iCyt Reflection Cell Sorter (iCyt Mission Technology, Champaign, IL).

Microscopic Studies

Livers and lymph nodes were flushed with 1×PBS and periodate-lysine-paraformaldehyde fixative (PLP), excised, and then incubated in PLP for 3 hrs at 4°C according to previous work[163]. After passage over a sucrose gradient, livers and lymph nodes were frozen in OCT, sectioned at 5 μm thickness, blocked with 2.4G2 solution (2.4G2 media containing anti-CD16/32, 30% chicken/donkey/horse serum, and 0.1% NaN_3), and stained with anti-B220 AF647 (RA3-6B2), anti-CD4 AF488 (RM4-5), anti-CD4 Brilliant Violet 421 (RM4-5), anti-CD31 Pacific Blue (MEC13.3), anti-CD105 AF647 (MJ7/18), anti-rabbit IgG Brilliant Violet 421 (pAb) (BioLegend), anti-Tim-3 AF647 (RMT3-23) (eBioscience), rabbit anti-HMG1/2/3 (pAb) (Santa Cruz Biotechnology), and anti-CD8α AF555 (210) (Sino Biological, Beijing, China). In select experiments, cells were also labeled with CFSE and Vybrant CM-DiI (Invitrogen). Confocal microscopy was performed on a Zeiss LSM-700 microscope, and the data were analyzed using Zen 2009 Light Edition software (Carl Zeiss MicroImaging GmbH, Jena, Germany).

Statistical Analysis

Significant differences between experimental groups were calculated using the two-tailed Student's t test or one-way ANOVA (with group comparisons ≥ 3). Data analysis was performed using Prism 5.0a software (GraphPad Software Inc., La Jolla, CA). Values of $P < 0.05$ were regarded as being statistically significant and noted as * < 0.05, ** < 0.01, and *** < 0.001.

CHAPTER 6

Conclusions and Future Directions

Main Findings: Regulation of the Intrahepatic $CD8^+$ T Lymphocyte

My thesis studies establish that antigen-specific $CD8^+$ T cells primed directly in the liver acquire a dysfunctional phenotype in response to viral challenge characterized by a decreased ability to produce pro-inflammatory cytokines and cytolytically kill target cells. The induction of tolerance is not a function of the pathogen in this model system (adenovirus), because priming at other sites, such as the skin-draining inguinal lymph node, leads to the expansion of functionally competent $CD8^+$ T_{eff} cells. Further, when these extrahepatic $CD8^+$ T_{eff} cells infiltrate the liver, they retain their effector function including cytokine production and cytolytic potential. It is apparent that dysfunction in the liver-primed $CD8^+$ effector T (T_{eff}) cell population begins at the early stage of viral infection because the liver microenvironment is unable to reshape competent $CD8^+$ T_{eff} cells primed in the skin into functionally exhausted cells once these cells migrate to the liver.

During the onset of intrahepatic viral infection, natural killer (NK) and $CD8^+$ T cell infiltration and/or expansion are accompanied by the upregulation of three core immunoregulatory pathways: IL-10, PD-1/PD-L1, and Tim-3. My studies indicate that Kupffer cell (KC) surface expression of PD-L1 is critical in dampening NK and $CD8^+$ T cell responses as demonstrated through targeted *Pdl1* silencing using PD-L1 siRNA encapsulated within lipidoid nanoparticles (LNP). A hepatocyte derived PD-L1 signal was deemed negligible, as PD-L1 siRNA delivered directly to hepatocytes, bypassing

entry into KCs, did not result in improvements in the antiviral immune response. Another layer of regulation existed beyond a unidirectional PD-1/PD-L1 signal because the $CD8^+$ T cell response could be manipulated based on the timing of PD-L1 LNP drug delivery. If NK cells were prematurely boosted, $CD8^+$ T cell effector function could not be improved. If NK cells were completely deleted, $CD8^+$ T cells could not be primed. If PD-L1 LNP was delivered after the expansion/influx of NK cells, $CD8^+$ T cell effector expansion and effector function were optimal. Therefore, I have identified a critical checkpoint where NK cell functional activity and global liver PD-1/PD-L1 signaling exist in a fine balance that controls $CD8^+$ T cell cytokine and cytolytic potentials. Nevertheless, KC PD-L1 expression is a major initiator of dysfunction highlighted by cell-specific drug targeting and targeted depletion of the KC population.

Without application of PD-L1 LNP, if the dysfunctional liver-primed $CD8^+$ T cells were allowed to expand in the natural setting, not only were these cells unable to produce pro-inflammatory cytokines or cytolytically kill targets, but they also acquired a T regulatory (T_{reg}) cell function on the *in vitro* and *in vivo* priming of naïve $CD8^+$ OT-I T cells. Even though the liver-primed $CD8^+$ T cells (herein renamed $CD8^+$ T_{reg} cells) expressed high levels of PD-1/PD-L1 and were capable of producing IL-10, these pathways became insignificant in dictating $CD8^+$ T_{reg} cell suppressor function as their blockades with antibodies did not dampen regulatory activity. In addition, $CD8^+$ T cell intrinsic PD-1/PD-L1 expression in the PD-L1 LNP model did not appear to play a role because $CD8^+$ T cell PD-1 and PD-L1 surface expression remained unaltered even though they expanded more proficiently and produced more cytokine when *Pdl1* was silenced within KCs (**Fig. 6.1**). Although PD-L1 did not appear to directly play a functional role in $CD8^+$ T cell suppression at the late phase antiviral immune response, PD-1/PD-L1 signaling

from antigen presenting cells (APC) during the early phase promoted the development of $CD8^+$ T_{reg} cells. PD-L1 LNP treatment at D5 seemed to slightly inhibit the ability of $CD8^+$ T_{reg} cells isolated at D7 from the livers of IV infected mice to dampen OT-I T cell expansion (evidenced by absolute number and division index) and CD25, IFN-γ, and CD107a expression (**Fig. 6.2**). This reversal of suppression was far from complete suggesting other early signaling events from immunoregulatory pathways (*e.g.* IL-10) may be involved in $CD8^+$ T_{reg} cell development.

Liver-primed $CD8^+$ T_{reg} cell suppression was discovered to be highly dependent on the negative signaling receptor Tim-3. Tim-3 expression on the surface of liver-primed $CD8^+$ T_{reg} cells was shown to directly bind the alarmin HMGB-1. Since HMGB-1 acts as a growth factor for T_{eff} cells (in manner similar to but mechanistically unrelated to IL-2-mediated proliferation), I conclude that Tim-3 displayed by $CD8^+$ T_{reg} cells sequesters HMGB-1 in order to mediate suppression. Moreover, I speculate that Tim-3 likely does not influence development of the $CD8^+$ T_{reg} cell because it is not expressed by immune cells in the early kinetics of the antiviral immune response within the liver. Overall, I conclude that PD-1/PD-L1 negative signaling diminishes the early antiviral immune response, whereas Tim-3 controls the contraction of the $CD8^+$ T cell pool during the late phase to viral infection of the liver (**Fig 6.3**).

Role of IL-10 in $CD8^+$ T Cell Dysfunction

Throughout the early phase of the immune response against intrahepatic adenoviral infection, IL-10 signaling is apparent as *Il10* mRNA and IL-10 cytokine are detected from D0 to D4 from whole liver samples and lipopolysaccharide (LPS) re-stimulated KC and dendritic cell (DC) populations within the liver (data not shown). In the past, my

laboratory has also shown that local liver IL-10 levels are elevated in mice expressing the HCV core protein under the *albumin* promoter. Further, treatment of these animals with anti-IL-10R antibody at the onset of infection results in a more rapid clearance of adenovirus in the livers of IV infected mice (data not shown). I did not specifically address the role of early IL-10 in shaping $CD8^+$ T cell immunity within the liver in my experiments because the IL-10 transcriptional reporter mouse (Vert-X) did not validate that APC and NK cell populations expressed eGFP, which correlates with *Il10* mRNA. The Vert-X mouse data indicated that most of the active *Il10* transcription was occurring within the liver-primed $CD8^+$ T cell pool, but this IL-10 had no impact on responder $CD8^+$ OT-I T cells in $CD8^+$ T_{reg} cell *in vitro* suppression assays. Therefore, the IL-10-production characteristic of $CD8^+$ T cells during chronic hepatitis C virus (HCV) infection probably has a minor role in imparting negative signals on the antiviral immune response[53,54]. IL-10-mediated regulation from T cells is thus probably limited to the IL-10-producing $CD4^+$ T_r1 cells that arise after HCV infection[52].

Nevertheless, constant exposure of KCs, DCs, and liver sinusoidal endothelial cells (LSEC) to LPS from portal blood via TLR4 ligation renders them poor APCs and potent IL-10 producers[19]. Further, Maris *et al.* have shown there is a critical window in which early IL-10 acts in limiting overall T cell expansion, IFN-γ production, and $CD8^+$ T cell cytolytic capacity[55]. Future experiments elucidating the role of early IL-10 signaling after intrahepatic viral infection are warranted. IL-10 derived from distinct APC subsets may either serve to dampen the antigen-specific $CD8^+$ T_{eff} cell response or promote the development of a *bona fide* population of $CD8^+$ T_{reg} cells within the liver. IL-10 production from $CD11b^+$ myeloid derived intestinal macrophages was shown to support the development of $FoxP3^+CD4^+$ T_{reg} cells by maintaining FoxP3 expression in a colitis

model[194]. IL-10 has also been shown to feedback on liver APC populations decreasing MHC II expression, co-stimulatory molecule expression, and IL-12 and TNF-α production[50,51,165]. Presentation of antigen by immature or semi-mature APCs has been shown to indirectly promote the development of CD4$^+$ T$_r$1 cells[48]. Given early PD-1/PD-L1 signaling from the KC population proved critical in promoting tolerance and these cells are also high producers of IL-10, it is possible both PD-1/PD-L1 and IL-10 signaling from this population both support the development of the CD8$^+$ T$_{reg}$ cell phenotype. Since the liver-primed CD8$^+$ T$_{reg}$ cell is FoxP3$^-$Helios$^+$ and maintains a repressed IL-2 axis, perhaps IL-10 signaling also leads to the transactivation of *Helios* as other researchers' findings consistently indicate that IL-10 directly inhibits IL-2 production[55].

Kupffer Cell PD-1/PD-L1 Signaling Modulates Intrahepatic NK and CD8$^+$ T Cell Effector Function

My research demonstrates that KC PD-L1 contributes to dysfunction in NK and CD8$^+$ T cells during the early phase of intrahepatic viral infection. PD-1 signaling in NK cells inhibits expansion/infiltration and effector function demonstrated in these series of experiments and by other laboratories, but the mechanism is unknown[122,123]. PD-1 contains an immunoreceptor tyrosine-based inhibitory motif (ITIM) and an immunoreceptor tyrosine-based switch motif (ITSM), where the latter recruits SHP-2 in T cells. Downstream PD-1 signals in NK cells have never been published. It is possible that the ITIM becomes relevant to PD-1 signaling in NK cells in addition to the ITSM. Nonetheless, PD-1 engagement of PD-L1 is expected to recruit tyrosine phosphatases to inhibit activating receptor signaling in NK cells.

My experiments show that prematurely boosting NK cells is detrimental to the effector function of $CD8^+$ T cells. As stated previously, this may be mediated by excessive IFN-γ negatively feedback from a hyperresponsive NK cell or the expansion of dysfunctional IL-10-producing $NKG2A^+Ly49^-$ NK cells[117,148]. Intrahepatic immune responses are believed to induce both a liver resident population of NK cells and a population that originates in the bone marrow, which migrates to the liver[121]. Experiments combining agents that block PD-L1 and selective ablation or depletion of NK cells are warranted in the future. For example, if mice are genetically manipulated or given a treatment to interfere with NK cell egress from the bone marrow, questions involving differential effects of PD-1/PD-L1 signaling in resident and migratory NK cell populations could be addressed. Walzer *et al.* have demonstrated that NK cells uniquely express $S1P_5$ receptor, and mice lacking the corresponding gene (endothelial differentiation gene 8; *Edg8*) have decreased NK cell trafficking to the blood, spleen, and lung. NK cells rather accumulate in the bone marrow and lymph nodes in these animals, and the number of NK cells in the liver remains unaffected suggesting that an independent population of liver resident NK cells exists[195]. Once PD-L1 signaling in these two populations of NK cells is understood, mechanisms relating to KC/NK cell cross-talk and related effects on the liver-primed $CD8^+$ T cells might be addressed.

This thesis work also suggests that blockade of PD-1/PD-L1 signaling during the early phase of adenovirus infection leads to the secretion of some factor or upregulation of a surface receptor that dampens liver-primed $CD8^+$ T cells. Microarray or multiplex analysis of liver samples may reveal molecular pathways activated that may lead to premature inhibition of the $CD8^+$ T cell response, and two candidates include IL-10 and excessive IFN-γ. The significance of these cytokines may perhaps be revealed if

congenically mismatched CD8$^+$ OT-I T cells from naïve or D5 adenovirus infected mice are transferred into adenovirus infected *Il10*$^{-/-}$ and *Infg*$^{-/-}$ animals that receive PD-L1 blocking agents or placebo treatments. In this experimental setup, host sources of IL-10 and IFN-γ and the relationship to the outcome of PD-1/PD-L1 signaling in CD8$^+$ T cell effector function may be exposed.

I have also found that MHC II$^+$ cells, CD4$^+$ T cells, and CD8$^+$ T cells form discrete clusters by D7 post-adenovirus infection within the liver, and the number of these clusters increases with PD-L1 LNP treatment. These cellular aggregates formed after viral infection are distinct from the hepatic granulomas and portal tract-associated lymphoid tissue (PALT) found by Yoneyama *et al.* after *Propionibacterium acnes* infection because the majority of cells in virally induced immune clusters are T cell derived, whereas in granulomas or PALTs DCs comprise the main cell population with few T cells contacting the peripheral DCs of the aggregation[196]. Since I discovered that KC PD-L1 plays a critical role in propagating antiviral immune dysfunction compared to LSEC and hepatocyte PD-L1, which is widespread histologically, perhaps the local concentrations of PD-1 and PD-L1 are critical for the negative signal. It is established that PD-1 microclustering on the surface of T cells is important for inhibiting the T cell receptor (TCR) signaling cascade[197]. There may be a mechanistic connection between cellular and molecular clustering that determines the outcome of PD-1/PD-L1 ligation.

Gal-9 and HMGB-1 Balance in the Liver Inflammatory Milieu

Both Gal-9 and HMGB-1 are upregulated during the progression of HCV infection[85,94]. This is likely to happen during adenoviral infection because virally lysed and cytolytically killed cells release HMGB-1, and activated APCs secrete HMGB-1 and Gal-9 as a result

of TLR stimulation and elevated IFN-γ, respectively[76,77,81,82,88,91,97]. It is also possible that cells secrete Gal-9 associated with the surface of exosomes, which is a characteristic of cancer and viral immune responses[76,87]. I did not identify a role for Gal-9 during intrahepatic infection in this adenovirus model, but I hypothesize that the balance between negative Gal-9 signals and positive HMGB-1 signals directly and/or indirectly affects the antiviral $CD8^+$ T cell response in the liver microenvironment.

Multiple viruses and TLR ligands should be used to determine which cells are capable of excreting Gal-9 and HMGB-1 within the liver. A detailed kinetic analysis may further characterize which points in the antiviral immune response, early or late phase, these ligands are poised to bind Tim-3. Since detection of Tim-3 was limited to $CD8^+$ T cells in these experiments and the half-life of Gal-9 is short ranging from 30 to 60 min, perhaps early Gal-9 secretion is negligible in regulating later arising adaptive immune responses[191]. Nevertheless, Gal-9 secretion at later phases of adenovirus infection and chronic HCV infection is liable to bind Tim-3 on the surface of $CD8^+$ T cells, regulating their effector activity.

The series of experiments in this thesis work demonstrate that Tim-3 likely binds HMGB-1 on the surface of liver-primed $CD8^+$ T cells when Gal-9 is predicted to be present in the inflammatory milieu. As previously mentioned, the binding sites for Gal-9 and HMGB-1 are distally located on Tim-3 mucin and immunoglobulin variable regions, respectively, and simultaneous recognition of both ligands is possible. Currently, it is unknown what downstream signaling events unfold from separate or simultaneous recognition of Gal-9 and HMGB-1. *In vitro* and *in vivo* experiments performed here suggest that the $CD8^+$ T_{reg} cell suppression effect was a Gal-9-independent, HMGB-1-dependent mechanism.

However, since Gal-9 and HMGB-1 are both present during the course of HCV infection, the quality of the Tim-3 signal imparted on the intrahepatic $CD8^+$ T cells is unknown. Further, prior research is limited because the RMT3-23 clone of anti-Tim-3 antibody is effective at blocking both Gal-9 and HMGB-1 affinity for Tim-3[103,191]. Two types of investigations would be helpful to understand Tim-3 signaling: (1) qualitative studies on the immune response after anti-Gal-9 and anti-HMGB-1 antibody blockades and (2) an intricate subcellular study of the TCR organization with altered Gal-9 and HMGB-1 avidities for Tim-3.

In summary, the liver may control the development of different $CD8^+$ T cell populations based on the concentrations of Tim-3 ligands, or the initial properties of the Tim-3 signal may influence signal 1, the TCR, leading to permanent downstream effects propagated in the viral-specific $CD8^+$ T cells originating from a single clone. PD-1 signal strength has been shown to be associated with the formation of microclusters, which is blocked by anti-PD-L1 antibody treatment[197]. Tim-3 conformational changes are associated with Gal-9 binding, but nothing is known regarding how the molecular structure or plasma membrane organization of Tim-3 impacts the TCR[81]. If the kinetics of Gal-9 and HMGB-1 are established together with an understanding of how Tim-3 surface organization is orchestrated within T cells, these data may shed light on how downstream signals originate from Tim-3. Moreover, new approaches to manipulating T cells in responses to pathogens and disease may be uncovered.

Sequestration of HMGB-1 by $CD8^+$ T_{reg} Cells

Prior studies have disclosed that both TCR-stimulated $CD4^+$ and $CD8^+$ T_{eff} cells are capable of engulfing HMGB-1 within $RAGE^+$ endosomes[101]. RAGE ligation of HMGB-1

leads to downstream NF-κB signaling and the proliferative expansion of both $CD4^+$ and $CD8^+$ T_{eff} cells, but the signaling cascade has not been fully characterized[96,100,102]. My research established that liver-primed $CD8^+$ T_{reg} cells indeed engulfed HMGB-1, and HMGB-1 co-localized with surface Tim-3 and surface/intracellular RAGE. Given the $CD8^+$ T_{reg} cells were unable to proliferate (existing in a terminally differentiated dysfunctional state), the significance of this is unknown. Perhaps the sequestration of HMGB-1 within $CD8^+$ T_{reg} cells does not result in an intracellular signal because Helios expression and lack of *Il2* transcription override HMGB-1-mediated NF-κB nuclear mobilization. Tim-3 may also intrinsically divert HMGB-1 from RAGE binding and subsequent positive signals within $CD8^+$ T_{reg} cells. Experiments using *Rage*$^{-/-}$ $CD8^+$ T_{reg} cells could provide evidence for the importance of RAGE expression in the context of Tim-3 expression. Alternatively, *Havcr2*$^{-/-}$ (Tim-$3^{-/-}$) $CD8^+$ T_{reg} cells may retain the ability to proliferate because HMGB-1 access to RAGE on the surface and within intracellular vesicles may well be restored. Nonetheless, the concentration of HMGB-1, which was dictated by Tim-3^+CD8^+ T_{reg} cells, did have a negative impact on the clonal expansion of naïve/early primed Tim-3^-CD8^+ T_{eff} cells in my model system.

PD-1 and Tim-3 Synergy

Investigations of PD-1 and Tim-3 are incomplete and only represent two molecular pathways responsible for perpetuating T cell tolerance. The PD-1/PD-L1 interaction has been investigated vigorously, but researchers currently believe PD-1/PD-L1 synergizes with Tim-3 enabling exhaustion within tolerized $CD8^+$ T cells[91]. Further, virus-specific PD-1^+Tim-3^+CD8^+ T cells exist in a higher state of dysfunction compared to single-positive cells during chronic infection[82,88]. McMahan *et al.*, through direct *ex vivo*

analysis of HCV-specific $CD8^+$ T cells, have shown that both anti-PD-L1 and anti-Tim-3 antibodies improve proliferation, but only anti-Tim-3 antibody treatment improves cytotoxic potential. This group concludes that PD-1 and Tim-3 signals may be acting at different stages of T cell differentiation[89]. My research highlights that lymphocyte PD-1 and Tim-3 expression are indeed temporally regulated, and synergy does not exist in the function of $CD8^+$ T_{reg} cells. PD-L1 expression on other non-immune cells (such as KCs and LSECs) does however continue into the late phase of the intrahepatic antiviral immune response. It is possible that PD-1/PD-L1 signaling from these cellular interactions influences the strength of the Tim-3 negative signal or the ability of Tim-3 to sequester HMGB-1. It would be interesting to pursue a line of questions pertaining to global inhibitory receptor signaling interdependence *in vivo*. Clinicians have cited this as a primary concern since inventing drugs that boost the immune response (specifically antiviral/anticancer T cells) and fine tune the balance between inhibitory cascades will be a major healthcare challenge in patients with different genetic backgrounds[127]. Understanding how immunoregulatory networks lead to chronic liver disease is important, but identifying biological processes that enable tolerance is also essential for uncovering mechanisms underlying deregulated immunity to other unsolved diseases.

Implications for Immunotherapies

Approximately 600 million people worldwide are in danger of developing chronic liver disease due to HBV and HCV infections, and only a subset of these patients respond to IFN-α/ribavirin therapy[127]. The Joint United Nations Programme on HIV/AIDS estimated that 33.4 million people lived with HIV, 2.4 million infections occurred, and 2 million deaths took place in 2011[198]. The World Health Organization declared 219 million acute

illnesses and 660,000 deaths occurred annually regarding malaria as of 2010[199]. Studies of IL-10, PD-1/PD-L1 and Tim-3 control of immune tolerance not only translate to these infectious diseases but also are govern the pathophysiology associated with cancer, autoimmune disease (*e.g.* type-1 diabetes), alloimmunity, and heart disease.

Given early blockade of PD-1/PD-L1 signaling boosted the expansion of polyfunctional $CD8^+$ T cells and late application of anti-Tim-3 antibody inhibited the ability of $CD8^+$ T_{reg} cells to suppress $CD8^+$ T_{eff} cells responding to viral challenge, more research is needed to determine the role of each immunoregulatory pathway in improving either the initial $CD8^+$ T_{eff} cell response or delaying the development of $CD8^+$ T_{reg} cells. In addition, blockade of early IL-10 signaling during antigen presentation was not assessed in these experiments, but the application of STAT3 inhibitors with small molecules or direct blockade of IL-10 with anti-IL-10R antibody may have a similar consequence on the dichotomy existing between effectors and regulators within the $CD8^+$ T cell response[200]. For translation of effective immunotherapies in the clinic, the duration of signal output and cell source of IL-10, PD-L1, and the ligands of Tim-3 (Gal-9, HMGB-1, and phosphatidylserine) during the pathology of a specified disease needs to be determined. There is no clinical precedent for combinatorial blockades of multiple immunoregulatory pathways simultaneously; therefore, safety is a primary concern. Patient genetic variability in these signaling networks may lead to personalized medical approaches for establishing the proper treatment regimen to minimize side effects[127].

A major drawback to blocking immunoregulatory pathways is the development of unwarranted autoimmunity. This possibility is even more likely with combinatorial blockades, and the side effects vary with different immunoregulatory pathways. For

example, anti-CTLA-4 antibody clinical trials were accompanied with the onset of autoimmunity, whereas anti-PD-L1 antibodies yielded fewer side effects[134]. My dissertation offers a feasible alternative to nonspecific antibody blockade approaches through the use of *in vivo* delivery of targeted PD-L1 siRNA to the disease-causing cell type (*i.e.* KCs). I hypothesize that KCs are a potent source of IL-10, and a similar additive effect of PD-L1/IL-10 LNP may yield a synergistic improvement in the antiviral $CD8^+$ T cell response. Since the source of Tim-3 within the infected liver is largely the T cell, delivery may be more difficult in a gene therapy approach as these cells do not phagocytize materials. Other alternatives to siRNA silencing exist where Tim-3 siRNA may be tethered to an anti-CD8 antibody to mediate delivery to $CD8^+$ T cells[138]. On the other hand, the ligands, Gal-9 and HMGB-1, may be more easily silenced. KCs and other APCs may act as potent sources of these ligands due to active secretion, or necrotic hepatocytes may supply these ligands on secreted exosomes (Gal-9) or as soluble factors (Gal-9 and HMGB-1). More investigations are needed to identify the best therapeutic strategy in blocking the different inhibitory pathways. Even though *in vivo* application of siRNA is still in its infancy, this technology is promising as there is less inherent danger in augmenting immunopathological effects or creating autoimmune symptoms unrelated to the disease of interest.

Figure 6.1

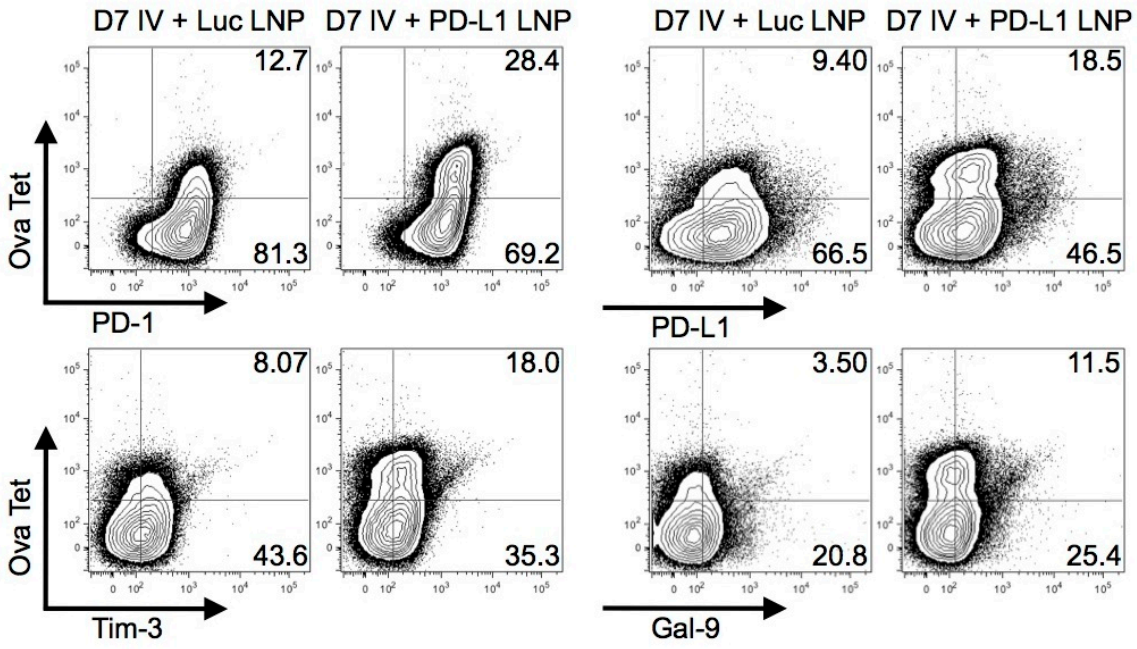
D7 IV + Luc LNP
D7 IV + PD-L1 LNP
D7 IV + Luc LNP
D7 IV + PD-L1 LNP
12.7
81.3
28.4
69.2
9.40
66.5
18.5
46.5
Ova Tet
PD-1
PD-L1
8.07
43.6
18.0
35.3
3.50
20.8
11.5
25.4
Ova Tet
Tim-3
Gal-9

Figure 6.1 PD-L1 LNP treatment does not alter PD-1/PD-L1 or Tim-3/Gal-9 expression on intrahepatic $CD8^+$ T cells. C57BL/6 mice were IV infected with 2.5×10^7 IU Ad-Ova and treated with Luc LNP or PD-L1 LNP at D5 post-infection. Expression of PD-1, PD-L1, Tim-3, and Gal-9 was determined directly *ex vivo* for Ova Tet^+ and Ova Tet^- populations of $CD8^+$ T cells at D7 post-infection (n = 3 per group). Numbers in the scatter plots represent percentages.

Figure 6.2

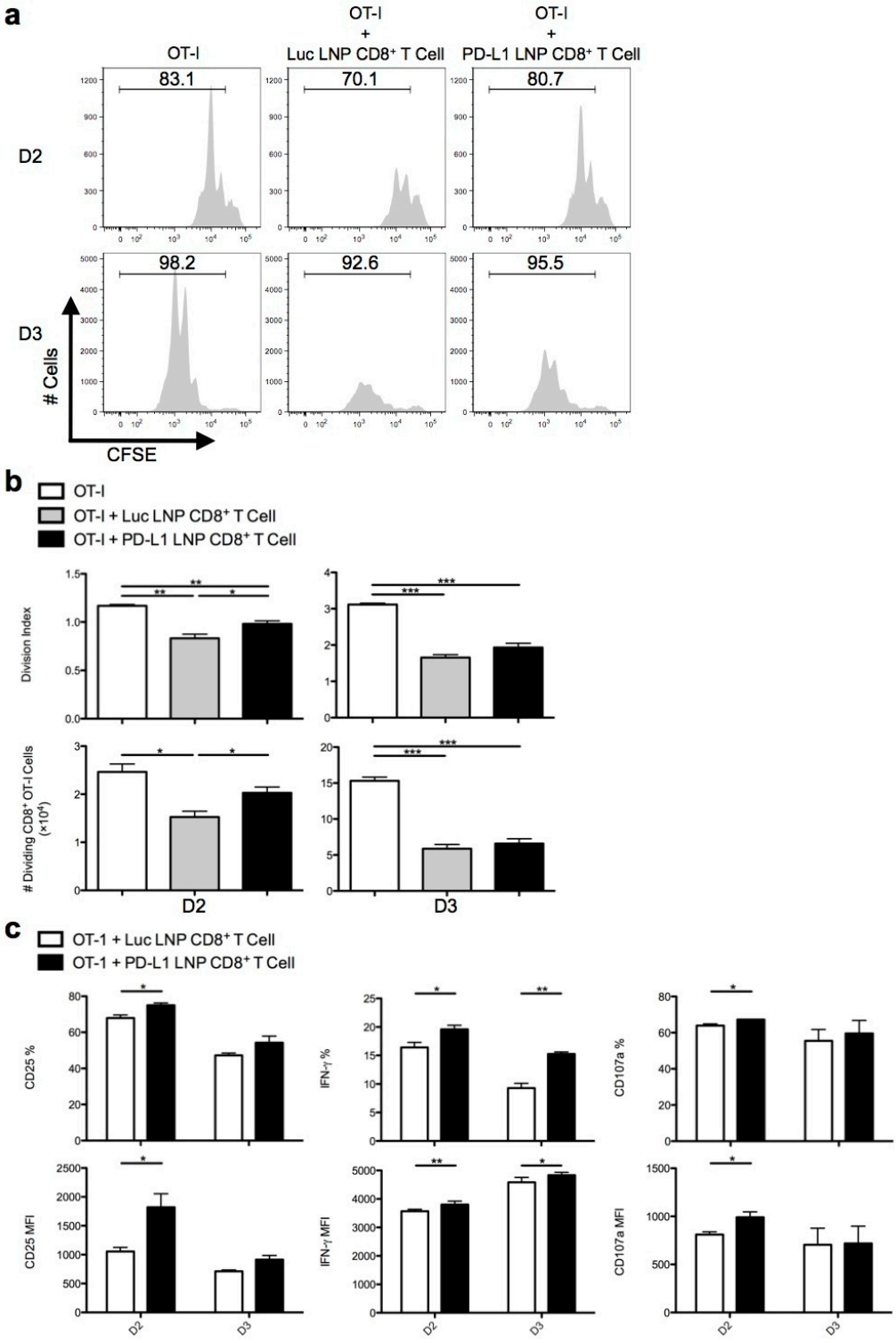
a
OT-I
OT-I + Luc LNP CD8+ T Cell
OT-I + PD-L1 LNP CD8+ T Cell
83.1
70.1
80.7
98.2
92.6
95.5
D2
D3
Cells
CFSE
b
OT-I
OT-I + Luc LNP CD8+ T Cell
OT-I + PD-L1 LNP CD8+ T Cell
Division Index
Dividing CD8+ OT-I Cells (×10⁴)
D2
D3
c
OT-1 + Luc LNP CD8+ T Cell
OT-1 + PD-L1 LNP CD8+ T Cell
CD25 %
IFN-γ %
CD107a %
CD25 MFI
IFN-γ MFI
CD107a MFI
D2
D3

Figure 6.2 PD-L1 LNP-treated $CD8^+$ T cells from the livers of IV infected animals are less effective at suppressing the activation and expansion of naïve $CD8^+$ OT-I T cells *in vitro*. C57BL/6 mice were IV infected with 2.5×10^7 IU Ad-Ova and treated with Luc LNP or PD-L1 LNP at D5 post-infection. (**a**) Bulk $CD8^+$ T cells were isolated from D7 IV livers then cultured with CFSE-labeled naïve $Thy1.1^+CD8^+$ OT-I T cells at a 1:1 ratio. SIINFEKL-pulsed BMDCs were used as the source of antigen, and co-cultures were analyzed at D3. (**b**) The number of dividing OT-I T cells and division index were calculated at D2 and D3 of culture. (**c**) CD25 expression was determined directly *ex vivo*, CD107a expression was ascertained after a 5 hr culture with GolgiStop + anti-CD107a Ab cocktail, and IFN-γ was quantified after a 5 hr re-stimulation with 2 μg/mL SIINFEKL peptide on D3 $Thy1.1^+CD8^+$ OT-I T cells (one-way ANOVA/Tukey's post test; n = 3 per group). Numbers in the histograms represent percentages. Mean ± s.e.m.; $^*P < 0.05$, $^{**}P < 0.01$, and $^{***}P < 0.001$.

Figure 6.3

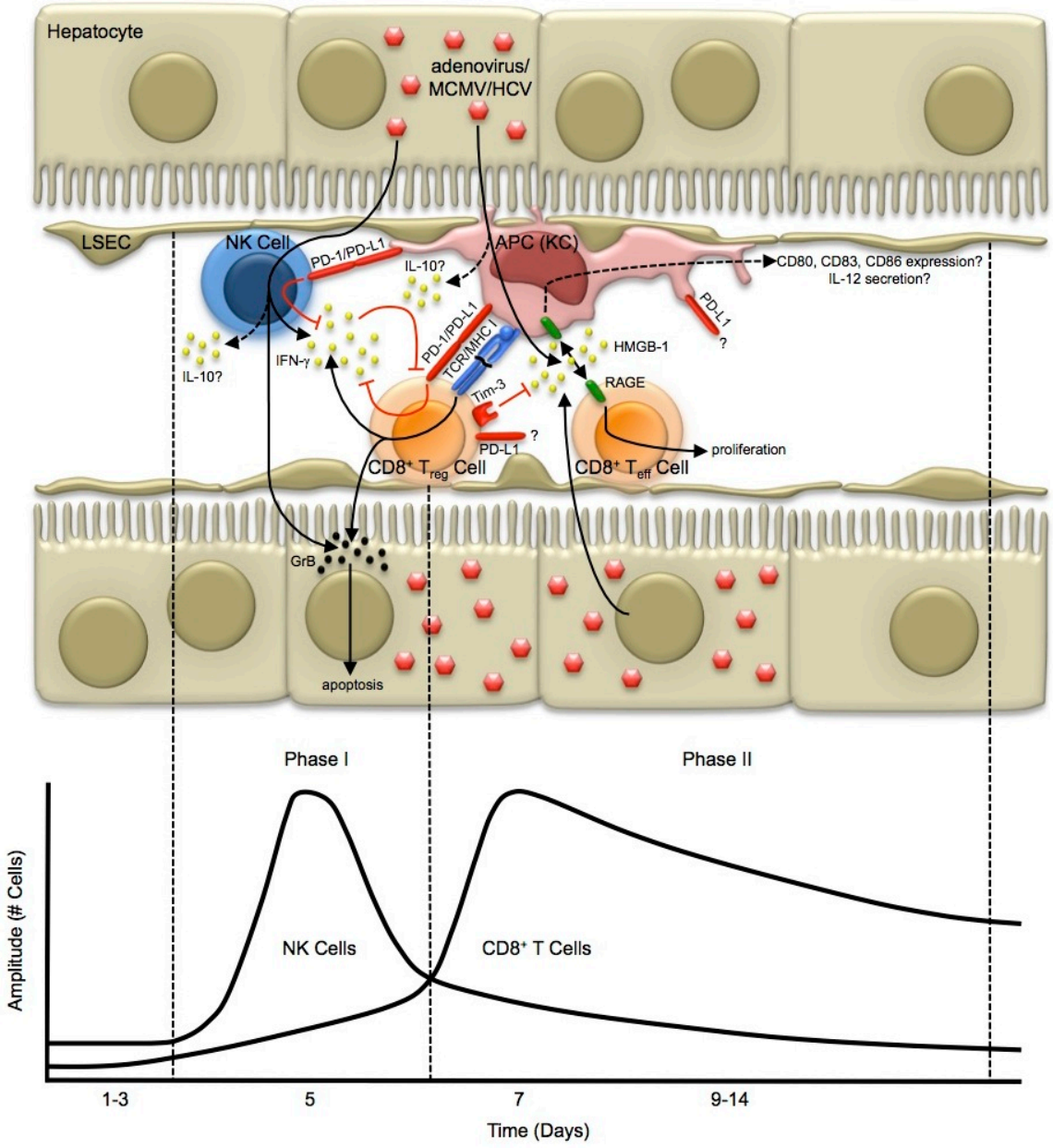
Hepatocyte
adenovirus/
MCMV/HCV
LSEC
NK Cell
PD-1/PD-L1
IL-10?
APC (KC)
CD80, CD83, CD86 expression?
IL-12 secretion?
PD-L1
?
IL-10?
IFN-γ
PD-1/PD-L1
TCR/MHC I
HMGB-1
Tim-3
RAGE
PD-L1
?
proliferation
CD8⁺ Treg Cell
CD8⁺ Teff Cell
GrB
apoptosis
Phase I
Phase II
Amplitude (# Cells)
NK Cells
CD8⁺ T Cells
1-3
5
7
9-14
Time (Days)

Figure 6.3 Model for immunosuppression during intrahepatic viral infection. The liver immune response can be divided into two phases: Phase I (early phase) characterized by a wave of NK cell expansion/infiltration and Phase II (late phase) where $CD8^+$ T cells proliferate robustly. Direct PD-1/PD-L1 interactions between KCs, NK cells, and $CD8^+$ T cells during the early phase inhibit the proliferation and effector function of both NK and $CD8^+$ T cells. Overexpansion of hyperresponsive NK cells (producing elevated IFN-γ) or hyporesponsive NK cells may negatively feedback on the $CD8^+$ T cell response if the PD-1/PD-L1 pathway is bypassed through anti-PD-L1 antibody blockade or targeted *Pdl1* silencing. The role for IL-10 production from KCs (or possibly immunoregulatory NK cells) during the early phase remains unknown. As the immune response progresses, the $CD8^+$ T_{eff} cells develop into $CD8^+$ T_{reg} cells, which is partially dependent on the early phase PD-1/PD-L1 interactions. The intrahepatic $CD8^+$ T_{reg} cells cannot proliferate, have a diminished IL-2 axis at the transcriptional level, and express Helios and GITR. PD-1/PD-L1 surface expression is maintained, and Tim-3 expression increases on the $CD8^+$ T_{reg} cells during the late phase. $CD8^+$ T_{reg} cell suppression of *de novo* naïve $CD8^+$ T cells is dependent on $CD8^+$ T_{reg} cell surface Tim-3-mediated sequestration of HMGB-1. HMGB-1 is an alarmin that acts as a growth factor for $CD8^+$ T cells and is likely secreted from virally activated APCs and necrosing hepatocytes. The role for late phase non-T cell PD-L1 is unknown, but $CD8^+$ T_{reg} cell PD-L1 does not contribute to suppression. Continued sequestration of HMGB-1 by $CD8^+$ T_{reg} cells may explain why acute HCV infection progresses into a chronic infection or why naïve and effector antiviral $CD8^+$ T cells remain tolerized in the chronic state.

Acknowledgments

I thank Alnylam Pharmaceuticals siRNA synthesis and formulation groups for providing PD-L1 siRNA and LNP nanoparticles. This project was in part formed through a collaboration initiated by Antonin de Fougerolles, and I am grateful for a pilot grant on behalf of Alnylam Pharmaceuticals. NIH Grants DK063222, U19 AI083024, and Immunology Training Fellowship T32 AI07496 supported this work.

Methods

Animals, Infections, and Treatments

Thy1.2$^{+/+}$ C57BL/6 mice were used in these series of experiments (Taconic Farms, Hudson, NY). *Thy1.1*$^{+/-}$ OT-I*(Tcra/Tcrb)*$^{+/-}$ mice were bred from *Thy1.1*$^{+/+}$ and OT-I*(Tcra/Tcrb)*$^{+/+}$*Rag1*^{tm1Mom} mice (Taconic Farms). Animals used were 6 to 10 weeks of age and housed in a pathogen-free facility under protocols approved by the Institutional Animal Care and Use Committee at the University of Virginia (Charlottesville, VA).

Replication-deficient type 5 adenovirus lacking the *E1* and *E3* genes and expressing the ovalbumin protein (Ad-Ova) under the control of the human *Cmv* promoter was provided by Timothy L. Ratliff (Iowa Gene Transfer Vector Core, University of Iowa, Iowa City, IA). Mice were infected with 2.5×10^7 infectious units (IU) Ad-Ova via intravenous (IV) injection in the caudal vein.

Mice were IV injected with 0.5 mg/kg LNP containing luciferase siRNA (Luc LNP) or PD-L1 siRNA (PD-L1 LNP) at day 5 relative to day 0 infection (Alnylam Pharmaceuticals, Cambridge, MA). Liver mononuclear cells were then collected, and $CD8^+$ T cells were isolated for use in *in vitro* suppression assays.

Liver Mononuclear Cell Isolation

Mononuclear cells were isolated from livers according to previous work[46,116,117]. Briefly, livers were flushed via the portal vein with 0.05% collagenase IV (Sigma-Aldrich, St. Louis, MO) in 1×PBS and washed with Iscove's Modified Dulbecco's Medium (IMDM) containing 10% newborn calf serum. Liver tissue was then homogenized and further digested with 0.05% collagenase IV in 1×PBS. Mononuclear cells were then isolated via

Histodenz (Sigma-Aldrich) gradient centrifugation, and the number of viable cells was determined based on 0.1% Trypan blue (Sigma-Aldrich) exclusion.

In vitro Suppression Assay

BMDCs were matured for one week in Roswell Park Memorial Institute (RPMI) Medium 1640 containing 10% HyClone fetal bovine serum, 15 mM HEPES Buffer, 50 μM βME, 20 ng/mL recombinant mouse IL-4 (rIL-4), and 20 ng/mL recombinant mouse GM-CSF (rGM-CSF) (eBioscience, San Diego, CA). 5×10^3 BMDCs were placed in each well of a 96-well round bottom plate, pulsed for 5 hrs with 10 ng/mL SIINFEKL or ICPMYARV peptides (AnaSpec, Fremont, CA), then cultured with 5×10^4 CFSE-labeled (Invitrogen, Carlsbad, CA) naïve Thy1.1$^+$CD8$^+$ OT-I T cells per reaction. CD8$^+$ T cells from SC or IV infected C57BL/6 mice were then added at the appropriate ratio. CD8$^+$ T cells were positively sorted using magnetic beads linked to anti-CD8α (Miltenyi Biotec, Auburn, CA) in all relevant experiments. βME was removed after peptide pulsing in a wash before T cell co-culture.

Flow Cytometry

The following mAbs were used for cell surface and intracellular staining: anti-CD25 APC (PC61) (BD Biosciences, Franklin Lakes, NJ), anti-Gal-9 PE (108A2) (BioLegend, San Diego, CA), anti-CD8α APC-eF780 (53-6.7), anti-CD107a eF660 (1D4B), anti-IFN-γ APC (XMG1.2), anti-PD-1 PE (J43), anti-PD-L1 PE (M1H5), anti-Thy1.2 eF450 (53-2.1), and anti-Tim-3 PE (RMT3-23) (eBioscience). H2-K^b Ova-tetramer (SIINFEKL) APC (MHC Tetramer Core Laboratory, Baylor College of Medicine, Houston, TX) was used to identify Ova-specific CD8$^+$ T cells. Cell surface staining of 1.5×10^6 mononuclear cells was performed by first blocking with anti-CD16/CD32 (2.4G2) (Lymphocyte Culture

Center, University of Virginia, Charlottesville, VA) followed by specific antibody labeling for 15 min at 4°C in FACS Buffer (1×PBS containing 2% fetal bovine serum and 0.1% NaN_3). Cells were fixed in BD Cytofix/Cytoperm (BD Biosciences). CD107a expression was assessed after a 5 hr culture with GolgiStop (BD Biosciences) + anti-CD107a Ab cocktail. For intracellular cytokine detection, cells were re-stimulated with 2 μg/mL SIINFEKL peptide (AnaSpec), blocked with 1 μL/mL GolgiPlug and 1 μL/mL GolgiStop, and permeabilized with BD Perm/Wash (BD Biosciences). Data were collected on a BD FACS Canto II (BD Immunocytometry Systems, San Jose, CA) and analyzed using FlowJo 8.8.6 software (Tree Star Inc., Ashland, OR).

Statistical Analysis

Significant differences between experimental groups were calculated using the two-tailed Student's t test or one-way ANOVA (with group comparisons ≥ 3). Data analysis was performed using Prism 5.0a software (GraphPad Software Inc., La Jolla, CA). Values of $P < 0.05$ were regarded as being statistically significant and noted as * < 0.05, ** < 0.01, and *** < 0.001.

References

1. Arrese, M. The liver in poetry: Neruda's “Ode to the Liver”. *Liver International* **28,** 901–905 (2008).
2. Rhodin, J. A. G. *Histology*. (1974).
3. Fawcett, D. W. & Bloom, W. *A textbook of histology*. (W.B. Saunders Company, 1986).
4. Ross, M. H., Romrell, L. J. & Kaye, G. I. *Histology*. (Lippincott Williams & Wilkins, 1995).
5. Cross, P. C. & Mercer, K. L. *Cell and Tissue Ultrastructure*. (W. H. Freeman, 1993).
6. Lehninger, A. L. *Lehninger Principles of Biochemistry*. (W H Freeman & Company, 2008).
7. Khan, B., Wilcox, H. G. & Heimberg, M. Cholesterol is required for secretion of very-low-density lipoprotein by rat liver. *Biochem. J.* **258,** 807–816 (1989).
8. Weiss, L. *Histology*. (North-Holland, 1983).
9. Young, B., Lowe, J. S., Stevens, A., Heath, J. W. & Deakin, P. J. *Wheater's Functional Histology*. (Churchill Livingstone, 2006).
10. Warren, A. *et al.* T lymphocytes interact with hepatocytes through fenestrations in murine liver sinusoidal endothelial cells. *Hepatology* **44,** 1182–1190 (2006).
11. Stains, C. U. S. Special Stains in Interpretation of Liver Biopsies. *Connection* 92 (2010).
12. Pappas, P. W. The use of a chrome alum-gelatin (subbing) solution as a general adhesive for paraffin sections. *Stain Technol* **46,** 121–124 (1971).

13. Calne, R. Y. *et al.* Induction of immunological tolerance by porcine liver allografts. *Nature* **223,** 472–476 (1969).

14. Crispe, I. N. *et al.* Cellular and molecular mechanisms of liver tolerance. *Immunol Rev* **213,** 101–118 (2006).

15. You, Q., Cheng, L., Kedl, R. M. & Ju, C. Mechanism of T cell tolerance induction by murine hepatic Kupffer cells. *Hepatology* **48,** 978–990 (2008).

16. Sriwatanawongsa, V., Davies, H. S. & Calne, R. Y. The essential roles of parenchymal tissues and passenger leukocytes in the tolerance induced by liver grafting in rats. *Nat Med* **1,** 428–432 (1995).

17. Breous, E., Somanathan, S., Vandenberghe, L. H. & Wilson, J. M. Hepatic regulatory T cells and Kupffer cells are crucial mediators of systemic T cell tolerance to antigens targeting murine liver. *Hepatology* **50,** 612–621 (2009).

18. Crispe, I. N. Hepatic T cells and liver tolerance. *Nat Rev Immunol* **3,** 51–62 (2003).

19. Crispe, I. N. The Liver as a Lymphoid Organ. *Annu Rev Immunol* **27,** 147–163 (2009).

20. Kern, M., Popov, A., Kurts, C., Schultze, J. L. & Knolle, P. A. Taking off the brakes: T cell immunity in the liver. *Trends Immunol* **31,** 311–317 (2010).

21. Bowen, D. G. The site of primary T cell activation is a determinant of the balance between intrahepatic tolerance and immunity. *Journal of Clinical Investigation* **114,** 701–712 (2004).

22. Klein, I. Complete differentiation of CD8+ T cells activated locally within the transplanted liver. *Journal of Experimental Medicine* **203,** 437–447 (2006).

23. Tiegs, G. & Lohse, A. W. Immune tolerance: What is unique about the liver. *Journal of Autoimmunity* **34,** 1–6 (2010).

24. Shin, H. & Wherry, E. J. CD8 T cell dysfunction during chronic viral infection. *Curr Opin Immunol* **19,** 408–415 (2007).

25. Wherry, E. J., Blattman, J. N., Murali-Krishna, K., van der Most, R. & Ahmed, R. Viral persistence alters CD8 T-cell immunodominance and tissue distribution and results in distinct stages of functional impairment. *Journal of Virology* **77,** 4911–4927 (2003).

26. Ghosh, S. S., Gopinath, P. & Ramesh, A. Adenoviral vectors: a promising tool for gene therapy. *Appl Biochem Biotechnol* **133,** 9–29 (2006).

27. Zaiss, A. K., Machado, H. B. & Herschman, H. R. The influence of innate and pre-existing immunity on adenovirus therapy. *J. Cell. Biochem.* **108,** 778–790 (2009).

28. Krebs, P., Scandella, E., Odermatt, B. & Ludewig, B. Rapid functional exhaustion and deletion of CTL following immunization with recombinant adenovirus. *J Immunol* **174,** 4559–4566 (2005).

29. Pipkin, M. E. *et al.* Interleukin-2 and Inflammation Induce Distinct Transcriptional Programs that Promote the Differentiation of Effector Cytolytic T Cells. *Immunity* 1–12 (2010). doi:10.1016/j.immuni.2009.11.012

30. Su, H. C. *et al.* CD4+ and CD8+ T cell interactions in IFN-gamma and IL-4 responses to viral infections: requirements for IL-2. *J Immunol* **160,** 5007–5017 (1998).

31. Rehermann, B. & Nascimbeni, M. Immunology of hepatitis B virus and hepatitis C virus infection. *Nat Rev Immunol* **5,** 215–229 (2005).

32. Neumann-Haefelin, C., Blum, H. E., Chisari, F. V. & Thimme, R. T cell response in hepatitis C virus infection. *J Clin Virol* **32,** 75–85 (2005).

33. Fried, M. W. *et al.* Improved outcomes in patients with hepatitis C with difficult-to-treat characteristics: randomized study of higher doses of peginterferon alpha-2a and ribavirin. *Hepatology* **48,** 1033–1043 (2008).

34. Large, M. K., Kittlesen, D. J. & Hahn, Y. S. Suppression of host immune response by the core protein of hepatitis C virus: possible implications for hepatitis C virus persistence. *J Immunol* **162,** 931–938 (1999).

35. Santolini, E., Migliaccio, G. & La Monica, N. Biosynthesis and biochemical properties of the hepatitis C virus core protein. *Journal of Virology* **68,** 3631–3641 (1994).

36. Chen, C. M., You, L. R., Hwang, L. H. & Lee, Y. H. Direct interaction of hepatitis C virus core protein with the cellular lymphotoxin-beta receptor modulates the signal pathway of the lymphotoxin-beta receptor. *Journal of Virology* **71,** 9417–9426 (1997).

37. Matsumoto, M. *et al.* Hepatitis C virus core protein interacts with the cytoplasmic tail of lymphotoxin-beta receptor. *Journal of Virology* **71,** 1301–1309 (1997).

38. Zhu, N. *et al.* Hepatitis C virus core protein binds to the cytoplasmic domain of tumor necrosis factor (TNF) receptor 1 and enhances TNF-induced apoptosis. *Journal of Virology* **72,** 3691–3697 (1998).

39. Hahn, C. S., Cho, Y. G., Kang, B. S., Lester, I. M. & Hahn, Y. S. The HCV core protein acts as a positive regulator of fas-mediated apoptosis in a human lymphoblastoid T cell line. *Virology* **276,** 127–137 (2000).

40. Bode, J. G. *et al.* IFN-alpha antagonistic activity of HCV core protein involves induction of suppressor of cytokine signaling-3. *FASEB J* **17,** 488–490 (2003).

41. Melén, K., Fagerlund, R., Nyqvist, M., Keskinen, P. & Julkunen, I. Expression of hepatitis C virus core protein inhibits interferon-induced nuclear import of STATs. *J. Med. Virol.* **73,** 536–547 (2004).

42. Widell, A. *et al.* Detection of hepatitis C core antigen in serum or plasma as a marker of hepatitis C viraemia in the serological window-phase. *Transfus Med* **12,** 107–113 (2002).

43. Yao, Z. Q., Nguyen, D. T., Hiotellis, A. I. & Hahn, Y. S. Hepatitis C virus core protein inhibits human T lymphocyte responses by a complement-dependent regulatory pathway. *J Immunol* **167,** 5264–5272 (2001).

44. Yao, Z. Q., Ray, S., Eisen-Vandervelde, A., Waggoner, S. & Hahn, Y. S. Hepatitis C virus: immunosuppression by complement regulatory pathway. *Viral Immunol* **14,** 277–295 (2001).

45. Yao, Z. Q., Eisen-Vandervelde, A., Ray, S. & Hahn, Y. S. HCV core/gC1qR interaction arrests T cell cycle progression through stabilization of the cell cycle inhibitor p27Kip1. *Virology* **314,** 271–282 (2003).

46. Lukens, J. R., Cruise, M. W., Lassen, M. G. & Hahn, Y. S. Blockade of PD-1/B7-H1 interaction restores effector CD8+ T cell responses in a hepatitis C virus core murine model. *J Immunol* **180,** 4875–4884 (2008).

47. Soguero, C. *et al.* Hepatitis C virus core protein leads to immune suppression and liver damage in a transgenic murine model. *Journal of Virology* **76,** 9345–9354 (2002).

48. Lutz, M. B. & Schuler, G. Immature, semi-mature and fully mature dendritic cells: which signals induce tolerance or immunity? *Trends Immunol* **23,** 445–449 (2002).

49. Couper, K. N., Blount, D. G. & Riley, E. M. IL-10: the master regulator of immunity to infection. *J Immunol* **180,** 5771–5777 (2008).

50. Kuwata, H. *et al.* IL-10-inducible Bcl-3 negatively regulates LPS-induced TNF-alpha production in macrophages. *Blood* **102,** 4123–4129 (2003).

51. Lang, R., Patel, D., Morris, J. J., Rutschman, R. L. & Murray, P. J. Shaping gene expression in activated and resting primary macrophages by IL-10. *J Immunol* **169,** 2253–2263 (2002).

52. Kaplan, D. E. *et al.* Peripheral virus-specific T-cell interleukin-10 responses develop early in acute hepatitis C infection and become dominant in chronic hepatitis. *J Hepatol* **48,** 903–913 (2008).

53. Abel, M. *et al.* Intrahepatic virus-specific IL-10-producing CD8 T cells prevent liver damage during chronic hepatitis C virus infection. *Hepatology* **44,** 1607–1616 (2006).

54. Accapezzato, D. *et al.* Hepatic expansion of a virus-specific regulatory CD8(+) T cell population in chronic hepatitis C virus infection. *Journal of Clinical Investigation* **113,** 963–972 (2004).

55. Maris, C. H., Chappell, C. P. & Jacob, J. Interleukin-10 plays an early role in generating virus-specific T cell anergy. *BMC Immunol* **8,** 8 (2007).

56. Filippi, C. M. & Herrath, von, M. G. IL-10 and the resolution of infections. *J Pathol* **214,** 224–230 (2008).

57. Hsu, W., Shu, S.-A., Gershwin, E. & Lian, Z.-X. The current immune function of hepatic dendritic cells. *Cell Mol Immunol* **4,** 321–328 (2007).

58. Brooks, D. G. *et al.* Interleukin-10 determines viral clearance or persistence in vivo. *Nat Med* **12,** 1301–1309 (2006).

59. Ejrnaes, M. *et al.* Resolution of a chronic viral infection after interleukin-10 receptor blockade. *J Exp Med* **203,** 2461–2472 (2006).

60. Oestreich, K. J., Yoon, H., Ahmed, R. & Boss, J. M. NFATc1 regulates PD-1 expression upon T cell activation. *The Journal of Immunology* **181,** 4832–4839 (2008).

61. Okazaki, T. & Honjo, T. PD-1 and PD-1 ligands: from discovery to clinical application. *International Immunology* **19,** 813–824 (2007).

62. Crawford, A. & Wherry, E. J. Inhibitory receptors: whose side are they on? *Nat Immunol* **8,** 1201–1203 (2007).

63. Dong, H., Zhu, G., Tamada, K. & Chen, L. B7-H1, a third member of the B7 family, co-stimulates T-cell proliferation and interleukin-10 secretion. *Nat Med* **5,** 1365–1369 (1999).

64. Freeman, G. J. *et al.* Engagement of the PD-1 immunoinhibitory receptor by a novel B7 family member leads to negative regulation of lymphocyte activation. *J Exp Med* **192,** 1027–1034 (2000).

65. Iwai, Y., Terawaki, S., Ikegawa, M., Okazaki, T. & Honjo, T. PD-1 inhibits antiviral immunity at the effector phase in the liver. *J Exp Med* **198,** 39–50 (2003).

66. Latchman, Y. *et al.* PD-L2 is a second ligand for PD-1 and inhibits T cell activation. *Nat Immunol* **2,** 261–268 (2001).

67. Loke, P. & Allison, J. P. PD-L1 and PD-L2 are differentially regulated by Th1 and Th2 cells. *Proc Natl Acad Sci USA* **100,** 5336–5341 (2003).

68. Tseng, S. Y. *et al.* B7-DC, a new dendritic cell molecule with potent costimulatory properties for T cells. *J Exp Med* **193,** 839–846 (2001).

69. Wang, S. *et al.* Molecular modeling and functional mapping of B7-H1 and B7-DC uncouple costimulatory function from PD-1 interaction. *J Exp Med* **197,** 1083–1091 (2003).

70. Chen, L. *et al.* B7-H1 up-regulation on myeloid dendritic cells significantly suppresses T cell immune function in patients with chronic hepatitis B. *J Immunol* **178,** 6634–6641 (2007).

71. Urbani, S. *et al.* PD-1 expression in acute hepatitis C virus (HCV) infection is associated with HCV-specific CD8 exhaustion. *Journal of Virology* **80,** 11398–11403 (2006).

72. Barber, D. L. *et al.* Restoring function in exhausted CD8 T cells during chronic viral infection. *Nature* **439,** 682–687 (2006).

73. Diehl, L. *et al.* Tolerogenic maturation of liver sinusoidal endothelial cells promotes B7-homolog 1-dependent CD8+ T cell tolerance. *Hepatology* **47,** 296–305 (2008).

74. Carter, L. *et al.* PD-1:PD-L inhibitory pathway affects both CD4(+) and CD8(+) T cells and is overcome by IL-2. *Eur J Immunol* **32,** 634–643 (2002).

75. Chikuma, S. *et al.* PD-1-mediated suppression of IL-2 production induces CD8+ T cell anergy in vivo. *The Journal of Immunology* **182,** 6682–6689 (2009).

76. Freeman, G. J., Casasnovas, J. M., Umetsu, D. T. & DeKruyff, R. H. TIM genes: a family of cell surface phosphatidylserine receptors that regulate innate and adaptive immunity. *Immunol Rev* **235,** 172–189 (2010).

77. Rodriguez-Manzanet, R., DeKruyff, R., Kuchroo, V. K. & Umetsu, D. T. The costimulatory role of TIM molecules. *Immunol Rev* **229,** 259–270 (2009).

78. Sakuishi, K., Jayaraman, P., Behar, S. M., Anderson, A. C. & Kuchroo, V. K. Emerging Tim-3 functions in antimicrobial and tumor immunity. *Trends Immunol* **32,** 345–349 (2011).

79. Cao, E. *et al.* T Cell Immunoglobulin Mucin-3 Crystal Structure Reveals a Galectin-9-Independent Ligand-Binding Surface. *Immunity* **26,** 311–321 (2007).

80. Sánchez-Fueyo, A. *et al.* Tim-3 inhibits T helper type 1–mediated auto- and alloimmune responses and promotes immunological tolerance. *Nat Immunol* **4,** 1093–1101 (2003).

81. Rangachari, M. *et al.* Bat3 promotes T cell responses and autoimmunity by repressing Tim-3–mediated cell death and exhaustion. *Nat Med* **18,** 1394–1400 (2012).

82. Golden-Mason, L. *et al.* Negative Immune Regulator Tim-3 Is Overexpressed on T Cells in Hepatitis C Virus Infection and Its Blockade Rescues Dysfunctional CD4+ and CD8+ T Cells. *Journal of Virology* **83,** 9122–9130 (2009).

83. Sehrawat, S., Suryawanshi, A., Hirashima, M. & Rouse, B. T. Role of Tim-3/Galectin-9 Inhibitory Interaction in Viral-Induced Immunopathology: Shifting the Balance toward Regulators. *The Journal of Immunology* **182,** 3191–3201 (2009).

84. Seki, M. *et al.* Galectin-9 suppresses the generation of Th17, promotes the induction of regulatory T cells, and regulates experimental autoimmune arthritis. *Clinical Immunology* **127,** 78–88 (2008).

85. Moorman, J. P. *et al.* Tim-3 Pathway Controls Regulatory and Effector T Cell Balance during Hepatitis C Virus Infection. *The Journal of Immunology* (2012). doi:10.4049/jimmunol.1200162

86. Cedeno-Laurent, F. & Dimitroff, C. J. Galectins and their ligands: negative regulators of anti-tumor immunity. *Glycoconj J* **29,** 619–625 (2012).

87. Klibi, J. *et al.* Blood diffusion and Th1-suppressive effects of galectin-9-containing exosomes released by Epstein-Barr virus-infected nasopharyngeal carcinoma cells. *Blood* **113,** 1957–1966 (2009).

88. Jin, H.-T. *et al.* Cooperation of Tim-3 and PD-1 in CD8 T-cell exhaustion during chronic viral infection. *Proc Natl Acad Sci USA* **107,** 14733–14738 (2010).

89. McMahan, R. H. *et al.* Tim-3 expression on PD-1+ HCV-specific human CTLs is associated with viral persistence, and its blockade restores hepatocyte-directed in vitro cytotoxicity. *Journal of Clinical Investigation* **120,** 4546–4557 (2010).

90. Sakuishi, K. *et al.* Targeting Tim-3 and PD-1 pathways to reverse T cell exhaustion and restore anti-tumor immunity. *Journal of Experimental Medicine* **207,** 2187–2194 (2010).

91. Fourcade, J. *et al.* Upregulation of Tim-3 and PD-1 expression is associated with tumor antigen-specific CD8+ T cell dysfunction in melanoma patients. *Journal of Experimental Medicine* **207,** 2175–2186 (2010).

92. Tang, D. & Lotze, M. T. Tumor immunity times out: TIM-3 and HMGB1. *Nature Publishing Group* **13,** 808–810 (2012).

93. Lotze, M. T. & Tracey, K. J. High-mobility group box 1 protein (HMGB1): nuclear weapon in the immune arsenal. *Nat Rev Immunol* **5,** 331–342 (2005).

94. Jung, J. H. *et al.* Hepatitis C Virus Infection Is Blocked by HMGB1 Released from Virus-Infected Cells. *Journal of Virology* **85,** 9359–9368 (2011).

95. Klune, J. & Dhupar, R. HMGB1: Endogenous Danger Signaling. *Mol. Med.* **14,** 1 (2008).

96. Riehl, A., Németh, J., Angel, P. & Hess, J. The receptor RAGE: Bridging inflammation and cancer. *Cell Commun Signal* **7,** 12 (2009).

97. Dumitriu, I. E. *et al.* Release of high mobility group box 1 by dendritic cells controls T cell activation via the receptor for advanced glycation end products. *J Immunol* **174,** 7506–7515 (2005).

98. Li, G., Liang, X. & Lotze, M. T. HMGB1: The Central Cytokine for All Lymphoid Cells. *Front Immunol* **4,** 68 (2013).

99. Moser, B. *et al.* Blockade of RAGE Suppresses Alloimmune Reactions In Vitro and Delays Allograft Rejection in Murine Heart Transplantation. *Am J Transplant* **7,** 293–302 (2007).

100. Moser, B. *et al.* Receptor for advanced glycation end products expression on T cells contributes to antigen-specific cellular expansion in vivo. *J Immunol* **179,** 8051–8058 (2007).

101. Akirav, E. M. *et al.* RAGE Expression in Human T Cells: A Link between Environmental Factors and Adaptive Immune Responses. *PLoS ONE* **7,** e34698 (2012).

102. Sundberg, E., Fasth, A. E. R., Palmblad, K., Harris, H. E. & Andersson, U. High mobility group box chromosomal protein 1 acts as a proliferation signal for activated T lymphocytes. *Immunobiology* **214,** 303–309 (2009).

103. Chiba, S. *et al.* Tumor-infiltrating DCs suppress nucleic acid–mediated innate immune responses through interactions between the receptor TIM-3 and the alarmin HMGB1. *Nature Publishing Group* **13,** 832–842 (2012).

104. Liu, Z., Falo, L. D. & You, Z. Knockdown of HMGB1 in Tumor Cells Attenuates Their Ability To Induce Regulatory T Cells and Uncovers Naturally Acquired CD8 T Cell-Dependent Antitumor Immunity. *The Journal of Immunology* **187,** 118–125 (2011).

105. Norris, S. *et al.* Resident human hepatic lymphocytes are phenotypically different from circulating lymphocytes. *J Hepatol* **28,** 84–90 (1998).

106. Wuensch, S. A., Spahn, J. & Crispe, I. N. Direct, help-independent priming of CD8+ T cells by adeno-associated virus-transduced hepatocytes. *Hepatology* **52,** 1068–1077 (2010).

107. Johnson, S. *et al.* Selected Toll-like receptor ligands and viruses promote helper-independent cytotoxic T cell priming by upregulating CD40L on dendritic cells. *Immunity* **30,** 218–227 (2009).

108. Brooks, D. G., Teyton, L., Oldstone, M. B. A. & Mcgavern, D. B. Intrinsic functional dysregulation of CD4 T cells occurs rapidly following persistent viral infection. *Journal of Virology* **79,** 10514–10527 (2005).

109. Xiong, Y. *et al.* Simian immunodeficiency virus (SIV) infection of a rhesus macaque induces SIV-specific CD8(+) T cells with a defect in effector function that is reversible on extended interleukin-2 incubation. *Journal of Virology* **75,** 3028–3033 (2001).

110. Groux, H., Bigler, M., de Vries, J. E. & Roncarolo, M. G. Interleukin-10 induces a long-term antigen-specific anergic state in human CD4+ T cells. *J Exp Med* **184,** 19–29 (1996).

111. Zajac, A. J. *et al.* Viral immune evasion due to persistence of activated T cells without effector function. *J Exp Med* **188,** 2205–2213 (1998).

112. Accapezzato, D. *et al.* Subversion of effector CD8+ T cell differentiation in acute hepatitis C virus infection: the role of the virus. *Eur J Immunol* **34,** 438–446 (2004).

113. Boyman, O., Kovar, M., Rubinstein, M. P., Surh, C. D. & Sprent, J. Selective stimulation of T cell subsets with antibody-cytokine immune complexes. *Science* **311,** 1924–1927 (2006).

114. Molloy, M. J., Zhang, W. & Usherwood, E. J. Cutting edge: IL-2 immune complexes as a therapy for persistent virus infection. *The Journal of Immunology* **182,** 4512–4515 (2009).

115. Williams, M. A., Tyznik, A. J. & Bevan, M. J. Interleukin-2 signals during priming are required for secondary expansion of CD8+ memory T cells. *Nature* **441,** 890–893 (2006).

116. Lukens, J. R., Dolina, J. S., Kim, T. S., Tacke, R. S. & Hahn, Y. S. Liver is able to activate naïve CD8+ T cells with dysfunctional anti-viral activity in the murine system. *PLoS ONE* **4,** e7619 (2009).

117. Lassen, M. G., Lukens, J. R., Dolina, J. S., Brown, M. G. & Hahn, Y. S. Intrahepatic IL-10 maintains NKG2A+Ly49- liver NK cells in a functionally hyporesponsive state. *The Journal of Immunology* **184,** 2693–2701 (2010).

118. Coles, R. M., Mueller, S. N., Heath, W. R., Carbone, F. R. & Brooks, A. G. Progression of armed CTL from draining lymph node to spleen shortly after localized infection with herpes simplex virus 1. *J Immunol* **168,** 834–838 (2002).

119. Folkl, A. & Bienzle, D. Structure and function of programmed death (PD) molecules. *Veterinary Immunology and Immunopathology* **134,** 33–38 (2010).

120. Fife, B. T. *et al.* Interactions between PD-1 and PD-L1 promote tolerance by blocking the TCR-induced stop signal. *Nat Immunol* **10,** 1185–1192 (2009).

121. Krueger, P. D., Lassen, M. G., Qiao, H. & Hahn, Y. S. Regulation of NK cell repertoire and function in the liver. *Crit. Rev. Immunol.* **31,** 43–52 (2011).

122. Benson, D. M. *et al.* The PD-1/PD-L1 axis modulates the natural killer cell versus multiple myeloma effect: a therapeutic target for CT-011, a novel monoclonal anti-PD-1 antibody. *Blood* **116,** 2286–2294 (2010).

123. Alvarez, I. B. *et al.* Role Played by the Programmed Death-1–Programmed Death Ligand Pathway during Innate Immunity against Mycobacterium tuberculosis. *J INFECT DIS* **202,** 524–532 (2010).

124. Narni-Mancinelli, E. *et al.* Tuning of Natural Killer Cell Reactivity by NKp46 and Helios Calibrates T Cell Responses. *Science* **335,** 344–348 (2012).

125. Wu, K., Kryczek, I., Chen, L., Zou, W. & Welling, T. H. Kupffer cell suppression of CD8+ T cells in human hepatocellular carcinoma is mediated by B7-H1/programmed death-1 interactions. *Cancer Research* **69,** 8067–8075 (2009).

126. Golden-Mason, L., Klarquist, J., Wahed, A. S. & Rosen, H. R. Cutting edge: programmed death-1 expression is increased on immunocytes in chronic hepatitis C virus and predicts failure of response to antiviral therapy: race-dependent differences. *J Immunol* **180,** 3637–3641 (2008).

127. Callendret, B. & Walker, C. A siege of hepatitis: Immune boost for viral hepatitis. *Nat Med* **17,** 252–253 (2011).

128. Keir, M. E., Freeman, G. J. & Sharpe, A. H. PD-1 regulates self-reactive CD8+ T cell responses to antigen in lymph nodes and tissues. *J Immunol* **179,** 5064–5070 (2007).

129. Dong, H. *et al.* B7-H1 determines accumulation and deletion of intrahepatic CD8(+) T lymphocytes. *Immunity* **20,** 327–336 (2004).

130. Ishida, Y., Agata, Y., Shibahara, K. & Honjo, T. Induced expression of PD-1, a novel member of the immunoglobulin gene superfamily, upon programmed cell death. *EMBO J.* **11,** 3887–3895 (1992).

131. Chen, Y. *et al.* Programmed Death (PD)-1-Deficient Mice Are Extremely Sensitive to Murine Hepatitis Virus Strain-3 (MHV-3) Infection. *PLoS Pathog* **7,** e1001347 (2011).

132. Okazaki, T. & Honjo, T. The PD-1–PD-L pathway in immunological tolerance. *Trends Immunol* **27,** 195–201 (2006).

133. Zou, W. & Chen, L. Inhibitory B7-family molecules in the tumour microenvironment. *Nat Rev Immunol* **8,** 467–477 (2008).

134. Melero, I., Hervas-Stubbs, S., Glennie, M., Pardoll, D. M. & Chen, L. Immunostimulatory monoclonal antibodies for cancer therapy. *Nat Rev Cancer* **7,** 95–106 (2007).

135. Fire, A. *et al.* Potent and specific genetic interference by double-stranded RNA in Caenorhabditis elegans. *Nature* **391,** 806–811 (1998).

136. Meade, B. R. & Dowdy, S. F. The road to therapeutic RNA interference (RNAi): Tackling the 800 pound siRNA delivery gorilla. *Discov Med* **8,** 253–256 (2009).

137. Novina, C. D. & Sharp, P. A. The RNAi revolution. *Nature* **430,** 161–164 (2004).

138. de Fougerolles, A., Vornlocher, H.-P., Maraganore, J. & Lieberman, J. Interfering with disease: a progress report on siRNA-based therapeutics. *Nat Rev Drug Discov* **6,** 443–453 (2007).

139. Hobo, W. *et al.* siRNA silencing of PD-L1 and PD-L2 on dendritic cells augments expansion and function of minor histocompatibility antigen-specific CD8+ T cells. *Blood* **116,** 4501–4511 (2010).

140. Bumcrot, D., Manoharan, M., Koteliansky, V. & Sah, D. W. Y. RNAi therapeutics: a potential new class of pharmaceutical drugs. *Nat. Chem. Biol.* **2,** 711–719 (2006).

141. Love, K. T. *et al.* Lipid-like materials for low-dose, in vivo gene silencing. *Proc Natl Acad Sci USA* **107,** 1864–1869 (2010).

142. Novobrantseva, T. I. *et al.* Systemic RNAi-mediated Gene Silencing in Nonhuman Primate and Rodent Myeloid Cells. *Mol Ther Nucleic Acids* **1,** e4 (2012).

143. Wahl, C., Bochtler, P., Chen, L., Schirmbeck, R. & Reimann, J. B7-H1 on hepatocytes facilitates priming of specific CD8 T cells but limits the specific recall of primed responses. *Gastroenterology* **135,** 980–988 (2008).

144. Kassel, R. *et al.* Chronically inflamed livers up-regulate expression of inhibitory B7 family members. *Hepatology* **50,** 1625–1637 (2009).

145. Andrews, D. M., Andoniou, C. E., Fleming, P., Smyth, M. J. & Degli-Esposti, M. A. The early kinetics of cytomegalovirus-specific CD8+ T-cell responses are not affected by antigen load or the absence of perforin or gamma interferon. *Journal of Virology* **82,** 4931–4937 (2008).

146. Waggoner, S. N., Cornberg, M., Selin, L. K. & Welsh, R. M. Natural killer cells act as rheostats modulating antiviral T cells. *Nature* **481,** 394–398 (2012).

147. Walzer, T. *et al.* Identification, activation, and selective in vivo ablation of mouse NK cells via NKp46. *Proc Natl Acad Sci USA* **104,** 3384–3389 (2007).

148. Liu, Z. X., Govindarajan, S., Okamoto, S. & Dennert, G. NK cells cause liver injury and facilitate the induction of T cell-mediated immunity to a viral liver infection. *J Immunol* **164,** 6480–6486 (2000).

149. Huang, L. & Liu, Y. In Vivo Delivery of RNAi with Lipid-Based Nanoparticles. *Annu. Rev. Biomed. Eng.* **13,** 507–530 (2011).

150. Boussif, O. *et al.* A versatile vector for gene and oligonucleotide transfer into cells in culture and in vivo: polyethylenimine. *Proc Natl Acad Sci USA* **92,** 7297–7301 (1995).

151. Mueller, S. N. *et al.* PD-L1 has distinct functions in hematopoietic and nonhematopoietic cells in regulating T cell responses during chronic infection in mice. *Journal of Clinical Investigation* **120,** 2508–2515 (2010).

152. Wolfrum, C. *et al.* Mechanisms and optimization of in vivo delivery of lipophilic siRNAs. *Nat Biotechnol* **25,** 1149–1157 (2007).

153. Gillard, G. O. *et al.* Thy1+ Nk cells from vaccinia virus-primed mice confer protection against vaccinia virus challenge in the absence of adaptive lymphocytes. *PLoS Pathog* **7,** e1002141 (2011).

154. Haeryfar, S. M. M. & Hoskin, D. W. Thy-1: more than a mouse pan-T cell marker. *J Immunol* **173,** 3581–3588 (2004).

155. Alter, G. & Altfeld, M. Mutiny or scrutiny: NK cell modulation of DC function in HIV-1 infection. *Trends Immunol* **32,** 219–224 (2011).

156. Schroder, K., Hertzog, P. J., Ravasi, T. & Hume, D. A. Interferon-gamma: an overview of signals, mechanisms and functions. *J Leukoc Biol* **75,** 163–189 (2004).

157. Lang, P. A. *et al.* Natural killer cell activation enhances immune pathology and promotes chronic infection by limiting CD8+ T-cell immunity. *Proc Natl Acad Sci USA* **109,** 1210–1215 (2012).

158. Wiesel, M. & Oxenius, A. From crucial to negligible: Functional CD8+T-cell responses and their dependence on CD4+T-cell help. *Eur J Immunol* **42,** 1080–1088 (2012).

159. Leuschner, F. *et al.* Therapeutic siRNA silencing in inflammatory monocytes in mice. *Nat Biotechnol* 1–9 (2011). doi:10.1038/nbt.1989

160. Cubillos-Ruiz, J. R. *et al.* Polyethylenimine-based siRNA nanocomplexes reprogram tumor-associated dendritic cells via TLR5 to elicit therapeutic antitumor immunity. *Journal of Clinical Investigation* (2009). doi:10.1172/JCI37716DS1

161. Frank-Kamenetsky, M. *et al.* Therapeutic RNAi targeting PCSK9 acutely lowers plasma cholesterol in rodents and LDL cholesterol in nonhuman primates. *Proc Natl Acad Sci USA* **105,** 11915–11920 (2008).

162. Ackerman, M. E. *et al.* A robust, high-throughput assay to determine the phagocytic activity of clinical antibody samples. *Journal of Immunological Methods* **366,** 8–19 (2011).

163. McLean, I. W. & Nakane, P. K. Periodate-lysine-paraformaldehyde fixative. A new fixation for immunoelectron microscopy. *J. Histochem. Cytochem.* **22,** 1077–1083 (1974).

164. Liu, Z. X., Govindarajan, S., Okamoto, S. & Dennert, G. Fas-mediated apoptosis causes elimination of virus-specific cytotoxic T cells in the virus-infected liver. *J Immunol* **166,** 3035–3041 (2001).

165. Mills, K. H. G. Regulatory T cells: friend or foe in immunity to infection? *Nat Rev Immunol* **4,** 841–855 (2004).

166. MacDonald, A. J. *et al.* CD4 T helper type 1 and regulatory T cells induced against the same epitopes on the core protein in hepatitis C virus-infected persons. *J INFECT DIS* **185,** 720–727 (2002).

167. Kapp, J. A. & Bucy, R. P. CD8+ suppressor T cells resurrected1 1 This work has been supported over the years by several research grants from the NIH, including the current Grant EY014877 from the NEI. *HIM* **69,** 715–720 (2008).

168. Bedke, T., Pretsch, L., Karakhanova, S., Enk, A. H. & Mahnke, K. Endothelial Cells Augment the Suppressive Function of CD4+CD25+Foxp3+ Regulatory T Cells: Involvement of Programmed Death-1 and IL-10. *J Immunol* (2010). doi:10.4049/jimmunol.0902458

169. Pandiyan, P., Zheng, L., Ishihara, S., Reed, J. & Lenardo, M. J. CD4+CD25+Foxp3+ regulatory T cells induce cytokine deprivation–mediated apoptosis of effector CD4+ T cells. *Nat Immunol* **8,** 1353–1362 (2007).

170. Dai, H. *et al.* Cutting Edge: Programmed Death-1 Defines CD8+CD122+ T Cells as Regulatory versus Memory T Cells. *J Immunol* (2010). doi:10.4049/jimmunol.1000661

171. Shafer-Weaver, K. A. *et al.* Cutting Edge: Tumor-Specific CD8+ T Cells Infiltrating Prostatic Tumors Are Induced to Become Suppressor Cells. *The Journal of Immunology* **183,** 4848–4852 (2009).

172. Efimova, O., Szankasi, P. & Kelley, T. W. Ncf1 (p47phox) Is Essential for Direct Regulatory T Cell Mediated Suppression of CD4+ Effector T Cells. *PLoS ONE* **6,** e16013 (2011).

173. Joosten, S. A. *et al.* Identification of a human CD8+ regulatory T cell subset that mediates suppression through the chemokine CC chemokine ligand 4. *Proc Natl Acad Sci USA* **104,** 8029–8034 (2007).

174. Takahashi, T. *et al.* Immunologic self-tolerance maintained by CD25(+)CD4(+) regulatory T cells constitutively expressing cytotoxic T lymphocyte-associated antigen 4. *J Exp Med* **192,** 303–310 (2000).

175. Kim, H.-J. *et al.* CD8+ T regulatory cells express the Ly49 Class I MHC receptor and are defective in autoimmune prone B6-Yaa mice. *Proc Natl Acad Sci USA* **108,** 2010–2015 (2011).

176. Strauss, L., Bergmann, C. & Whiteside, T. L. Human circulating CD4+CD25highFoxp3+ regulatory T cells kill autologous CD8+ but not CD4+ responder cells by Fas-mediated apoptosis. *The Journal of Immunology* **182,** 1469–1480 (2009).

177. Daniel, V., Sadeghi, M., Wang, H. & Opelz, G. CD4+CD25+Foxp3+IFNÎ³+ CD178+ human induced Treg (iTreg) contribute to suppression of alloresponses by apoptosis of responder cells. *HIM* **74,** 151–162 (2013).

178. Salti, S. M. *et al.* Granzyme B Regulates Antiviral CD8+ T Cell Responses. *The Journal of Immunology* **187,** 6301–6309 (2011).

179. Gotot, J. *et al.* Regulatory T cells use programmed death 1 ligands to directly suppress autoreactive B cells in vivo. *Proc Natl Acad Sci USA* **109,** 10468–10473 (2012).

180. Kitazawa, Y. *et al.* Involvement of the Programmed Death-1/Programmed Death-1 Ligand Pathway in CD4+CD25+ Regulatory T-Cell Activity to Suppress Alloimmune Responses. *Transplantation* **83,** 774–782 (2007).

181. Singh, A., Dey, A. B., Mohan, A., Sharma, P. K. & Mitra, D. K. Foxp3+ Regulatory T Cells among Tuberculosis Patients: Impact on Prognosis and Restoration of Antigen Specific IFN-γ Producing T Cells. *PLoS ONE* **7,** e44728 (2012).

182. Getnet, D. *et al.* A role for the transcription factor Helios in human CD4+CD25+ regulatory T cells. *Molecular Immunology* **47,** 1595–1600 (2010).

183. Huang, C.-T. *et al.* Role of LAG-3 in Regulatory T Cells. *Immunity* **21,** 503–513 (2004).

184. Blackburn, S. D. & Wherry, E. J. IL-10, T cell exhaustion and viral persistence. *Trends Microbiol* **15,** 143–146 (2007).

185. Sun, J., Madan, R., Karp, C. L. & Braciale, T. J. Effector T cells control lung inflammation during acute influenza virus infection by producing IL-10. *Nat Med* **15,** 277–284 (2009).

186. Crispín, J. C. & Tsokos, G. C. Transcriptional regulation of IL-2 in health and autoimmunity. *Autoimmunity Reviews* **8,** 190–195 (2009).

187. Baine, I., Basu, S., Ames, R., Sellers, R. S. & Macian, F. Helios Induces Epigenetic Silencing of Il2 Gene Expression in Regulatory T Cells. *The Journal of Immunology* **190,** 1008–1016 (2013).

188. Kalia, V. *et al.* Prolonged Interleukin-2Rα Expression on Virus-Specific CD8+ T Cells Favors Terminal-Effector Differentiation In Vivo. *Immunity* **32,** 91–103 (2010).

189. Xu, D. *et al.* Circulating and liver resident CD4+CD25+ regulatory T cells actively influence the antiviral immune response and disease progression in patients with hepatitis B. *J Immunol* **177,** 739–747 (2006).

190. Guy, C. S. *et al.* Distinct TCR signaling pathways drive proliferation and cytokine production in T cells. *Nature Publishing Group* **14,** 262–270 (2013).

191. Kanzaki, M. *et al.* Galectin-9 and T Cell Immunoglobulin Mucin-3 Pathway Is a Therapeutic Target for Type 1 Diabetes. *Endocrinology* **153,** 612–620 (2012).

192. Said, E. A. *et al.* Programmed death-1-induced interleukin-10 production by monocytes impairs CD4+ T cell activation during HIV infection. *Nat Med* **16,** 452–459 (2010).

193. Madan, R. *et al.* Nonredundant Roles for B Cell-Derived IL-10 in Immune Counter-Regulation. *The Journal of Immunology* **183,** 2312–2320 (2009).

194. Murai, M. *et al.* Interleukin 10 acts on regulatory T cells to maintain expression of the transcription factor Foxp3 and suppressive function in mice with colitis. *Nat Immunol* **10,** 1178–1184 (2009).

195. Walzer, T. *et al.* Natural killer cell trafficking in vivo requires a dedicated sphingosine 1-phosphate receptor. *Nat Immunol* **8,** 1337–1344 (2007).

196. Yoneyama, H. *et al.* Regulation by chemokines of circulating dendritic cell precursors, and the formation of portal tract-associated lymphoid tissue, in a granulomatous liver disease. *J Exp Med* **193,** 35–49 (2001).

197. Yokosuka, T. *et al.* Programmed cell death 1 forms negative costimulatory microclusters that directly inhibit T cell receptor signaling by recruiting phosphatase SHP2. *Journal of Experimental Medicine* **209,** 1201–1217 (2012).

198. Who, U.Unicef. Global HIV/AIDS Response: Epidemic update & health sector progress towards universal access. *Progress report. November* (2011).

199. Newman, R. D. World Malaria Report 2011. (2012).

200. Schust, J., Sperl, B., Hollis, A., Mayer, T. U. & Berg, T. Stattic: a small-molecule inhibitor of STAT3 activation and dimerization. *Chem Biol* **13,** 1235–1242 (2006).